AD-A274 038

AFIT/GE/ENG/93D-06

DTIC
ELECTE
DEC 23 1993
S A

OBJECT IMAGING ACCOMPLISHED WITH AN
INTEGRATED CIRCUIT ROBOTIC TACTILE
SENSOR INCORPORATING A PIEZOELECTRIC
POLYVINYLIDENE FLUORIDE THIN FILM

THESIS

JOHN M. EMMERT, Captain, USAF

AFIT/GE/ENG/93D-06

93-30986

93 12 22 099

AFIT/GE/ENG/93D-06

OBJECT IMAGING ACCOMPLISHED WITH AN INTEGRATED CIRCUIT

ROBOTIC TACTILE SENSOR INCORPORATING A PIEZOELECTRIC

POLYVINYLIDENE FLUORIDE THIN FILM

THESIS

Presented to the Faculty of the Graduate School of

Engineering of the Air Force Institute of Technology

Air University

In Partial Fulfillment of the

Requirements for the Degree of

Master of Science in Electrical Engineering

JOHN M. EMMERT, B.S.E.E.

Captain, USAF

December 1993

Approved for public release; distribution unlimited

Preface

The purpose of this undertaking was to develop a piezoelectric tactile sensor for use on a robotic hand. In order to accomplish this task, I had help from many people. I wish to thank Dr. Victor M. Bright and Dr. Edward S. Kolesar (currently at Texas Christian University) for advising me during this undertaking. I would also like to thank the members of my thesis committee, Major Mark Mehalic, Dr. Curtis H. Spenny, and Captain Thomas Jenkins. In addition, I would like to thank Mr. William Trop and Mr. Chris O'Brien for technical laboratory support, and Mr. Larry Callahan for his wire bonding assistance.

A special thanks goes to my wife, Jorie, for her support throughout this research endeavor. She was very understanding and supportive throughout the entire project.

Table of Contents

iv

vi

List of Figures

List of Tables

AFIT/GE/ENG/93D-06

Abstract

The purpose of this research effort was to investigate the performance of a piezoelectric tactile sensor design and appropriately refine it. The sensor was fabricated from an 8 x 8 electrode array MOS integrated circuit. Each taxel in the array was 400 μm x 400 μm. A 6 mm x 6 mm piece of piezoelectric polyvinylidene fluoride was adhered to the electrode array using a urethane dielectric adhesive to form the active sensing area of the sensor.

In order to minimize electrical crosstalk inherent in the sensor design, the integrated circuit used as the base of the sensor was specifically designed to determine the cause of electrical crosstalk. Specifically, the spacing and configuration of the lines connecting the taxels to the amplifiers and the pads to the amplifiers of the integrated circuit were investigated. Additionally, to enhance the range of the tactile sensor's output signal, a high input impedance differential amplifier with a linear range from 1 to 17 V was designed and tested for incorporation into the tactile sensor's integrated circuit. The unique feature of the differential amplifier was that it used a power supply of only 12 V.

Using the center to center taxel spacing as the criteria for spatial resolution, the spatial resolution of the piezoelectric tactile sensor is 0.7 mm. The lower force limit of the sensor was determined to be 1 g while the upper limit, limited by amplifiers with a range from 2.5 to 7 V, was found to be 130 g. The dynamic range of the sensor is 130:1. The sensor force sensitivity was determined to be between 7.35 g. The pyroelectric bandwidth of the sensor was determined to be 0.083 Hz, and the temperature sensitivity of the sensor was 0.39 °C.

OBJECT IMAGING ACCOMPLISHED WITH AN INTEGRATED CIRCUIT ROBOTIC TACTILE SENSOR INCORPORATING A PIEZOELECTRIC POLYVINYLIDENE FLUORIDE THIN FILM

1. Introduction

1.1. Background

The advent of automation and automated manufacturing processes has motivated the need for pressure (force) sensing robotic grippers [1]. Currently, most automated manufacturing processes are accomplished with robots or specialized machinery without precision sensory information. These "machines" follow preprogrammed scripts that do not necessarily consider the information available from their immediate surroundings. This situation is often satisfactory for repetitive tasks performed in an invariant environment. Many of these tasks are often dangerous, and the robot removes the necessity of human intervention. However, there is an increased demand for robots or machines that can be influenced by sensory information [1].

Most robots used in industry have no tactile sensory capabilities [2]. The strength of their grip is defined by the task at hand, and frequently the force applied to hold an object firmly is excessive. To utilize their complete functionality, grippers must not only firmly grasp an object, but they should also possess the ability to discern the tactile image of the object [3]. This tactile image may also provide sensory information such as the object's texture and composition. Also, menial tasks could be performed by robots with this information,

including: determining the location of randomly placed objects, measuring tolerances, recognizing objects and their orientation, sensing potentially dangerous situations, and detecting substandard parts and controlling quality on an assembly line [1,2]. A robotic hand with a tactile sensing capability could ultimately be utilized to autonomously determine the object it is gripping [3].

Complex tactile sensors are required to bridge the gap between the automated and autonomous robotic functions. A tactile sensor should have a resolution of 0.1 to 10.0 mm [3]. It should respond to a stimulus in less than 10 ms and have a dynamic range that spans 1 to 1000 grams [3]. Finally, it must be robust and tolerate a hostile environment [3].

1.2. Summary of Current Knowledge

The piezoelectric tactile sensor in this research effort represents the culmination of several projects and research efforts at AFIT [4-10]. Capt Pirolo initially investigated 16 fundamental macroscopic piezoelectric polymer tactile sensor array configurations [4]. His research revealed that an array of square-pads, as shown in Figure 1.1, was a better performing configuration compared to the arrangement of overlapping rectangular stripes shown in Figure 1.2. He also determined that a 40 μm thick polyvinylidene fluoride (PVDF) film exhibited higher piezoelectric activity and was more desirable (from a sensor fabrication perspective) compared to the 25 μm thick PVDF film [4].

Capt Reston investigated the pressure sensitivity and coupling (electrical and mechanical) of a piezoelectric tactile integrated
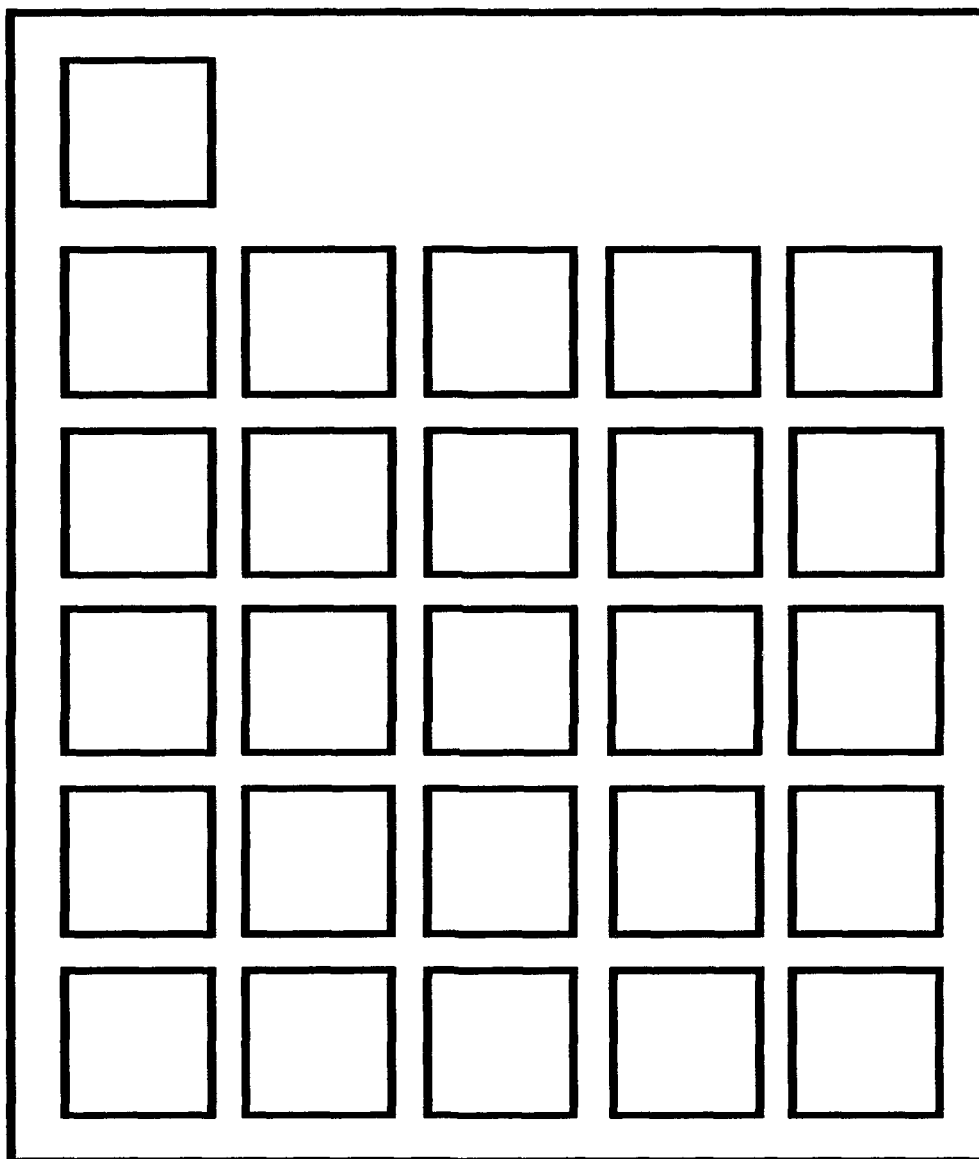
Figure 1.1. Array of square electrode pads. The electrode pads are 3 mm x 3 mm. Two electrode pad spacings were tested (0.5 and 0.75 mm). The pad in the upper left corner was used as a reference electrode [4].
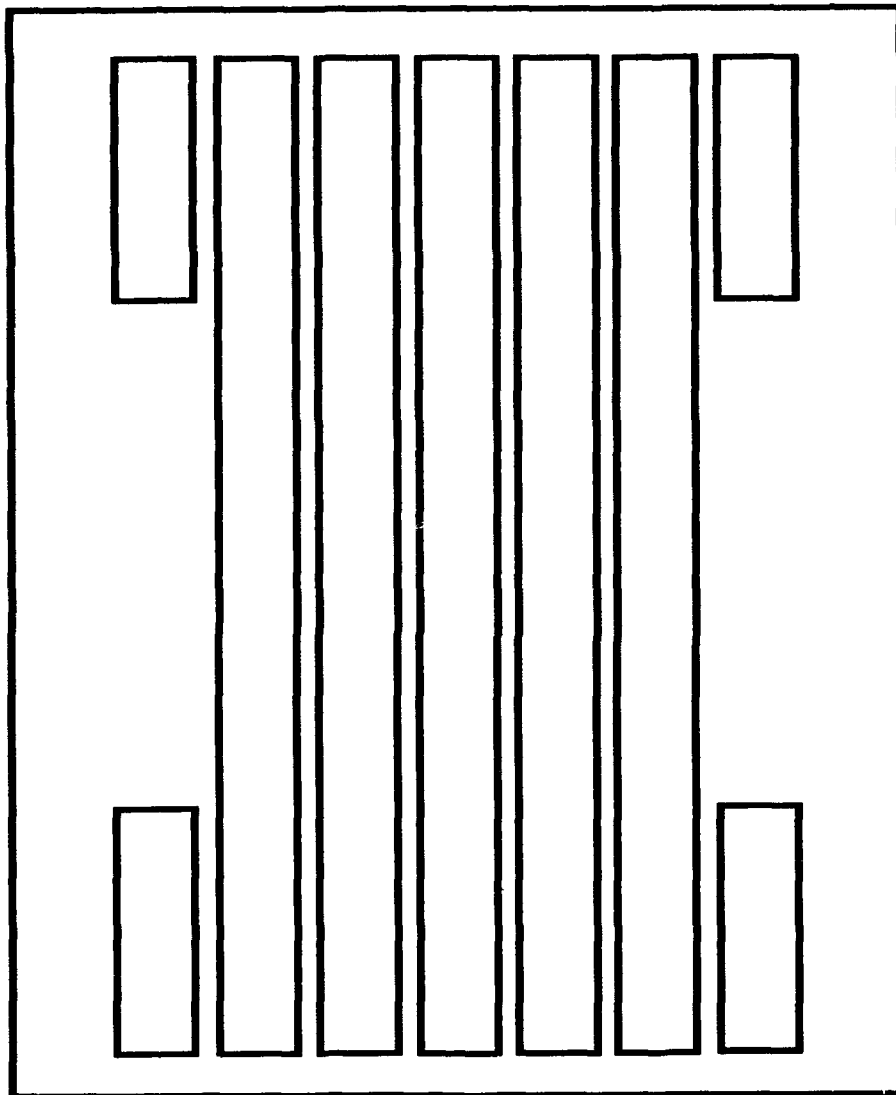
Figure 1.2. Array of rectangular-shaped stripe electrode pads. The primary (long) pads are 37.5 mm x 3 mm, and the reference (short) pads are 9 mm x 3 mm [4].

circuit based sensor [5]. Capt Reston, fabricated, and tested a sensor with an overall 6 mm x 6 mm active area (the size of an adult's fingertip). The active area consisted of a 5 x 5 array of square electrodes (600 μm x 600 μm each that were separated from each other by 600 μm) [5]. The configuration of this sensor design is shown in Figure 1.3. It was determined that a 25 μm thick PVDF film exhibited a linear response for loads spanning 0.8 to 76 grams with no detectable coupling between nearest-neighbor electrodes [5].

Capt Ford designed, fabricated, and evaluated a 16 x 16 piezoelectric integrated circuit tactile sensor electrode array [6]. The layout of this sensor design is shown in Figure 1.4. Unfortunately, the finished sensor did not function as intended. The integrated circuit design relied upon transmission gates to access the electrical response of the PVDF film. The incompatible RC-time constants of the PVDF film and the transmission gates allowed leakage currents to compromise the operation of the sensor [6]. However, further investigation of Capt Reston's 5 x 5 sensor led to new and valuable information. Four PVDF film attachment adhesives were determined to be compatible with the sensor. Three of the adhesive types were liquid based, and they included: an acrylic-based adhesive, a urethane-based adhesive, and a silicon-based adhesive (manufactured by Miller-Stephenson Chemical Company, Danbury, CT 06810). The other useful candidate was a low viscosity, nonpolar adhesive (Epoxy Technology Incorporated, Billerica, MA 01821) [6]. Also, Capt Reston defined the need and functional utility of an initial biasing state that was achieved across the entire sensor array; this situation produced enhanced and reproducible tactile sensing results [6].
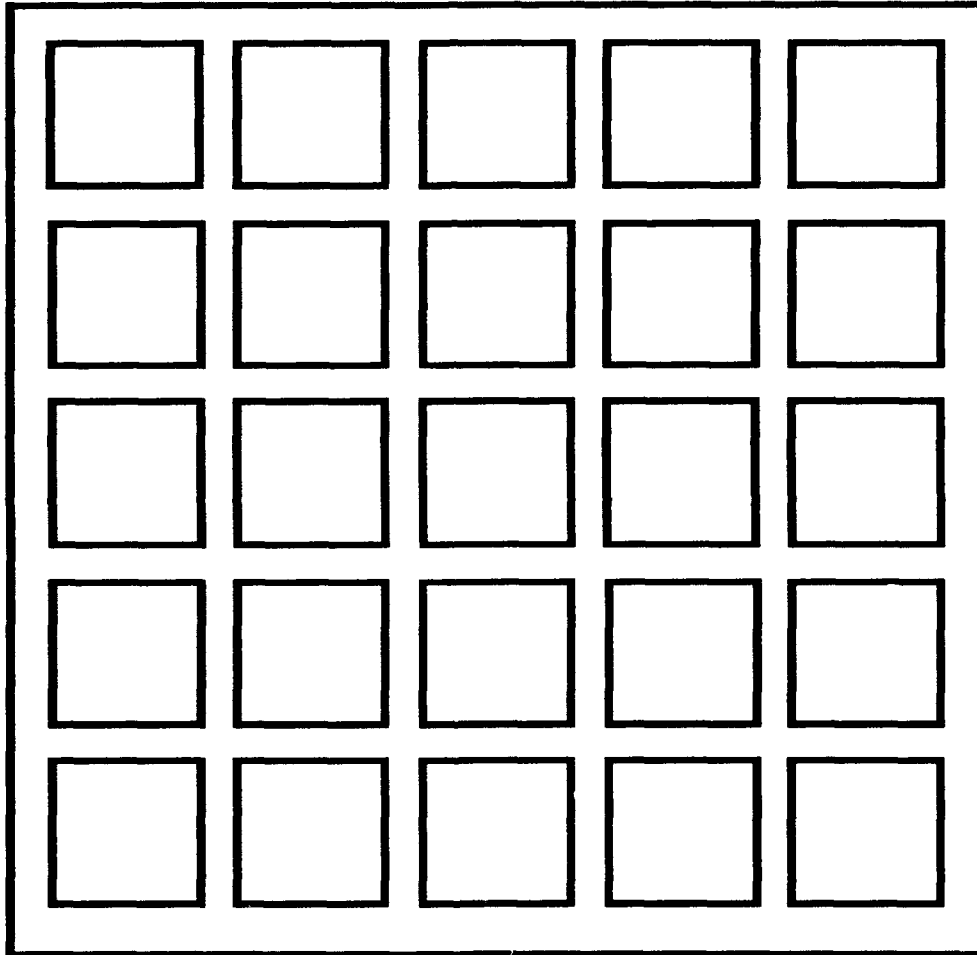
Figure 1.3. Integrated circuit 6 mm x 6 mm sensor array. The electrode pads are 600 μm x 600 μm, and they are separated from each other by 600 μm [5].
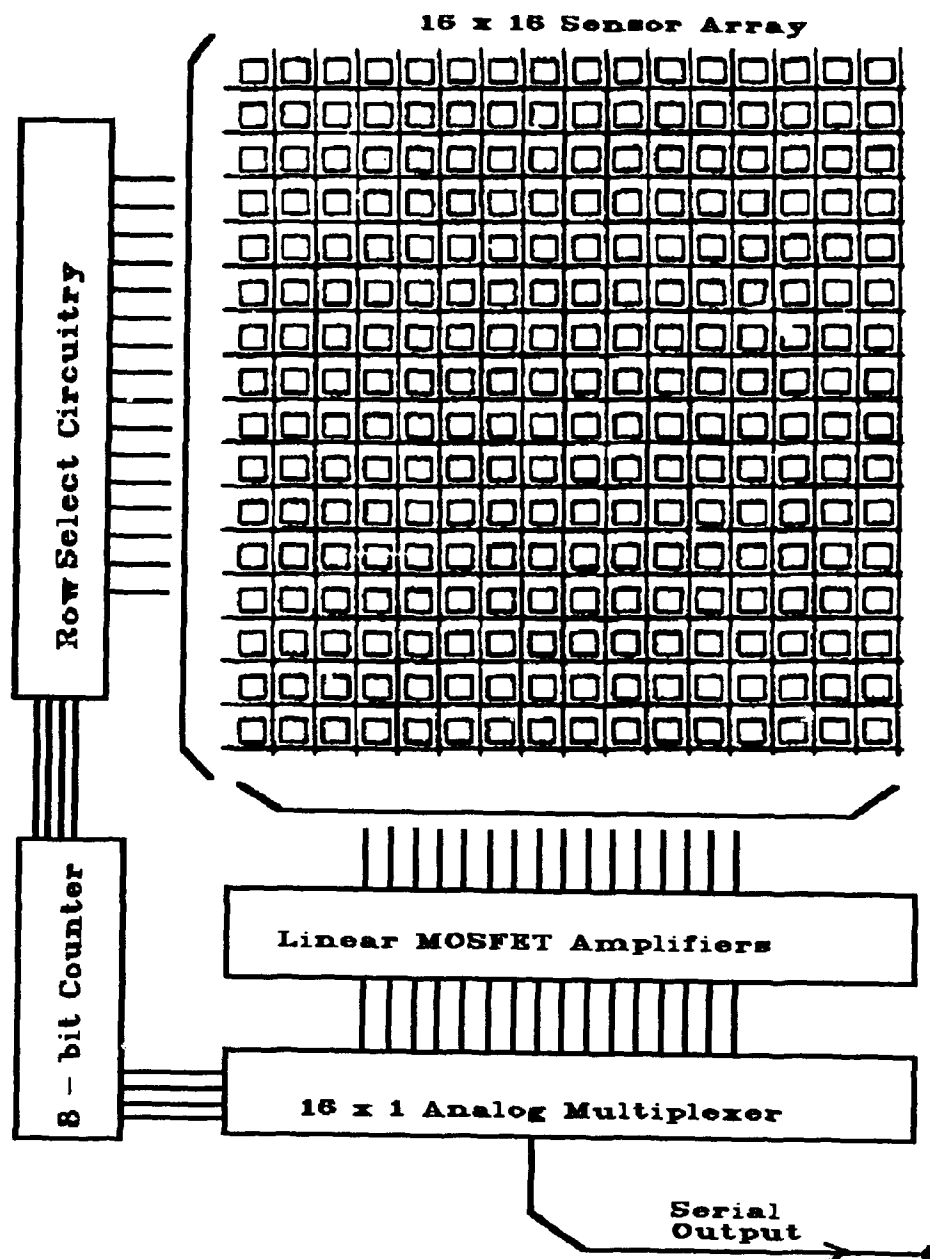
Figure 1.4. Integrated circuit 6.25 mm x 6.25 mm sensor array. The electrode pads are 250 μm x 250 μm, and they are separated from each other by 150 μm [6].

Capt Fitch fabricated a 7 x 7 tactile integrated circuit sensor array with *in situ* output multiplexing circuitry. This sensor concept is shown in Figure 1.5. Capt Fitch intensely studied the charge amplifier biasing issue [7]. An unforseen problem with charge leakage forced him to reduce the size of his active array to a 3 x 3 configuration that included an external output multiplexing circuit [7]. Capt Fitch determined that the problem was caused by two phenomena: a design error in the *in situ* multiplexer circuit and faulty wire bonds [7]. Characterization of the reduced 9-element taxel array revealed a linear output range for loads spanning 3 to 81 grams [7]. Additionally, there was little or no crosstalk between the nearest-neighbor taxels [7], and the sensor was capable of recognizing several simple shapes [7]. Finally, it was concluded that the urethane PVDF film adhesive exhibited superior electrical and mechanical performance characteristics [7].

Capt Dyson designed, fabricated, and characterized an operational piezoelectric tactile integrated circuit sensor [8]. This sensor consisted of an 8 x 8 taxel array of equally spaced aluminum electrodes [8]. The design is shown in Figure 1.6. A 40 μm thick piezoelectric PVDF film was utilized to obtain a linear response for applied loads spanning 0.8 to 135 grams [8]. Capt Dyson determined there was considerable electrical crosstalk between several of the closely spaced sensor element aluminum conductors (for spacings less than 10 μm) [8]. Additionally, it was verified that the urethane adhesive's physical and electrical properties were superior to the *Loctite* or polyamide materials [8].
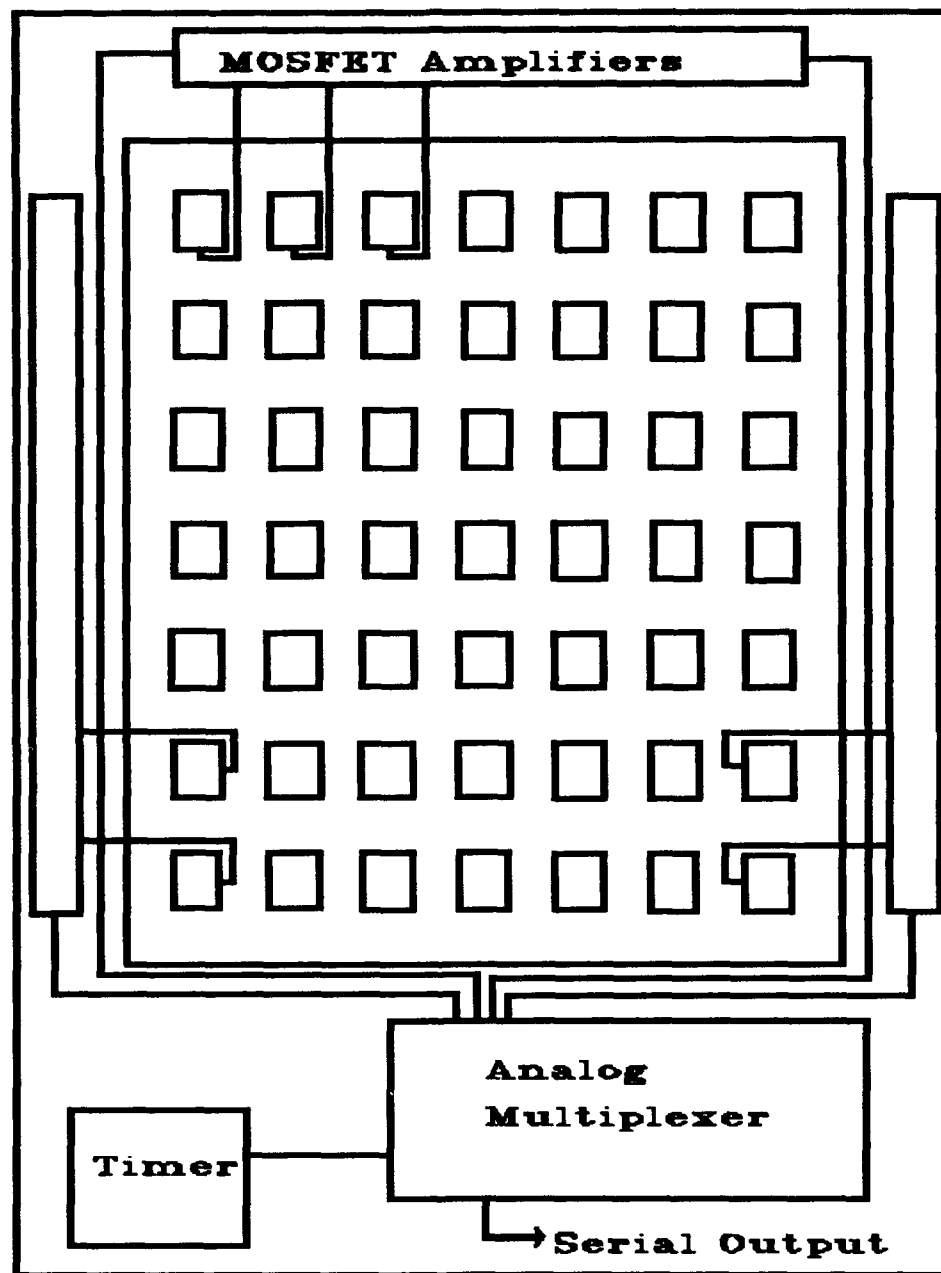
Figure 1.5. Integrated circuit 5.2 mm x 5.2 mm sensor array. The
electrode pads are 400 μm x 400 μm, and they are
separated from each other by 400 μm [7].
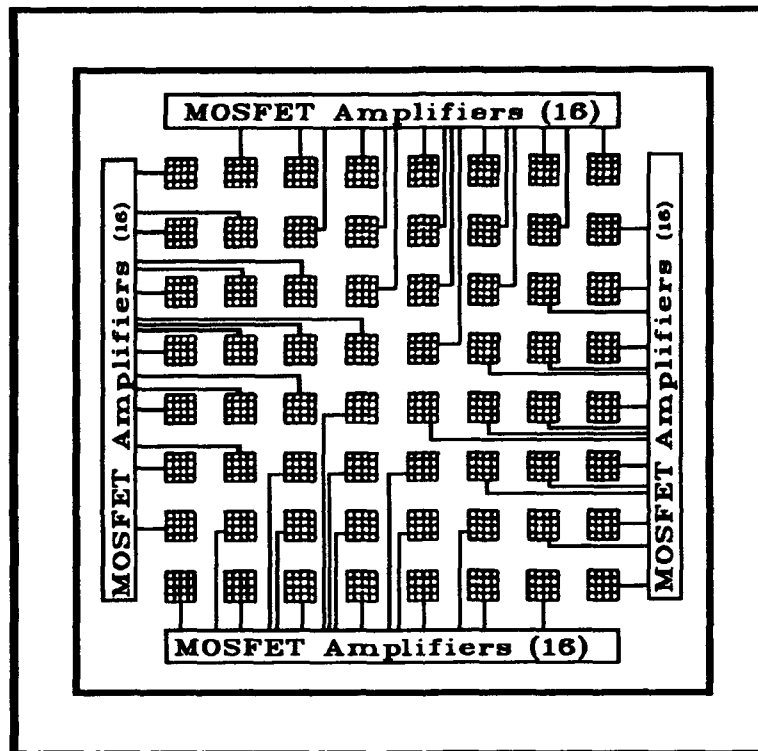
Figure 1.6. Integrated circuit 5.3 mm x 5.3 mm sensor array. The electrode pads are 400 μm x 400 μm, and they are separated from each other by 300 μm [8].

1-10

Capt Yauilla further investigated the tactile integrated circuit sensor designed by Capt Dyson. He determined that the amplifier's linear output voltage response spanned 2 to 7 V [9]. The performance of an alternative external multiplexing circuit that was used to bias the sensor's 8 x 8 taxel array was also investigated. It was reported that the MAX327CPE analog switches (Maxim Integrated Products, 120 San Gabriel Dr., Sunnyvale, CA 94086) exhibited superior performance when they were compared to other switch technologies (for example, magnetically-triggered reed relay switches) used for this biasing function [9].

1.3. Problem Statement

This research effort investigates the performance of a piezoelectric tactile sensor design and appropriately refines it. Additionally, the linear range of the tactile sensor's amplifiers are enhanced, the electrical crosstalk of the sensor is characterized and minimized. Pyroelectric characteristics need to be investigated. The specific areas of interest are expanded below:

1.3.1. Investigation of a Revised Charge Signal Amplifier Design.
The previous research has consistently motivated the need for a charge signal amplifier with an enhanced linear operating region [8]. The current integrated circuit amplifier was designed by Capt Dyson [8]. Neglecting temperature effects, it was theoretically determined that the 40 μm thick piezoelectric PVDF film could generate a voltage that spanned 0.37 to 37 V for applied loads spanning 1 to 100 grams. Ideally, a charge amplifier for the 40 μm thick PVDF film used in Capt Dyson's research would have a linear output range spanning 0 to 37 V.

Therefore, the power supply voltage (V_{DD}) for an ideal amplifier would necessarily be on the order of 37 V. Utilizing a supply voltage (V_{DD}) of 15 V, Capt Dyson designed an amplifier with a linear range that extended from approximately 2 to 8 V with a gain on the order of 1.25 [8]. Simulations were used to model the amplifier's response to a series of voltage inputs. After testing it was determined that the amplifier's linear range was actually 2.5 to 7 V, and that it possessed a gain of 0.98 for a 14-volt V_{DD} [8]. In subsequent testing, Capt Yauilla established that the linear range of the amplifier spanned 2 to 7 V, and that it possessed a gain of 1.01 for a 12-volt V_{DD} [9].

Extensive testing by Capt Dyson also revealed another problem with the amplifier's design. The integrated circuit taxel sensor utilized 64 amplifiers that were of the same design. When they were operated for extended periods of time, the output of some of the amplifiers latched at either V_{DD} or ground. By monotonically increasing V_{DD} with respect to time, Capt Dyson determined that a 14-volt V_{DD} was excessive, and it caused several of the amplifier circuits to malfunction. It was empirically observed that when V_{DD} was 12 V or less, the amplifier's failure phenomena did not occur [8]. Consequently, to incorporate an amplifier with a linear range that is closer to the ideal amplifier's linear range, the amplifier design must be enhanced to accommodate a larger supply voltage. Thus, an effort is made in this research to increase V_{DD} from 12 to 20 V.

1.3.2. Characterization of Taxel Crosstalk. The cumulative research indicates that electrical crosstalk prevails in the integrated circuit sensor designed by Capt Dyson [8]. The closeness of the

conductors (10 μm separation) routed from the bonding pads to the charge signal amplifiers is the apparent source of the electrical crosstalk. Research was performed to characterize the electrical crosstalk of the integrated circuit design in order to minimize its affect on the tactile sensor's performance.

1.3.3. Investigation of Pyroelectric Effects. Most piezoelectric materials, including PVDF, are also pyroelectric [11]. A pyroelectric material is one which exhibits a change in the magnitude of the open circuit voltage as the temperature of the material is changed [12]. It is not desirable for a pressure or tactile sensor to be pyroelectric since a grasped object will likely be at a different temperature compared to the sensor. Intimate contact between a tactile sensor that is pyroelectric, and an object that is at a different temperature, will cause a false tactile sensor response. That is, the tactile sensor's response to a temperature change could be interpreted as the sensor's response solely to an externally applied force. The pyroelectric nature of the sensor must be characterized.

1.4. Assumptions

1.4.1. Prior research established that the urethane adhesive exhibited superior mechanical and electrical characteristics [7,8]. Therefore, the urethane adhesive is also utilized in this research effort. It is not evaluated separately, but its effects are lumped into the overall tactile sensor system's performance.

1.4.2. Steady-state conditions are established for each measurement in order to make the analysis as consistent as possible.

1.4.3. The integrated circuits fabricated by Metal-Oxide-Semiconductor Implementation System (MOSIS) function very similar to the HSPICE analysis performed during the design process.

1.4.4. The test fixture (designed by Capt Fitch) is capable of applying test loads that make uniform contact with the integrated circuit tactile sensor.

1.5. *Scope of the Effort*

An integrated circuit tactile sensor is designed, fabricated, and tested. This research effort has several specific goals:

1.5.1. *Investigation of a Revised Charge Signal Amplifier Design.* Two design avenues for an amplifier with an enhanced linear range are pursued:

a) *Enhancement of the Power Supply Voltage.* One possible way to enhance the linear range of the amplifier is to increase the supply voltage of the existing amplifier design. Consequently, a similar amplifier is designed, fabricated, and tested. The goal is to enhance the 12-volt V_{DD} limitation. The amplifier circuit is designed using the MAGIC CAD tool, and then the circuit is simulated using the HSPICE circuit simulation software (the simulation indicates the ideal amplifier response). After the amplifier circuit design was completed, the circuit was fabricated using the MOSIS TinyChip format. Tests were conducted to verify whether the amplifier's supply voltage limitation had been enhanced.

b) Revised Amplifier Design with an Enhanced Linear Operating Range. Assuming that the useful operating range of the amplifier cannot be enhanced by simply increasing the magnitude of V_{DD}, a revised amplifier design is pursued. A revised integrated circuit charge amplifier is designed, fabricated, and tested. The amplifier design is simulated using the HSPICE and MAGIC CAD software tools. After the amplifier circuit design was completed, it was fabricated using the MOSIS TinyChip format. Tests were conducted on the fabricated circuits to verify the amplifier's linear operating range and voltage gain.

1.5.2. Characterization of the Tactile Sensor's Taxel Crosstalk. The electrical crosstalk and sensor response were characterized. Electrical crosstalk characterization was defined as the percent of electrical coupling experienced by the electrodes. This objective was accomplished in three parts:

a) Electrical Crosstalk Problem Associated with the Original Integrated Circuit Design. The electrical crosstalk of an integrated circuit (without the piezoelectric PVDF film) used in the previous research effort was characterized.

b) Electrical Crosstalk Issue Associated with the Revised Integrated Circuit Design. The electrical crosstalk of the new integrated circuit (without the piezoelectric PVDF film) designed to minimize electrical crosstalk was characterized.

c) *Tactile Sensor Fabrication Process.* Once the electrical crosstalk evaluation of the original and revised integrated circuits had been accomplished, tactile sensors were fabricated using these integrated circuits. After sensor fabrication, the revised integrated circuit tactile sensor's response was characterized.

1.5.3. Investigation of the Tactile Sensor's Pyroelectric Effects. The response of a piezoelectric tactile sensor to temperature variations will be investigated. Several transient and steady-state temperature fluctuations (nondestructive) will be investigated.

1.6. Approach

Using the materials listed in Appendix A, the research effort was accomplished in three main parts: design, fabrication, and evaluation.

1.6.1. Design. First, the integrated circuits were designed using a very large scale integrated circuit design tool called MAGIC. The amplifier integrated circuits will be designed with the TinyChip format which has a size limitation of approximately 2000 μm x 2000 μm and a pin limitation of 40 pins. The integrated circuits for the tactile sensors were designed using MAGIC and utilizing MOSIS' pin-grid-array (PGA) format. The PGA format limits the size of the integrated circuit to approximately 7900 μm by 9200 μm and the pin count to 132 pins. After the integrated circuit preliminary design was completed, the circuits were tested using the HSPICE circuit simulation software.

1.6.2. Fabrication. Once the design phase was completed, the integrated circuits were fabricated by MOSIS. While waiting for the circuit fabrication, test equipment was configured in the Cooperative

Electronics and Materials Laboratory at the Air Force Institute of Technology.

1.6.3. *Evaluation.* After the fabrication phase, the circuits were tested. The amplifiers were tested to verify an enhanced linear range compared to the previous amplifier design, and the sensor integrated circuit was evaluated for crosstalk.

After the initial evaluation was complete, the test results were evaluated. A decision was made concerning the type of amplifier to add to the tactile sensor integrated circuit. The pyroelectric characterization of the sensor was presented. Finally, the signal lines on the tactile sensor integrated circuit were rerouted to provide a minimum number of turns in the conductors.

2. Piezoelectric Tactile Sensor Technologies

2.1. Introduction

Robots have used tactile sensors for more than twenty years to determine spatial information concerning the objects they interact with. Tactile sensing involves the continuous sensing of static or dynamic forces in a patterned profile [2,3]. More recently, piezoelectric tactile sensors, sensors fabricated with piezoelectric materials, have become prominent in the field of tactile sensing.

Many materials exhibit the piezoelectric effect and, therefore, could be used to fabricate piezoelectric tactile sensors. As one would expect, materials that possess high piezoelectric coefficients (a measure of a material's piezoelectric effect) produce better sensors than materials that possess low piezoelectric coefficients [13]. Vinylidene-fluoride-based polymers possess high piezoelectric coefficients and are very flexible, therefore, they make good piezoelectric tactile sensors [13]. Recently, many piezoelectric tactile sensors have been fabricated using the vinylidene-fluoride-based polymer, polyvinylidene fluoride (PVDF).

This chapter reviews the state of the art tactile sensors. First, it introduces ideal figures of merit (or performance criteria) to establish the quality of tactile sensor technologies. Then, several current tactile sensor technologies, other than those relying upon piezoelectricity, are discussed. Next, current PVDF piezoelectric tactile sensor technologies are examined. Finally, a comprehensive

table is presented with the figures of merit for each of the discussed sensor technologies.

2.2. Piezoelectric Tactile Sensor Figures of Merit

The ideal qualitative figures of merit to which tactile sensors should be designed were defined by Harmon [3,14]. A piezoelectric tactile sensor should be skin-like, highly elastic, robust, patterned in an array, and smart [3]. Harmon [3] also defined several quantitative figures of merit that can be used for direct comparison of piezoelectric tactile sensors. A piezoelectric tactile sensor should have a minimal array resolution of 4 x 4 sensing elements, a spatial resolution on the order of 1 mm, a dynamic range of 1000:1, a frequency of response of 100 Hz (or 0.01 s), a threshold sensitivity of 1 gram, and an upper detectable limit of at least 1000 grams [3,14].

2.3. Alternate Tactile Sensor Technologies

In this section, recent capacitive, piezoresistive, magneto-strictive, ultrasonic, and optical tactile sensors are presented for later comparison with the current piezoelectric tactile sensor developments.

2.3.1. Capacitive. When a force applied to a capacitor changes the shape of the capacitor, the overall capacitance of the device is changed. The change in capacitance due to an externally applied force is the principle of operation of capacitive tactile sensors. Recently, several articles have been published concerning capacitive tactile sensing [15–17]. The figures of merit for one of the capacitive tactile

sensors will be presented for comparison with the piezoelectric tactile sensor's figures of merit.

Suzuki et al. have recently fabricated a capacitive tactile sensor with an array resolution of 32 x 32 elements [17]. The spatial resolution of their sensor is 0.5 mm, and the response frequency of their sensor is 196 Hz. The upper detectable limit of the sensor is 1 g [17]. One of the primary disadvantages of this sensor is its lack of flexibility. No information was provided concerning the dynamic range or the threshold sensitivity of this sensor. In summary, this sensor exceeds Harmon's ideal array resolution, spatial resolution, and response frequency criteria, but it falls short of the flexibility and upper detectable limit criteria.

2.3.2. Piezoresistive. When a material experiences a change in resistivity due to an externally applied force, the material is said to be piezoresistive [18]. These materials may be utilized to fabricate piezoresistive tactile sensors [18,19,20]. The figures of merit for one of the piezoresistive tactile sensors will be presented for comparison with the piezoelectric tactile sensor's figures of merit.

Liu et al. have recently fabricated a piezoresistive tactile sensor with an array resolution of 4 x 4 elements [19]. Their sensor has a spatial resolution of 0.86 mm and a lower threshold of 3 grams [19]. The detectable limit was calculated to be on the order of 42 grams [19]. The dynamic range is on the order of 14:1. However, since the sensor was designed with silicon processing, its overall structure is not very flexible. No iniormation was provided on the response frequency of the sensor. Liu's sensor greatly exceeds Harmon's

ideal detectable limit and dynamic range criteria. It also satisfies or exceeds the spatial and array resolution criteria, but it is not flexible and does not satisfy Harmon's minimum threshold criteria.

2.3.3. *Magnetostrictive*. Magnetostrictive materials experience a change in magnetic field when they are influenced by an externally applied force [21]. The change in magnetic field of the magnetostrictive material may be used to fabricate a tactile sensor [22,23]. The figures of merit for one of the magnetostrictive tactile sensors will be presented for comparison with the piezoelectric tactile sensor's corresponding figures of merit.

Clark has described a high resolution tactile sensor based on changing magnetic fields [23]. The sensor has an array resolution of 64 x 64 taxels and a spatial resolution of 100 μm [23]. The response frequency of the sensor is approximately 125 Hz, and it is flex-ible [23]. No information was provided on the dynamic range, threshold sensitivity, or the upper detectable limit of the sensor.

2.3.4. *Ultrasonic*. Most ultrasonic sensors are used to sense large obstacles and obstructions [24-26]; however, there have been tactile sensors produced with ultrasonic technology [27]. This section will introduce the figures of merit for one such ultrasonic tactile sensor for comparison with the piezoelectric tactile sensor's figures of merit.

Grahn and Astle have designed and fabricated several ultrasonic tactile sensors [27]. One of their sensors has an array resolution of 3 x 4 elements and a spatial resolution of 1 mm [27]. The threshold sensitivity of the sensor is 0.6 grams, and the response frequency is

14 kHz [27]. Using the dynamic range of 2000:1, the upper detectable limit is approximately 1200 grams [27]. In summary, this design satisfies all of Harmon's criteria except for the minimal array element density.

2.3.5. Optical. Optical tactile sensors typically rely on an external force to change the path of a propagating light's signal in order to characterize the force that induced the change in the path [28]. Many optical tactile sensors have been fabricated over the last few years [29-32]. The figures of merit for one of the optical tactile sensors will be presented for comparison with the piezoelectric tactile sensor's figures of merit.

Walker et al. have fabricated a 3 x 3 optical tactile sensor [29]. The response frequency of the sensor is 60 Hz [29]. The spatial resolution, threshold sensitivity, detectable limit, and dynamic range were not presented.

2.4. PVDF Piezoelectric Tactile Sensors

Since Muller and Conragan [33] produced the first piezoelectric-semiconductor, electromechanical transducer in 1967, single element piezoelectric transducers have evolved into piezoelectric tactile sensors. In this section, figures of merit for several recent piezoelectric tactile sensors are presented and compared to the ideal figures of merit established by Harmon.

2.4.1. Multi-Purpose Tactile Sensor for Robot Manipulators. Tzou and Pandita designed and fabricated a piezoelectric tactile sensor that also serves as an acceleration sensor [34]. The sensor was designed

using a polymeric piezoelectric material. The sensor can be used to measure the acceleration of a robot arm as it moves from one position to another and to detect force or pressure when the sensor surface comes into contact with an object [34].

This sensor is depicted in Figure 2.1 and Figure 2.2 [34]. The sensor only has one element, so its array and spatial resolution are severely limited [34]. The sensor is not flexible, and its frequency response is 2200 Hz [34]. No information was reported concerning its dynamic range, its threshold sensitivity, or its upper detectable limit. This sensor clearly satisfies the 100 Hz criteria, but its performance is limited with respect to array and spatial resolution.
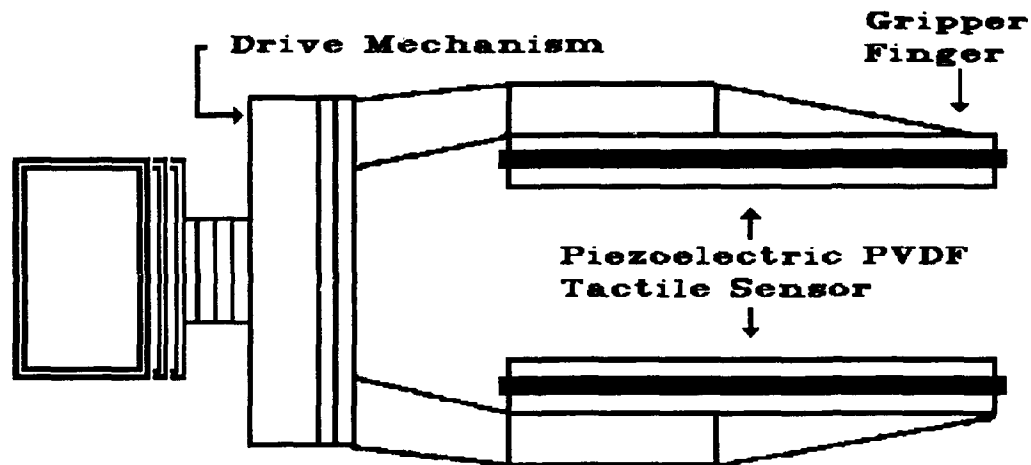
Figure 2.1. Robotic hand with piezoelectric PVDF tactile/acceleration sensor [34].
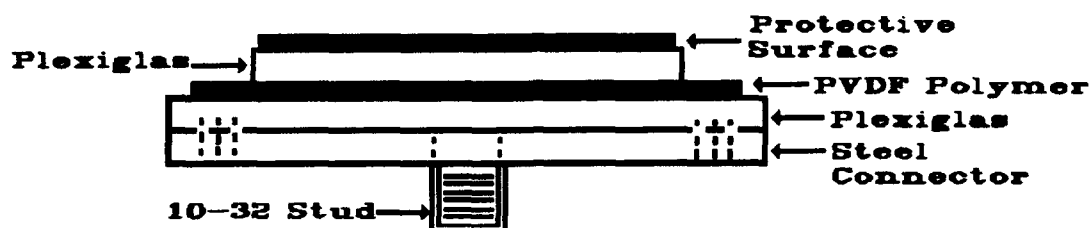
Figure 2.2. Piezoelectric PVDF tactile/acceleration sensor [34].

2.4.2. PVDF Tactile Sensor for Industrial Robots. Park et al. developed a piezoelectric tactile sensor for use with industrial robots, which is capable of determining the shape of objects [35].

The sensor is shown in Figure 2.3. The spatial resolution of the sensor is 2.5 mm, and the array has a resolution of 8 x 8 elements [35]. The sensor's dynamic range is approximately 100:1 [35]. The threshold sensitivity of the sensor is 2.5 grams, and the upper detectable limit of the sensor is 250 grams [35]. There was no information reported on the frequency response or flexibility of the sensor. In summary, this sensor exceeds Harmon's array resolution criteria, but it has a limited spatial resolution, dynamic range, threshold sensitivity, and upper detectable limit.

Silver Impregnated Silicon Rubber

Sensing Elements (0.1" center to center)

Substrate (3" x 1" x 0.04")

Multiplexers

Amplifiers

Aluminum
Support
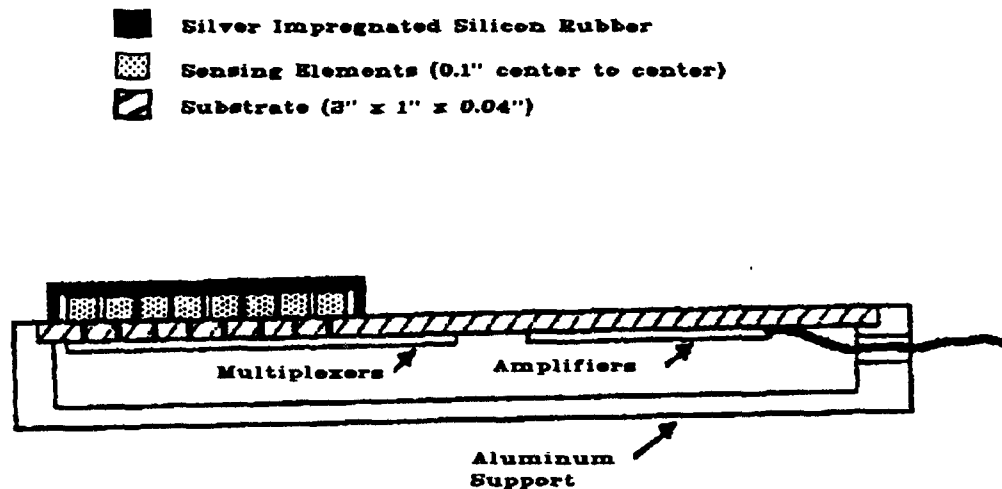
Figure 2.3. Cross section of tactile sensing device [35].

2.4.3. Tactile Sensor Similar to the Human Hand. Omata and
Terunuma fabricated a piezoelectric tactile sensor that can detect the
elastic nature of an object (the hardness or softness of an object)
[36]. This piezoelectric tactile sensor uses frequency feedback to
provide information concerning the acoustic impedance of an object. The
object's acoustic impedance is then used to determine the hardness or
softness of an object [36]. The single element sensor determines the
shape of an object by making multiple passes over the object.

The sensor is shaped like a typical probe, and it is shown in
Figure 2.4. It has a spatial resolution of 0.001 mm and an array
resolution of 1 element [36]. The sensor's frequency response is
approximately 0.5 Hz [36]. No information was provided on the dynamic
range, the threshold sensitivity, or the upper detection limit of the

2-8

sensor. This sensor exceeds Harmon's ideal spatial resolution criteria, but its array resolution and frequency response are limited.

Equivalent Impedance Zo

Impedance of Object Zx

Vibrational Pickup

PZT

Amplifier

(a) **(b)**
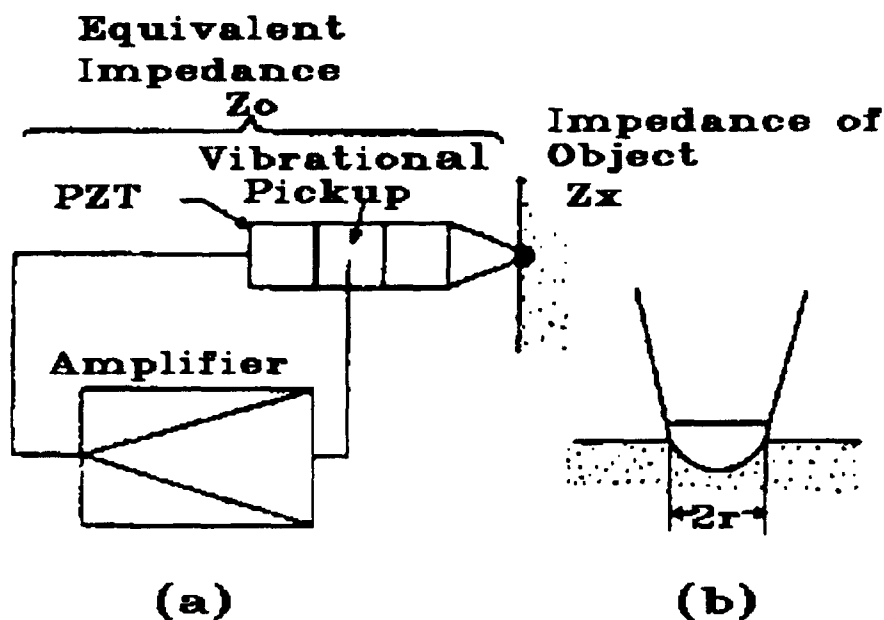
Figure 2.4. (a) Piezoelectric tactile sensor which determines the elastic nature of an object [36]. (b) Sensor's probe tip [36].

2.4.4. Stress-Component-Selective Tactile Sensor. Domenici and De Rossi developed a piezoelectric tactile sensor that can detect normal and transverse stresses when an object is contacted [37]. This unique trait distinguishes this sensor from other tactile sensors because of its ability to discriminate the fine physical detail of an object, even in the absence of conformal contact. The transverse (shear) stress component, in addition to the normal (compressive) stress component, supplies the necessary information to establish a surface's texture without requiring the sensor to have the same shape as the surface [37]. This feature can be understood by observing a round object. A sensor

that only detects the normal stress tensor component must conform to the surface of the round object to obtain shape information. However, a sensor that is also capable of sensing the transverse stress component can discern that the object is curved even if the sensor's surface is flat.

A schematic of the sensor is shown in Figure 2.5. It has a spatial resolution of 0.6 mm and an array resolution of 7 x 6 elements [37]. The dynamic range of the sensor is approximately 40:1 [37]. No information was reported concerning its frequency response, the threshold sensitivity, or the sensor's upper detection limit. The sensor designed by Domenici and De Rossi exceeds Harmon's ideal spatial and array resolution criteria, but it does not satisfy the dynamic range criteria.
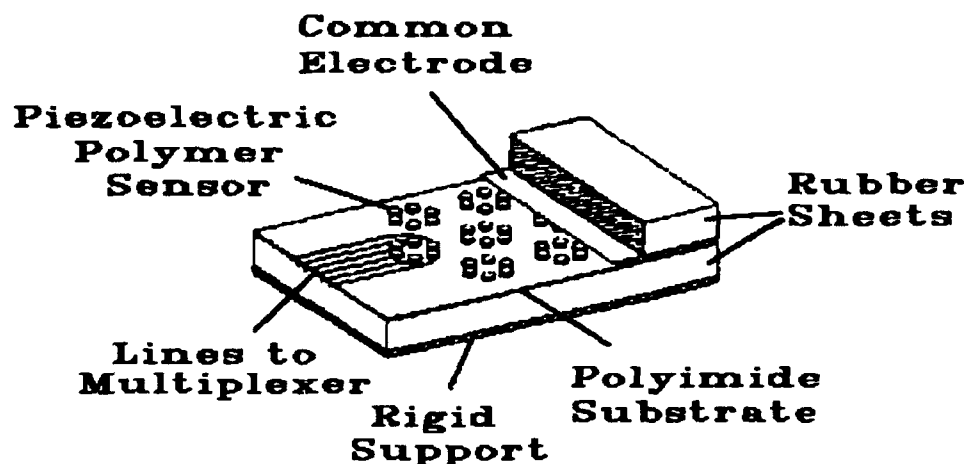
Figure 2.5. Stress-component-selective piezoelectric tactile sensor [37].

2.5. Conclusion

Several types of tactile sensors have been reviewed. Table 2.1 summarizes the characteristics of each sensor's quantitative figures of merit as presented in this literature review. None of the sensors presented possesses all of the ideal characteristics defined by Dr. Harmon [3]. However, each sensor has unique characteristics that make it viable for particular applications.

Table 2.1.   Summary of Figures of Merit for Several Tactile Sensors.

Sensor	Spatial Resolution (mm)	Array Resolution	Dynamic Range	Frequency Response (Hz)	Threshold Sensitivity (gram)	Upper Limit (gram)
Ideal Criteria	1	4 x 4	1000:1	100	1	1000
Suzuki [17] (Capacitive)	0.5	32 x 32	-	196	-	1
Liu [19] (Piezo-resistive)	0.86	4 x 4	14:1	-	3	42
Clark [23] (Magneto-strictive)	0.1	64 x 64	-	125	-	-
Grahn [27] (Ultrasonic)	1	3 x 4	2000:1	14 k	0.6	1200
Walker [29] (Optical)	-	3 x 3	-	60	-	-
Tzou [34] (Piezoelectric)	0	1	-	2200	-	-
Park [35] (Piezoelectric)	2.5	8 x 8	100:1	-	2.5	250
Omata [36] (Piezoelectric)	0.001	1	-	0.5	-	-
Domenici [37] (Piezoelectric)	0.6	6 x 7	40:1	-	-	-

3. Piezoelectric and Pyroelectric Phenomena in the Beta-Phase Polyvinylidene Fluoride Thin Film Polymer

3.1. Introduction

In this chapter, the piezoelectric and pyroelectric phenomena are explained relative to the beta-phase polyvinylidene fluoride (β-PVDF) material. First, piezoelectricity and pyroelectricity are defined. Then, the quantitative analysis used to determine the electric field and dipole moment of an electric dipole element are derived. Next, given certain macroscopic material coefficients, the quantitative results used to model the piezoelectric and pyroelectric effects in solids are presented. Finally, the microscopic structure of β-PVDF is linked to the macroscopic equations used to model its piezoelectric and pyroelectric effects.

3.2. Definition of Piezoelectricity and Pyroelectricity

3.2.1. Piezoelectricity Definition.
Since the discovery of piezoelectricity by Pierre and Jacques Curie in 1880 [38], several definitions have been advanced for piezoelectricity. Cady explained that "piezo-" comes from the Greek word for "press" [12]. He defined direct piezoelectricity as "electric polarization produced by mechanical strain in crystals belonging to certain classes, the polarization being proportional to the strain and changing sign with it" [12]. Furthermore, he defined the converse effect as "a piezoelectric crystal becomes strained, when electrically polarized, by an amount proportional to the polarizing field" [12]. Webster's dictionary gives a similar but more rigorous definition of piezoelectricity; it is defined to be the

"generation of electricity or of electric polarity in dielectric crystals subjected to mechanical stress, and conversely, generation of stress in such crystals subjected to an applied voltage" [39]. Both of the definitions indicate the presence of a direct and indirect piezoelectric effect; however, they disregard two important classes of materials that are also piezoelectric: ceramics and polymers. In this thesis, the direct piezoelectric effect is defined to be the electric polarization of certain materials produced by an externally applied mechanical strain, and the converse piezoelectric effect is defined to be the mechanical strain of certain materials produced by an externally applied electric field.

3.2.2. Pyroelectricity Definition. Similar to piezoelectricity, several definitions have been given for pyroelectricity, but they are all very similar to the definition presented by Walter Cady. He explained that "pyro-" comes from the Greek word for "fire" [12]. He defined pyroelectricity as "the change with temperature of positive and negative polarization charges on certain portions of crystals belonging to certain classes" [12], and he showed vectorial pyroelectricity as "a relation between a scalar (temperature) and a vector (polarization)" [12]. Similar to the converse piezoelectric effect, he defined the electrocaloric effect as the converse of the pyroelectric effect. Once again, no mention was made of other classes of materials that exhibit the pyroelectric phenomenon, but the important fact is that a pyroelectric material undergoes a change in its polarization when exposed to a change in temperature. Therefore, a change in temperature causes a pyroelectric material to become electrified.

To further refine the definition of pyroelectricity, the two types of pyroelectricity (primary and secondary) will be presented. Primary pyroelectricity is that which would be produced in a completely clamped material [12]. Secondary pyroelectricity is associated with an unconstrained material. Since all pyroelectric materials are also piezoelectric, a change in temperature causes an unconstrained crystal to change shape [12]. The change in shape causes a secondary polarization due to the piezoelectric effect (secondary pyroelectricity) [12]. Secondary pyroelectricity can be further partitioned into pyroelectricity due to uniform and nonuniform heating. Typically, the term secondary pyroelectricity implies pyroelectricity due to uniform heating, and the term tertiary implies pyroelectricity due to nonuniform heating [12].

Both terms, piezoelectricity and pyroelectricity, are used to describe materials that exhibit the piezoelectric phenomenon. Piezoelectric and pyroelectric coefficients are used to describe the corresponding effects in materials. Typically, materials that exhibit strong piezoelectric and/or pyroelectric effects have large piezoelectric and pyroelectric coefficients.

3.3. Electric Field and Dipole Moment of an Electric Dipole

The fundamental electric dipole forms the basis for the model of β-PVDF which will be presented later in this chapter. In this section, the quantitative expressions used to determine the electric field and dipole moment of an electric dipole are derived, but first the coordinate system is defined to facilitate the presentation of the microscopic and macroscopic models for the piezoelectric and

pyroelectric effects. The cartesian coordinate system shown in Figure 3.1 will be used to be consistent with most of the published literature [40]. In Figure 3.1, the 1-direction corresponds to the x-axis, the 2-direction corresponds to the y-axis, and the 3-direction corresponds to the z-axis.
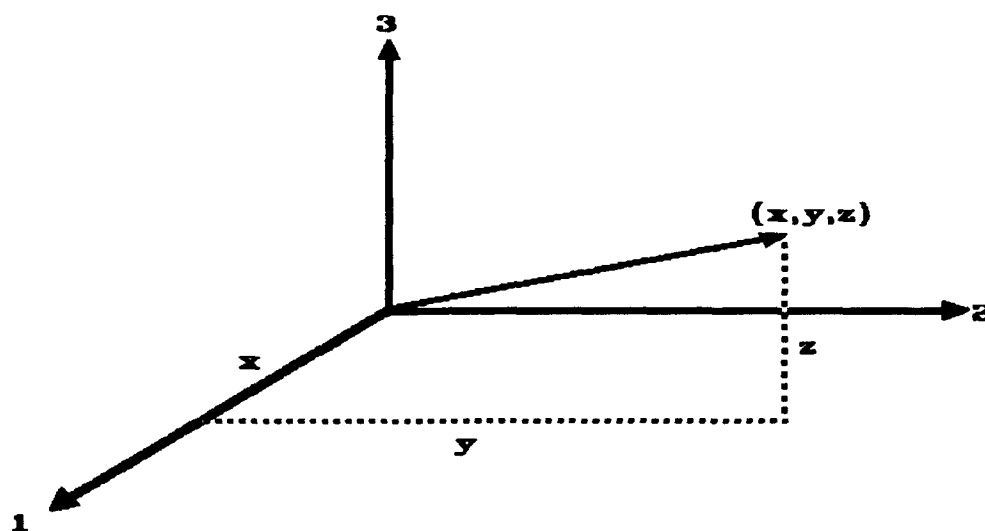
Figure 3.1. Cartesian coordinate axis definition [40].

3.3.1. *Electric Field of an Electric Dipole.* The development of a model for the piezoelectric and pyroelectric effects in crystalline and partially crystalline substances begins with the microscopic model of an electric dipole depicted in Figure 3.2. By invoking Gauss' Law, the electric potential at the point P due to the point charges +Q and –Q can be determined as [41,42]:
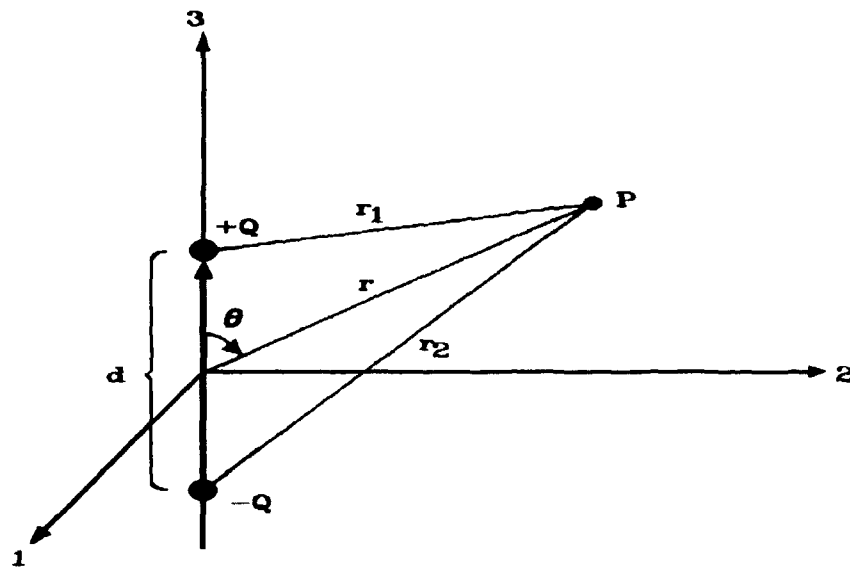
Figure 3.2. Fundamental electric dipole structure [42].

$$V = \frac{Qd\cos\theta}{4\pi e_r \epsilon_o r^2} \qquad (3.1)$$

where

V is the potential at point P due to +Q and -Q (V),

Q is the net charge of the particle (C),

d is the distance between +Q and -Q (m),

θ is the angle between the 3-axis and r (radians),

ϵ_r is the relative permittivity of the medium (unitless),

ϵ_o is the permittivity of a vacuum (F·m^{-1}),

r is the distance between the origin and P (m).

Equation (3.1) can be partitioned into four fundamental parts [41]:

$$V = Qd \cdot \cos\theta \cdot \frac{1}{r^2} \cdot \frac{1}{4\pi\epsilon_r\epsilon_o} \qquad (3.2)$$

where

Qd is the magnitude of the dipole moment between +Q and -Q ($C\cdot m$),

$\cos\theta$ is the angle factor (unitless),

$1/r^2$ is the distance factor (m^{-2}),

$1/(4\pi\epsilon_r\epsilon_o)$ is a material parameter ($F^{-1}\cdot m$).

Using spherical coordinates, the electric field at point P can be determined by forming the negative of the gradient of the electric potential at point P [41]:

$$\mathbf{E} = \hat{\mathbf{r}}E_r + \hat{\boldsymbol{\theta}}E_\theta \qquad (3.3)$$

where

$$E_r = \frac{Qd\cos\theta}{2\pi\epsilon_r\epsilon_o r^3} \quad \text{and} \quad E_\theta = \frac{Qd\sin\theta}{4\pi\epsilon_r\epsilon_o r^3} \quad .$$

Equation (3.3) can be converted to cartesian coordinates [4]:

$$\mathbf{E} = \left(\frac{Qd}{4\pi\epsilon_r\epsilon_o r^3}\right)[\hat{\mathbf{1}}3\cos\theta\sin\theta\sin\phi + \hat{\mathbf{2}}3\cos\theta\sin\theta\cos\phi + \hat{\mathbf{3}}3\cos^2\theta] \quad . \quad (3.4)$$

3.3.2. Dipole Moment of an Electric Dipole. The electric dipole moment of the two point charges shown in Figure 3.2 is given as [42,43]:

$$\mathbf{p} = Q\mathbf{d} \qquad (3.5)$$

where $\mathbf{p}$ is the vector dipole moment of two charged particles ($C\cdot m$), and $\mathbf{d}$ is the vector directed from -Q to +Q (m). The equation (3.5) for the dipole moment of an electric dipole forms the basis used to model macroscopic piezoelectric and pyroelectric effects.

3.4. Macroscopic Piezoelectric and Pyroelectric Equations

In this section, the linear macroscopic equations used to model the piezoelectric and pyroelectric effects in solids are presented. First, stress and strain are defined. Then, a relationship is presented that relates stress and strain in a solid. Then, the macroscopic piezoelectric and pyroelectric relationships for solids are presented. The relationships presented in this section, along with supporting coefficients, can be used to model the macroscopic piezoelectric and pyroelectric effects in β-PVDF.

3.4.1. Stress.

To develop a definition of stress, the concept of a force is considered. Force is a vector quantity. A force acting on a surface can be interpreted in terms of a normal and a tangential component. Often, these components are known as pressure and shearing stress, respectively [12]. Using force as a starting point, stress is defined as force per unit area applied to the surface of a material. Applied to an elastic solid, stress can be considered to be composed of pairs of equal and opposite forces per unit area [12]. Within a solid, stress is represented by a second rank tensor, T_{ij} [40,44]. The double subscript notation is used to represent stress. The i, or first subscript in T_{ij} is the direction normal to the surface that is acted upon. The j, or second subscript indicates the direction of the driving force. Initially, it appears as if the stress tensor has nine components. However, in the absence of body torque, which is typically the case when dealing with the macroscopic description of stress, it is immaterial whether sliding (rotation of the solid) takes place when considering shear stress [12,44]. Therefore, $T_{ij} = T_{ji}$ and the overall

stress tensor is reduced from nine to six values. Furthermore, the six components of stress are typically partitioned into three compression and three shearing components.

Using the six components of stress as a basis, the matrix notation for stress can be reduced to a vector notation [44]. First, the compressional stresses (T_{11}, T_{22}, and T_{33}) depicted in Figure 3.3 can be considered. They are represented by identical subscripts in matrix notation, and they are usually represented by a single subscript of the same value (T_1, T_2, and T_3) in vector notation. There are also three shear components ($T_{23} = T_{32} = T_4$, $T_{13} = T_{31} = T_5$, and $T_{12} = T_{21} = T_6$) as depicted in Figure 3.4. T is the standard symbol used for stress as defined by the IEEE standard on piezoelectricity [40]. The 6 components of stress can be written in a more compact form:

$$T = \begin{bmatrix} T_1 \\ T_2 \\ T_3 \\ T_4 \\ T_5 \\ T_6 \end{bmatrix} = \begin{bmatrix} T_{11} \\ T_{22} \\ T_{33} \\ T_{23} = T_{32} \\ T_{13} = T_{31} \\ T_{12} = T_{21} \end{bmatrix} \qquad (3.6)$$

or

$$T = T_i$$

where T_i is the stress in a solid ($N \cdot m^{-2}$), and i is an integer, 1 to 6. The standard sign convention defines stress as negative for compressional force and positive for extentional force [12].

3.4.2. *Strain.* Strain is a measure of the degree of deformation of a material that is under stress. To understand the concept of strain, a vector, u, that is connecting two points in a solid material

3-8
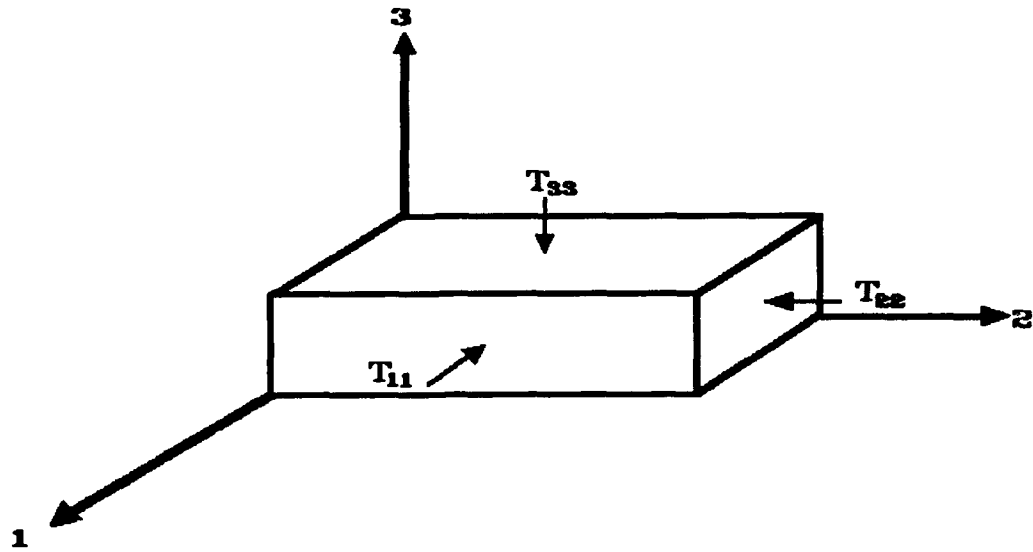
Figure 3.3. Normal stress components.

that is in equilibrium can be considered. Strain is the change in the
vector, **u**, when the solid is deformed by stress [44]. The tensor
quantities δ_{ij} are defined as the ratios of the change in the vector **u**
(Δ**u**) relative to the components of **u** [44]:

$$\delta_{ij} = \lim_{u \to 0}\left(\frac{\Delta u_i}{u_j}\right) \qquad (3.7)$$

where i and j are the direction subscripts. When i = j, the quantities
δ_{ij} measure the increase in length per unit length of **u** in the $\hat{\imath}$
direction. When i ≠ j, the quantities δ_{ij} are equal to the angular
rotation towards the $\hat{\imath}$ axis of a line parallel to the $\hat{\jmath}$ axis before the
rotation [44]. Assuming pure shears, to eliminate the rotational terms,
the strain, S_{ij}, can be defined by the following equations [44]:

3-9
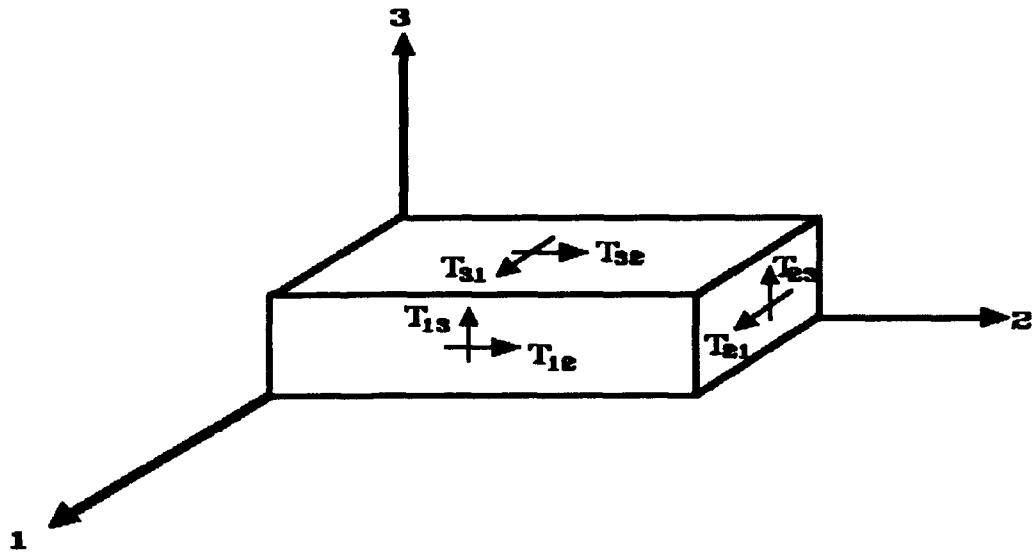
Figure 3.4. Shear stress components.

$$S_{ij} = \frac{1}{2} (\delta_{ij} + \delta_{ji}) \qquad\qquad (3.8)$$

where i = j and

$$S_{ij} = \delta_{ij} + \delta_{ji} \qquad\qquad (3.9)$$

where i ≠ j.

Similar to stress, there are 6 components of strain, and positive strain corresponds to positive stress [12]. In reduced notation, the strain is also represented by a vector [40]:

$$
\mathbf{S} = \begin{bmatrix} S_1 \\ S_2 \\ S_3 \\ S_4 \\ S_5 \\ S_6 \end{bmatrix} = \begin{bmatrix} S_{11} \\ S_{22} \\ S_{33} \\ S_{23} = S_{32} \\ S_{13} = S_{31} \\ S_{12} = S_{21} \end{bmatrix} \tag{3.10}
$$

or

$$
S = S_i \tag{3.11}
$$

where S_i is the resultant material strain due to stress, and i is an integer ranging from 1 to 6. It should also be noted, that by staying within the limits of elastic deformation, a material under stress (strain) will return to its original state when the stress (strain) is removed.

3.4.3. Hooke's Law. Strains are related to stresses with the fourth rank elastic compliance tensor [12,44]. In matrix notation, the equation for strain as a function of an externally applied stress is [44]:

$$
\begin{bmatrix} S_1 \\ S_2 \\ S_3 \\ S_4 \\ S_5 \\ S_6 \end{bmatrix} = \begin{bmatrix} s_{11} & s_{12} & s_{13} & s_{14} & s_{15} & s_{16} \\ s_{21} & s_{22} & s_{23} & s_{24} & s_{25} & s_{26} \\ s_{31} & s_{32} & s_{33} & s_{34} & s_{35} & s_{36} \\ s_{41} & s_{42} & s_{43} & s_{44} & s_{45} & s_{46} \\ s_{51} & s_{52} & s_{53} & s_{54} & s_{55} & s_{56} \\ s_{61} & s_{62} & s_{63} & s_{64} & s_{65} & s_{66} \end{bmatrix} \cdot \begin{bmatrix} T_1 \\ T_2 \\ T_3 \\ T_4 \\ T_5 \\ T_6 \end{bmatrix} \tag{3.12}
$$

where s_{11} through s_{66} are the elastic compliance coefficients ($m^2 \cdot N^{-1}$). In vector notation, equation (3.12) can be expressed in a more compact form as:

$$
\mathbf{S} = s\mathbf{T} \quad . \tag{3.13}
$$

The converse relation, otherwise known as Hooke's law, defines the stress due to an applied strain [12,44]:

$$
\begin{bmatrix} T_1 \\ T_2 \\ T_3 \\ T_4 \\ T_5 \\ T_6 \end{bmatrix} = \begin{bmatrix} c_{11} & c_{12} & c_{13} & c_{14} & c_{15} & c_{16} \\ c_{21} & c_{22} & c_{23} & c_{24} & c_{25} & c_{26} \\ c_{31} & c_{32} & c_{33} & c_{34} & c_{35} & c_{36} \\ c_{41} & c_{42} & c_{43} & c_{44} & c_{45} & c_{46} \\ c_{51} & c_{52} & c_{53} & c_{54} & c_{55} & c_{56} \\ c_{61} & c_{62} & c_{63} & c_{64} & c_{65} & c_{66} \end{bmatrix} \cdot \begin{bmatrix} S_1 \\ S_2 \\ S_3 \\ S_4 \\ S_5 \\ S_6 \end{bmatrix}
\tag{3.14}
$$

where c_{11} through c_{66} are the elastic stiffness coefficients ($N \cdot m^{-2}$). In reduced vector notation:

$$
\mathbf{T} = c\mathbf{S} \quad .
\tag{3.15}
$$

3.4.4. Macroscopic Piezoelectric and Pyroelectric Relations.

With stress and strain as the fundamental building blocks, the macroscopic piezoelectric and pyroelectric material relationships are presented. First, the polarization of a piezoelectric material can be related to an applied strain in the absence of an externally applied electric field by the following matrix relationship [12]:

$$
\begin{bmatrix} P_1 \\ P_2 \\ P_3 \end{bmatrix} = \begin{bmatrix} e_{11} & e_{12} & e_{13} & e_{14} & e_{15} & e_{16} \\ e_{21} & e_{22} & e_{23} & e_{24} & e_{25} & e_{26} \\ e_{31} & e_{32} & e_{33} & e_{34} & e_{35} & e_{36} \end{bmatrix} \cdot \begin{bmatrix} S_1 \\ S_2 \\ S_3 \\ S_4 \\ S_5 \\ S_6 \end{bmatrix}
\tag{3.16}
$$

where P_i is the polarization vector component due to an applied strain ($C \cdot m^{-2}$), and e_{11} through e_{36} are the piezoelectric stress coefficients ($m^2 \cdot C^{-1}$). In vector form, equation (3.16) becomes:

$$
\mathbf{P} = e\mathbf{S} \quad .
\tag{3.17}
$$

The polarization of a piezoelectric material can be related to an externally applied stress in the absence of an externally applied electric field by the following matrix relationship [12]:

$$
\begin{bmatrix} P_1 \\ P_2 \\ P_3 \end{bmatrix} = \begin{bmatrix} d_{11} & d_{12} & d_{13} & d_{14} & d_{15} & d_{16} \\ d_{21} & d_{22} & d_{23} & d_{24} & d_{25} & d_{26} \\ d_{31} & d_{32} & d_{33} & d_{34} & d_{35} & d_{36} \end{bmatrix} \cdot \begin{bmatrix} T_1 \\ T_2 \\ T_3 \\ T_4 \\ T_5 \\ T_6 \end{bmatrix}
\tag{3.18}
$$

where d_{11} through d_{36} are the piezoelectric strain coefficients ($C \cdot N^{-1}$), and in vector form:

$$
\mathbf{P} = d\mathbf{T} \quad .
\tag{3.19}
$$

Next, by the direct piezoelectric effect, the polarization of a piezoelectric material can be related to an externally applied electric field, in the absence of an externally applied stress or strain, by the following relationship [45]:

$$
\begin{bmatrix} P_1 \\ P_2 \\ P_3 \end{bmatrix} = \begin{bmatrix} \chi_{11} & \chi_{12} & \chi_{13} \\ \chi_{21} & \chi_{22} & \chi_{23} \\ \chi_{31} & \chi_{32} & \chi_{33} \end{bmatrix} \cdot \begin{bmatrix} E_1 \\ E_2 \\ E_3 \end{bmatrix}
\tag{3.20}
$$

where χ_{11} through χ_{33} are the electric susceptibility tensors ($F \cdot m^{-1}$), and E_i is the externally applied electric field ($V \cdot m^{-1}$), and in vector form:

$$
\mathbf{P} = \chi\mathbf{E} \quad .
\tag{3.21}
$$

Also, by the converse piezoelectric effect, the strain of a piezoelectric material can be related to an externally applied electric field, in the absence of an externally applied stress, by the following relationship [12]:

3-13

$$\begin{bmatrix} S_1 \\ S_2 \\ S_3 \\ S_4 \\ S_5 \\ S_6 \end{bmatrix} = \begin{bmatrix} d_{11} & d_{21} & d_{31} \\ d_{12} & d_{22} & d_{32} \\ d_{13} & d_{23} & d_{33} \\ d_{14} & d_{24} & d_{34} \\ d_{15} & d_{25} & d_{35} \\ d_{16} & d_{26} & d_{36} \end{bmatrix} \cdot \begin{bmatrix} E_1 \\ E_2 \\ E_3 \end{bmatrix} \qquad (3.22)$$

and in vector form:

$$\mathbf{S} = d^T \mathbf{E} \qquad (3.23)$$

where d^T is the transposed piezoelectric strain coefficient matrix
$(m^2 \cdot V^{-1})$ defined in equation (3.18). Similarly, by the direct
piezoelectric effect, the stress of a piezoelectric material can be
related to an externally applied electric field, in the absence of an
externally applied strain by the following relationship [12]:

$$\begin{bmatrix} T_1 \\ T_2 \\ T_3 \\ T_4 \\ T_5 \\ T_6 \end{bmatrix} = \begin{bmatrix} e_{11} & e_{21} & e_{31} \\ e_{12} & e_{22} & e_{32} \\ e_{13} & e_{23} & e_{33} \\ e_{14} & e_{24} & e_{34} \\ e_{15} & e_{25} & e_{35} \\ e_{16} & e_{26} & e_{36} \end{bmatrix} \cdot \begin{bmatrix} E_1 \\ E_2 \\ E_3 \end{bmatrix} \qquad (3.24)$$

and in vector form:

$$\mathbf{T} = e^T \mathbf{E} \qquad (3.25)$$

where e^T is the transposed piezoelectric stress coefficient matrix
defined in equation (3.16). Additionally, the electric field in a
piezoelectric material can be related to an applied strain, in the
absence of an externally applied stress, by the following relation-
ship [12]:

$$
\begin{bmatrix} E_1 \\ E_2 \\ E_3 \end{bmatrix} = - \begin{bmatrix} h_{11} & h_{12} & h_{13} & h_{14} & h_{15} & h_{16} \\ h_{21} & h_{22} & h_{23} & h_{24} & h_{25} & h_{26} \\ h_{31} & h_{32} & h_{33} & h_{34} & h_{35} & h_{36} \end{bmatrix} \cdot \begin{bmatrix} S_1 \\ S_2 \\ S_3 \\ S_4 \\ S_5 \\ S_6 \end{bmatrix} \tag{3.26}
$$

and in vector form:

$$
\mathbf{E} = - \mathbf{h}\mathbf{S} \tag{3.27}
$$

where h is the piezoelectric stress or voltage constant coefficient matrix $(V \cdot m^{-1})$. Similarly, the electric field in a piezoelectric material can be related to an externally applied stress, in the absence of an externally applied strain, by the following relationship [12]:

$$
\begin{bmatrix} E_1 \\ E_2 \\ E_3 \end{bmatrix} = - \begin{bmatrix} g_{11} & g_{12} & g_{13} & g_{14} & g_{15} & g_{16} \\ g_{21} & g_{22} & g_{23} & g_{24} & g_{25} & g_{26} \\ g_{31} & g_{32} & g_{33} & g_{34} & g_{35} & g_{36} \end{bmatrix} \cdot \begin{bmatrix} T_1 \\ T_2 \\ T_3 \\ T_4 \\ T_5 \\ T_6 \end{bmatrix} \tag{3.28}
$$

and in vector form:

$$
\mathbf{E} = - \mathbf{g}\mathbf{T} \tag{3.29}
$$

where g is the piezoelectric strain or voltage constant coefficient matrix $(V \cdot m \cdot N^{-1})$. With the basic piezoelectric relationships defined, the principle of linear superposition can be used to combine several of the equations to obtain a set of equations that represent the combination of two or more applied forcing functions. The following equation from the direct effect, represents the polarization of a piezoelectric material due to an externally applied electric field and an applied strain [12]:

$$P = \chi'' \mathbf{E} + e\mathbf{S} \tag{3.30}$$

where χ'' is the clamped susceptibility of the material $(F \cdot m^{-1})$. It should be noted that the clamped condition implies that the piezoelectric material is subject to constant strain (or constrained), and since the material is constrained, χ'' neglects the effects of applied strain. Similarly, the converse effect yields the stress in a material due to an externally applied electric field and an applied strain [12]:

$$T = c\mathbf{S} - e^T \mathbf{E} \quad . \tag{3.31}$$

The direct effect can also be used to find the polarization in a solid due to the application of an externally applied electric field and stress [12]:

$$P = \chi' \mathbf{E} + d\mathbf{T} \tag{3.32}$$

where χ' is the free susceptibility of the material $(F \cdot m^{-1})$. The free susceptibility condition implies that the piezoelectric material is subject to constant stress, and since the stress is constant, χ' neglects the effects of the applied stress. The converse effect can be used to obtain an expression for the strain in a solid due to an externally applied electric field and stress [12]:

$$S = s\mathbf{T} + d^T \mathbf{E} \quad . \tag{3.33}$$

The following equation represents the electric field in a piezoelectric material due to an applied strain and polarization [12]:

$$\mathbf{E} = -h\mathbf{S} + \frac{\mathbf{P}}{\chi''} \quad . \tag{3.34}$$

Similarly, the stress in a material due to an applied strain and polarization is [12]:

$$\mathbf{T} = c\mathbf{S} - h^T\mathbf{P} \quad . \tag{3.35}$$

The electric field in a piezoelectric solid can also be found due to the application of an externally applied stress and polarization [12]:

$$\mathbf{E} = -g\mathbf{T} + \frac{\mathbf{P}}{\chi'} \quad . \tag{3.36}$$

Similarly, an expression for the strain in a solid due to an externally applied stress and polarization is [12]:

$$\mathbf{S} = s\mathbf{T} + g^T\mathbf{P} \quad . \tag{3.37}$$

In order to compensate for the pyroelectric effect, the mechanism and the modeling equations for the pyroelectric effect need to be thoroughly understood. Pyroelectricity represents the linear reversible change of polarization due to a change in temperature [44]. The change in polarization can be related to the change in temperature through the following equation [44]:

$$\Delta P_i = p_i \Delta T \tag{3.38}$$

where

ΔP_i is the change in polarization due to a change in the temperature ($C \cdot m$),

p_i is the ith pyroelectric coefficient ($C \cdot m^{-2} \cdot K^{-1}$),

ΔT is the change in temperature (K).

Therefore, for a given polarization state of a piezoelectric material, the change in the polarization due to the pyroelectric effect (change in temperature) is given by equation (3.38).

3.5. *Piezoelectric and Pyroelectric Effect in the PVDF Polymer*

Now that the macroscopic modeling equations for the piezoelectric and pyroelectric effects have been presented, the theory of piezoelectricity and pyroelectricity in the PVDF polymer will be developed. First, the types of the PVDF polymer and how they are synthesized will be presented. Then, the structure of the β–phase PVDF polymer (one of the types of the PVDF polymers) will be qualitatively related to its polarization. Finally, the pyroelectricity property of PVDF will be discussed, and a model will be presented to account for its pyroelectric coefficients.

The PVDF polymer film can be fabricated by utilizing a number of manufacturing techniques including chill wheel extrusion, thermal lamination, or solvent casting [46]. The PVDF polymer film is composed of long chains of the $(-CH_2-CF_2-)_n$ monomer where the carbon–hydrogen and polar carbon–fluorine bonds are available in several orientations, and n is on the order of 2000 [44,47]. The available orientations can be partitioned into four phases (forms): α (II), β (I), γ (III), and δ (IV) [48]. Typically, a PVDF polymer film sample will possess a degree of crystallinity on the order of 50% [49], and the most important of the phases are the α– and β–phases [47,50].

The α–phase is formed synthetically through a slow–cooled melt or acetone solution, and the bonds formed are in a trans-gauche-trans-gauche′ (TGTG′) configuration as shown in Figure 3.5 [47]. The α–phase

molecules are arranged in an antiparallel structure in such a manner that the net polarization of the α-phase unit cell is zero [48].
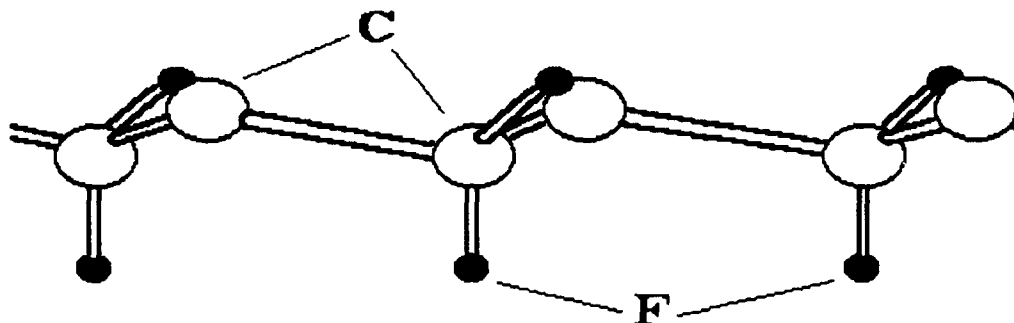
Figure 3.5. Trans-gauche-trans-gauche' configuration of α-phase PVDF [47].

The γ- and δ-phases are less important, to this thesis effort, compared to the α- and β-phases, and they are only mentioned here for clarity and completeness. The γ-phase has a conformation intermediate between the α- and β-phases (T_3GT_3G'), and it is formed by high temperature annealing or high pressure crystallization of the α-phase. The δ-phase is formed by poling the α-phase [44].

The most important phase of PVDF, relative to piezoelectric tactile sensors, is the β-phase. Several techniques have been developed and several articles written concerning the poling of PVDF film to form the β-phase [49,51,52,53,54]. The common theme of these articles is that β-phase PVDF (β-PVDF) is formed by poling the α-phase PVDF

film [54]. Poling is the mechanical stretching (in a direction

parallel to the plane of the film) under the conditions of a high

electric field (applied orthoganally to the plane of the film) and high

temperature. Typically, the poling fields for creating β-phase PVDF are

greater than 120 MV·m^{-1} [44]. After poling, the TGTG' chains in α-phase

PVDF become β-phase PVDF all trans (T) chains as shown in Figure 3.6.
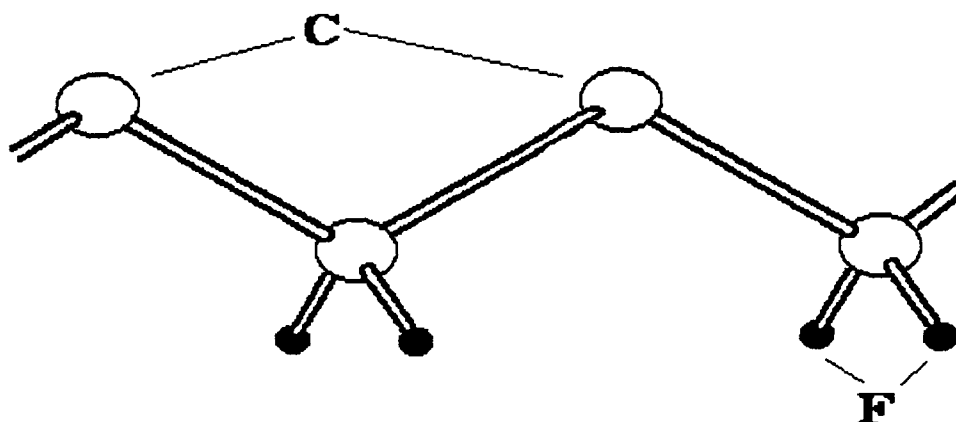
Figure 3.6. All trans configuration found in β-PVDF [47].

3.5.1. Microscopic Model for β-PVDF. In this section, a model of

the piezoelectric and pyroelectric effects will be presented. The

purpose of this modeling effort is to relate the microscopic β-PVDF

material parameters to the coefficients used in the macroscopic

equations for the piezoelectric and pyroelectric effects. First, the

model is described. As such, the model presents a dipole description of

β-PVDF. Next, the Lorentz factor will be developed. Finally, the

equations which link the macroscopic piezoelectric and pyroelectric coefficients to the microscopic description of β-PVDF are presented. The section concludes by comparing the experimentally obtained macroscopic coefficients with the derived coefficients.

The molecular structure of β-PVDF is shown in Figure 3.7. Since the discovery of piezoelectricity in PVDF [55], several models for the piezoelectric effect in semicrystalline β-PVDF have been developed [56-61]. The model used in this thesis was developed by R. Al-Jishi and P. L. Taylor [56,57]. It accounts for the semicrystallinity of the β-PVDF polymer, and it agrees well with experimental results [44]. The model uses a crystalline structure to model the crystalline portion of the β-PVDF polymer, and it introduces a weighting factor to account for its semicrystallinity. Ultimately the model is used to determine the macroscopic piezoelectric and pyroelectric coefficients of the β-PVDF polymer from the microscopic material parameters.

The model represents the crystalline portion of the β-PVDF polymer with a base-centered orthorhombic crystal lattice structure that is shown in Figure 3.8, where each lattice point represents one CH_2-CF_2 monomer as shown in Figure 3.9 [56]. Each primitive unit cell of the β-PVDF polymer is composed of two CH_2-CF_2 molecules. The two, simple, base-centered orthorhombic cells in Figure 3.8 can be separated into two sub-lattices, one of which is shown in Figure 3.10. The two sub-lattices will be designated s_1 and s_2. The lattice spacings of the unit cell shown in Figure 3.8, Figure 3.9, and Figure 3.10 are a = 8.58 Å, b = 4.91 Å, and c = 2.56 Å [56]. From the basic structure of the β-PVDF polymer shown in Figure 3.7, the dipole moment of a single monomer, which is primarily due to the moments of the C-F bonds, is calculated to
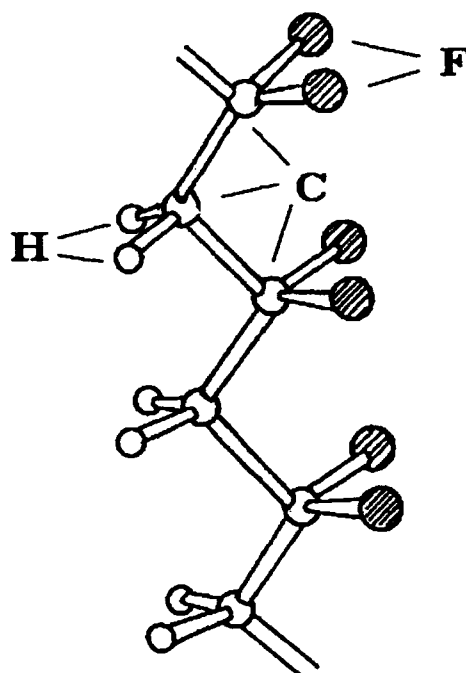
Figure 3.7. Molecular structure of the β-phase PVDF polymer [11].

be $7.0 \cdot 10^{-30}$ (C·m) in the direction of the b lattice constant (the 3-direction) [56]. Relative to a macroscopic PVDF thin film, the 1-direction is the poling stretch direction, and the 3-direction is perpendicular to the plane of the film.

Each lattice point in the crystal representation of the β-PVDF polymer can be thought of as a dipole. If the net charge on the positive particle is Q and the net charge on the negative particle is -Q, then the dipole moment of each β-PVDF lattice site can be calculated with the following equation [56]:

$$p_o = Qd \tag{3.39}$$

where

p_o is the dipole moment of each lattice site (C·m),
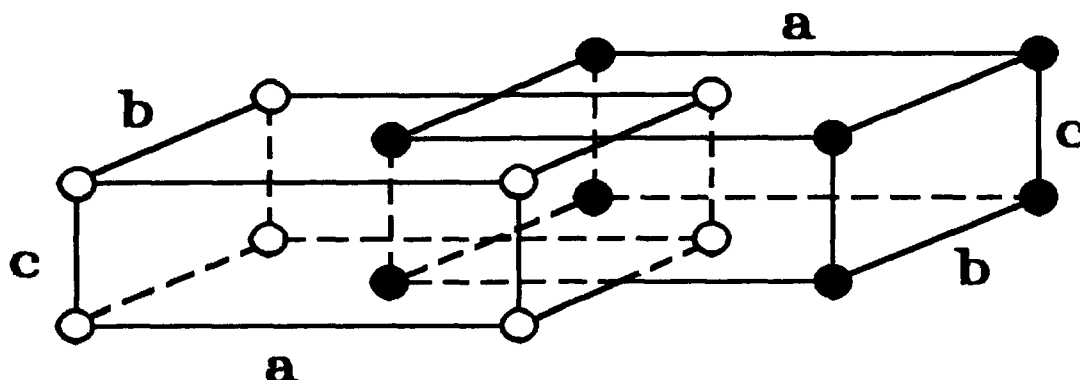
Figure 3.8. Base-centered orthorhombic crystal structure used to model
the crystalline form of the β-PVDF polymer [57].

Q is the net charge on the positive particle (C),

d is the distance between the positive and negative particle (m).

The calculated value of p_0 is $7.0 \cdot 10^{-30}$ C·m, and the direction of p is

3 [56]. The net polarizability of each PVDF molecule is the net sum of

the electronic polarization, P_E, and the structural polarization,

P_A [56]. P_A is due to changes in molecular bond length, and since

$P_A \ll P_E$, only P_E, which is due to the displacement of electrons, is

considered in the model [56]. Therefore, it is assumed that a change in

p_0 is a function of Q, and d is constant.

The next step in the model's development is the determination of

the Lorentz factor, L, which is a scaling factor used to find the

electric field at a site due to the effects of neighboring dipoles [56].

(a)

(b)
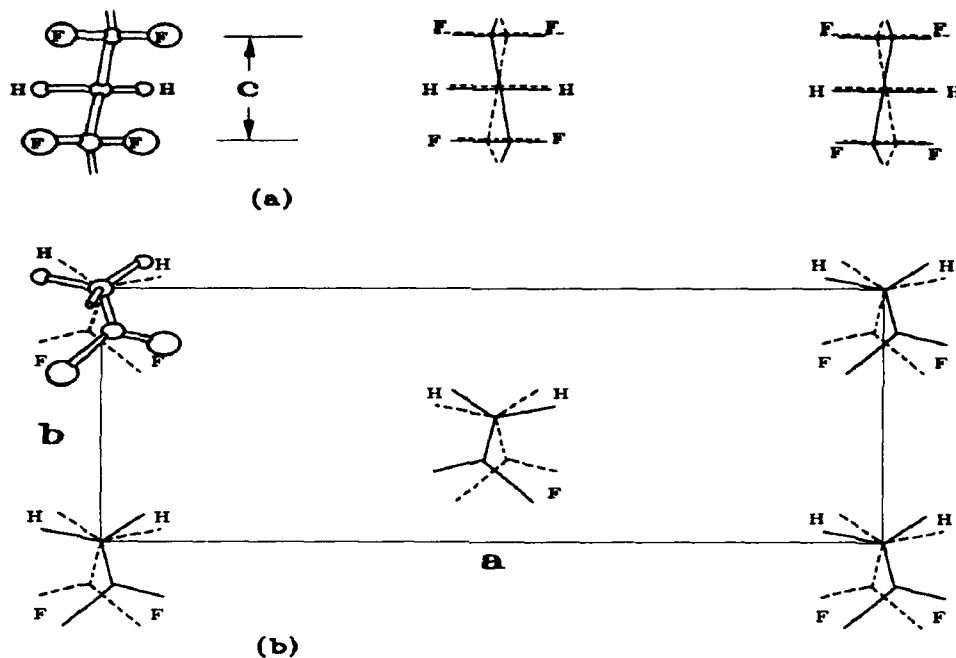
Figure 3.9. (a) Top view of the unit cell for the β-PVDF polymer. (b) Side view of the unit cell for the β-PVDF polymer [56].

At any arbitrary monopole site (in this case, arbitrarily choose an s_1 lattice site), the Lorentz factor is given by the following equation [56]:

$$L = \frac{1}{2}\left[L(s_1) + L(s_2)\right] \qquad (3.40)$$

where $L(s_1)$ is the Lorentz factor for sub-lattice s_1 (unitless) and $L(s_2)$ is the Lorentz factor for sub-lattice s_2 (unitless). $L(s_1)$ is found by calculating the electric field due to s_1, but the contribution of the other monopole that forms the dipole at the site must be excluded in the calculation. Assuming d/b is not $\ll 1$ [56]:
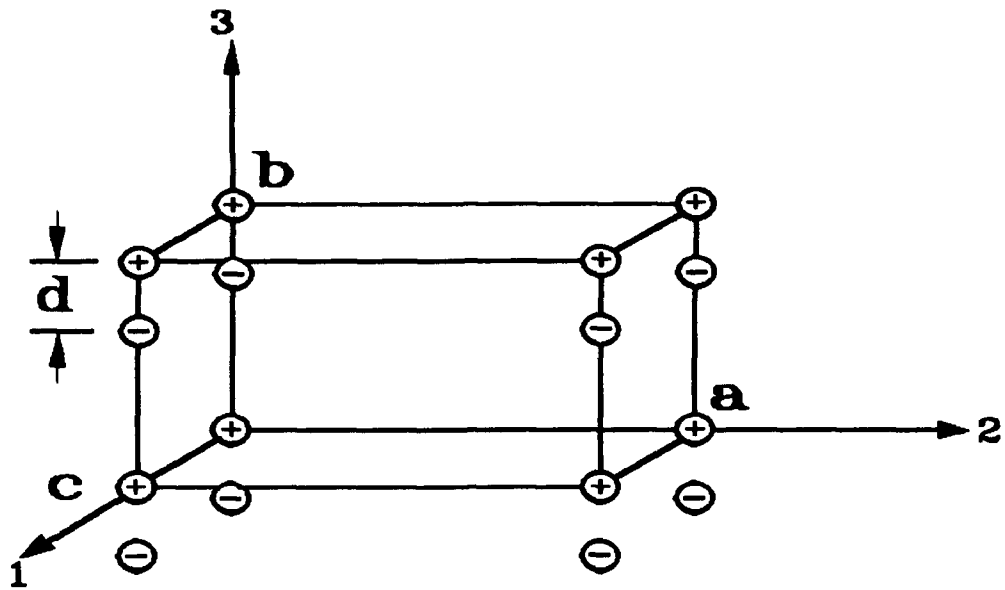
Figure 3.10.   Unit cell of the simple orthorhombic crystal used to represent the β-PVDF polymer film. Each lattice point is occupied by a monomer that is represented by a dipole [56].

$$L(s_1) = L(s_1, a) + L(s_1, b) \, , \tag{3.41}$$

where

$$L(s_1, a) = 1 + 2\frac{b}{d}\{2 \sum_{i_1, i_2 = 1}^{\infty} \frac{\sinh(2\pi k_i d)}{\exp(2\pi k_i b) - 1}$$

$$+ \sum_{i=1}^{\infty} \frac{\sinh(2\pi i d/a)}{\exp(2\pi i b/a) - 1} \tag{3.42}$$

$$+ \sum_{i=1}^{\infty} \frac{\sinh(2\pi i d/c)}{\exp(2\pi i b/c) - 1}\} \, ,$$

and

$$L(s_1,b) = -\frac{b}{a}\{2 \sum_{i_1,i_2=1}^{\infty} \exp(-2\pi k_i d)$$

$$+ \sum_{i=1}^{\infty} \exp(-2\pi i d/c)\} - \frac{b}{2a} + \frac{abc}{4\pi d^3} \, , \tag{3.43}$$

with

$$k_i^2 = \frac{i_1^2}{a^2} + \frac{i_2^2}{c^2} \, . \tag{3.44}$$

If $d/b \ll 1$, then equation (3.43) should be replaced by [56]:

$$L(s_1,b) = \left(-\frac{abc}{4}\right) \sum_{m,n}^{m^2a^2+n^2c^2 \leq R^2} (d^2+m^2a^2+n^2c^2)^{-3/2} \tag{3.45}$$

where $m = n = 0$ is excluded, and m and n are restricted to a disc of radius R centered on $(0,0,d)$. If R is equal to infinity, the equation will be exact, but if R is taken to be approximately $100a$, the error is less than 1% [56]. Similarly, the Lorentz factor for the s_2 sub-lattice can be found with the following equation [56]:

$$L(s_2) = \frac{2a}{d} \sum_{i_1=1}^{\infty} \left\{ \sum_{i_2=1}^{\infty} \frac{i_1}{bk_i'\sinh(\pi k_i'a)} + \frac{1}{2\sinh(\pi i_1 a/b)} \right\} \cdot \sin[2\pi i_1(b/2-d)/b] \, , \tag{3.46}$$

where

$$k_i'^2 = \frac{i_1^2}{b^2} + \frac{i_2^2}{c^2} \, . \tag{3.47}$$

A plot of $L(s_1)$, $L(s_2)$, and L versus d is shown in Figure 3.11.

The Lorentz factor, L, can be used in the following equation to determine the equilibrium crystal polarization for the β–PVDF polymer [56]:
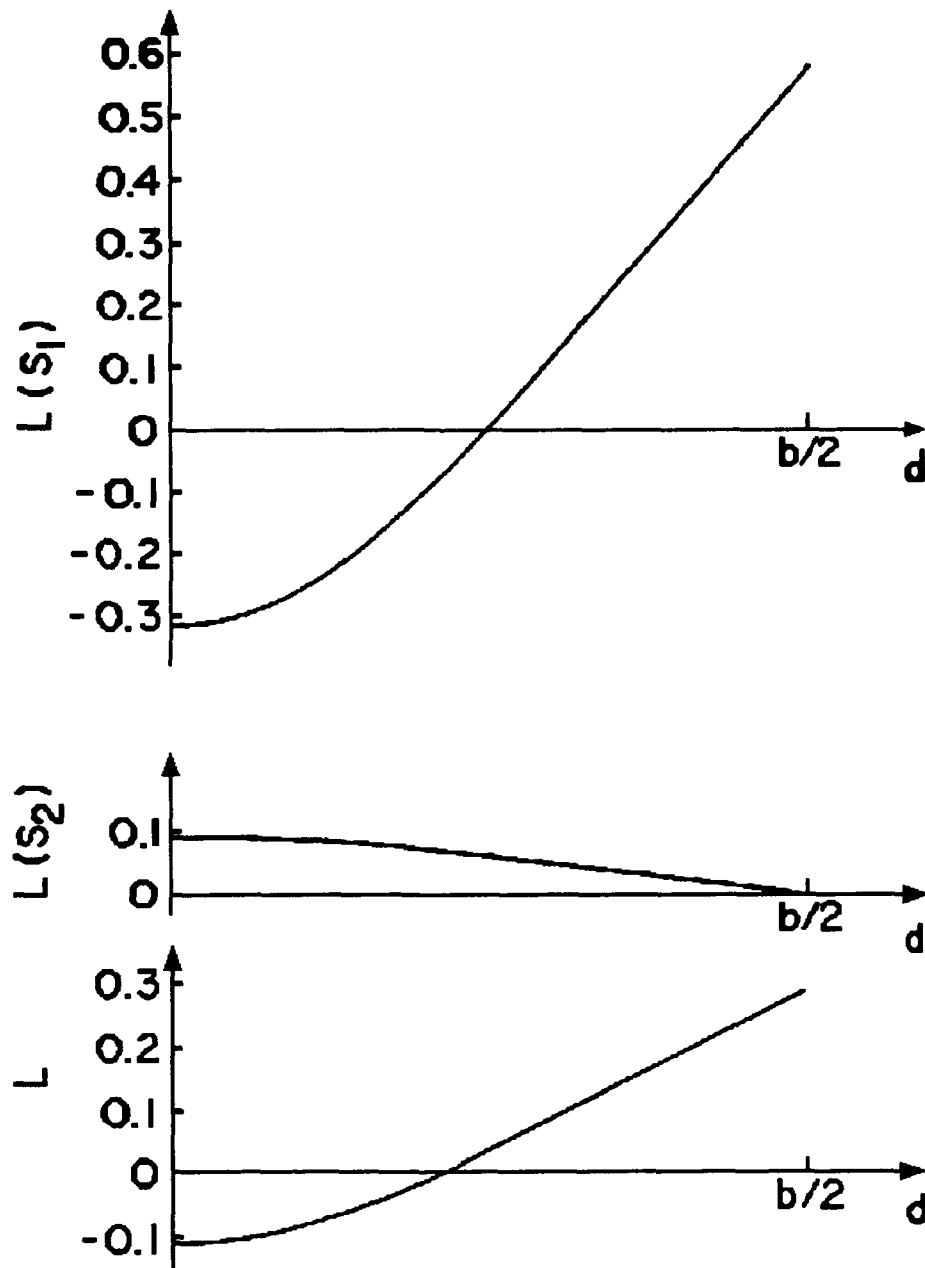
Figure 3.11.   The Lorentz factors $L(s_1)$, $L(s_2)$, and L as a
function of the separation of two monopoles, d [56].

$$P = [1 + L(\epsilon_r - 1)] P_o \qquad (3.48)$$

where

$$P_o = np_o \quad \text{and} \quad n = \frac{2}{abc} . \qquad (3.49)$$

To find P, a value must be defined for d. To determine d, a simple dipole is used to represent a single CF_2 molecule in the PVDF chain [56]. With a CF-bond length of 0.135 nm and a F-C-F angle of 109°, the dipole moment, p_o, of a CF_2 molecule has been calculated to be $7 \cdot 10^{-30}$ C·m, where the charge on each F atom was found to be 0.28·q, where q is the elementary charge $1.609 \cdot 10^{-19}$ C [56]. An equivalent simple dipole model for this system would have $Q = 6.89 \cdot 10^{-20}$ C and $d = 10^{-10}$ m [56]. From Figure 3.11, for $d = 10^{-10}$ m, L is equal to approximately -0.007. Using $\epsilon_r = 4$ [56] and substituting the above values into equation (3.49) yields a value of $P = 0.127$ C·m^{-2}.

To determine the macroscopic piezoelectric and pyroelectric coefficients for the β-PVDF polymer, Al-Jishi and Taylor used the equations developed by Purvis and Taylor [62]. Purvis and Taylor developed a model for the piezoelectric and pyroelectric effects of the β-PVDF polymer; however, their model assumed that the β-PVDF polymer was totally crystalline [62]. Al-Jishi and Taylor refined the equations and included a weighting factor to account for the semi-crystallinity of the β-PVDF polymer. The following equation is used to determine the piezoelectric coefficients for the β-PVDF polymer [56]:

$$d_{3i} = \xi P \left\{ (\epsilon_r - 1) \left[\left[\frac{\partial L}{\partial \ln a} - L \right] s_{2i} + \left[\frac{\partial L}{\partial \ln b} - L \right] s_{3i} + \left[\frac{\partial L}{\partial \ln c} - L \right] s_{1i} \right] - s_{s3i} \right\}, \qquad (3.50)$$

where ξ is the volume fraction of crystalline PVDF, S_{1i} through S_{3i} are the elastic compliances of the single crystals (see Table 3.1), and S_{s3i} are the elastic compliances of the semi-crystalline film (see Table 3.1). Similarly, the following equation is used to determine the pyroelectric coefficients for the semi-crystalline β-PVDF polymer [56]:

$$P_3 = \xi P \left\{ (\epsilon_r - 1) \left[\left[\frac{\partial L}{\partial \ln a} - L \right] \alpha_2 + \left[\frac{\partial L}{\partial \ln b} - L \right] \alpha_3 + \left[\frac{\partial L}{\partial \ln c} - L \right] \alpha_1 \right] - \alpha_{s3} \right\} \qquad (3.51)$$

where the α_is are the linear thermal expansion coefficients (see Table 3.1). The partial derivatives were calculated with the appropriate β-PVDF polymer dimensions [56]:

$$\frac{\partial L}{\partial \ln a} = -0.19 \ , \quad \frac{\partial L}{\partial \ln b} = -0.83 \ , \quad \frac{\partial L}{\partial \ln c} = 0.85 \ .$$

Table 3.2 shows the values calculated from these equations, the experimentally measured quantities, and the percent error for the β-PVDF polymer. In the worst case, d_{32} is in error by a factor of approximately 58%; however, the two most important quantities relative to this research, d_{33} and p_3, are accurate to within 50%.

3.6. Conclusion

The equations used to model the piezoelectric and pyroelectric effects, both microscopic and macroscopic, have been presented. Table 3.3 summarizes the experimentally determined coefficients for the β-PVDF polymer. These coefficients can be used with the equations presented in this chapter to predict the piezoelectric and pyroelectric response of the β-PVDF polymer. The predicted responses will be used in the next chapter during design of the proposed piezoelectric tactile sensor.

Table 3.1. Properties of the β-PVDF Polymer [56].

Properties	i = 1	2	3
S_{1i} $(10^{-11}$ $m^2 \cdot N^{-1})$	4.44	-1.82	-0.832
S_{2i} $(10^{-11}$ $m^2 \cdot N^{-1})$	-1.82	7.41	-1.15
S_{3i} $(10^{-11}$ $m^2 \cdot N^{-1})$	-0.832	-1.15	6.78
S_{s3i} $(10^{-11}$ $m^2 \cdot N^{-1})$	-15.37	-15.37	40.0
α_i $(10^{-4}$ $K^{-1})$	0.130	1.45	1.45
α_{si} $(10^{-4}$ $K^{-1})$			1.45

Table 3.2. Piezoelectric and Pyroelectric Coefficients for the
β–PVDF polymer [56,63].

Coefficients	Calculated	Experimental	% Error
d_{31} $(10^{-12}$ $C \cdot N^{-1})$	15.0	9.5	58
d_{32} $(10^{-12}$ $C \cdot N^{-1})$	4.85	9.5	48
d_{33} $(10^{-12}$ $C \cdot N^{-1})$	-29.2	-19.5	49
p_3 $(10^{-5}$ $C \cdot m^{-2} \cdot K^{-1})$	-2.78	-1.9	46

Table 3.3. Material Coefficients for the β-PVDF polymer [11,56,58,63,64].

Coefficient	Units	Value
d_{31}	$C \cdot N^{-1}$	$9.5 \cdot 10^{-12}$
d_{32}	"	$9.5 \cdot 10^{-12}$
d_{33}	"	$-19.5 \cdot 10^{-12}$
p_3	$C \cdot m^{-2} \cdot K^{-1}$	$-3.2 \cdot 10^{-5}$
s_{11}	$m^2 \cdot N^{-1}$	$4.44 \cdot 10^{-11}$
s_{12}	"	$-1.82 \cdot 10^{-11}$
s_{13}	"	$-0.832 \cdot 10^{-11}$
s_{21}	"	$-1.82 \cdot 10^{-11}$
s_{22}	"	$7.41 \cdot 10^{-11}$
s_{23}	"	$-1.15 \cdot 10^{-11}$
s_{31}	"	$-0.832 \cdot 10^{-11}$
s_{32}	"	$-1.15 \cdot 10^{-11}$
s_{33}	"	$6.78 \cdot 10^{-11}$
e_{31}	$m^2 \cdot C^{-1}$	$69 \cdot 10^{-3}$
e_{32}	"	$9 \cdot 10^{-3}$
e_{33}	"	$-108 \cdot 10^{-3}$
g_{31}	$V \cdot m \cdot N^{-1}$	$216 \cdot 10^{-3}$
g_{32}	"	$19 \cdot 10^{-3}$
g_{33}	"	$-190 \cdot 10^{-3}$
c	$N \cdot m^{-2}$	$(s_{ij})^{-1}$

4. Design and Fabrication of the Piezoelectric Tactile Sensor and Support Circuitry

4.1. Introduction

The design and fabrication process of the piezoelectric tactile sensor investigated in this thesis effort has been refined through many research efforts [4-10]. The piezoelectric tactile sensor has been designed and fabricated to allow easy test and evaluation. In this chapter, the procedures for the design and fabrication of the piezoelectric tactile sensor and the configuration of the supporting external circuitry are described. The chapter begins by explaining the design and fabrication process of the integrated circuit used as the foundation of the sensor. Also, there is a brief explanation of the amplifier design used to extend the linear range of the tactile sensor. Then, the process of attaching the piezoelectric film to the integrated circuit is presented. Next, the configuration of the external circuitry used to transfer the integrated circuit tactile sensor's information to the test equipment is discussed. This chapter concludes by presenting the design of a heater that was used to characterize the pyroelectric effects of the tactile sensor.

4.2. Integrated Circuit Design

The integrated circuit that serves as the foundation of the piezoelectric tactile sensor was designed using MAGIC software, and it is depicted in Figure 4.1. After completing the sensor portion of the circuit design, the amplifier design used was evaluated with HSPICE software, and then the sensor was fabricated and packaged by MOSIS in a

132 pin grid array (PGA) package. The integrated circuit is composed of three main components: taxel array, charge signal amplifiers, and interconnect lines. This section explains the design and test of each of these components.

4.2.1. *Taxel Array*. The taxel array is composed of 64 taxels arranged in an 8 x 8 electrode array configuration. Each taxel measures 400 μm by 400 μm and it is separated from its nearest neighbors by 300 μm. A block diagram of the circuit is shown in Figure 4.2. The overall dimensions of the array are 5.3 mm by 5.3 mm, and the overall die dimensions are approximately 7.9 mm by 9.2 mm. The taxel's metal electrodes are expo ed with a glass-cut so that the PVDF film can be attached to the taxels with a urethane dielectric adhesive.

There were two primary objectives that led to the design oi the taxel array. The first resulted from the research of Capt Pirolo [4]. He found that the square electrode pattern exhibited superior results compared to several other array configurations. The second objective was pin count. The MOSIS package has 132 pins available for connection to external circuitry. Also, each taxel requires two pins, one for biasing and one for an output connection. Consequently, the size was limited to the 8 x 8 design. The remaining four pins were used for power supply (V_{DD}) and ground connections. The assignment of the pins is shown in Figure 4.2. The pins used for input biasing are connected to the pads on the right and left edges of Figure 4.2. The number that follows each I corresponds to the taxel associated with that input bias pin. Similarly, the pins used for the output connection are connected to the pads on the top and bottom edges of Figure 4.2.

4-2
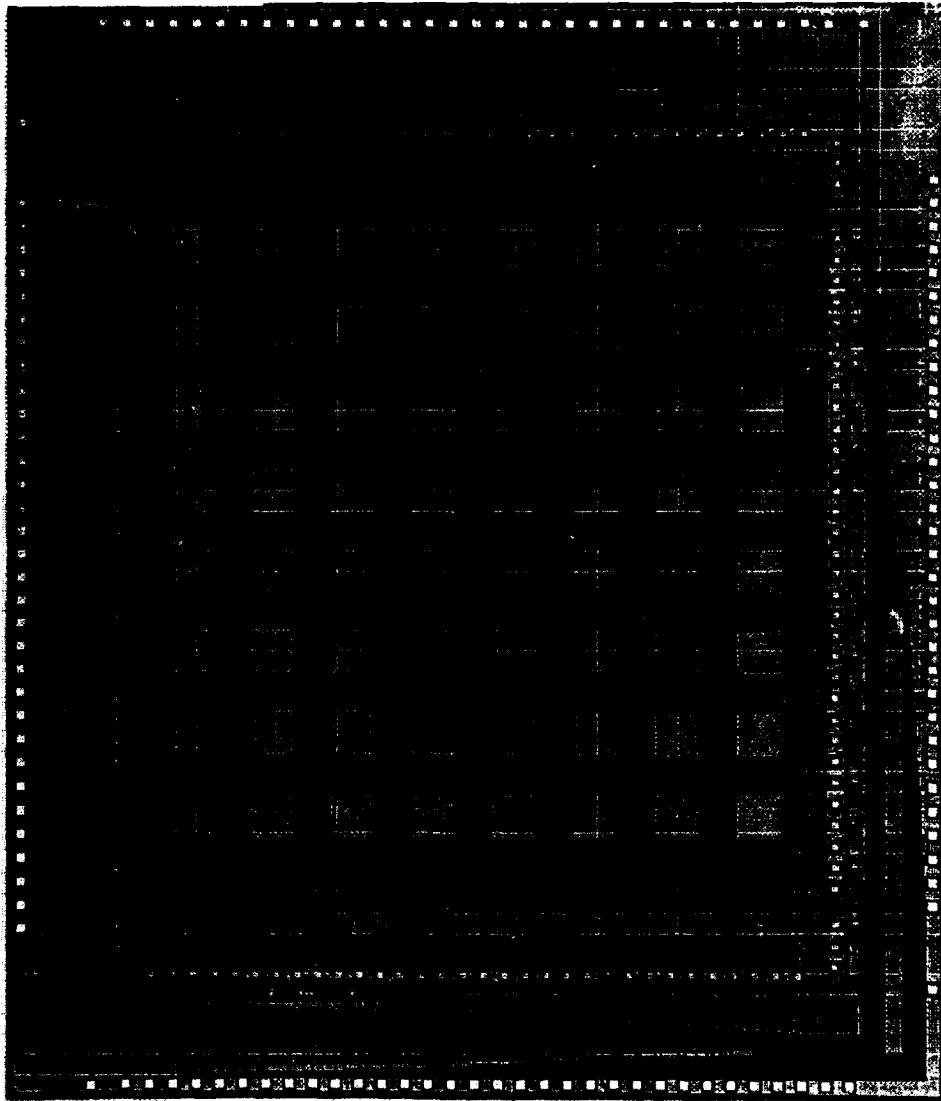
Figure 4.1. 5.3 mm x 5.3 mm piezoelectric integrated circuit sensor array. The sensing electrode pads are 400 μm x 400 μm each, and they are separated from each other by 300 μm.
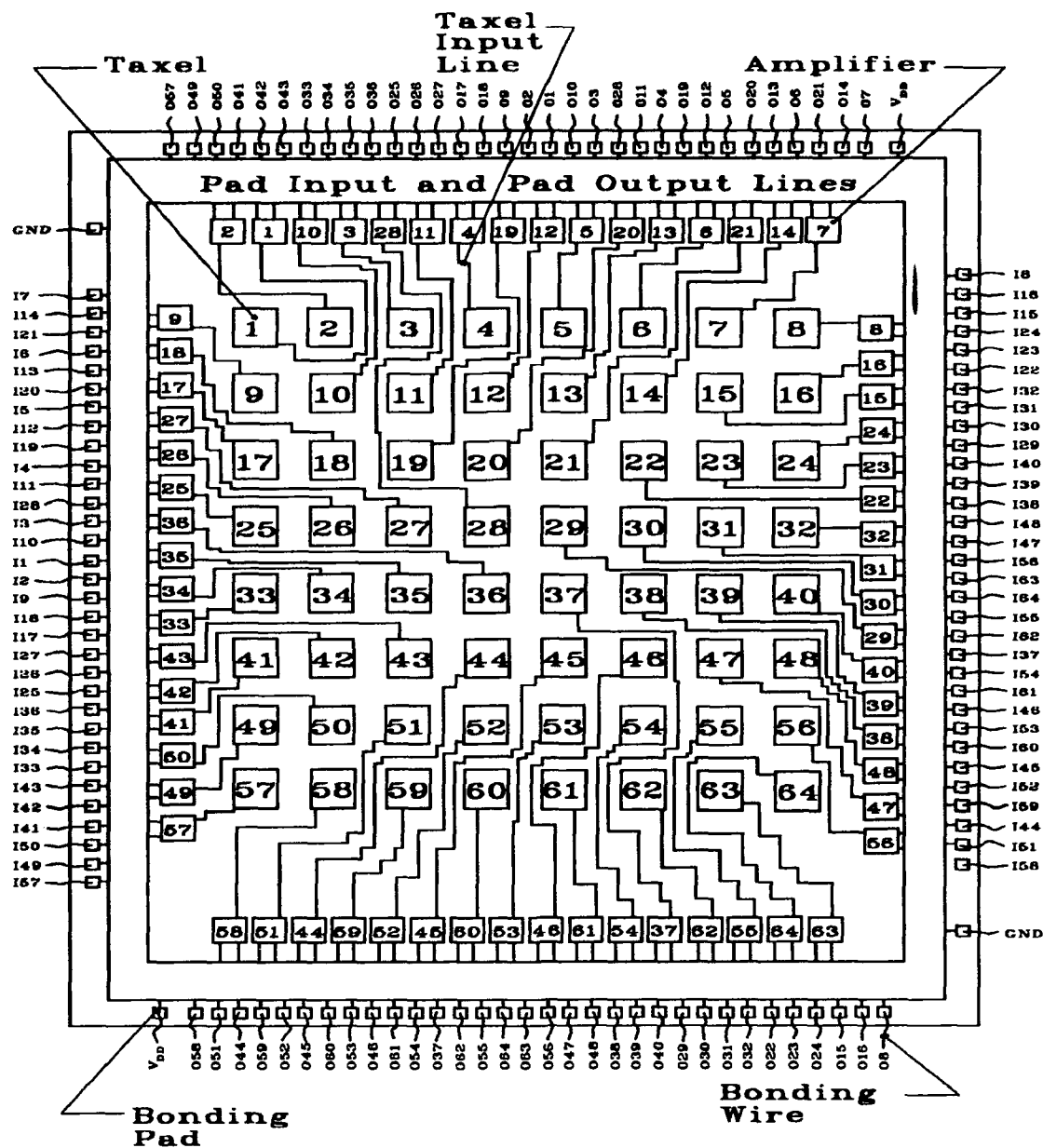
Figure 4.2. Block diagram of the integrated circuit used as the base
of the piezoelectric tactile sensor.

In summary, the taxel array on the integrated circuit is composed of an 8 x 8 array of square-shaped taxels. The pins on the integrated circuit are divided so that 64 are input bias pins, 64 are output pins, 2 are ground connections, and two are V_{DD} connections.

4.2.2. *Charge Signal Amplifiers*. When a force is applied to a piezoelectric PVDF film, charge is developed on the surface of the film. For a reasonably wide dynamic range, the relative magnitude of the charge generated on the surface of the film is linearly proportional to the magnitude of the externally applied force [11]. The tactile integrated circuit sensor utilized in this research effort is fabricated by attaching the piezoelectric PVDF film to the 8 x 8 array of charge sensing electrodes. When a compressive force is applied to the film that is sandwiched between a ground electrode and a sensing electrode, charge is generated on the surface of the sensing electrode that is characteristic of the force applied to the film. The magnitude of the charge generated (Q; Q = CV) on each of the sensor electrodes can be multiplexed to form a tactile image of the object that is contacting the sensor.

A charge amplifier acts as a high impedance buffer between each taxel electrode and its corresponding multiplexer interface, as shown in Figure 4.3. The amplifier's input impedance must be compatible with the output impedance of the PVDF film (on the order of 10^{15} Ω). Figure 4.4 shows the equivalent circuit for the PVDF electrical impedance calculations. The output electrical impedance of the film can be found from Figure 4.4 [11]:

$$Z = \frac{1}{\frac{1}{R} + j2\pi fC} = \frac{R}{1 + j2\pi fRC} \qquad (4.1)$$

$$C = \frac{\epsilon A}{t} \qquad (4.2)$$

and

$$R = \rho \frac{t}{A} \qquad (4.3)$$

where

Z is the electrical impedance of the film (Ω),

f is the frequency of operation (DC to 100 Hz),

R is the resistance of the film (Ω),

C is the capacitance of the film (F),

ρ is the volume resistivity of the film (10^{13} $\Omega \cdot$m) [11],

ϵ is the permittivity of the film ($1.01 \cdot 10^{-10}$ F$\cdot$m^{-1}) [63],

A is the surface area of a sensor electrode ($1.6 \cdot 10^{-7}$ m^2),

t is the thickness of the film ($4 \cdot 10^{-5}$ m).

A piezoelectric tactile sensor with human-like properties will typically possess a bandwidth from DC to 100 Hz [65]. At DC, the impedance of the PVDF film can be found by setting f = 0 Hz. At f = 100 Hz, j2πfRC is much greater than 1. Therefore, at f = 100 Hz, the denominator in equation (4.1) can be approximated by j2πfRC, and since the resistance (R) in the numerator and the denominator cancel, the impedance becomes predominantly reactive:

$$Z = \frac{1}{j2\pi fC} \Big|_{f=100 \text{ Hz}} . \qquad (4.4)$$
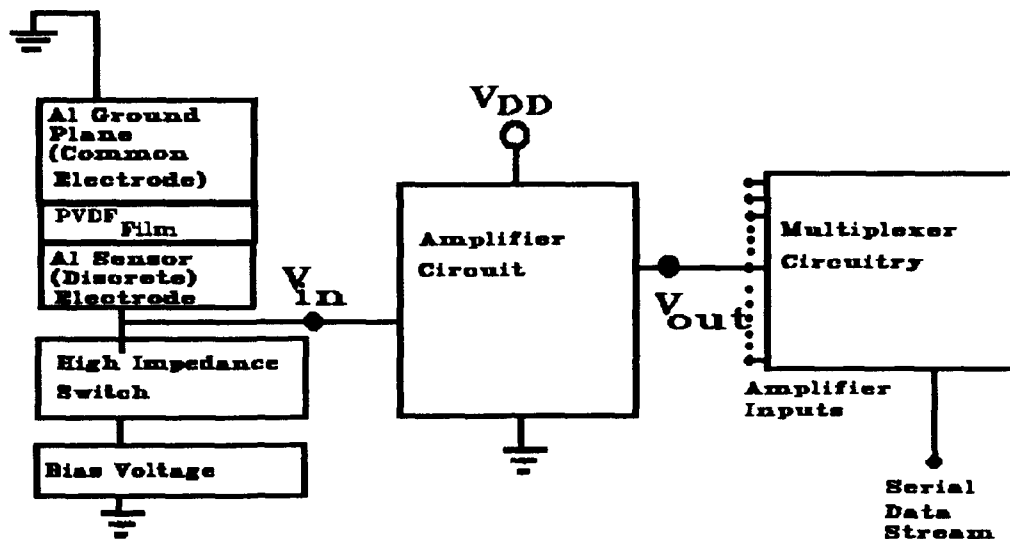
Figure 4.3. Charge amplifier located between a taxel sensor electrode and the multiplexing circuitry.

Therefore, the extremum values of the electrical impedance are:

$Z = 2.5 \cdot 10^{15}$ Ω at DC, and $Z = -j \cdot 3.9 \cdot 10^{09}$ Ω at $f = 100$ Hz. Ideally, for operating frequencies spanning DC to 100 Hz, the amplifier must have an input impedance greater than 2.5×10^{15} Ω.

Since the generated piezoelectric charge is linearly proportional to the externally applied force, the amplifier should have a correspondingly large linear range of output voltage. The magnitude of the generated voltage (V) can be related to the magnitude of the externally applied force (F) by the piezoelectric charge constant (d_{33}) and the temperature change ($\Delta T = T - T_o$) by the pyroelectric constant (p_3) using the following theoretical equation [11,41]:
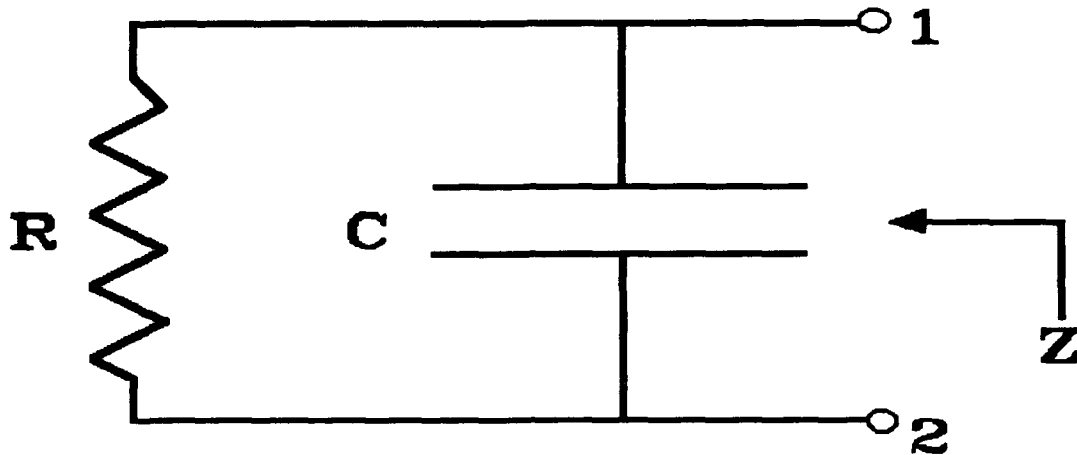
Figure 4.4. Equivalent electrical circuit for the PVDF impedance
calculations.

$$V = \frac{d_{33}tmg}{\epsilon A} + \frac{p_3 t \Delta T}{\epsilon} \tag{4.5}$$

where g is the acceleration due to gravity (9.81 $m \cdot s^{-1}$). Using values

from Equation (4.3) and Table 3.3, and since the tactile sensor is

intended to measure loads spanning 1 to 100 grams, the corresponding

voltage will span 0.47 to 47 V at constant temperature. Thus, the ideal

amplifier should have a linear range from 0 to 47 V.

The amplifier used in the integrated circuit tactile sensor that

was fabricated for crosstalk testing was a design that had been

previously proven to work [8]; however, two new amplifiers that have

extended linear ranges were designed, simulated, fabricated, and tested.

The best amplifier design will be incorporated into the integrated

circuit for subsequent fabrication. The details for realizing the two

amplifier designs with an extended linear region and high input

impedance will be discussed in the following paragraphs.

A. *Extending the Linear Region by Increasing the Power Supply.*

In order to increase the linear region of the charge amplifier, a method

of increasing the power supply voltage of the amplifier was

investigated. The amplifier design shown in Figure 4.5 was designed

with minimum sized transistors. It is the same amplifier that was

proven to work in a previous research effort [8], and it is the same

amplifier used in the integrated circuit that was fabricated for this

research effort. since some of the amplifiers broke down when used at

voltages exceeding 12 V over extended periods of time, a better

amplifier design (able to withstand higher supply voltages) was

investigated using the MOSIS TinyChip format.
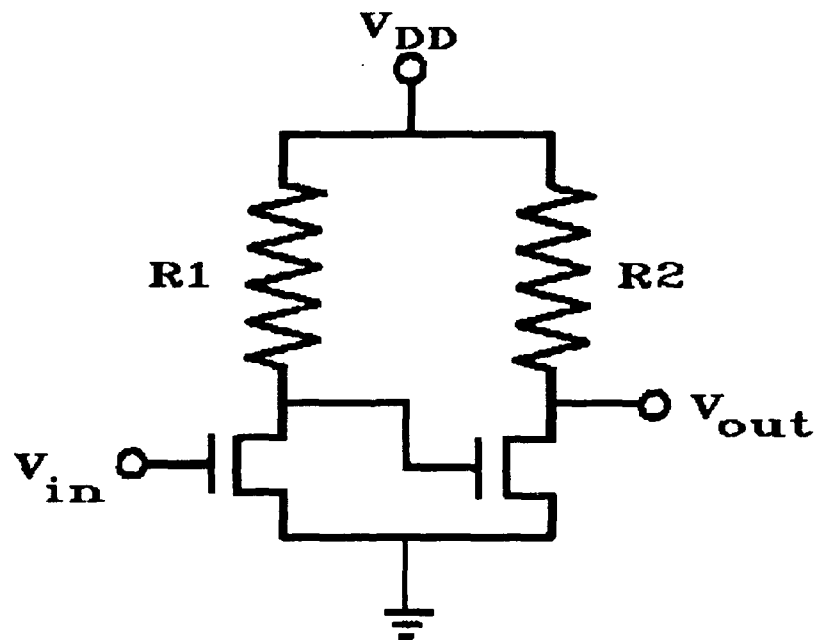
Figure 4.5. Original amplifier design [8].

If the gate lengths of the transistors in an amplifier are very short, the channel's electric fields could induce excessive substrate currents and cause device degradation with time [66]. A practical V_{DD} value for a particular gate length (L) can be found from the following empirical relation [67]:

$$V_{DD} = 6.1 \times \left[\frac{L}{2}\right]^{1/2} \tag{4.6}$$

where V_{DD} is the desired supply voltage (V) and L is the gate length (μm). By algebraic manipulation, the gate length (L) can be expressed as a function of the supply voltage; that is:

$$L = 2 \times \left[\frac{V_{DD}}{6.1}\right]^2 \tag{4.7}$$

The gate length as a function of V_{DD} is plotted in Figure 4.6. To take advantage of this behavior, the gate lengths of the transistors in the amplifier shown in Figure 4.5 were monotonically increased in an attempt to decrease the channel's corresponding electric fields and increase the V_{DD} limit. The varying transistor sizes were used to relate the dependence of transistor size on the power supply voltage (V_{DD}). In order to maintain continuity, eight different amplifier designs were fabricated on the same chip using the TinyChip format offered by MOSIS. The gate widths (W) and the gate lengths (L) of the MOSFETs in the amplifiers are shown in Table 4.1, and the resistor values remained unchanged with R1 = 7 kΩ and R2 = 5 kΩ. The first amplifier was identical to the one used in the actual sensor integrated circuit design where the width (W) of the gate in the transistor on the left (input) is 5 μm, the width of the gate in the transistor on the right (output) is 3 μm, and the length (L) of the gate in both transistors is 2 μm [8].

4-10

This situation corresponds to a design with minimum-sized features (MOSIS 2-μm CMOS fabrication process), and the design utilized in the previous research effort [8]. The subsequent amplifiers were designed with increasing transistor lengths (and corresponding widths) to investigate the possibility of increasing the linear range by increasing the power supply, V_{DD}.

Table 4.1. Gate Length (L) and Width (W) for the Transistors Shown in Figure 4.5.

Amplifier Number	Left Transistor (Input)		Right Transistor (Output)		Optimum Predicted V_{DD} (V)
	W (μm)	L (μm)	W (μm)	L(μm)	
1	5	2	3	2	6.1
2	40	16	24	16	17.3
3	85	34	51	34	25.2
4	125	50	75	50	30.5
5	165	66	99	66	35.0
6	205	82	123	82	39.1
7	245	98	147	98	42.7
8	285	114	171	114	46.1

B. *Extending the Linear Region by Using a Differential Amplifier*. In order to approach the problem of extending the linear range of the tactile sensor from a different perspective, a new amplifier was designed to solve the linear region limitation problem. Several amplifier designs were investigated, but a differential amplifier with a step-down amplification feature was chosen because of its favorable
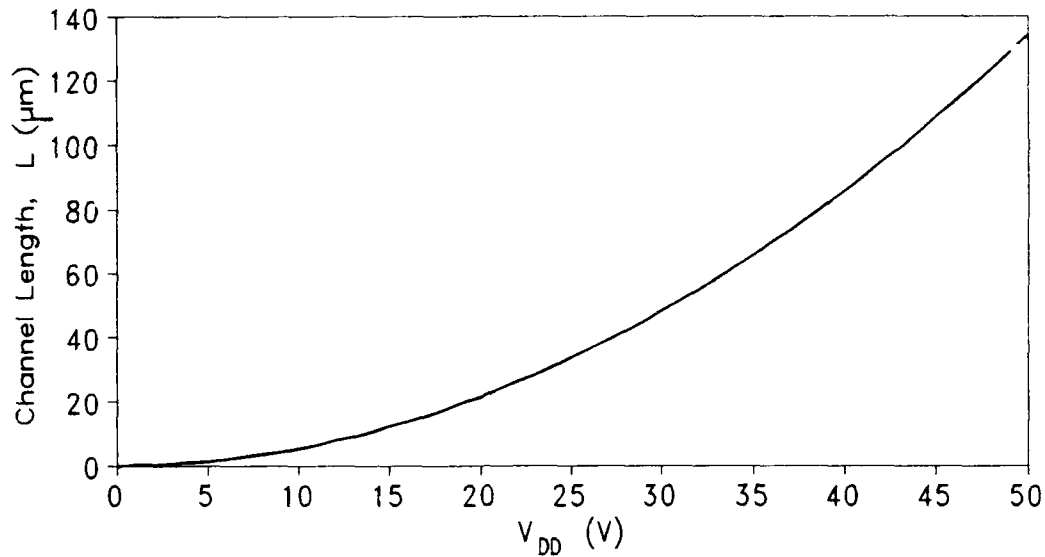
Figure 4.6. MOSFET channel length (L) as a function of the supply voltage (V_{DD}).

linear response for low voltage inputs and its ability to operate with a 12 V V_{DD} supply voltage (an amplifier with a 12 V limit on V_{DD} was previously shown to operate without degradation over extended time periods [8]). The greatest advantage of this amplifier design is its ability to amplify signals that exceed the V_{DD} supply voltage. The differential amplifier used in this effort is shown in Figure 4.7, and the values of the components in the differential amplifier are found in Table 4.2. The HSPICE equivalent circuit is found in Appendix C, and it was fabricated by MOSIS using their TinyChip format.

Once the amplifier designs were fabricated by MOSIS using their TinyChip format they were tested. The evaluation procedure for the TinyChips is discussed in Chapter 5. After evaluation, the best design
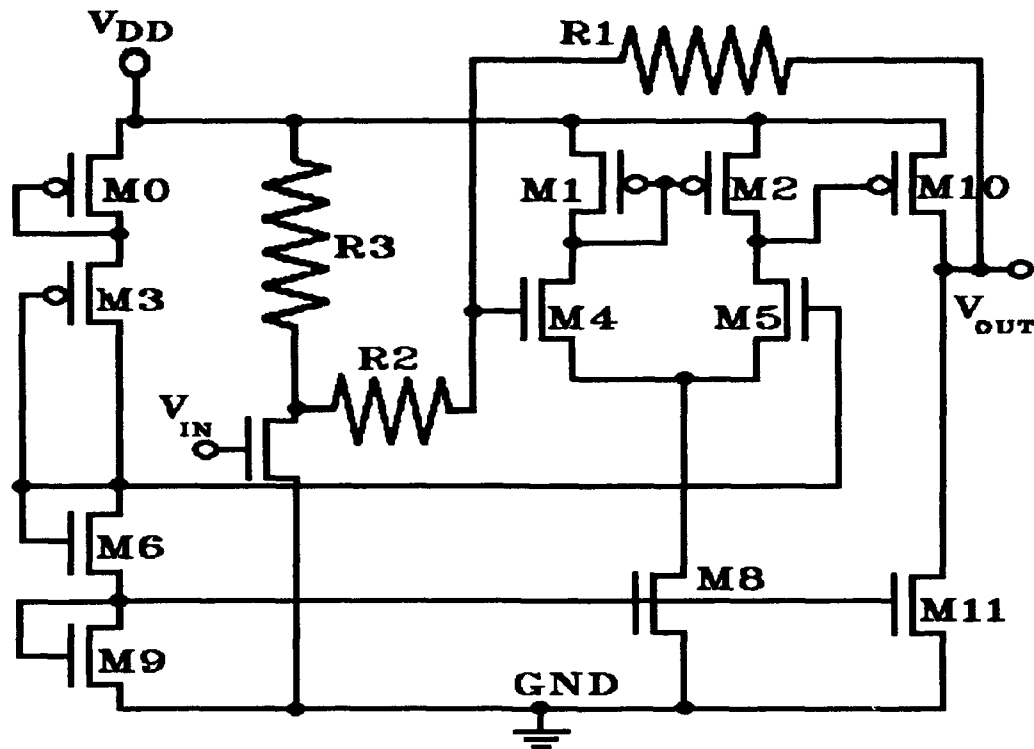
Figure 4.7. Differential amplifier design.

was incorporated into the integrated circuit tactile sensor for
subsequent fabrication.

   4.2.3. *Interconnecting Lines*. In an attempt to eliminate the
electrical crosstalk reported by Capt Dyson [8], the interconnecting
lines of the tactile sensor were rerouted. The lines were rerouted to
determine the potential cause of electrical crosstalk behavior. Before
presenting how the lines were rerouted, it is necessary to define the
types of lines found in the integrated circuit design. There are three
types of interconnecting lines in the integrated circuit design: pad
input lines (64), taxel input lines (64), and pad output lines (64). A
block diagram depicting the three types of lines is shown in Figure 4.8.
The taxel amplifiers (64) are the junctions for these lines. The pad
input lines connect each of the 64 input bond pads to the inputs of

Table 4.2. Transistor and Resistor Values for the Differential
            Amplifier.

Element	Parameters	
V_{DD}	12 V	
M0	L = 4 μm	W = 4 μm
M1	L = 3 μm	W = 3 μm
M2	L = 3 μm	W = 3 μm
M3	L = 4 μm	W = 4 μm
M4	L = 2 μm	W = 9 μm
M5	L = 2 μm	W = 9 μm
M6	L = 4 μm	W = 4 μm
M7	L = 2 μm	W = 5 μm
M8	L = 2 μm	W = 8 μm
M9	L = 4 μm	W = 8 μm
M10	L = 2 μm	W = 60 μm
M11	L = 2 μm	W = 120 μm
R1	4 kΩ	
R2	1 kΩ	
R3	7 kΩ	

their corresponding taxel amplifiers. (The 64 input bond pads are used
to connect the integrated circuit die to the 64 integrated circuit input
bias pins through bonding wires.) The taxel input lines connect each of
the 64 taxels to the inputs of their corresponding taxel amplifiers.
The pad output lines connect each of the 64 output bond pads to the
outputs of their corresponding taxel amplifiers. (The 64 output bond
pads are used to connect the integrated circuit die to the 64 integrated
circuit output pins through bond wires.)

Now that the three basic types of interconnecting lines have been
presented, their routing and orientation will be explained. A block

4-14
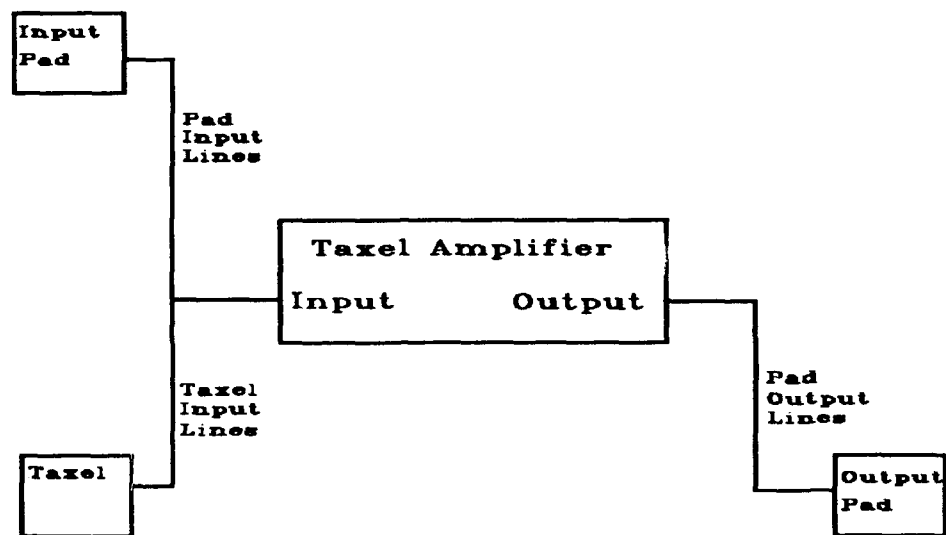
Figure 4.8. Block diagram depicting the three types of interconnecting lines found in the integrated circuit design. This drawing is typical for each of the 64 taxels.

diagram of the initial (or old) tactile sensor integrated circuit design

is shown in Figure 1.6. A revised integrated circuit design is

presented in Figure 4.1. The initial integrated circuit shown in

Figure 1.6 was designed with the pad input lines separated by 6 to

17 μm, with the majority of those lines separated by 6 to 8 μm. The

taxel input lines in the old integrated circuit were routed with various

spacings, but all of the spacings were greater than 50 μm. The pad

output lines in the old integrated circuit were routed with 5 to 15 μm

spacing between the lines. In order to explain how the interconnecting

lines in the new or revised integrated circuit were rerouted for

electrical crosstalk testing, the old integrated circuit in Figure 1.6

can be divided into four sections by drawing an internal X that connects

opposite corners. This allows Figure 1.6 to be described by four quadrants: upper, lower, left, and right. The taxel input lines in the upper and lower quadrants of Figure 1.6 were rerouted so that the taxel input lines from adjacent sensor taxels did not run parallel to each other over extended lengths. The pad input lines in the right and left quadrants of Figure 1.6 were rerouted so that all of the pad input lines were at least 25 μm apart. The 25 μm value was identified by Capt Dyson as an acceptable separation between integrated circuit conductors thesis [8]. Since the routing of the pad output lines in the old integrated circuit was not identified as a contributor to electrical crosstalk, the pad output line routing was left alone.

4.3. Piezoelectric PVDF Film Application

In this section, the details for adhering the piezoelectric PVDF film to the surface of the integrated circuit are presented. After this step is accomplished, the sensor will be complete. The final step is to establish the external circuit necessary to bias the sensor's input pins and multiplex its output. The methodology for fabricating the piezoelectric tactile sensor has undergone many iterations. The general procedure for fabricating the piezoelectric tactile sensor started with Pirolo's research, and it was refined by Reston, Ford, Fitch, Dyson, and Yauilla [4-9].

4.3.1. Film Preparation. The first step in the process is to determine the polarity of the PVDF film. The process for accomplishing this task is described in Appendix B. Once the polarity of the film is determined, the film should be prepared for adhesion by etching the (+) side of the 4" x 4" piece of PVDF with ferric chloride for 30 minutes at

room temperature, rinsing it in deionized water, and drying it with nitrogen (this removes the aluminum coating from the (+) side of the film). Then, several 6 mm x 6 mm pieces are cut from the sheet and store for sensor fabrication.

4.3.2. Film Attachment. To fabricate the tactile sensor, the piezoelectric PVDF film must be attached to the integrated circuit (IC). The procedure for attaching the film to the IC was recorded by Capt Dyson [8]. The following steps describe how to attach a sample of the piezoelectric PVDF film to an IC with an overall surface area measuring 7.9 mm x 9.2 mm, and a tactile sensing area that measures 5.3 mm x 5.3 mm [8].

A. Neutralize the charge on the 6 mm x 6 mm PVDF film by immersing it in an electrically-grounded solution composed of 200 ml of deionized water and 1 drop of HCl.

B. Thoroughly dry the PVDF film with nitrogen gas.

C. Place 1 drop of urethane adhesive (Miller-Stephenson Chemical Co., MS-270/22) in the center of the PVDF film with a 3 cc syringe. Smooth the adhesive with a glass slide and center the film on the tactile array.

D. Place a piece of cellophane tape over the PVDF film.

E. Place a square microscope slide on the cellophane tape that is centered on the sensor.

F. Place the entire package one large paper binding clip to ensure proper bonding of the PVDF film to the sensor. The placement of the paper binding clip is critical toward achieving a uniform compressive force (F) across the surface of the PVDF film.

G. Place the entire package in a vacuum system and reduce the pressure to 100 μm of mercury for 30 minutes.

H. Cure for 1 hour at 65°C.

I. Verify proper film adhesion.

I.1. Use the optical microscope to visually inspect the quality of the bond.

I.2. Verify there are no bubbles on the surface of the sensor.

I.3. Verify there are no tears in the film.

I.4. Verify that the corners of the film have 90° angles.

I.5. Verify that the corners of the film are uniformly and consistently bonded to the IC.

I.6. Apply a load to the sensor and verify the taxel outputs.

I.7. Verify there are no electrodes shorted together (shorts between electrodes indicate that the aluminum was not properly removed from the PVDF film's surface).

I.8. Verify all taxels respond to an applied load.

J. If the PVDF film did not adhere properly:

J.1. Remove the PVDF film with acetone (solvent for the urethane adhesive).

J.2. Place the IC in the plasma asher to remove the residual adhesive and acetone.

K. When the film is properly bonded, use conductive silver epoxy to connect a 1-mil diameter wire to the top surface electrode on the piezoelectric PVDF film. Connect the other end to the gold wire bond on

the IC's ceramic package. (This serves as a ground conductor for the top surface electrode.)

4.4. *External Circuit Configuration*

The external circuitry consists of four main parts: input biasing network, output multiplexing circuitry, power supplies, and data collection equipment. A block diagram of the equipment and their relative interconnections are shown in Figure 4.9. In this section, the setup and configuration of each of these parts will be presented.
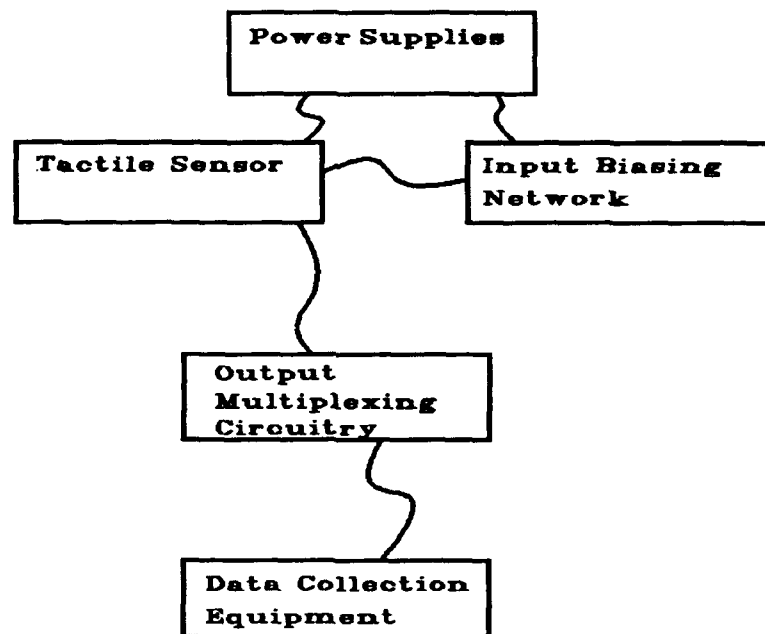
Figure 4.9. Block diagram of the piezoelectric tactile sensor external support circuitry.

4.4.1. Input Biasing Network. The input biasing network is necessary to ensure that the voltage levels of all the taxels begin in a uniform initial state. The initial state also ensures that the

amplifier inputs are set to the lower end of the taxel amplifier's linear range. Once this initial state is reached, the bias voltage is removed, and sensor readings are taken.

To achieve a uniform initial state, a high impedance switching network, shown in Figure 4.10, is used to interface with each taxel. The switches, when "ON", connect the taxels to a bias voltage. When the switches are switched to the "OFF" position, the bias voltage is disconnected from the taxel and the switch becomes a high impedance leakage path for the initial state charge residing on the PVDF film. It is critical to the operation of the sensor to minimize the charge leakage through the "OFF" switch. Capt Yauilla determined that the MAXIM MAX327 high impedance switches provided an adequately high impedance to limit charge leakage from the PVDF film [9]; therefore, this IC switch was incorporated into the input biasing network for the piezoelectric tactile sensor.

4.4.2. *Output Multiplexing Circuitry.* The output multiplexing circuitry is used to connect the integrated circuit tactile sensor to external instrumentation that, in turn, processes the sensor output data to form an image of the applied load. The MAXIM MAX328 Ultra-Low Leakage Monolithic CMOS Analog Multiplexers provided a low-distortion analog signal to the digital storage oscilloscope (DSO).

Eight multiplexers were used to serialize the output of the sensor. A ninth MAX328 multiplexer was used to drive the enable lines of the other eight multiplexers. A decoder (TI 74156) driven by a binary counter (TI 74161), which in turn is driven by an external clock,
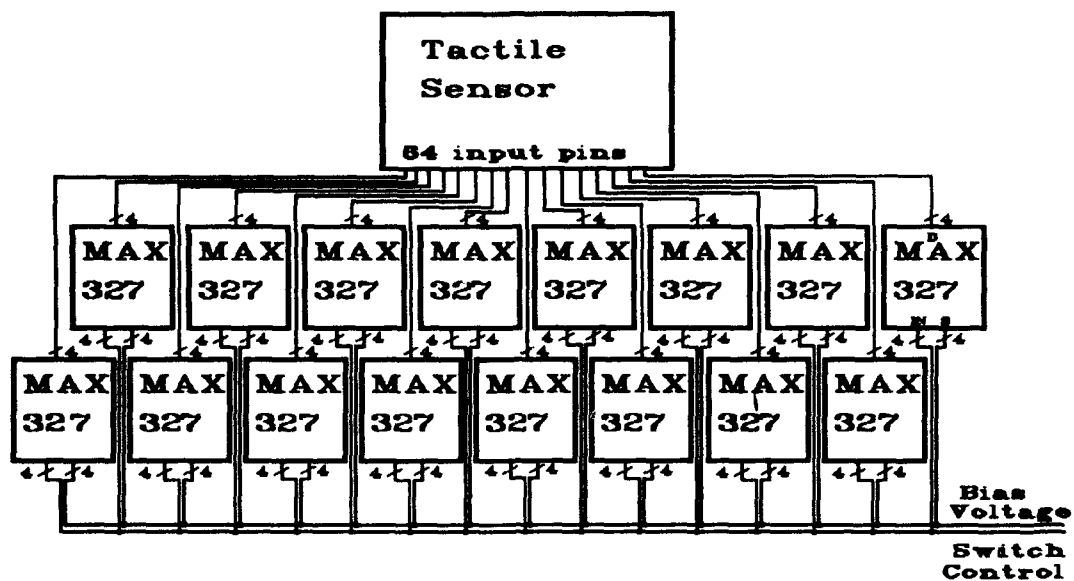
Figure 4.10.   Input biasing network for the piezoelectric tactile
                  sensor.

provided the timing signal required to realize a consistent serialized

output.   The output multiplexing circuitry is shown in Figure 4.11.

4.4.3. *Power Supplies*.   The power supplies were necessary to

drive the input biasing network, the output multiplexing circuitry, and

the tactile sensor.   The HP 6624A DC power supply provided four of the

voltage levels necessary for sensor operation.   Channel 1 of the HP

6624A was set to 0 or 5 V and used as a switch, Channel 2 was set to

4.5 V and used as the reference voltage level for the input bias

network, channel 3 and 4 were set to 12 and -12 V, respectively, and

used as the power supplies for the MAXIM chips (channel 3 was also used

as V_{DD}).   The fifth DC supply was a HP 6632A DC power supply which

provided the 5 V, V_{CC} voltage levels for the Texas Instrument IC's.
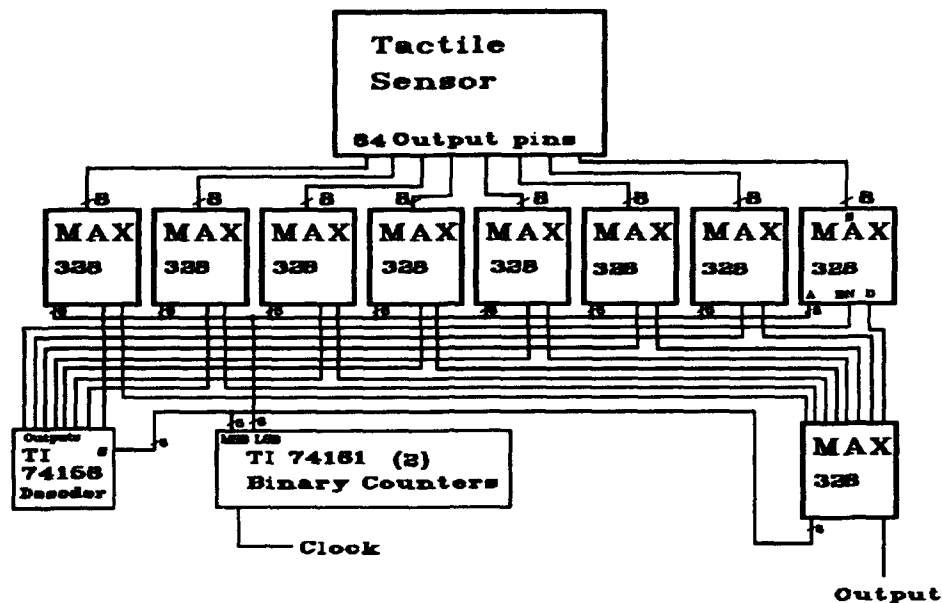
Figure 4.11.   Output multiplexing circuitry for the piezoelectric
                tactile sensor.

4.4.4. *Data Collection Equipment*. The final equipment used for

the tactile sensor's operation consisted of a HP digital storage

oscilloscope (DSO) and a Z-248 computer fitted with an HPIB interface

card that was IEEE-488 compatible. The first input channel of the DSO

was connected to the of the multiplexing circuitry's output that is

shown in Figure 4.11. The second channel of the DSO was connected to

one of the decoder outputs for triggering purposes.

4.5. *Heater for Pyroelectric Characterization*.

In this section, the design of the heater used for pyroelectric

characterization is described. Uniform tactile sensor heating was

accomplished by placing the voltage-controlled heater (Figure 4.12) on

top of the integrated circuit tactile sensor. The heater was designed

4-22

using a DC controlled off-the-shelf kapton heating element. The kapton
heater was mounted on a 31.8 mm x 31.8 mm square sheet of copper that
was 3.2 mm thick. A 15 mm diameter hole was drilled through the copper
washer to create an opening for a thermocouple or a piezoelectric load.
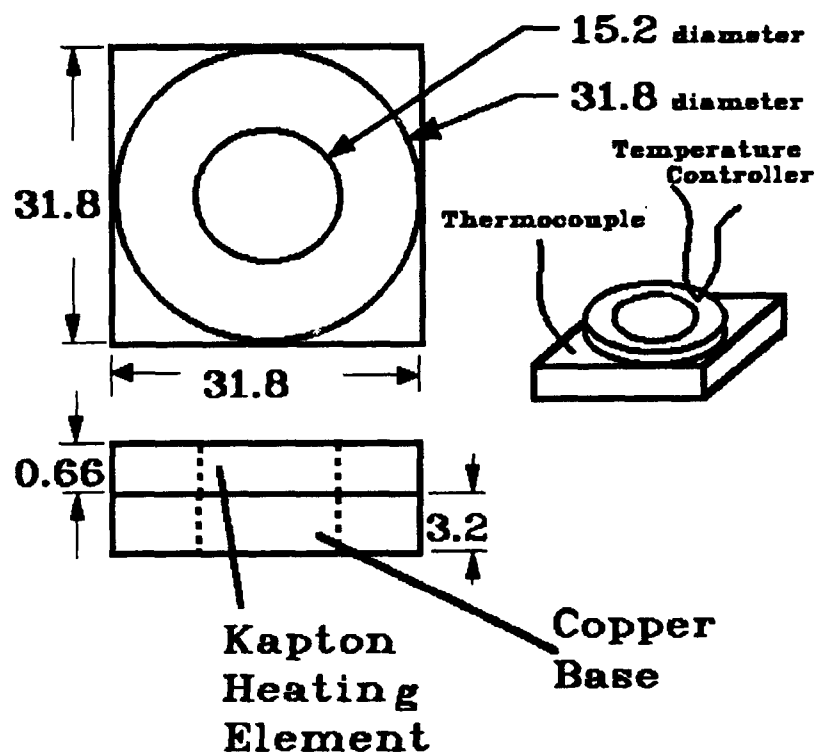
Figure 4.12.   Heat source for pyroelectric testing (units in mm).

5. Procedures for Evaluating the performance of the
Piezoelectric Tactile Sensor

5.1. Introduction

A critical part of the thesis effort is test and evaluation. In order to show that design criteria have been satisfied, experimental validation was accomplished. Several items were designed specifically for the experimental verification phase of the piezoelectric tactile sensor's research. The hardware consisted of eight integrated circuit amplifiers designed to enhance the linear region of the tactile sensor, and an integrated circuit tactile sensor designed specifically for crosstalk testing. In addition, a heater was designed to facilitate the pyroelectric characterization of the sensor. In conjunction with the hardware, several computer programs were either enhanced or generated to operate and evaluate the tactile sensor or support instrumentation.

The test procedure used in this thesis effort is hierarchical. First, low-level component tests were performed. Performance was validated experimentally on those components associated with the sensor, and then higher-level system tests were performed that involved the integrated circuit without the PVDF film attached. Finally, complete tactile sensors were fabricated (PVDF film was attached) and overall system tests were performed. Ultimately, the results were used to modify the existing hardware for future piezoelectric tactile sensor fabrication and performance tests.

This chapter presents the procedures used to evaluate the performance of the piezoelectric tactile sensor. First, the details

used to evaluate the new amplifier designs and criteria used to determine the best design will be explained. Next, the process used to evaluate the electrical crosstalk associated with the new and old integrated circuit designs will be explained. Then, the procedure for determining the piezoelectric tactile sensor's response will be presented. The sensor responses will include: force sensitivity, pressure accuracy, voltage predictability, and object imaging capability. Finally, the procedure for pyroelectric characterization will be presented.

5.2. Evaluation Procedures for Power Supply Enhancement

In order to determine which of the amplifier designs will best extend the operational force sensitivity range of the tactile sensor, the amplifier designs needed to be experimentally evaluated. To accomplish this task, the experimental test phase was partitioned into two segments: long-term and short-term performance tests. Long-term testing was accomplished on the seven amplifier configurations designed with extended channel lengths (testing was also performed on the original amplifier design as a control). Short term testing was done on both the extended channel length amplifiers and the differential amplifier. The following paragraphs describe, in detail, the testing procedure.

5.2.1. Evaluation of the Amplifiers with Enhanced Channel Lengths. Once the seven amplifier designs incorporating extended gate lengths were complete, they were fabricated by MOSIS using their TinyChip format. When the completed TinyChips arrived from MOSIS, the

amplifiers were tested without PVDF film being attached to the amplifiers' electrodes.

Long-term testing of the amplifiers designed with various sized transistors was accomplished over several days. Each of the eight amplifier designs described in Table 4.1 was tested individually. The V_{DD} supply voltage of the amplifier under test was connected to a variable DC power supply, as shown in Figure 5.1. The V_{DD} supply voltage was then biased to 10 V for a 24-hour period. After 24 hours, V_{DD} was increased by 0.5 V every 15 minutes until the amplifier ceased to work, or until a 50 V limit on V_{DD} was attained. Throughout the test, the amplifier's input voltage, V_{IN}, was adjusted so the output voltage of the amplifier, V_{OUT}, remained in the amplifier's linear region. For each of the eight amplifiers tested, the output voltages were stored on a computer disk via the IEEE-488 bus connection. The computer program used to control the test instrumentation and store the data is listed in Appendix D. The data from the test will be presented in Chapter 6, and an attempt will be made to relate the channel length of the amplifier to the maximum allowable V_{DD} voltage level.

Short term tests were accomplished on each of the amplifier designs described in Table 4.1. First, HSPICE was used to simulate the V_{OUT} versus V_{IN} characteristic curve for each of the eight amplifier designs. Next, the simulations were validated experimentally by measuring V_{OUT} versus V_{IN} with the test configuration shown in Figure 5.1. The computer program used to measure and store the data is listed in Appendix D.
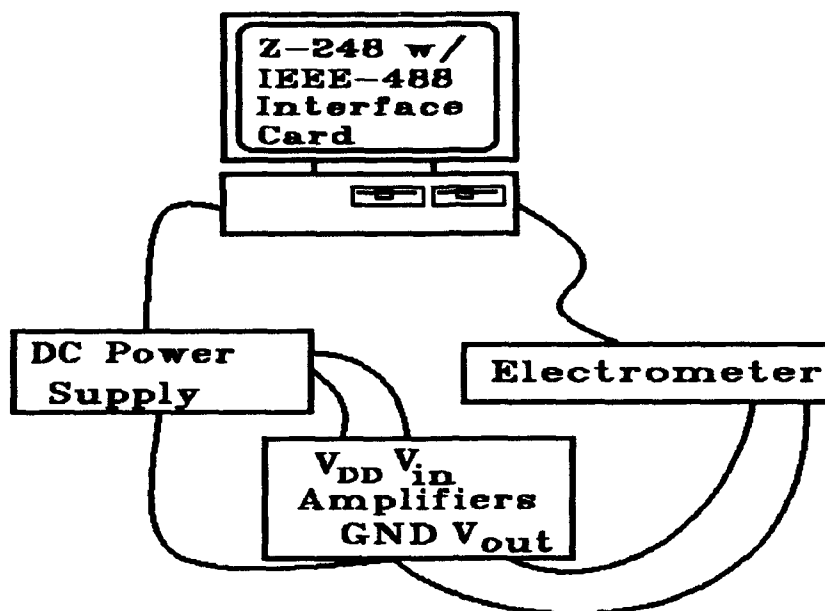
Figure 5.1. Test configuration for establishing the amplifier V_{DD} limitations.

5.2.2. Evaluation of the Differential Amplifier. The design for the differential amplifier was validated using HSPICE simulation software. The simulation consisted of predicting the output voltage, V_{OUT}, of the amplifier as the input voltage, V_{IN}, ranged from 0 to 20 V with V_{DD} set to 12 V. The HSPICE file used for simulation is presented in Appendix C. After simulation, a TinyChip design with eight identical differential amplifiers on each IC was sent to MOSIS for fabrication. When the TinyChips arrived from fabrication, they were experimentally validated using the test configuration shown in Figure 5.1. The test involved measuring V_{OUT} as V_{IN} varied from 0 to 20 V when V_{DD} remained constant at 12 V. The data was stored on a computer disk via the IEEE-

488 bus connection. The computer program used to operate the test instrumentation is listed in Appendix D.

5.3. Electrical Crosstalk

A critical aspect of this research effort involved determining the cause of the taxel electrical crosstalk observed in the previous studies [4-10]. (For this research, electrical crosstalk is defined as a DC voltage level that is developed on the output of a taxel's amplifier due to the electrical response of some other taxel.) This objective led to a redesign of the integrated circuit piezoelectric tactile sensor. The redesign involved rearranging the configuration of the bond pad input lines and taxel input lines to facilitate specific electrical crosstalk tests. Specifically tested were the spacing parameters associated with the pad input lines and the relative position of the taxel input lines.

The basis of the test methodology for the electrical crosstalk performance measurements was to test both the old and the new integrated circuit tactile sensor designs, and then compare the results. To establish a starting point, a taxel numbering system, shown in Figure 4.2, was adopted. This taxel numbering system was also used when the additional circuitry was associated with each taxel. For example, the taxel input line associated with taxel number 1 will be called "taxel input line 1." Also, the amplifier connected to taxel input line 1 will be defined as "amplifier 1" (see Figure 4.2). Similarly, the input of amplifier 1 is also connected to pad input line 1, and the output of amplifier 1 is connected to pad output line 1. Both the old and the new integrated circuits will be described using the same taxel numbering scheme. However, it should be noted that although the taxel

numbers (amplifier numbers, taxel input line numbers, pad input line numbers, and pad output line numbers) are the same, the relative order or position of the pad input, taxel input, and pad output lines for the old and new integrated circuit designs are different. For example, the old integrated circuit has the pad input lines from amplifier number 6 and number 13 directly adjacent to the pad input line from amplifier 21, while the new integrated circuit design has pad input lines from amplifier number 6 and number 14 directly adjacent to the pad input line from amplifier number 21.

Now that the taxel numbering scheme has been explained, the method used to accomplish the electrical crosstalk measurements will be presented. In order to collect test data, the test configuration shown in Figure 5.2 was used. In the previous research efforts, several minutes were required to process the actual measured results and display them on the computer screen. To enhance the speed of this process, a new method for processing the sensor data was developed. The new method used "up front" data processing to process the data as soon as it was retrieved from the digital storage oscilloscope. This feature reduced the time required for processing the data from several minutes to approximately three seconds.

The electrical crosstalk data was collected by biasing a single taxel input line and recording the output voltage response from all 64 taxels. For example to determine the crosstalk due to taxel 7's associated pad input line, taxel input line, and pad output line, taxel 7's pad input line was stimulated with a DC voltage. A 6.21 V DC stimulation voltage was used to be consistent with previous research. The outputs of all 64 taxel amplifiers were multiplexed and stored using
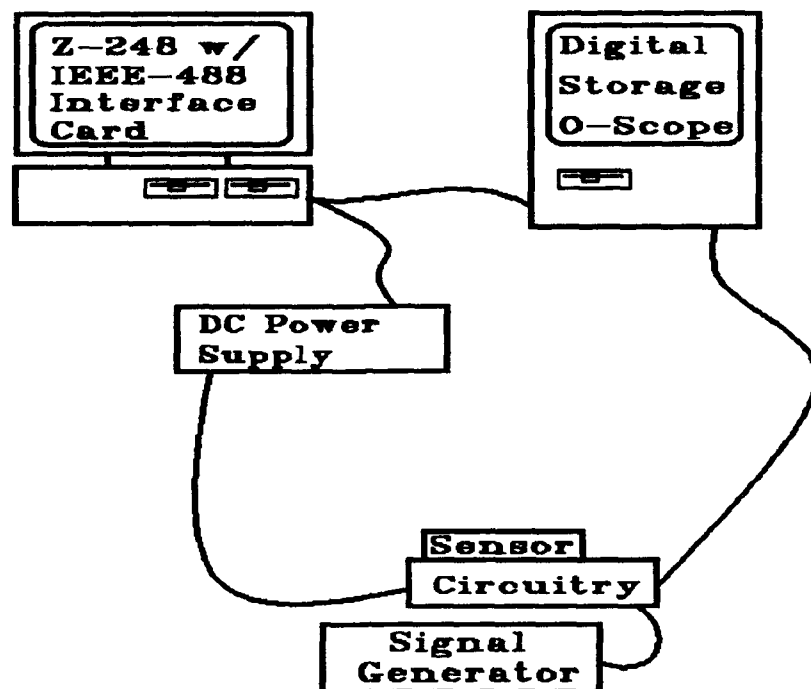
Figure 5.2. Instrumentation configuration used to accomplish the electrical crosstalk measurements.

the IEEE 488 bus interface and a computer. The output voltage response of each taxel's amplifier was determined using a two step process.

The two step process implemented to determine the output voltage response of each taxel's amplifier consisted of a pre-stimulus step and a post-stimulus step. The concept for the two step process stems from the characteristics of the sensor. With the integrated circuit tactile sensor circuitry biased for operation, but no load or input stimulus applied to the taxels, the output voltage of each taxel's amplifier migrates to a voltage level that is characteristic of that taxel. This output voltage level is constant for each taxel's amplifier, but it varies from integrated circuit to integrated circuit; therefore, to determine the change in the voltage level of a taxel's amplifier due to an applied stimulus (in tnis case, crosstalk attributable to a single

5-7

taxel's pad input line voltage level change) a pre-stimulus sensor
reading on all 64 taxels is accomplished and recorded. Then a single
taxel's pad input line is stimulated with a DC voltage level (for
example taxel 7's pad input bias line). One second after the input
stimulus is applied, the post-stimulus reading of all 64 taxels is
accomplished and recorded. The sensor's response then becomes the
difference between the post-stimulus and pre-stimulus sensor
measurements.

To accomplish a sensor reading (pre-stimulus or post-stimulus),
the outputs of the integrated circuit amplifiers must be multiplexed
using high impedance analog multiplexers. The output of the multiplexer
circuitry is displayed and stored on a digital storage oscilloscope
(DSO). The DSO stores 500 data points per channel. Since the data from
the 64 taxels is displayed across the DSO screen, each taxel output is
represented by 7 to 8 DSO data points. The program used to retrieve and
store the data points takes three data points from the middle of the set
of 7 to 8 data points used to represent each taxel's response. These
three data points are compared to each other to insure the voltage
levels of the three points only differ within a reasonable limit (a
reasonable limit was established empirically by examining the 500 data
points from several sensor measurements). If this condition is
satisfied, the three data points are averaged to form a sensor taxel
reading, otherwise the program interrupts and an error message is
displayed. Since the multiplexed taxel data is not in the same order as
the taxel numbering scheme, the taxel data is reordered in ascending
order starting with the reading from taxel number one. These 64 taxel

readings compose the sensor reading. Using this method, sensor readings can be accomplished in approximately one second.

Now that the method for taking sensor readings has been explained, the methodology for determining the sensor's electrical crosstalk will be described. As stated earlier, the source of the electrical crosstalk was initially thought to be caused by the relative spacing of the pad input lines [8]; therefore, the spacing of the integrated circuit pad input lines was varied as explained in Chapter 4. To determine how the spacing of the lines affected crosstalk, the old integrated circuit (designed by Capt Dyson [8]) and the new integrated circuit were tested. The order of the pad input lines and the pad output lines on the new integrated circuit design is: 2 1 10 3 28 11 4 19 12 5 20 13 6 21 14 7 8 16 15 24 23 22 32 31 30 29 40 39 38 48 47 56 63 64 55 62 37 54 61 46 53 60 45 52 59 44 51 58 57 49 50 41 42 43 33 34 35 36 25 26 27 17 18 9 and back to 2 (see Figure 4.2). It is noted that the order of the lines indicates which lines (and also bond pads) are directly adjacent to each other. For example, on the new integrated circuit, pad input lines 2 and 10 lie directly adjacent to pad input line 1, and pad output lines 2 and 10 lie directly adjacent to pad output line 1. The order of the pad input lines and pad output lines on the old integrated circuit is: 1 2 10 3 11 19 4 12 20 28 5 13 21 6 14 7 8 16 15 24 23 22 32 31 30 29 40 39 38 48 47 56 64 63 55 62 54 46 61 53 45 37 60 52 44 59 51 58 57 49 50 41 42 43 33 34 35 36 25 26 27 17 18 9 and back to 1. In order to determine the worst case electrical crosstalk, some of the longest pad input lines, the pad input lines corresponding to taxel 28 and 29, were stimulated on both the old and the new integrated circuit for comparison. Similarly, in order to validate that the cause of the

electrical crosstalk was the placement of the pad input lines, the taxels whose pad input lines were the shortest, the pad input lines corresponding to taxel 8 on the new and old integrated circuit, were stimulated. Since the pad input line on taxel 8 does not run next to any other pad input line, if the electrical crosstalk is caused solely by the pad input line placement, then when taxel 8 is stimulated, the output of the integrated circuit will show no electrical crosstalk. Once the electrical crosstalk for the various taxels is determined, the percent change of the output of the electrode that is experiencing electrical crosstalk is calculated using the following equation:

$$\%\text{crosstalk} = \left(\frac{\Delta V_i}{\Delta V_{\text{stimulated}}} \right) \times 100\% \tag{5.1}$$

where $\%_{\text{crosstalk}}$ is the percent crosstalk due to the stimulated taxel's pad input line, taxel input line, and/or pad output line; ΔV_i is the change in the ith taxel amplifier's output voltage (V); and $\Delta V_{\text{stimulated}}$ is the change in the stimulated taxel amplifier's output voltage (V). The distance between the pad input lines and pad output lines experiencing electrical crosstalk was recorded for comparison between the old and the new circuit design.

After the electrical crosstalk of the old and new integrated circuits was quantified, tactile sensors were fabricated from the new integrated circuit design (the PVDF film was attached) and characterized. (Specific sensor fabrication procedures are outlined in Chapter 4.)

5.4. Tactile Sensor Response Characterization

After the electrical crosstalk of the revised integrated circuit tactile sensor was quantified, its static applied load response was characterized. Sensor characterization included quantifying the sensitivity, accuracy, and predictability of the sensor's response. To facilitate the characterization of the tactile sensor's response, several basic terms need to be defined. Load is defined as the force that is applied to the surface of the sensor. A gram of force (gmf) will be used to describe the load applied to the tactile sensor and the response of the tactile sensor. Grams of force (gmf) is defined as the amount of force, with an associated characteristic mass, exerted on the tactile sensor. For example, a 50 g object will exert a 50 gmf (0.491 N) on the surface of the sensor when the object is placed on the active area of the sensor.

A brief explanation of how the data was taken is also in order. Similar to the method explained for accomplishing the electrical crosstalk measurements, the method for implementing the load measurements is significantly improved relative to the prior research [8]. In prior research, several minutes elapsed between the instant a sensor measurement for a given load was accomplished and the time that the measured data was processed and displayed on the computer screen. To enhance the speed up these processes, a new method for processing the sensor data was developed. The new method employs "up front" data processing to process the data as soon as it is retrieved from the digital storage oscilloscope. This concept reduced the time required for processing the measured data from several minutes to approximately three seconds.

Sensor response data was gathered by stimulating different combinations of taxels with a square, round, and rectangular shaped load, using the load application device shown in Figure 5.3, and recording the multiplexed voltage response of all 64 taxels. For example to determine the response of the sensor to a load applied to certain taxels on the sensor, the load was applied and the outputs of all 64 taxels were multiplexed and stored using the IEEE 488 bus interface and a computer. The output voltage response of each taxel was determined by implementing a two-step process similar to the one that was explained in the crosstalk section described earlier in this chapter.
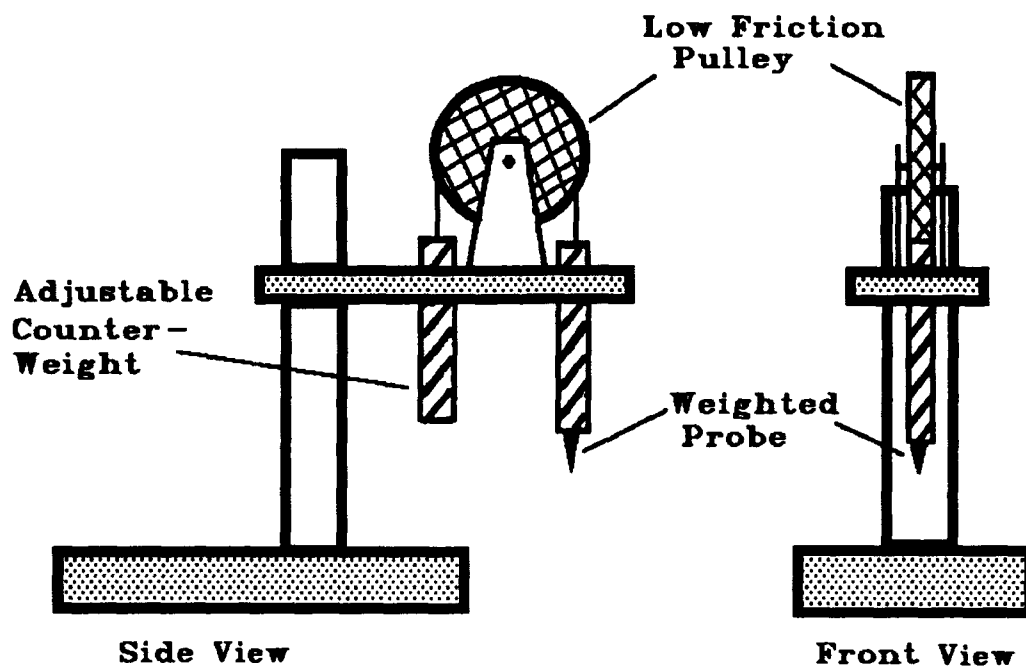
Figure 5.3. Test load application device.

The two-step process implemented to determine the output voltage response of each taxel to a load consisted of a pre-load and a post-load

step. The concept for this two step process was motivated by the characteristics of the sensor. When the integrated circuit tactile sensor circuitry was pre-biased for operation, but with no load applied, the output voltage of each taxel's amplifier migrated to a voltage level that was characteristic of that amplifier. When the pre-bias was removed, the output of each amplifier decayed to a voltage level that was nearly constant for each taxel, but it varied from integrated circuit to integrated circuit. Therefore, to eliminate this characteristic decay from the sensor's response, a pre-load response is subtracted from the loaded response. All 64 taxels are pre-biased with a voltage level to insure they possess a known initial bias state that is near the lower end of the amplifier's linear region. This bias state is recorded using the DSO. The bias is removed and after one second, a second unloaded sensor measurement is accomplished. The difference between these two measurements, known as the unloaded sensor measurement, is recorded for each taxel. Next, the bias is reapplied to each taxel. Just before the load is applied, the bias is removed. The load is then applied within one second after the bias is removed, and the loaded sensor measurement is accomplished. The difference between the unloaded and loaded sensor measurement is used to form the sensor's response for each taxel relative to the load. The sensor's response is then recorded. Now that the method for accomplishing loaded sensor measurements has been explained, the methodology for determining the sensor's characteristics will be described.

5.4.1. *Sensor Force Sensitivity*. The sensor's force sensitivity is defined as the minimum force differential that the sensor can

resolve. In order to determine the force sensitivity, the sensor must first be calibrated. The test configuration shown in Figure 5.4 was used to experimentally calibrate the sensor. A relationship for the average response value relative to the force applied to a sensor's taxel and the voltage output from the sensor's amplifier was determined to calibrate the sensor. To accomplish this task, a square-shaped load (approximately 400 μm x 400 μm, or the size of one taxel) was applied to the sensor and its weight was incrementally increased from 1 to 150 g. The loads (1 to 150 g) were each applied to five different taxels (5, 21, 29, 43, and 57). Assuming the load was distributed uniformly across the loaded taxels, the average value of the taxel amplifier outputs, taxel response, for a given load were plotted versus the value of the applied load. The average taxel response (V_{ave}) for a given load magnitude was calculated using the following relation:

$$V_{ave} = \frac{\sum V_i}{N} \qquad (5.2)$$

where V_{ave} is the average taxel response of the loaded taxels (V), V_i is taxel response of the i_{th} loaded taxel (V), and N is the total number tested taxels. Average taxel response versus load data was curve fitted, using a linear least-squares technique, to generate a taxel response versus load calibration curve. The sensor's force sensitivity was found by taking the slope of the taxel response versus load calibration curve and multiplying it times the minimum input voltage differential detectable at the output of the sensor's amplifiers. The electrometer was used in conjunction with the Micromanipulator probe station to determine the minimum input voltage differential detectable at the output of the sensor's amplifiers.
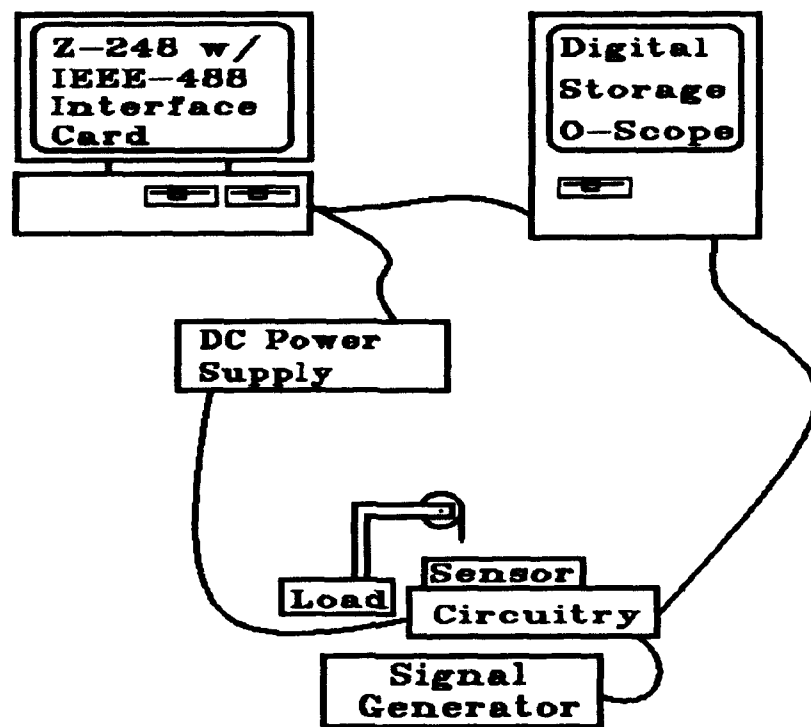
Figure 5.4. Test configuration for measuring the sensor's response due
to an externally applied load.

5.4.2. *Sensor Pressure Accuracy*. The sensor's pressure accuracy
is defined as the percent difference between the taxel response
indicated by the tactile sensor and the taxel response calculated using
the calibration equation. The average taxel response was determined for
several loads (1 to 150 gmf), and correspondingly, the calculated taxel
response was determined for the same loads. The percent difference
between the average taxel response and the calculated taxel response was
plotted versus the applied load.

5.4.3. *Sensor Voltage Predictability*. The sensor's voltage
predictability is defined as the percent difference between the voltage
change indicated by the tactile sensor versus the value calculated using
the fundamental piezoelectric equations. Loads spanning 1 to 150 grams

5-15

were applied to the surface of the tactile sensor. The corresponding taxel responses were measured using the configuration shown in Figure 5.4. The indicated change in the voltage (V_i) of the i_{th} taxel due to a load applied to the i_{th} taxel was measured and recorded. The predicted change in voltage (V_{pi}) of the i_{th} taxel due to a load applied to the i_{th} taxel can be found from the following equation:

$$V_{pi} = \frac{d_{33} t m g}{\epsilon A} \qquad (5.3)$$

where

V_{pi} is the predicted voltage developed on the i_{th} taxel (V),

d_{33} is the piezoelectric charge constant (19.5 pC·N^{-1}) [63],

t is the thickness of the PVDF film (40·10^{-6} m),

m is the mass of the load applied to the i_{th} taxel (kg),

g is the acceleration due to gravity (9.81 m·s^{-2}),

ϵ is the permittivity of the PVDF film (1.01·10^{-10} F·m^{-1}) [63],

A is the area of the i_{th} electrode covered by the load (m^2).

5.4.4. Sensor Object Imaging Capability. Square (2.5 mm x 2.5 mm), round (2-mm diameter), and rectangular (0.7 mm x 6 mm) shaped loads were applied to the surface of the tactile sensor (50, 75, and 100 g masses were used for each shape). The multiplexed signal from the tactile sensor was stored using the program listed in Appendix D. The voltage level change, or taxel response, (post-load minus pre-load) was plotted for each taxel using a bar graph format, and a three-dimensional plot of the amplitudes for each taxel was generated using the MATLAB simulation software. A threshold voltage was established empirically. If the change in voltage (post-load minus pre-load) on a taxel exceeded

this threshold value, that taxel was considered "ON", and if the change in voltage (post-load versus pre-load) on a taxel did not exceed this threshold value, that taxel was considered "OFF". A two-dimensional plot of the "ON" taxels (represented by black squares) and "OFF" taxels (represented by white squares) was visually compared to the position of the actual test load shapes.

Additionally, a data processing algorithm was established for comparing the actual shape of the load to the shape seen by the sensor. The idea behind the algorithm was to account for the "dead space" between the taxels on the integrated circuit. The algorithm can be understood by letting the area covered by the taxels and the area between the taxels be represented by nodes. There are three types of nodes. The first node type, indicated by the shaded region labeled Node 1 in Figure 5.5, is used to represent the area of the taxels. The second node type, indicated by the shaded region labeled Node 2 in Figure 5.5, is used to represent the area between two adjacent taxels. The third node type, indicated by the shaded region labeled Node 3 in Figure 5.5, is used to represent the area surrounded by four taxels. When a taxel is "ON", its Node 1 is represented by a solid black square. When a taxel is "OFF", its Node 1 is represented by a solid white square. A node connecting two taxels (Node 2) is represented by a solid black rectangle if both of the taxels are "ON", a solid white rectangle if both of the taxels are "OFF", or a rectangle with a black border and white center if either one of the taxels is "ON" and the other is "OFF". A node connecting four taxels (Node 3) is represented by a solid black square if at least three of the four taxels are "ON" or if two of the four taxels that are nonadjacent are "ON"; a solid white square if all

four taxels are "OFF"; or a square with a black border and white center if two of the four taxels that are adjacent are "ON" and the other two are "OFF". After the nodal representation of the object seen by the sensor is complete, the centers of the rectangles or squares that have black borders and white centers are then considered to form a rudimentary border which encompasses the area of the load. For validation of the algorithm, the area enclosed by connecting the centers of the nodes with black borders and white centers was compared to the area of the actual applied load. The data acquisition program used to determine the nodal representation of the sensor is part of the SHAPE.BAS program listed in Appendix D.
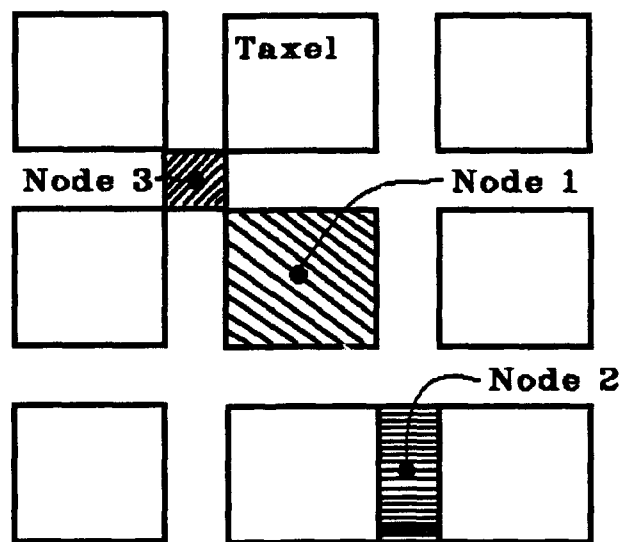
Figure 5.5. The node representation for the algorithm used to determine an ojects area. The shaded area indicates the rectangular or square shape associated with each node.

5.5. *Investigation of the Tactile Sensor's Pyroelectric Effects*

The piezoelectric PVDF film also responds to temperature changes. When the temperature in the vicinity of the film changes, the voltage

across the PVDF film increases or decreases depending upon the film's orientation (polarization).

The pyroelectric response of the piezoelectric tactile sensor due to uniform heating was characterized. Uniform tactile sensor heating was accomplished by placing a voltage-controlled heater (Figure 4.12) on top of the integrated circuit tactile sensor. During the test, the voltage response (taxel response) of the individual taxels was measured with a digital storage oscilloscope (DSO), and it was stored on the microcomputer equipped with an IEEE-488 interface card. The program for the data analysis was written using the BASIC computer language and is documented in Appendix D. The bandwidth, sensitivity, accuracy, and predictability of the sensor's response to uniform heating was characterized.

5.5.1. Temperature Polarity Test. The tactile sensor system was tested to establish its pyroelectric polarity response relative to that associated with its piezoelectric response. The pyroelectric response was recorded when the sensor was uniformly heated (after heating, its response as it cooled was observed relative to the discussion (Appendix B) covering the polarity determination of the PVDF film sample that was to be attached to the IC sensor). The output voltage of the amplifiers should decrease when the sensor is heated. The test configuration is shown in Figure 5.6. The procedure for implementing this test is simple. A small heater (Figure 4.12) was used to heat the sensor. The response of the tactile sensor was recorded, and its response polarity was determined.
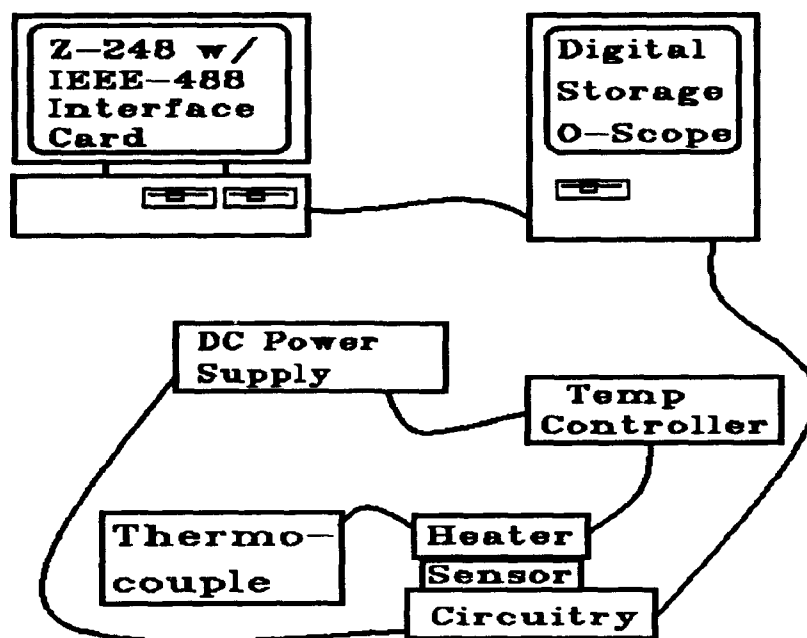
Figure 5.6. Test configuration for accomplishing the pyroelectric response evaluation.

5.5.2. Temperature Response Bandwidth. The pyroelectric response bandwidth of the tactile sensor is an indication of the time required for the sensor to react to a temperature change. The pyroelectric response bandwidth of the piezoelectric tactile sensor is defined as the inverse of the thermal time constant of the sensor. The thermal time constant is defined as the thermal excitation time constant. Thermal excitation of the sensor occurred when it experienced a positive change in temperature. The thermal excitation time constant can be predicted from the following equation [11]:

$$\tau_{PET} = R_T C_T \qquad (5.4)$$

where τ_{PET} is the predicted thermal excitation time constant of the sensor (s), R_T is the thermal resistance of the PVDF film ($K \cdot W^{-1}$), and C_T is the thermal capacitance of the film ($J \cdot K^{-1}$). The thermal resistance (R_T) describes the losses which occur when heat propagates through the film, and it can be calculated using the following equation [68]:

$$R_T = \frac{t}{GA} \qquad (5.5)$$

where t is the thickness of the film (m), G is the thermal conductivity of the film ($W \cdot K^{-1} \cdot m^{-1}$), and A is the surface area of a taxel (m^2). On the other hand, the thermal capacitance (C_T) of the film is a measure of the film's thermal energy storage capacity. The thermal capacitance of the film can be calculated using the following equation [69]:

$$C_T = C_V m \qquad (5.6)$$

where C_V is the constant volume specific heat of the film ($J \cdot kg^{-1} \cdot K^{-1}$) and m is the mass of the film on one taxel (kg). Using Equation (5.4) through Equation (5.6), with $t = 4 \cdot 10^{-5}$ m, $G = 0.13$ $W \cdot K^{-1} \cdot m^{-1}$ [11], $A = 1.6 \cdot 10^{-7}$ m^2, $C_V = 2.4 \cdot 10^6$ $J \cdot kg^{-1} \cdot K^{-1}$ [11], and $m = 1.14 \cdot 10^{-8}$ kg, the predicted value for the thermal excitation time constant is $\tau_{PET} = 52$ seconds. The predicted pyroelectric response bandwidth of the sensor can be found using the following equation:

$$BW_{predicted} = \frac{1}{\tau_{PET}} \qquad (5.7)$$

where $BW_{predicted}$ is the predicted pyroelectric response bandwidth of the PVDF film (Hz). Using $\tau_{PET} = 52$ seconds, $BW_{predicted}$ becomes 0.19 Hz. The measured tactile sensor pyroelectric response bandwidth will be defined as the inverse of the average of the thermal excitation time constant

for the sensor's response relative to a change in temperature that can be modeled as a step-input function (ΔT versus time).

5.5.3. *Sensor Temperature Sensitivity.* Temperature sensitivity is defined as the minimum temperature differential that the sensor can resolve. To experimentally determine the sensor's thermal sensitivity, the sensor needed to be thermally calibrated. The test configuration shown in Figure 5.5 was used for thermal calibration. The temperature sensitivity was determined by implementing the following test protocol:

A. The heater in Figure 4.12 is positioned on top of the sensor.

B. The temperature of the heater and sensor will be recorded via the thermocouple.

C. The voltage output of the tactile sensor will be recorded.

D. The temperature of the heater and sensor will be increased to $29 \pm 1°C$.

E. The response of the sensor will be recorded. (The response of the sensor is defined by the following equation:

$$\Delta V_{Thermal} = \sum \frac{\Delta V_i}{N} \qquad (5.8)$$

where $\Delta V_{Thermal}$ is the average change in voltage of the sensor (V), ΔV_i is the change in voltage of the i_{th} taxel (V), and N is the total number of taxels.

F. The temperature of the heater will be decreased to room temperature.

G. The sensor will be allowed to cool to room temperature. (A heat sink may be used to expedite cooling the sensor.)

H. Steps A. through G. will be repeated with the temperature of the heater increased to 31 ± 1°C instead of 29 ± 1°C.

I. Steps A. through G. will be repeated with the temperature of the heater increased to 33 ± 1°C instead of 29 ± 1°C.

J. Steps A. through G. will be repeated with the temperature of the heater increased to 36 ± 1°C instead of 29 ± 1°C.

K. Steps A. through G. will be repeated with the temperature of the heater increased to 39 ± 1°C instead of 29 ± 1°C.

L. Steps A. thorough K. will be repeated three times over a three day period.

A relationship between the change in temperature and the taxel response from the sensor's amplifiers was established to calibrate the sensor. Assuming that the temperature was uniformly distributed across the surface of the sensor, the taxel response was plotted versus the change in temperature. The taxel response for each ΔT was calculated using the following equation:

$$\Delta V_{ave} = \frac{\Delta V_i}{N} \tag{5.9}$$

where ΔV_{ave} is the average taxel response of the taxels (V), ΔV_i is the taxel response of the i_{th} taxel (V), and N is the total number of taxels tested. The average taxel response versus ΔT data points were curve fitted using a linear least-squares technique to form a taxel response versus ΔT calibration curve. The slope of the taxel response versus ΔT curve was used to determine the temperature sensitivity of the sensor. The temperature sensitivity is found by multiplying the slope of the calibration curve by the minimum input voltage differential detectable at the output of the sensor's amplifiers.

5.5.4. *Sensor Temperature Accuracy.* Temperature accuracy is defined as the percent difference between the average taxel response of the sensor and the taxel response calculated using the calibration equation as a function of an applied temperature differential. The sensor's temperature accuracy will be represented by plotting the percent difference between the average taxel response and the calculated taxel response for several ΔT's.

5.5.5. *Sensor Temperature Predictability.* The sensors's temperature predictability is defined as the percent differenc ·f the change in voltage of the sensor due to a change in temperature versus the change in voltage predicted by the fundamental pyroelectric equations. The same data used in the sensor temperature accuracy test was used to complete this analysis.

The change in voltage of the sensor can be calculated using the following equation:

$$\Delta V_{indicated} = \sum \frac{\Delta V_i}{N} \tag{5.10}$$

where $\Delta V_{indicated}$ is the indicated voltage change of the tactile sensor (V), ΔV_i is the change in voltage of the i_{th} taxel after the temperature is changed (V), and N is the total number of taxels. The predicted DC output of the detector due to the pyroelectric effect is given by the following equation [11]:

$$\Delta V = \frac{A_v p t \Delta T}{\epsilon} \tag{5.11}$$

where

ΔV is the sensor's output voltage (V),

A_v is the voltage gain of the amplifiers,

p is the pyroelectric coefficient ($C \cdot m^{-2} \cdot K^{-1}$),

t is the PVDF film thickness (m),

ΔT is the temperature change of the PVDF film (K),

ϵ is the permittivity of the PVDF film ($1.01 \cdot 10^{-10}$ $F \cdot m^{-1}$) [63].

6. Tactile Sensor Performance Results and Analysis

6.1. Introduction

This chapter presents the tactile sensor's performance results and analysis. First, the results and analysis for enhancement of the amplifier's linear range is presented. Then, the data and analysis for the electrical crosstalk and tactile sensor performance characterization will be presented. Finally, the data for the pyroelectric performance characterization will be presented.

6.2. Evaluation Results and Analysis for Signal Range Enhancement

One of the primary goals of this thesis was to enhance the linear signal range of the piezoelectric tactile sensor. In order to accomplish this goal, it was necessary to enhance the linear range of the tactile sensor's amplifiers. The data for the amplifier with increased channel length and the data for the differential amplifier is presented and analyzed. The results are then used to determine which amplifier design should be added to the integrated circuit tactile sensor.

6.2.1. *Amplifiers with Increased Channel Length*. The data for the amplifiers with increased channel length is shown in Figure 6.1 through Figure 6.12. For this analysis, two terms are defined: amplifier degradation and amplifier breakdown. Since, the long term simulation data (presented later in this section) indicated the amplifier output should increase linearly as the V_{DD} supply voltage was increased linearly, amplifier degradation is defined as occurring

6-1
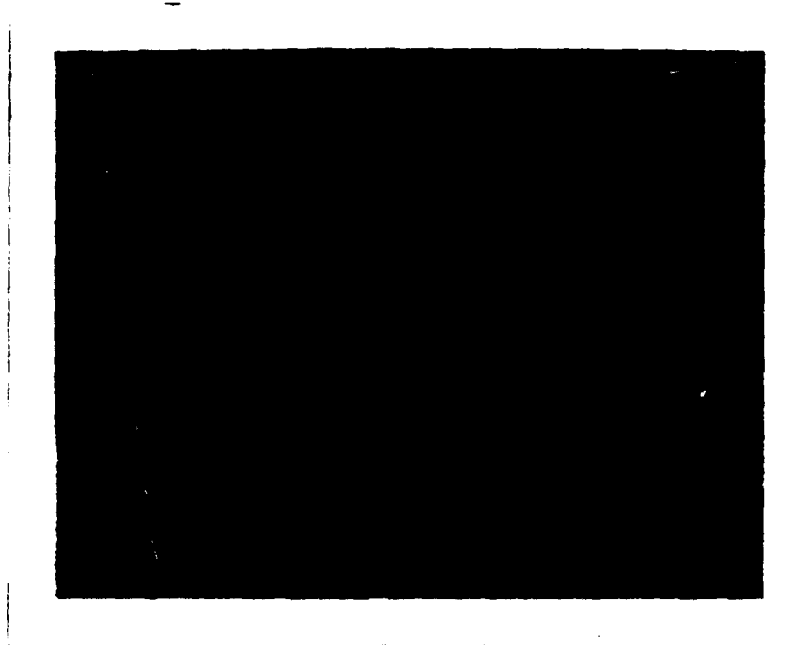
Figure 6.3. Picture of failed via.
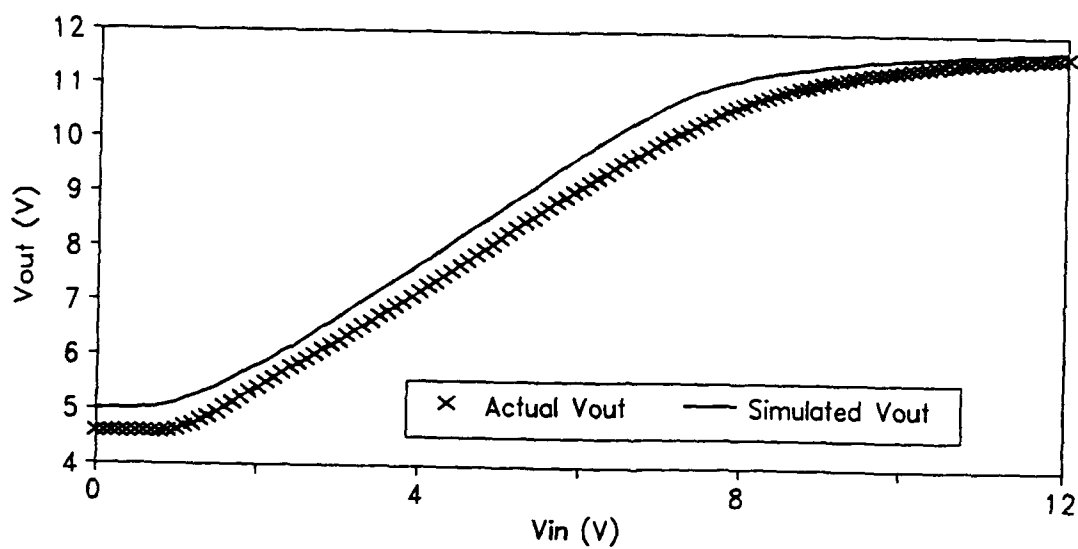
Figure 6.4. V_{out} versus V_{in} for the amplifier with channel length of 2 μm.
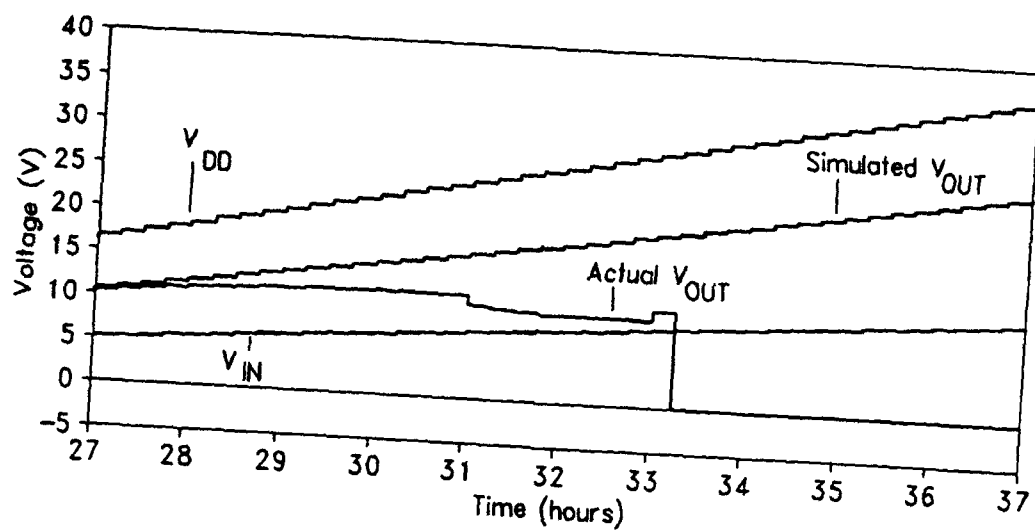
Figure 6.1. Data for the long term amplifier test for the MOSFETs with channel length of 2 μm.
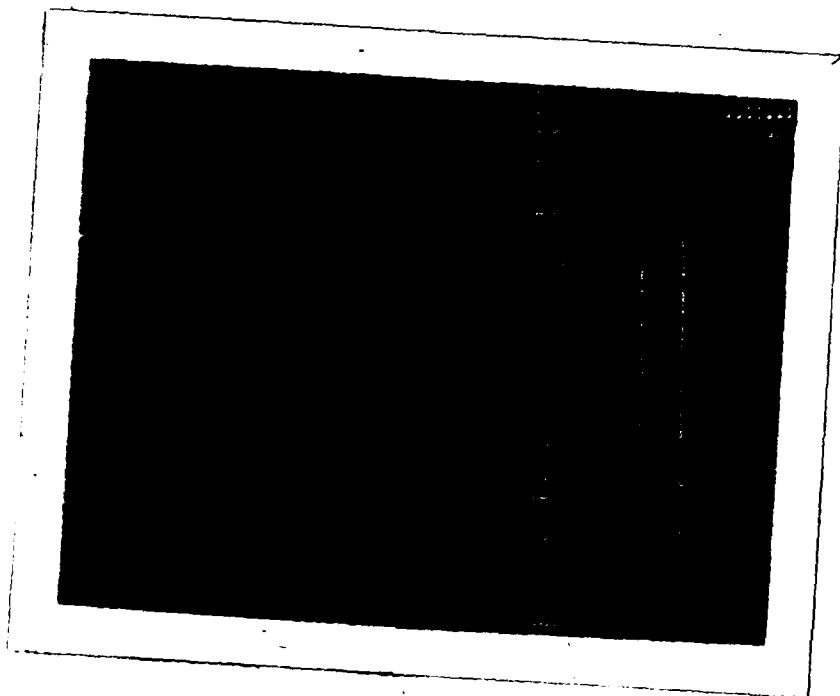
Figure 6.2. Picture of failed via.
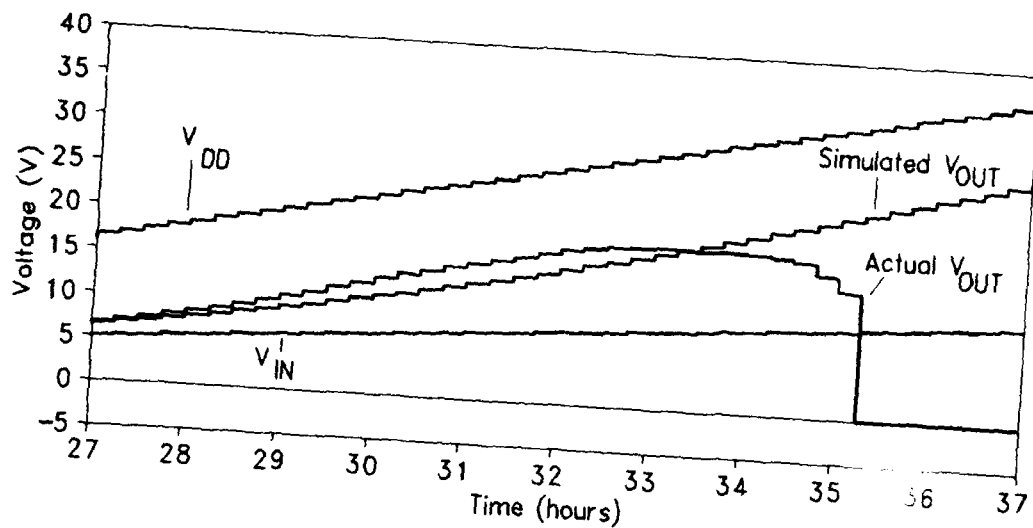
Figure 6.5. Data for the long term amplifier test for the MOSFETs with channel length of 18 μm.
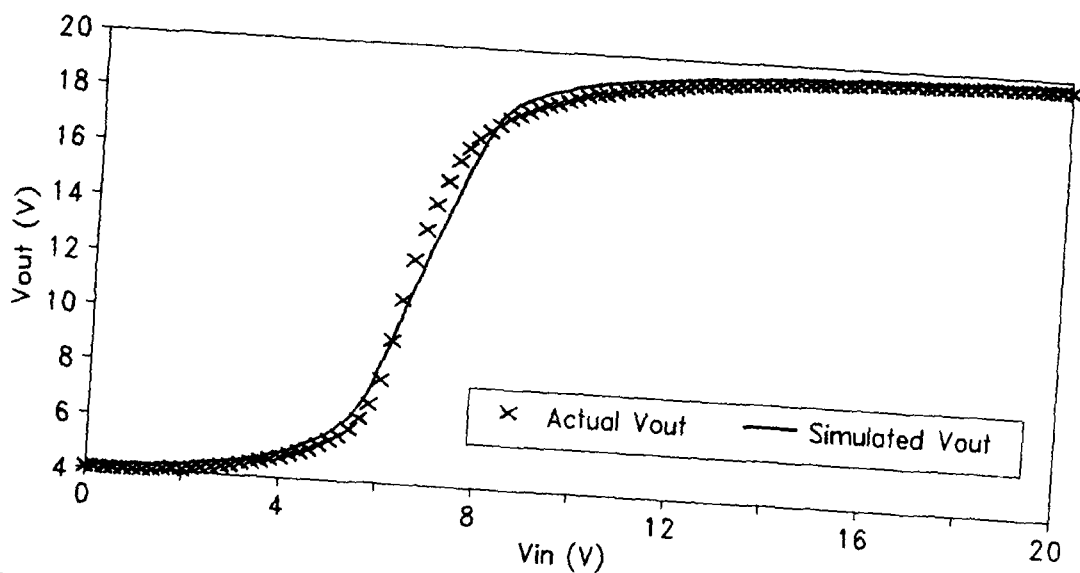
Figure 6.6. V_{out} versus V_{in} for the amplifier with channel length of 18 μm.
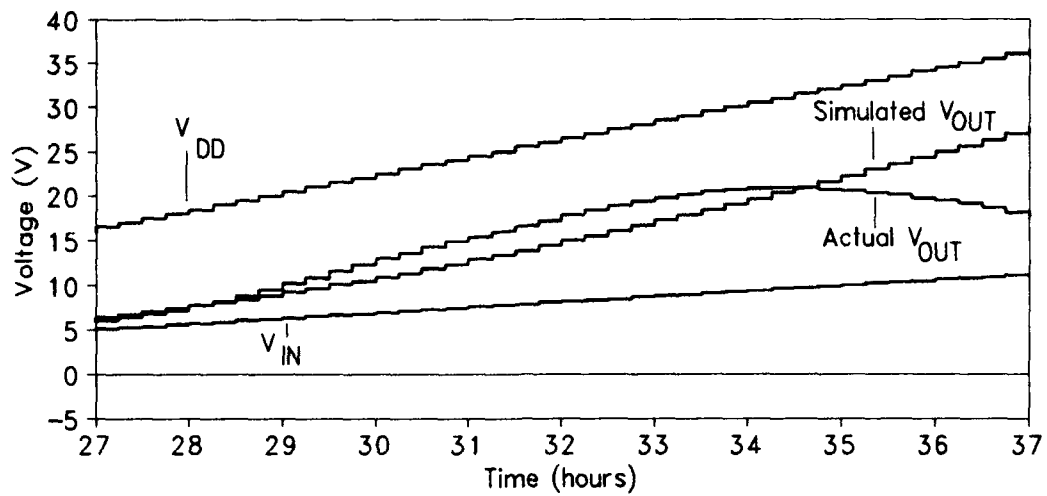
Figure 6.7. Data for the long term amplifier test for the MOSFETs with channel length of 34 μm.
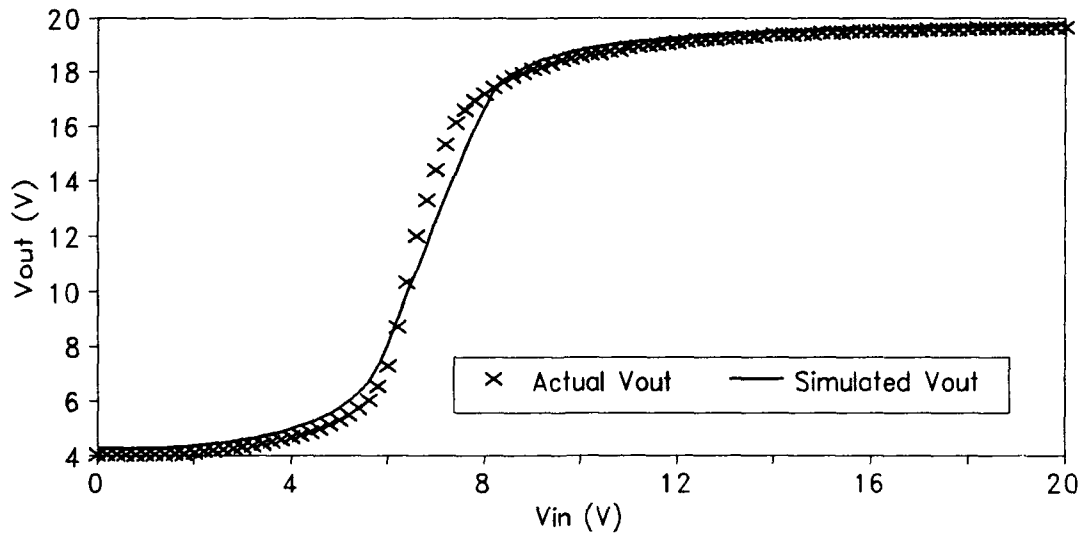
Figure 6.8. V_{out} versus V_{in} for the amplifier with channel length of 34 μm.
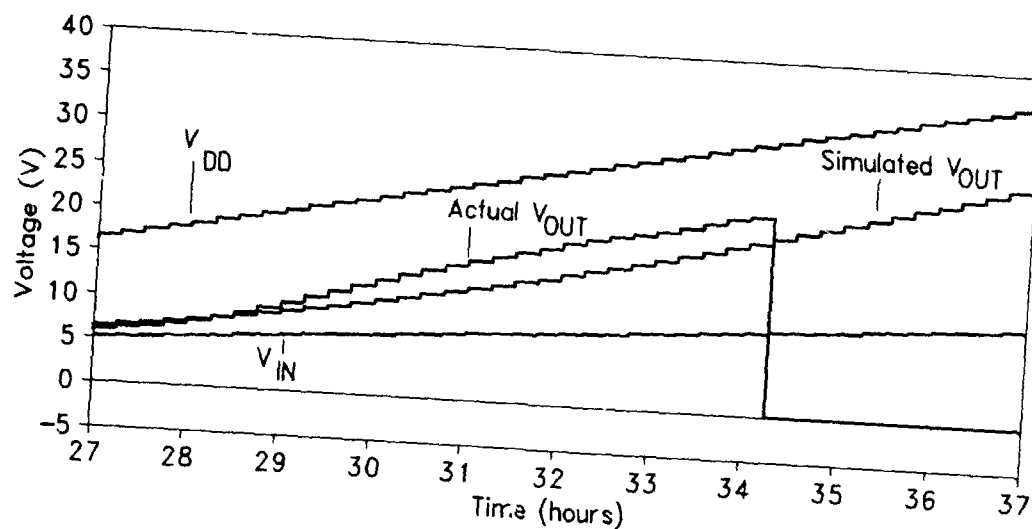
Figure 6.9. Data for the long term amplifier test for the MOSFETs with channel length of 66 μm.
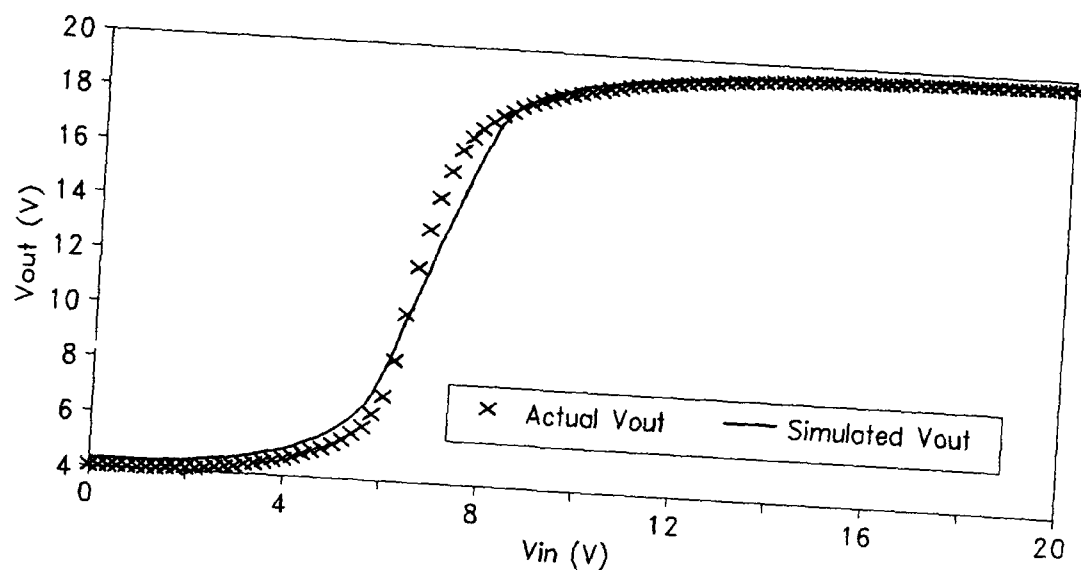
Figure 6.10. V_{out} versus V_{in} for the amplifier with channel length of   66 μm.
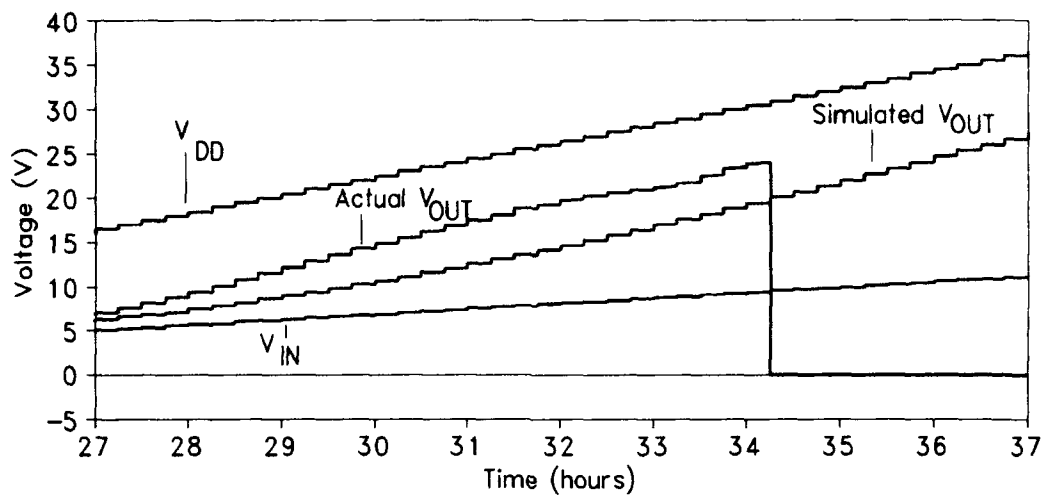
Figure 6.11.   Data for the long term amplifier test for the MOSFETs with channel length of 114 μm.
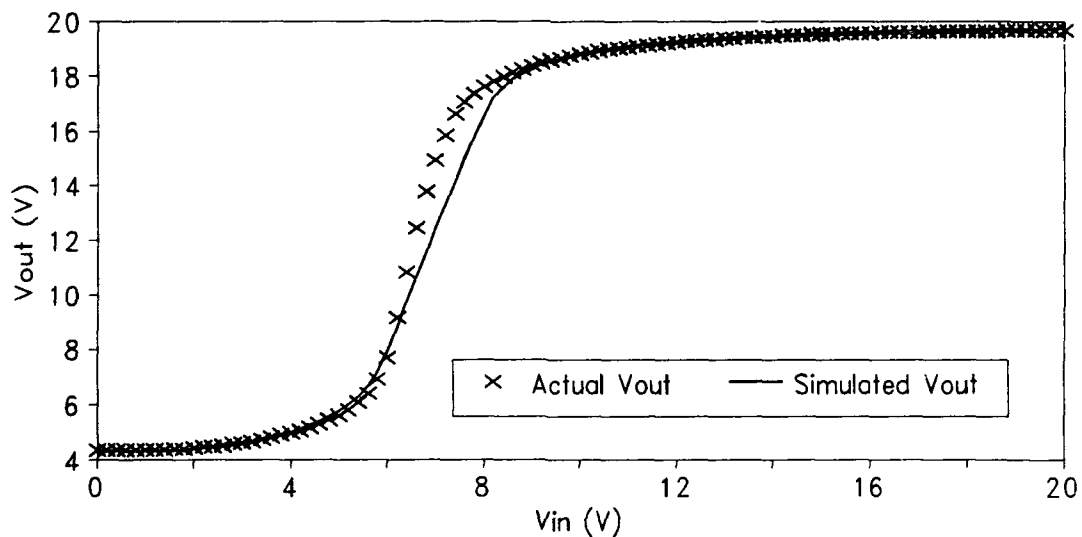
Figure 6.12. V_{out} versus V_{in} for the amplifier with channel length of 114 μm.

when the amplifier output voltage, V_{OUT}, deviates by more than 5% of the

value that V_{OUT} would be if V_{OUT} had continued to increase linearly with

V_{DD}. Five percent was considered significant by considering a 5% change

in V_{OUT} was on the order of 1 V, and a 1 V change in V_{OUT} is well beyond

the minimum input voltage differential detectable at the output of the

sensor's amplifiers (this fact will be verified late in this chapter).

It should be noted that amplifier degradation is not permanent.

Amplifier breakdown is defined as occurring when the amplifier

permanently breaks down. It will be shown later in this section that

amplifier breakdown occurred when the via failed.

Figure 6.1 shows the output of the amplifier with a channel length

of 2 μm as V_{DD} was increased from 10 to 50 V over a 48-hour time period.

Amplifier degradation occurred after approximately 27.75 hours when V_{DD}

was 17 V. Amplifier breakdown occurred after 33.25 hours when V_{DD}

reached 28.5 V. Visual inspection of the amplifier revealed that the

amplifier breakdown was due to breakdown of the via connecting the

diffused resistors to the V_{DD} supply line. Figure 6.2 and Figure 6.3

are representative pictures of failed via for two of the five amplifier

tests. Figure 6.4 shows the output voltage versus the input voltage for

the amplifier with a channel length of 2 μm and V_{DD} of 12 V (12 V was

chosen for V_{DD} because it was previously shown to be the maximum

operating voltage for extended operation of this amplifier design [8]).

The plot indicates that the performance of the amplifier is consistent

with the HSPICE simulation results, and there is a strong correlation

between the simulation plot and the actual measured amplifier output.

The average percent difference between the actual and predicted output

was 7%; therefore, the amplifier was considered to be consistent with the predicted operation.

Figure 6.5 shows the output of the amplifier with a channel length of 18 μm as V_{DD} was increased from 10 to 50 V over a 48-hour time period. Amplifier degradation occurred after approximately 32.5 hours when V_{DD} was 27 V. Amplifier breakdown occurred after 35.25 hours when V_{DD} reached 32.5 V. Visual analysis of the amplifier revealed that amplifier breakdown was caused by breakdown of the via connecting the diffused resistors to the V_{DD} supply line. Figure 6.2 and Figure 6.3 are representative pictures of failed via for two of the five amplifier tests. Figure 6.6 depicts the output voltage versus the input voltage for the amplifier with a channel length of 18 μm and V_{DD} of 20 volts (an increase in V_{DD} from 12 to at least 20 V was a design goal of this thesis effort). The plot indicates that the performance of the amplifier is consistent with the HSPICE simulation, with a worst case percent error of 11%; thus, this amplifier design could be operated with a 20 V V_{DD} power supply.

Figure 6.7 depicts the output of the amplifier with a channel length of 34 μm as V_{DD} was increased from 10 to 50 V over a 48-hour time period. Amplifier degradation occurred after 33.5 hours when V_{DD} was 29 V. Amplifier breakdown occurred after 37.5 hours when V_{DD} reached 37.5 V. Visual analysis of the amplifier revealed that amplifier breakdown was caused by breakdown of the via connecting the diffused resistors to the V_{DD} supply line. Figure 6.2 and Figure 6.3 are representative pictures of failed via for two of the five amplifier tests. Figure 6.8 depicts the output voltage versus the input voltage for the amplifier with channel length of 34 μm and V_{DD} of 20 V. The

graph indicates that the performance of the amplifier is consistent with the HSPICE simulation, with a maximum percent error of 12%; thus, this amplifier design could be operated with a 20 V power supply.

Figure 6.9 and Figure 6.11 depict the output of the amplifier designs with channel lengths of 66 and 114 μm, respectively, as V_{DD} was increased from 10 to 50 V over a 48-hour time period. There was no apparent amplifier degradation until amplifier breakdown occurred. Amplifier breakdown occurred at 34.5 hours when V_{DD} reached 31.5 V, and it was caused by breakdown of the via connecting the diffused resistors to the V_{DD} supply line on the amplifier. Figure 6.2 and Figure 6.3 are representative pictures of failed via for two of the five amplifier tests. Figure 6.10 and Figure 6.12 depict the output versus the input for the amplifiers with channel lengths of 66 and 114 μm, respectively, and a V_{DD} of 20 V. The outputs are consistent with the HSPICE simulation, with maximum percent error of 13%, so the amplifiers could be operated with a 20-volt V_{DD}.

Figure 6.13 depicts the voltage where amplifier degradation occurred versus the channel length of the amplifier. The linear least-squares fit of the data yields the following equation for the channel length (L) versus the V_{DD} value:

$$L = 2.67 \cdot V_{DD} - 46.88 \qquad (6.1)$$

Only the data from amplifiers that exhibited amplifier degradation prior to amplifier breakdown were included in Figure 6.13. With the data presented above, it can be assumed that amplifier degradation was caused by transistor failure, and amplifier breakdown was caused by failure of the via. This assumption is supported by Figure 6.9 and Figure 6.11

where amplifier breakdown occurred before amplifier degradation. Using this assumption and the data in Figure 6.13, it is hypothesized that a transistor channel length of at least 10 μm is required to support a 20 V V_{DD}; however, since no data concerning current in the channels of the transistors was taken in this research, the assumption and the hypothesis warrant further investigation.
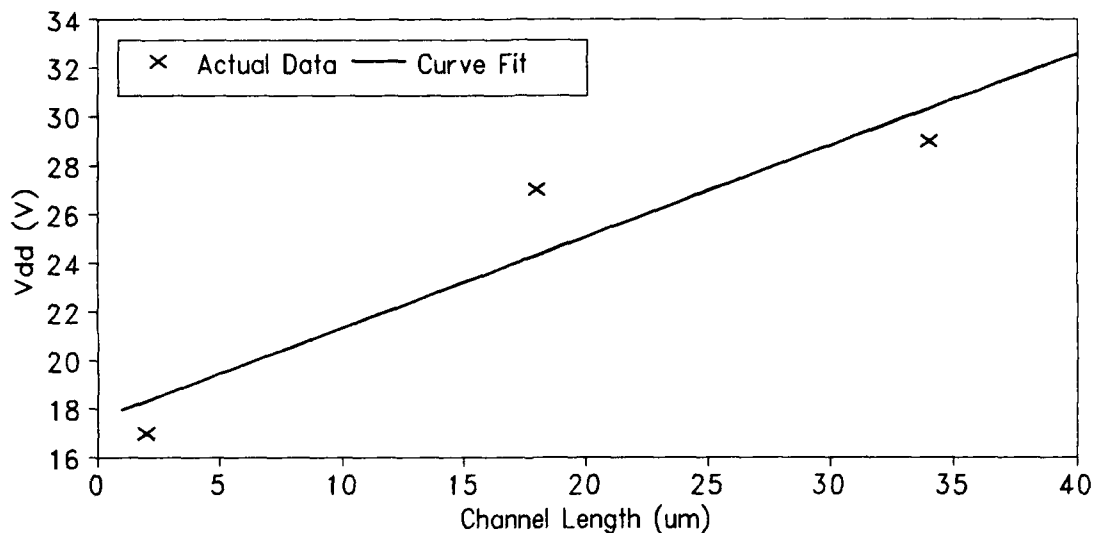
Figure 6.13.   Data for determining the optimum amplifier power supply voltage, V_{DD}, as a function of the MOSFET's channel length, and the linear-least squares curve fit of the data.

6.2.2. Differential Amplifier. Figure 6.14 shows the output voltage versus the input voltage for the simulated and measured values associated with the differential amplifier design. V_{DD} was set to 12 V. The actual output of the amplifier agrees well with the HSPICE analysis, with maximum percent error of 20%. It should be noted that the

amplifier is a step-down amplifier design that is capable of amplifying input signals with amplitudes that exceed the V_{DD} power supply voltage. In the linear range of the amplifier, the gain is 0.5, and the linear input range of the amplifier is 1 to 17 V.
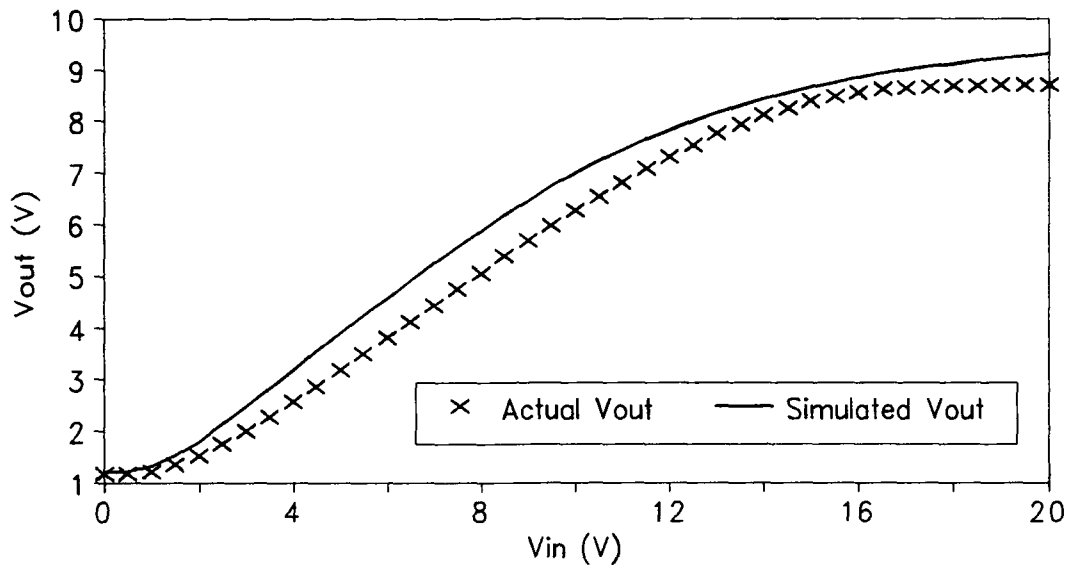
Figure 6.14. V_{out} versus V_{in} for the differential amplifier.

6.2.3. *Summary and Conclusion.* Two methods for enhancing the operational range of the piezoelectric tactile sensor were pursued in this thesis effort. The first method revealed that the V_{DD} supply voltage could be enhanced to values above 20 V. However, the amplifiers fabricated to support this conclusion were designed for proof of concept, and they did not possess large linear ranges. The objective of the analysis was to show that the range of the amplifier could be enhanced by extending the channel length of the MOSFET transistor's. In order to make an amplifier employing this technology that is compatible

with the piezoelectric tactile sensor integrated circuit, the transistor

and resistor sizes need to provide an expanded linear region, while

maintaining a critical MOSFET channel length that is greater than or

equal to 10 μm. The second method pursued a new amplifier design to

replace the existing amplifier in the piezoelectric tactile sensor. To

accomplish this objective, a differential amplifier design was used.

The results revealed the amplifier has a linear range from 1 to 17 V,

and the operating voltage for the amplifier is $V_{DD} - 12$ V. Since the

differential amplifier design possesses a favorable linear range and

only requires a 12 V operating bias (compared to the amplifier designed

with a longer MOSFET channel length), this amplifier design was selected

for adding to the CIF file of the piezoelectric tactile sensor. It

should be noted, however, that a differential amplifier designed with a

minimum MOSFET channel length of 10 μm could combine the best of both

design concepts and could ultimately be extended to an even larger

linear range with a smaller V_{DD} operating bias requirement.

6.3. Electrical Crosstalk

In this section, the results of the electrical crosstalk

evaluation procedures are presented. Figure 6.15 through Figure 6.36

document the resulting electrical crosstalk due to biasing the conductor

lines associated with various clusters of taxels. The data in

Figure 6.15 through Figure 6.36 was analyzed, and the results are

summarized in Table 6.1 and Table 6.2 for the revised and old integrated

circuit design, respectively.

The first column in Table 6.1 and Table 6.2 identifies the taxel

number whose pad input line was stimulated in an attempt to observe
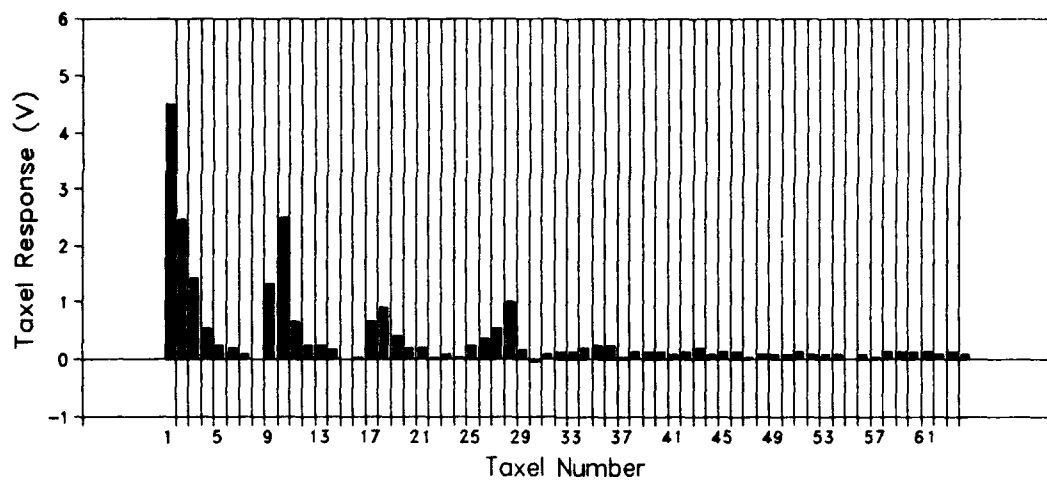
Figure 6.15.   Crosstalk on the new integrated circuit design due to an applied voltage on taxel number 1.
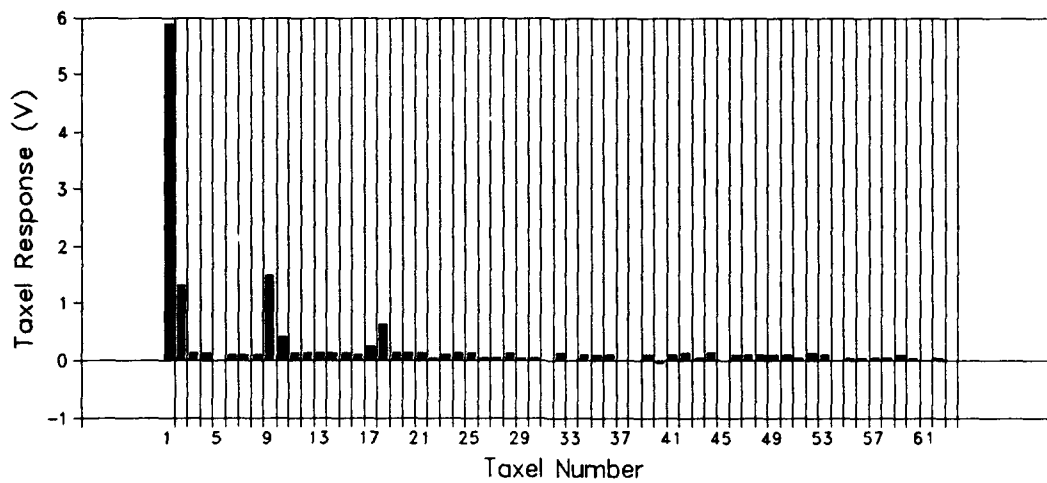
Figure 6.16.   Crosstalk on the old integrated circuit due to an applied voltage on taxel number 1.
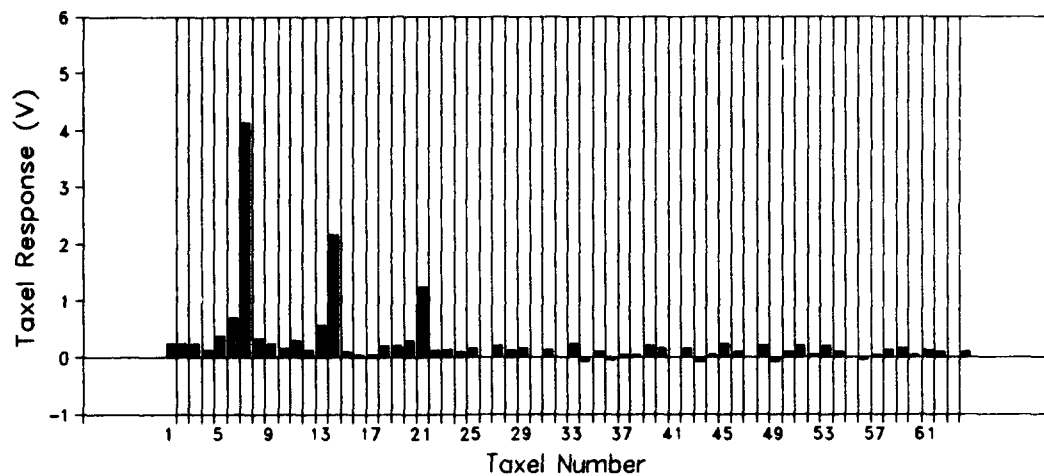
Figure 6.17.   Crosstalk on the new integrated circuit due to an applied voltage on taxel number 7.
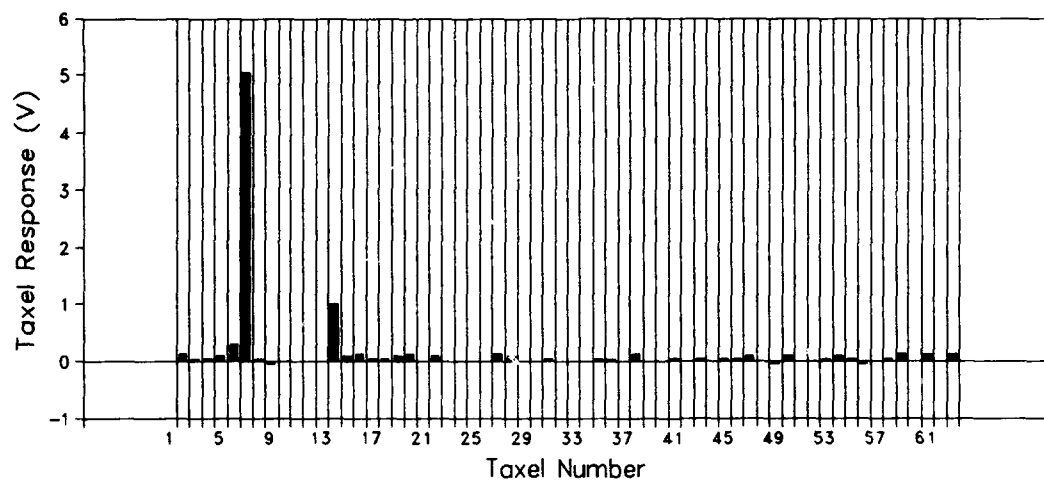
Figure 6.18.   Crosstalk on the old integrated circuit due to an applied voltage on taxel number 7.

6-15
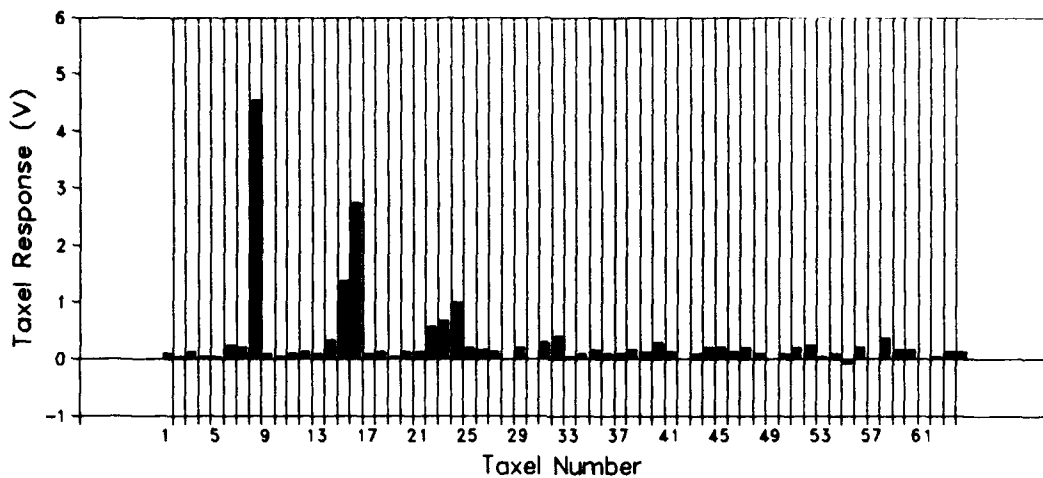
Figure 6.19.   Crosstalk on the new integrated circuit due to an
applied voltage on taxel number 8.
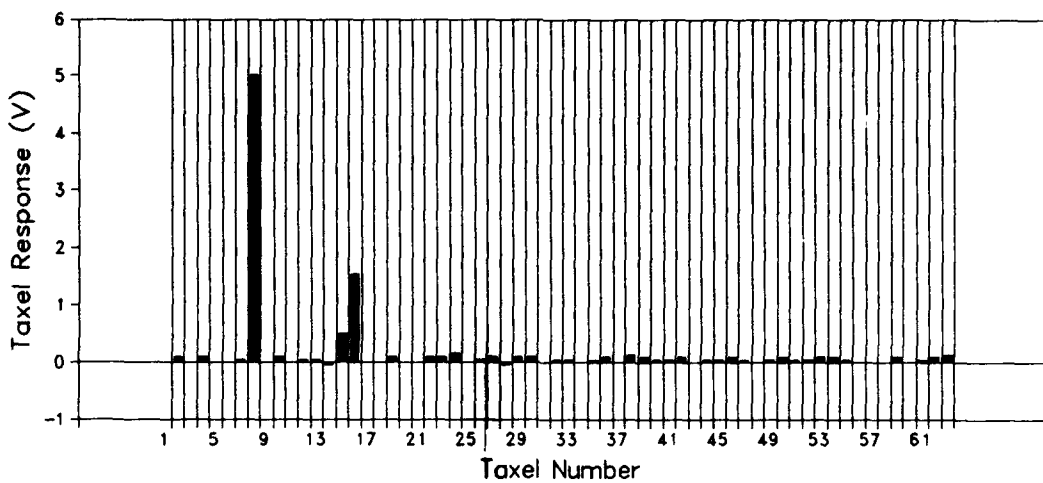
Figure 6.20.   Crosstalk on the old integrated circuit due to an
applied voltage on taxel number 8.
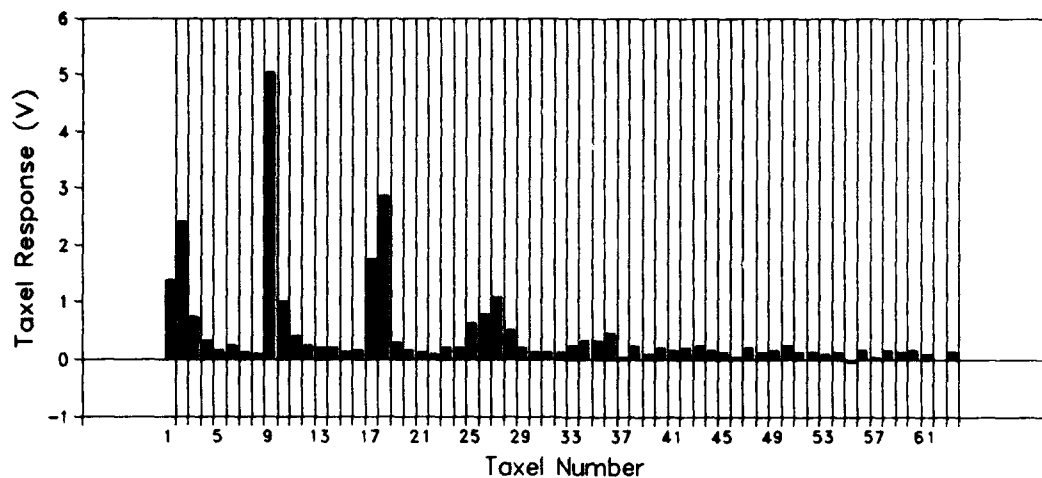
Figure 6.21.   Crosstalk on the new integrated circuit due to an applied voltage on taxel number 9.
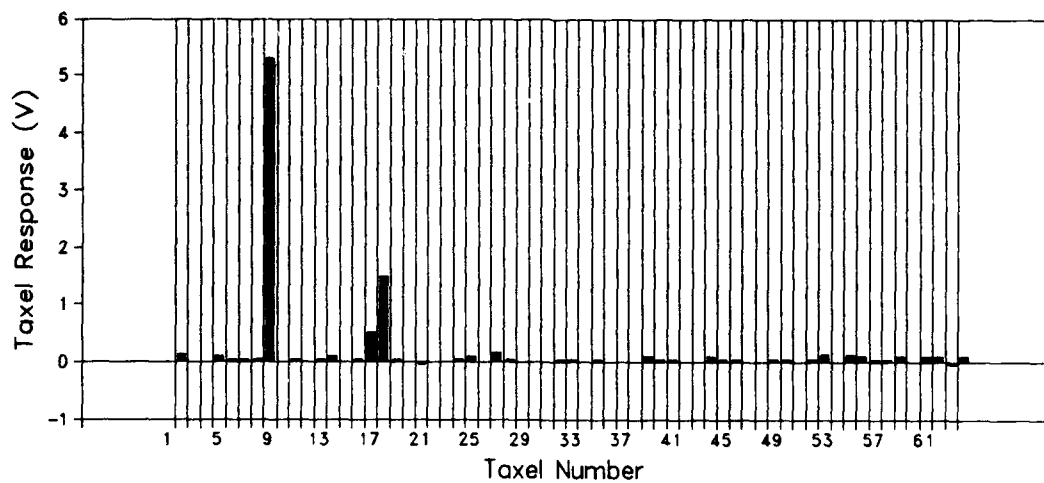
Figure 6.22.   Crosstalk on the old integrated circuit due to an applied voltage on taxel number 9.

6-17
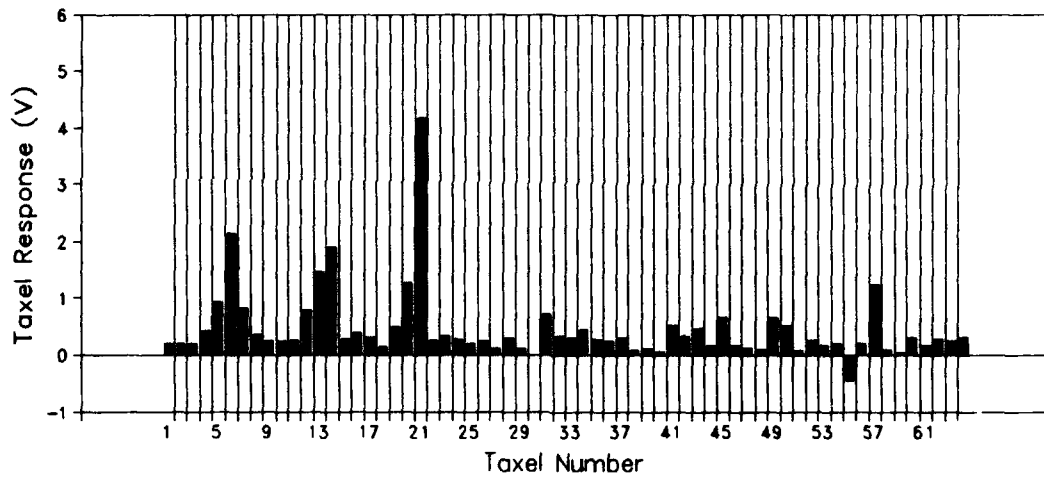
Figure 6.23.   Crosstalk on the new integrated circuit due to an applied voltage on taxel number 21.
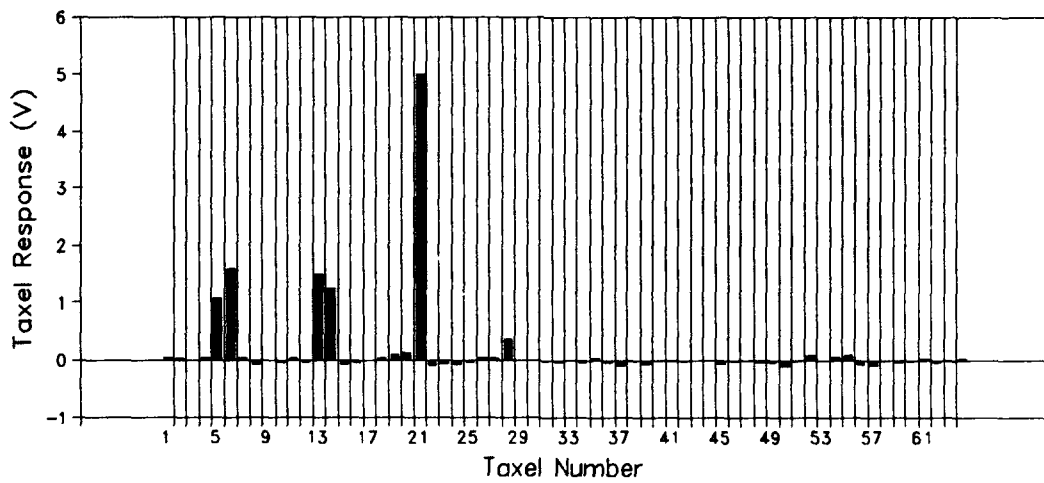
Figure 6.24.   Crosstalk on the old integrated circuit due to an applied voltage on taxel number 21.
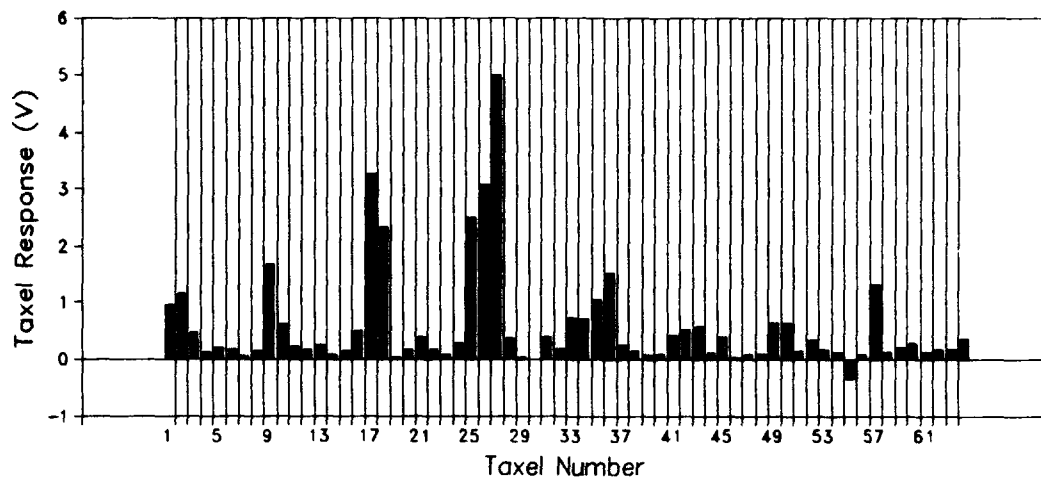
Figure 6.25.   Crosstalk on the new integrated circuit due to an
                applied voltage on taxel number 27.
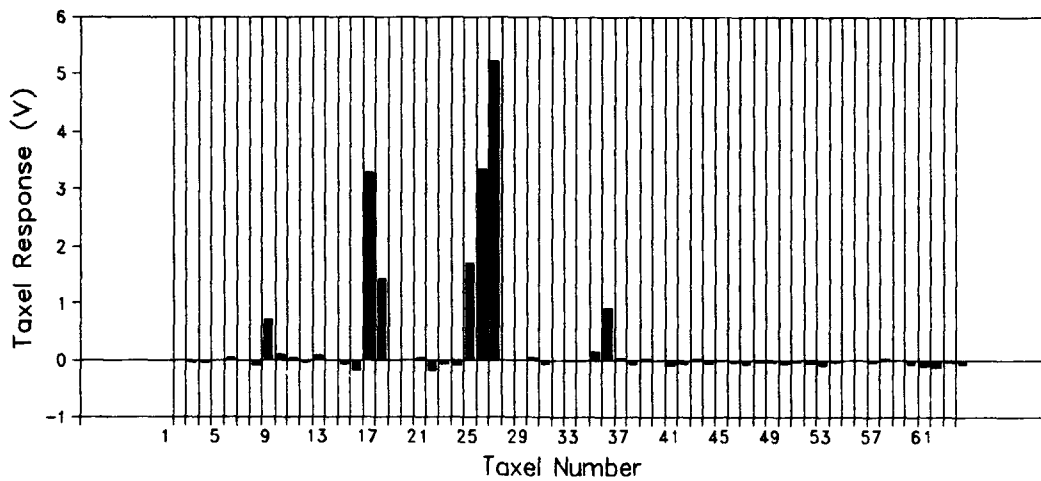
Figure 6.26.   Crosstalk on the old integrated circuit due to an
                applied voltage on taxel number 27.
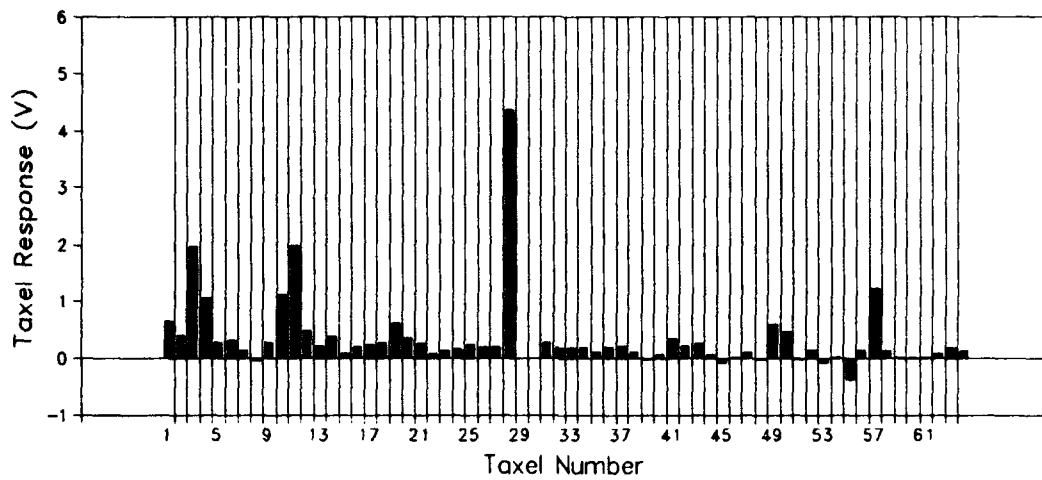
Figure 6.27.   Crosstalk on the new integrated circuit due to an
                    applied voltage on taxel number 28.
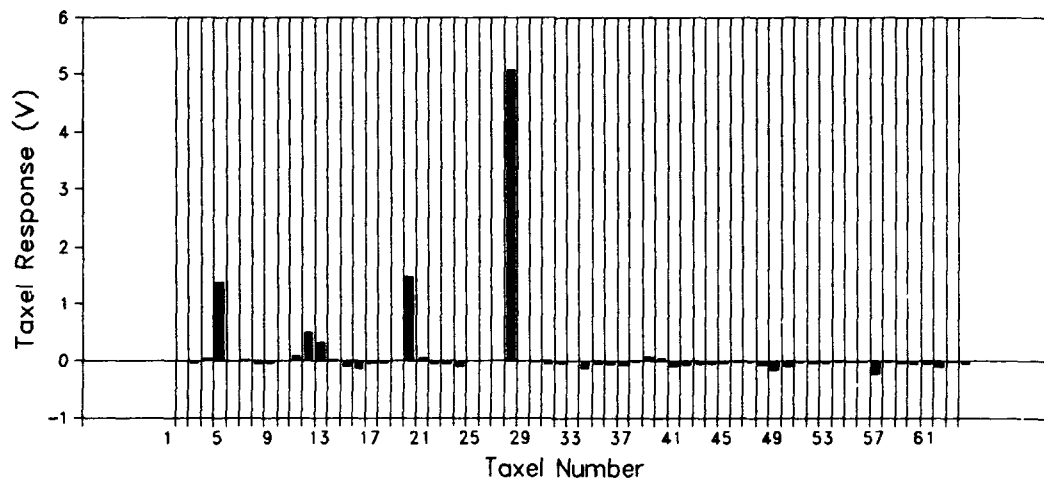
Figure 6.28.   Crosstalk on the old integrated circuit due to an
                    applied voltage on taxel number 28.

6-20
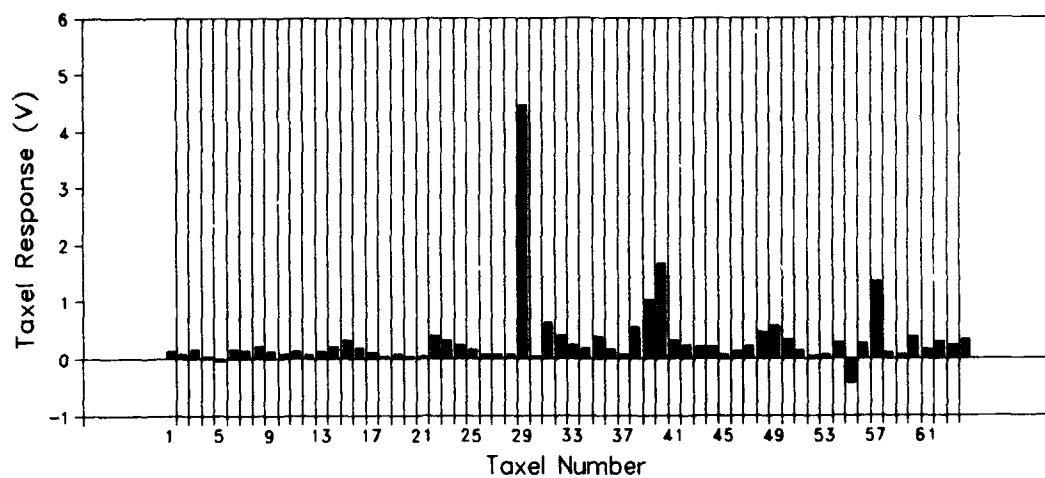
Figure 6.29.   Crosstalk on the new integrated circuit due to an
                    applied voltage on taxel number 29.
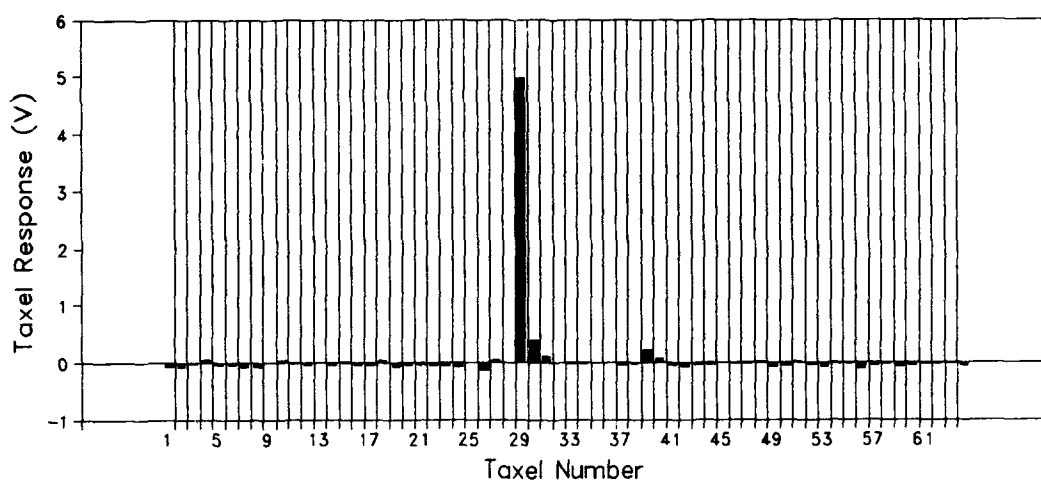
Figure 6.30.   Crosstalk on the old integrated circuit due to an
                    applied voltage on taxel number 29.
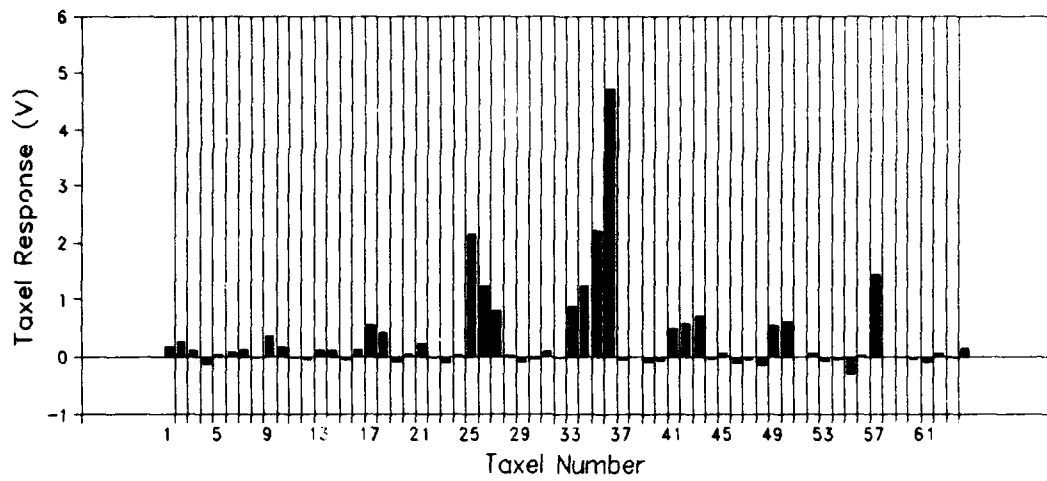
Figure 6.31.   Crosstalk on the new integrated circuit due to an applied voltage on taxel number 36.
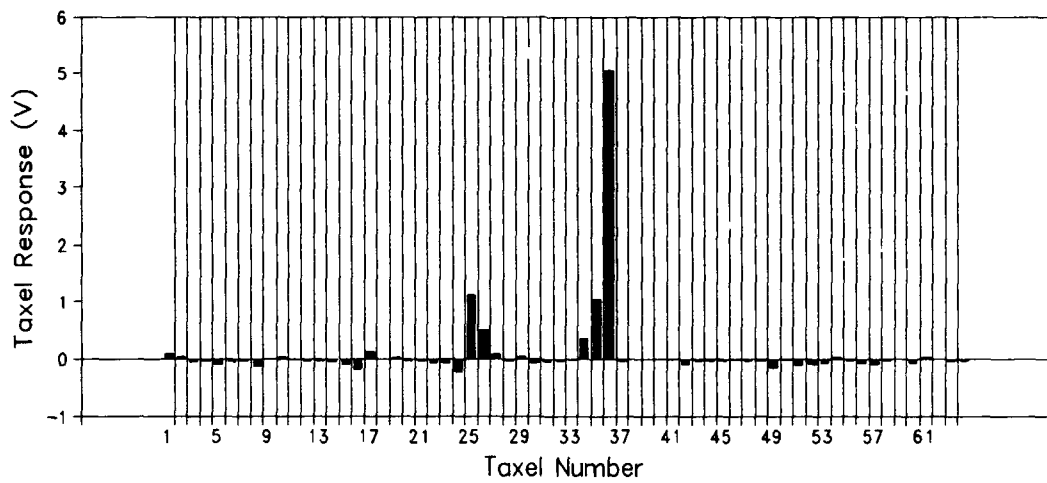
Figure 6.32.   Crosstalk on the old integrated circuit due to an applied voltage on taxel number 36.
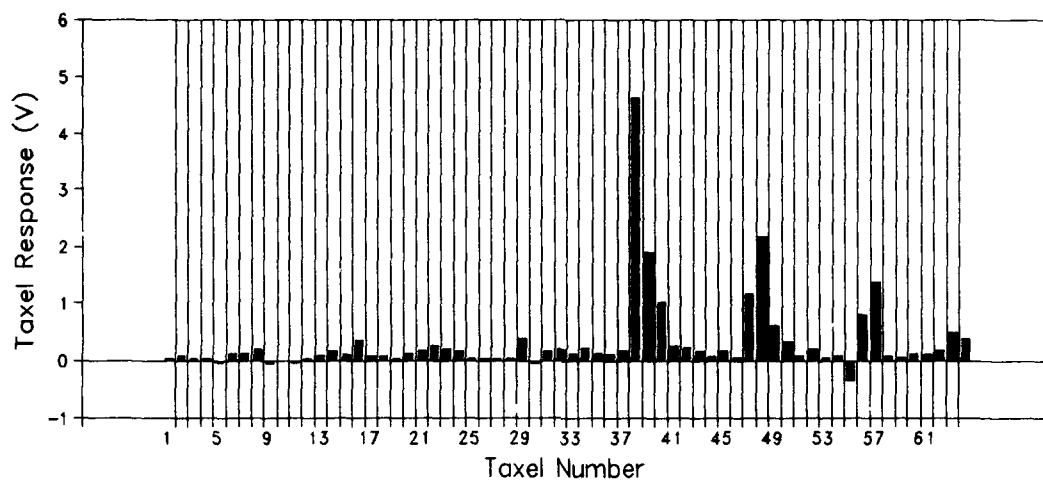
Figure 6.33.   Crosstalk on the new integrated circuit due to an applied voltage on taxel number 38.
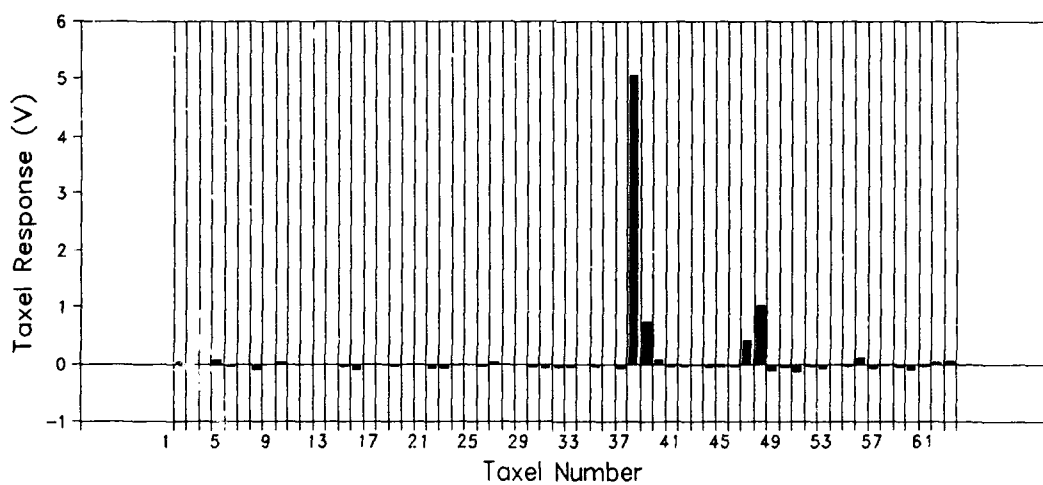
Figure 6.34.   Crosstalk on the old integrated circuit due to an applied voltage on taxel number 38.
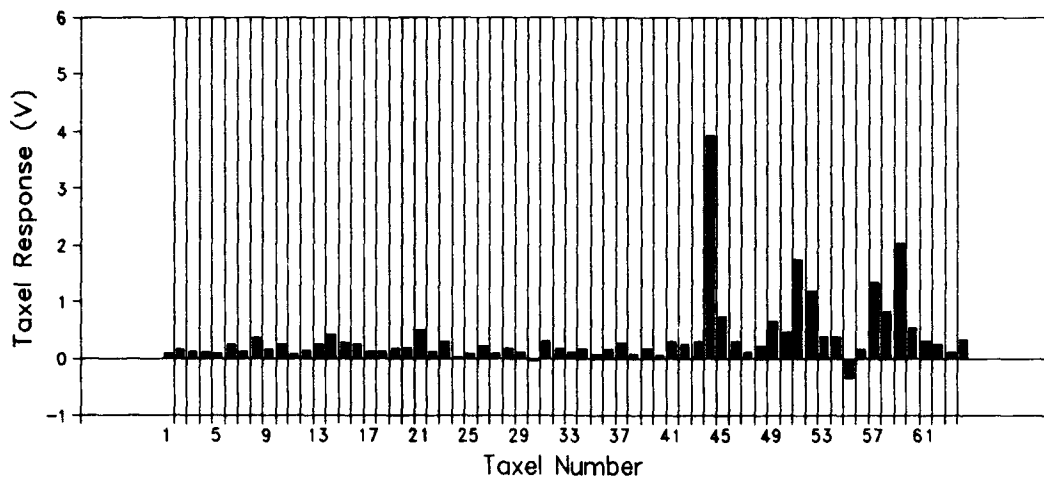
Figure 6.35.   Crosstalk on the new integrated circuit due to an
                applied voltage on taxel number 44.
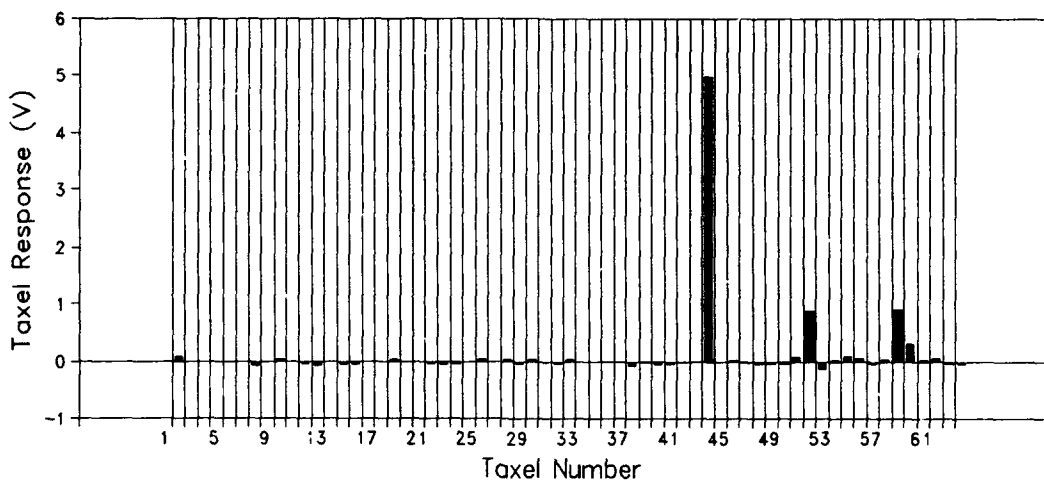
Figure 6.36.   Crosstalk on the old integrated circuit due to an
                applied voltage on taxel number 44.

Table 6.1   Electrical Crosstalk Data for the New IC design.

New IC Design		Pad Input Line Spacing (μm)	Pad Output Line Spacing (μm)	Percent Electrical Crosstalk (%)
Stimulated Taxel #	Adjacent Line #			
1	9	119	33	28
	2	8	16	53
	10	9	14	53
	3	25	32	31
7	21	18	Not Adjacent	29
	14	6	8	49
	8	Not Adjacent	Not Adjacent	0
	16	Not Adjacent	Not Adjacent	0
8	14	Not Adjacent	Not Adjacent	0
	7	Not Adjacent	Not Adjacent	0
	16	25	6	54
	15	54	15	30
9	17	54	26	30
	18	25	12	56
	2	104	13	45
	1	119	33	25
21	13	19	21	33
	6	7	7	52
	14	8	8	43
	7	18	Not Adjacent	21
27	25	54	23	47
	26	25	9	57
	17	25	6	58
	18	54	17	46

Table 6.1 (continued)

28	10	29	30	27
	3	12	12	45
	11	14	16	45
	4	30	36	25
29	31	54	15	0
	30	25	5	0
	40	25	5	38
	39	54	16	31
36	34	54	15	23
	35	25	5	48
	25	25	5	46
	26	54	16	23
38	40	54	17	21
	39	25	6	41
	38	25	9	43
	48	54	23	24
44	52	19	21	30
	59	8	7	50
	51	7	8	46
	58	18	Not Adjacent	25

Table 6.2   Electrical Crosstalk Data for the Old IC Design.

Old IC Design		Pad Input Line Spacing (μm)	Pad Output Line Spacing (μm)	Percent Electrical Crosstalk (%)
Stimulated Taxel #	Adjacent Line #			
1	18	21	32	10
	9	8	13	25
	2	11	16	20
	10	23	34	7
7	6	18	Not Adjacent	0
	14	6	8	20
	8	Not Adjacent	Not Adjacent	0
	16	Not Adjacent	Not Adjacent	0
8	14	Not Adjacent	Not Adjacent	0
	7	Not Adjacent	Not Adjacent	0
	16	17	5	30
	15	41	15	10
9	17	22	33	10
	18	9	15	28
	1	ε	13	0
	2	23	33	0
21	5	24	23	20
	13	8	10	30
	6	7	7	30
	14	19	19	24
27	25	24	17	29
	26	8	6	60
	17	7	9	60
	18	19	23	25

Table 6.2 (continued)

28	12	27	25	0
	20	12	10	28
	5	9	12	26
	13	25	27	0
29	31	15	15	0
	30	6	5	8
	40	8	5	5
	39	23	16	0
36	34	15	15	9
	35	6	5	20
	25	8	5	20
	26	23	16	10
38	40	21	17	0
	39	8	6	16
	48	9	9	20
	47	24	23	10
44	60	24	23	8
	52	8	10	18
	59	7	7	18
	51	19	19	0

electrical crosstalk. The second column (divided into sections of 4 rows for each stimulated taxel) identifies the number of the pad input/output conductor lines that are immediately adjacent (rows 2 and 3 of each stimulated taxel's section) and secondarily adjacent (rows 1 and 4 of each stimulated taxel's section) to the stimulated taxel. The third column identifies the distance (in micrometers) between the pad input conductor lines of the stimulated taxel and the corresponding adjacent pad input conductor lines defined in the second column. The fourth column contains the distance (in micrometers) between the pad output conductor lines of the stimulated taxel and the corresponding adjacent pad output conductor lines defined in the second column. The fifth column in Table 6.1 and Table 6.2 identifies the percent of electrical crosstalk observed between the conductor lines associated with the stimulated taxel and the conductor lines associated with the adjacent taxels that are identified in the second column.

From Figure 6.15 through Figure 6.36, it is clear that the electrical crosstalk found is related to the placement of the pad input lines and pad output lines of the integrated circuit. From the results in Table 6.1, the new integrated circuit design exhibited, on the average, 48.52% electrical crosstalk on outputs whose conductor lines are directly adjacent to the stimulated taxels, and 28.9% electrical crosstalk is observed on those outputs whose conductor lines are secondarily adjacent to those of the stimulated taxel. From the results in Table 6.2, the old integrated circuit design exhibited, on the average, 26.77% electrical crosstalk on outputs whose conductor lines are directly adjacent to the stimulated taxels, and 14.3% electrical

crosstalk is observed on those outputs whose conductor lines are secondarily adjacent to those of the stimulated taxel.

No mathematical relationship was successfully developed to explain the percent electrical crosstalk observed relative to the separation of the pad input lines and the pad output lines of the sensor. Also, no relationship was found between the length of the pad input, taxel input, or pad output lines and electrical crosstalk. However, the data shows that, for this circuit, electrical crosstalk is dominated by something besides the distance between the pad input and pad output lines. The data shows the electrical crosstalk is directly related to the order of the pad input and pad output lines of the sensor. In other words, the taxels whose pad input and/or pad output lines were directly adjacent or secondarily adjacent to the input/output lines of the taxel being stimulated exhibited electrical crosstalk.

In order to verify the assumption that the electrical crosstalk is related to the order of the bonding pads, a simple test was performed. An arbitrary taxel, taxel 17, was chosen as a test case. First, an electrical crosstalk reading was taken by stimulating the pad input line associated with taxel 17. Then since taxel 27 has a pad input line directly adjacent to that of taxel 17, the bonding wire that connects the bonding pad, associated with the pad input line for taxel 27, to the integrated circuit package was removed. A second electrical crosstalk reading was taken to compare to the first.

Since the pad input line of taxel 27 is directly adjacent to that of taxel 17, the data from the initial reading (reading before the bonding wire was removed) should show electrical crosstalk on taxel 27 of approximately 48%. Figure 6.37 shows that this is indeed the case,

and an arrow on the graph indicates the electrical crosstalk associated with taxel 27 which is approximately 47%. With the bonding wire of taxel 27 removed, the data from the second reading should show one of two things. If the electrical crosstalk was due to the pad input or pad output lines on the integrated circuit die, the electrical crosstalk would approximately the same as it was before the bonding wire was removed; however, if the electrical crosstalk was due to some aspect of the integrated circuit package or the external circuitry, then there would be no electrical crosstalk associated with taxel 27. Figure 6.38 shows the electrical crosstalk after taxel 27's input bonding wire was removed. The arrow in Figure 6.38 points to the electrical crosstalk associated with taxel 27. Since it is below the noise level of the circuit (approximately 0.02 V), it was concluded that the electrical crosstalk was due to some aspect of the integrated circuit package or the external circuitry.

To determine if the electrical crosstalk was due to the integrated circuit package, resistance measurements were made on the circuit. First, the integrated circuit was placed in the Micromanipulator probe station. Then, the resistance between several adjacent bonding pads (both output and input bonding pads) was measured. Using the electrometer, the resistance between adjacent pads was on the order of 5 $G\Omega$. The high resistance indicates the electrical crosstalk was not caused by the packaging of the integrated circuit. To further verify this assumption, the isolated integrated circuit was biased for operation and a single taxel (taxel 17) was stimulated with a microprobe. None of the voltage outputs on any of the adjacent lines
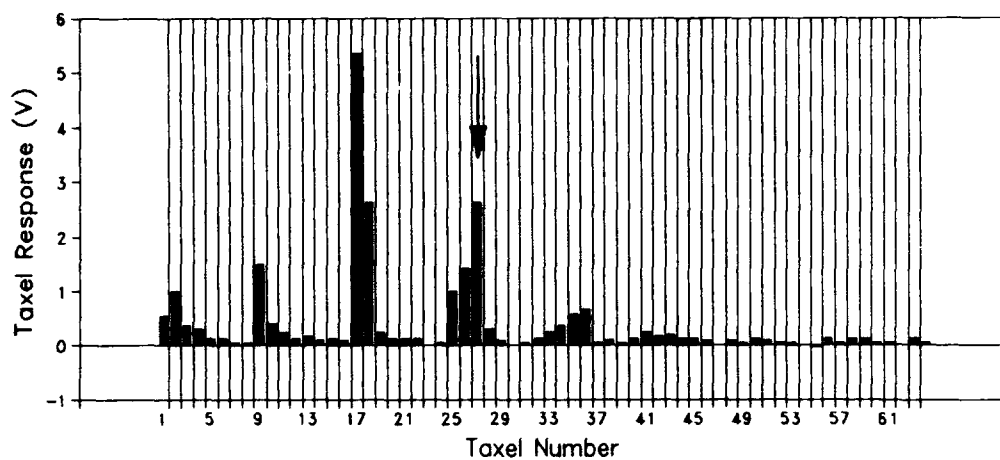
Figure 6.37.   Electrical crosstalk associated with taxel 17 before
                the bond wire on taxel 27 was removed.
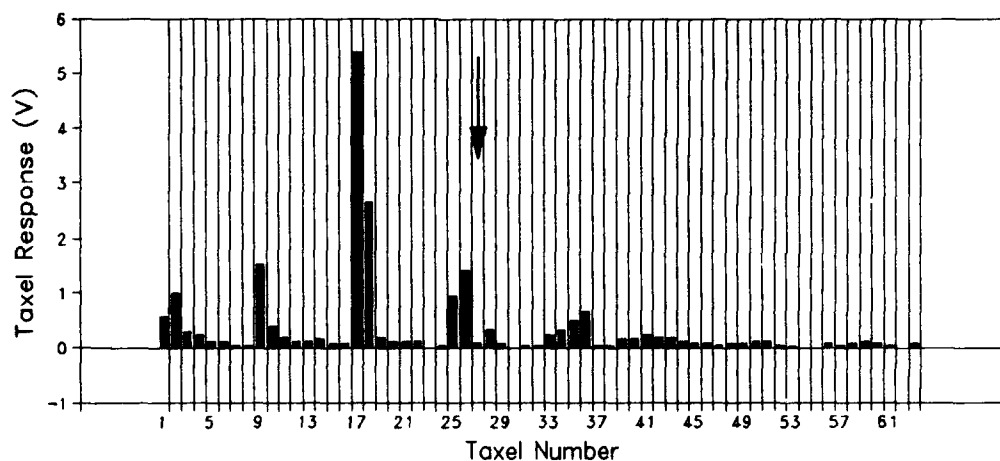
Figure 6.38.   Electrical crosstalk associated with taxel 17 after
                the bond wire on taxel 27 was removed.

indicated electrical crosstalk. Therefore, it was concluded that the electrical crosstalk was due to some aspect of the external circuitry.

To determine if the electrical crosstalk was due to the external circuitry, the proto-board and associated circuitry were tested. With the integrated circuit removed from the proto-board, the resistance between the outputs of adjacent high-input impedance switches was measured. When the switches were "ON", the resistance between adjacent switch outputs was on the order of 4.26 kΩ, and when the switches were "OFF", the resistance between adjacent switch outputs was on the order of 5 GΩ. The value of the resistance between the outputs of the switches when the switches are "ON" in conjunction with the method for taking electrical crosstalk data is the probable cause of the electrical crosstalk found in this research.

Since the stimulating input used to test for electrical crosstalk was applied to a single taxel with the switches in the "ON" position, the adjacent pad input lines should have a nonzero voltage drop on them due to the 4.26 kΩ impedance between the outputs of adjacent switches. When the switches were opened to take electrical crosstalk readings, the high impedance between the outputs of adjacent switches and the high input impedance of the sensor amplifiers caused the charge associated with the nonzero voltage drop to be trapped at the input of adjacent amplifiers. This nonzero voltage drop at the input, and associated output voltage, caused false electrical crosstalk readings. Therefore, it is concluded that the electrical crosstalk found in this research was not due to the integrated circuit tactile sensor or the associated external circuitry, but the method used to determine if electrical crosstalk is present.

6-33

6.3.1. Summary and Conclusion. It was found that a mistake in the method of taking electrical crosstalk data was the cause of the electrical crosstalk found in this research.

6.4. Tactile Sensor Response Characterization

This section presents the sensor's force performance characterization data and analysis. First, the force sensitivity data is presented and analyzed. Next, the sensor's pressure accuracy and voltage predictability are investigated. Finally, the object imaging data is presented and analyzed.

6.4.1. Sensor Force Sensitivity. Figure 6.39 depicts the data used to calibrate the sensor. The vertical lines in Figure 6.39 are the range of the response of the five taxels to the load given on the x-axis. The solid squares are the average of the taxel response to the given load, and the solid line is the linear least squares curve fit of the solid squares. The equation of the least squares curve fit is:

$$\text{Load} = 147.17 \cdot V - 12.39 \qquad (6.2)$$

where the load is given in gmf and V is the taxel response (V). Equation 6.2 is defined as the calibration equation for the sensor. From the calibration equation, the slope of the curve fit is 147.17 gmf/V. Using a 12 V V_{DD} power supply, the minimum input voltage differential detectable at the output of the sensor's amplifiers was 0.05 V. By multiplying this by the slope, it was determined that the force sensitivity was 7.35 g. It should also be noted that the noise floor of the sensor was found by averaging the taxel response for several sensor readings where no load was applied to the sensor. The

value determined for the noise floor was 0.02 V. Using this value for the noise floor and the data in Figure 6.39, the lower detectable limit of the sensor is at most 1 g.
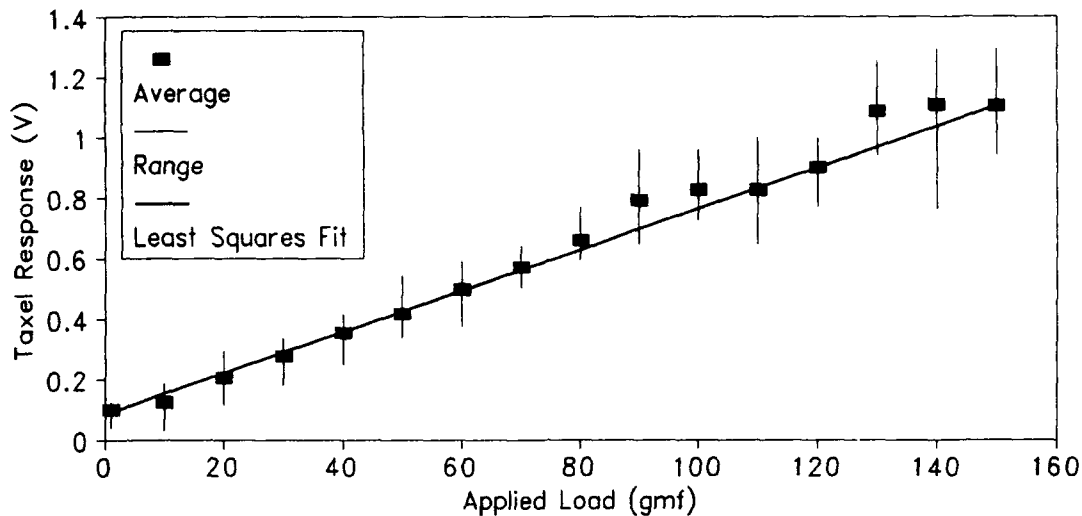
Figure 6.39.   Calibration curve for the tactile sensor.

6.4.2. *Sensor Pressure Accuracy*. Figure 6.40 shows the percent difference between the average taxel response and the taxel response calculated with a form of Equation 6.1 versus the applied load. The percent difference for the 10 gmf load is approximately 40%. This is due to the fact that the low end of the amplifier's linear range is being used to amplify the signal, and some of the readings taken with 10 gmf may be in the nonlinear range of the amplifier. The rest of the percent differences were all less than 15%. Using all but the 10 gmf load, the sensor force reading is accurate to within 15% of the actual load applied to the sensor.
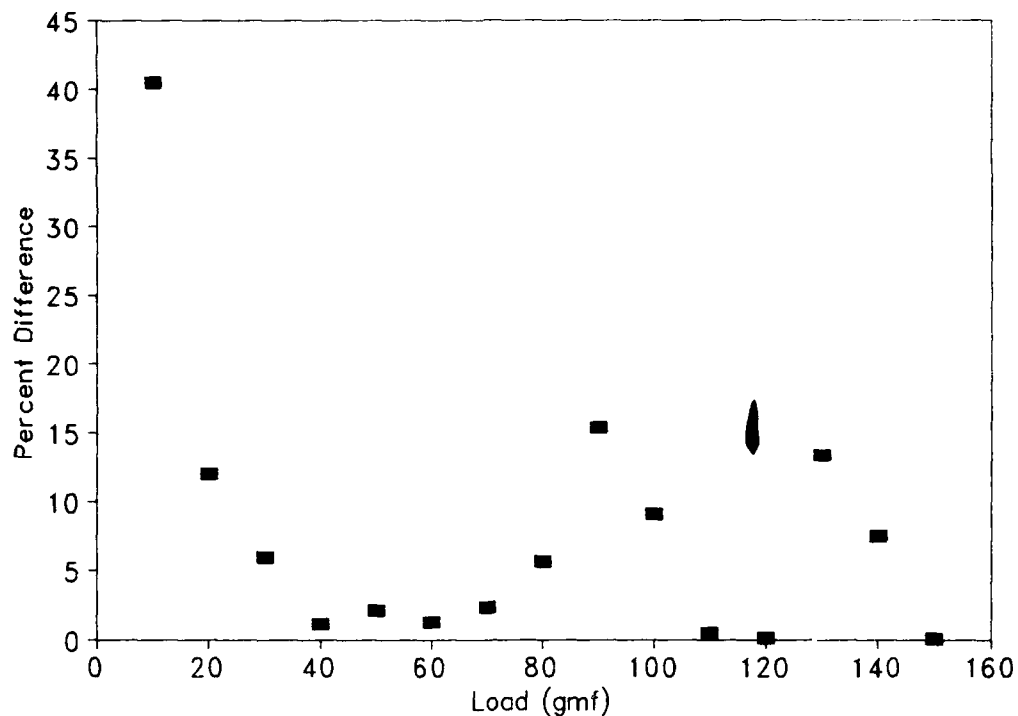
Figure 6.40.   The percent difference between the average taxel
                voltage response and the voltage response found
                using the calibration equation.

6.4.3. *Sensor Voltage Predictability*. Equation 5.3 used to model

the sensor's response to a load did not accurately predict the actual

data. One possible cause for the difference between the predicted and

actual output is charge leakage. When a load is applied and a

measurement is accomplished with the sensor, there is a transient

voltage spike that is observed on the digital storage oscilloscope

(DSO); however, this transient value is not captured when the reading is

stored on the DSO. Another possible cause for the unpredictability of

the sensor's response is the dielectric adhesive used to bond the PVDF

film to the integrated circuit. The adhesive not only provides a path

for charge leakage, it also mechanically damps the response of the film

to the applied load. These are two likely causes that contribute to the significant disparity between the sensor's measured and predicted responses.

6.4.4. *Sensor Object Imaging Capability*. Figure 6.41 through Figure 6.63 show the data for demonstrating the sensor's object imaging capability. The data presented in this section is representative of the data measured for the square (2.5 mm x 2.5 mm), rectangular (0.7 mm x 6 mm), and circular (2 mm diameter) shaped loads. Due to the similarities and quantity of data, only a representative portion is presented in this thesis for analysis. In a realistic application, the sensor would likely be used where a single-valued threshold voltage could be established. It was determined empirically that a reproducible threshold voltage level for establishing which taxels are "ON" and which are "OFF", was 0.2 V. This voltage level corresponds to a load of 17 gmf (Figure 6.39).

Figure 6.41 depicts the rectangular shaped load (0.7 mm x 6 mm) applied diagonally to the tactile sensor. Figure 6.42 through Figure 6.45 show the sensor's response to the rectangular shaped load applied diagonally with 50 gmf. Figure 6.42 shows the taxel response (change of the taxel output voltage due to the application of a load) of each taxel to the load. Figure 6.43 shows the normalized response of each sensor taxel in a 3-dimensional format. In Figure 6.44, the taxels with a measurement exceeding the 0.2 V threshold are depicted by solid squares, and the taxels with voltage levels less than the 0.2 V threshold are depicted as empty squares. Figure 6.45 shows the response of the sensor to the algorithm used to determine the load's shape
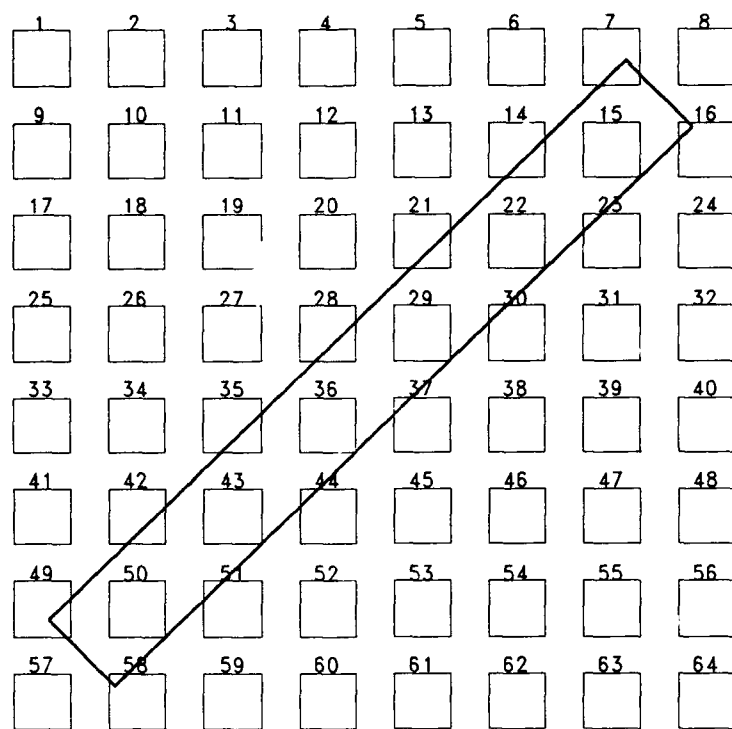
Figure 6.41.   Two-dimensional representation depicting the actual
                taxel coverage of the rectangular load applied
                diagonally to the sensor's surface.
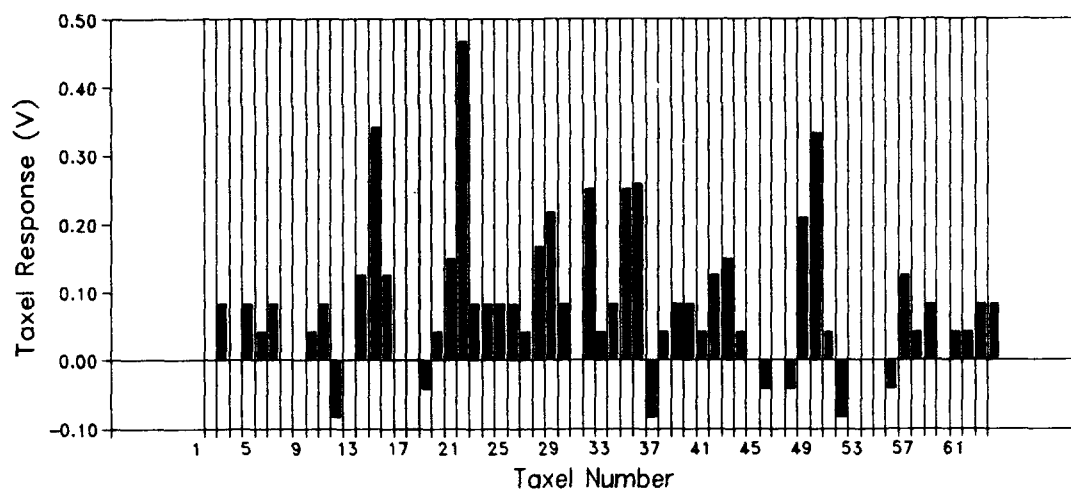
Figure 6.42.   Taxel response of the sensor to a 0.7 mm x 6 mm
                 rectangular load applied diagonally with 50 gmf.
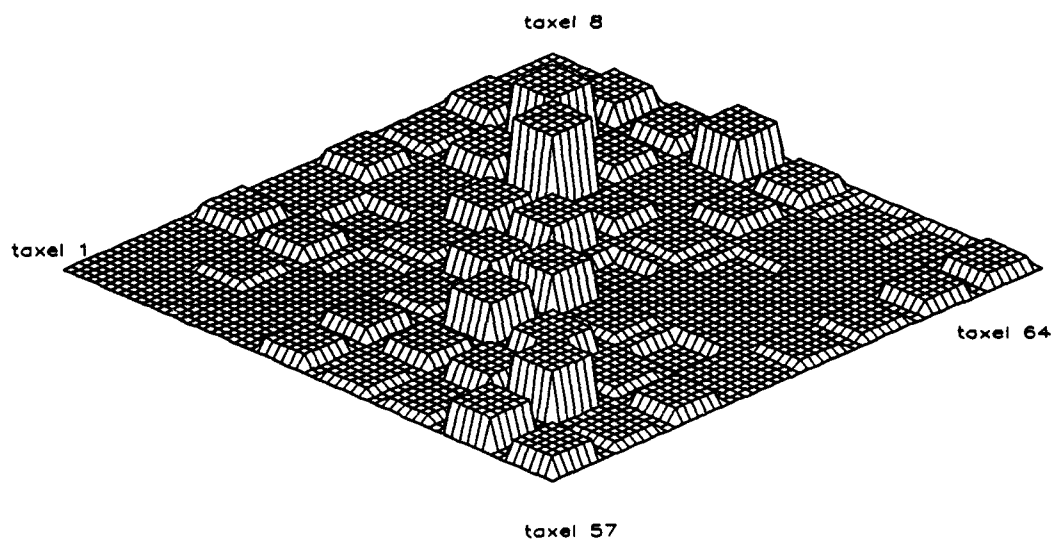
Figure 6.43.   Three-dimensional depiction of the response of the
                 sensor to a 0.7 mm x 6 mm load applied diagonally
                 with 50 gmf.
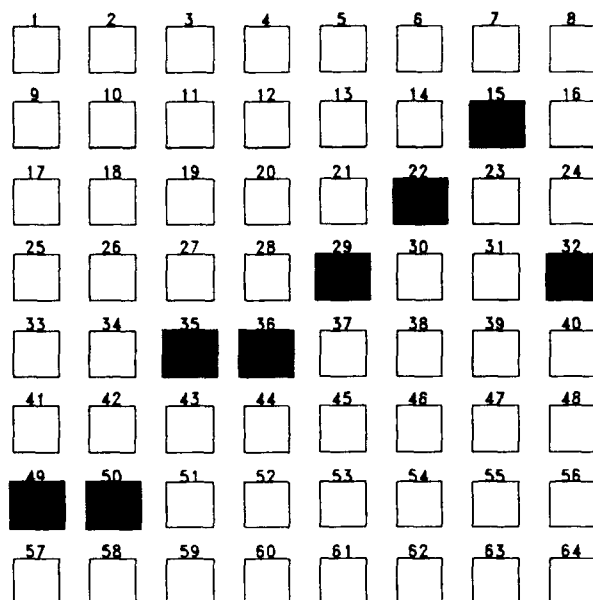
Figure 6.44.   Two-dimensional representation of the sensor
response showing which taxels are above the 0.2 volt
threshold for the 0.7 mm x 6 mm load applied
diagonally with 50 gmf.
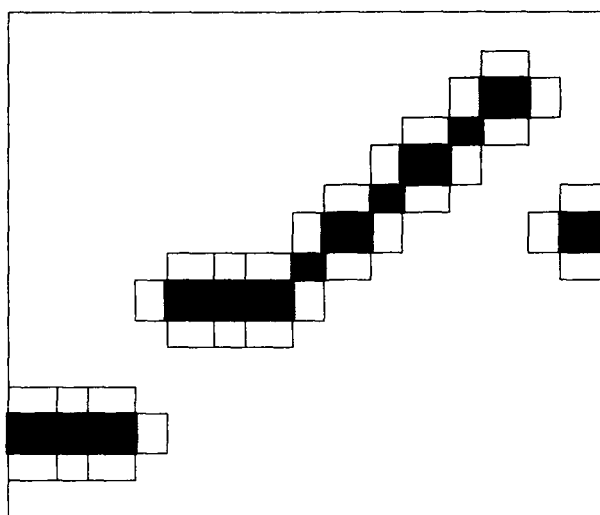
Figure 6.45.   Depiction of the sensor response using a first order
shape fitting algorithm to the 0.7 mm x 6 mm load
applied diagonally with 50 gmf.
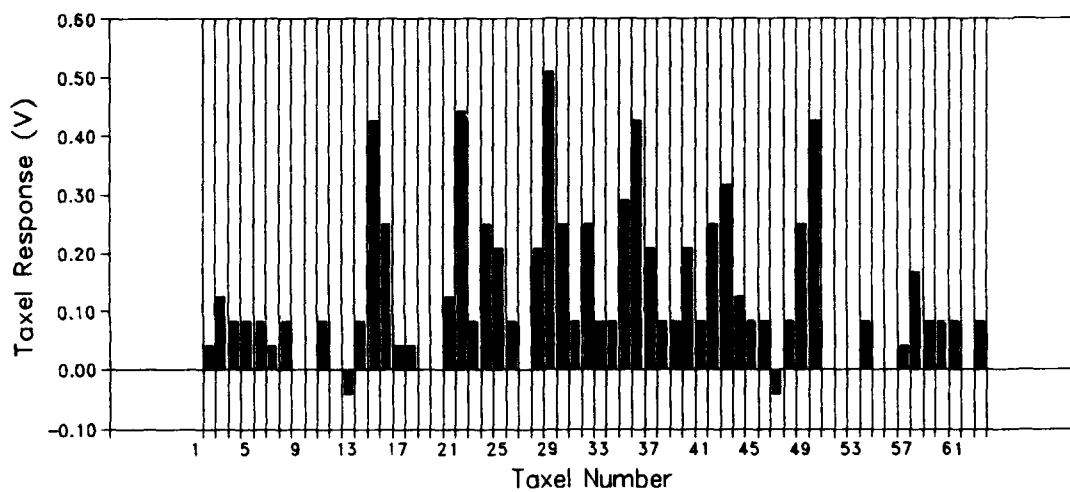
Figure 6.46.   Taxel response of the sensor to a 0.7 mm x 6 mm rectangular load applied diagonally with 75 gmf.
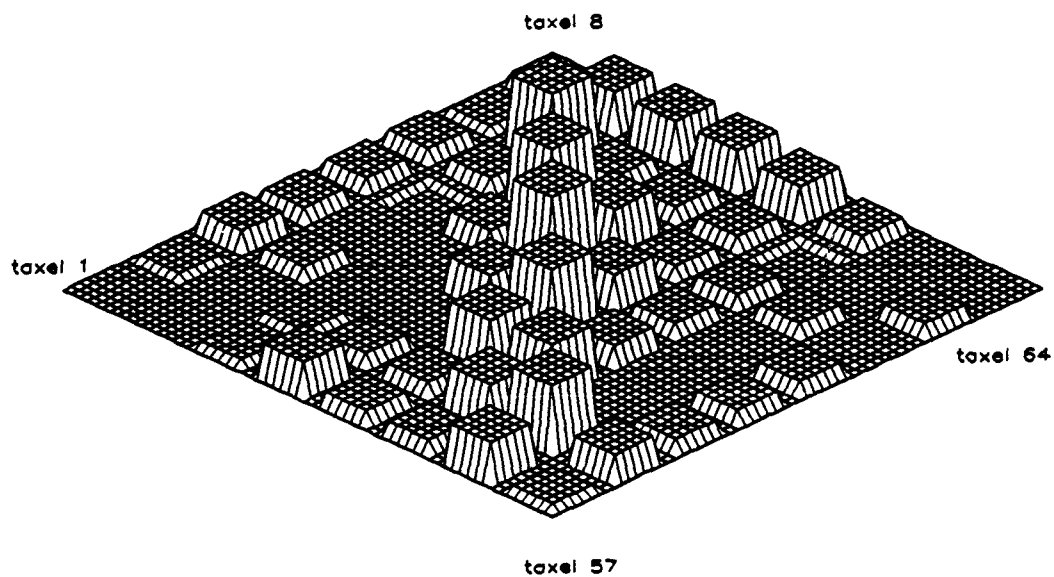
Figure 6.47.   Three-dimensional depiction of the response of the sensor to a 0.7 mm x 6 mm load applied diagonally with 75 gmf.
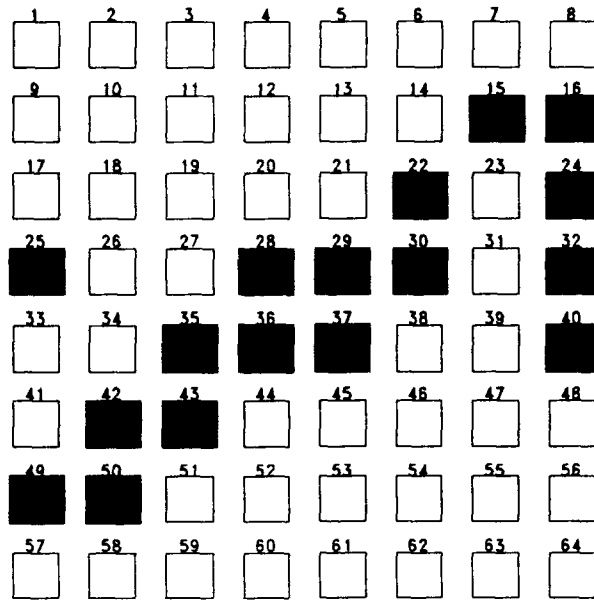
Figure 6.48.   Two-dimensional representation of the sensor response showing which taxels are above the 0.2 volt threshold for the 0.7 mm x 6 mm load applied diagonally with 75 gmf.
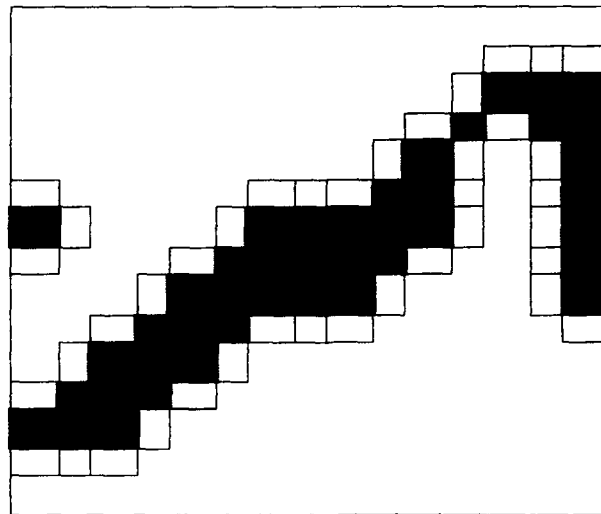
Figure 6.49.   Depiction of the sensor response using a first order shape fitting algorithm to the 0.7 mm x 6 mm load applied diagonally with 75 gmf.
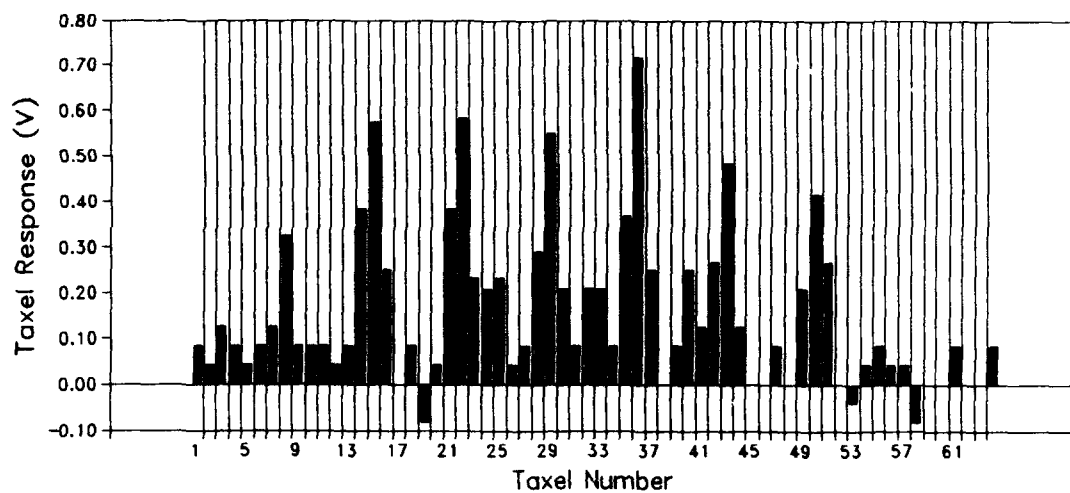
Figure 6.50.   Taxel response of the sensor to a 0.7 mm x 6 mm
                 rectangular load applied diagonally with 100 gmf.
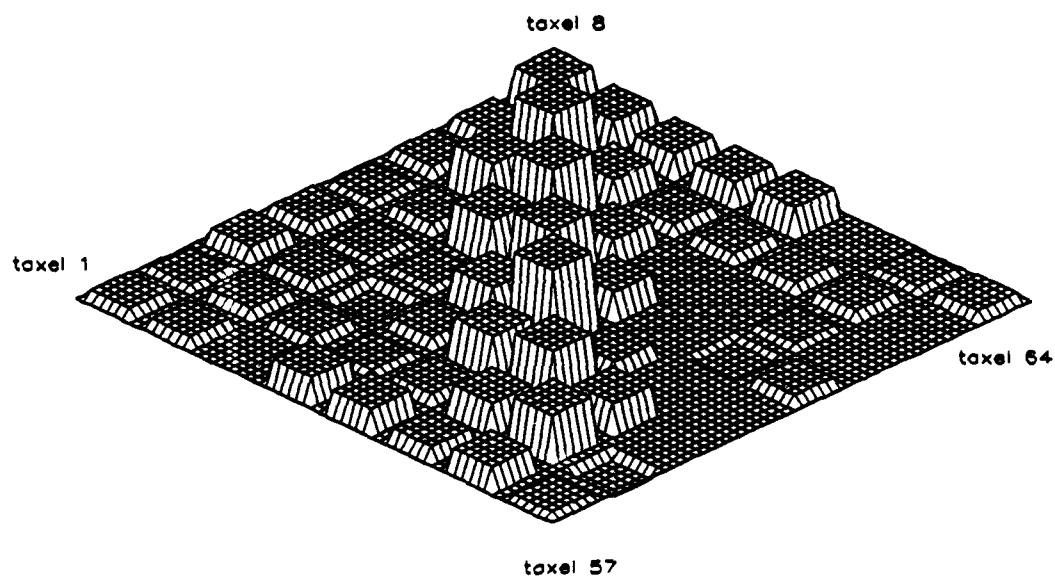
Figure 6.51.   Three-dimensional depiction of the response of the
                 sensor to a 0.7 mm x 6 mm load applied diagonally
                 with 100 gmf.
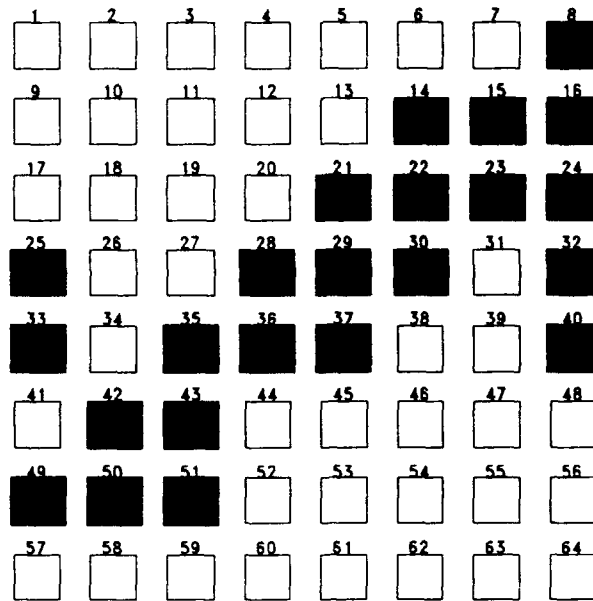
Figure 6.52.   Two-dimensional representation of the sensor
                 response showing which taxels are above the 0.2 volt
                 threshold for the 0.7 mm x 6 mm load applied
                 diagonally with 100 gmf.
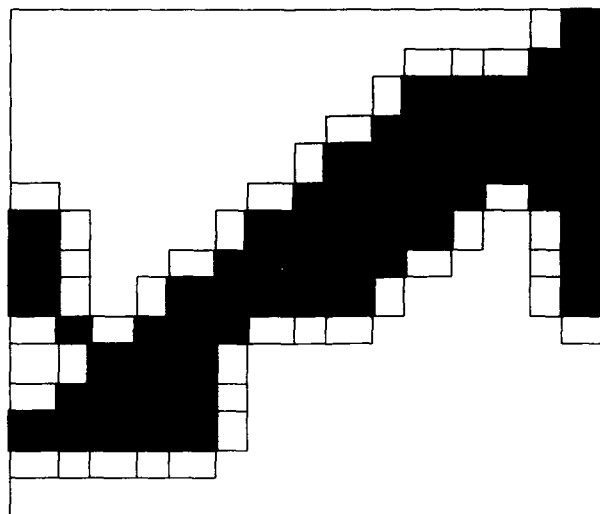
Figure 6.53.   Depiction of the sensor response using a first order
                 shape fitting algorithm to the 0.7 mm x 6 mm load
                 applied diagonally with 100 gmf.
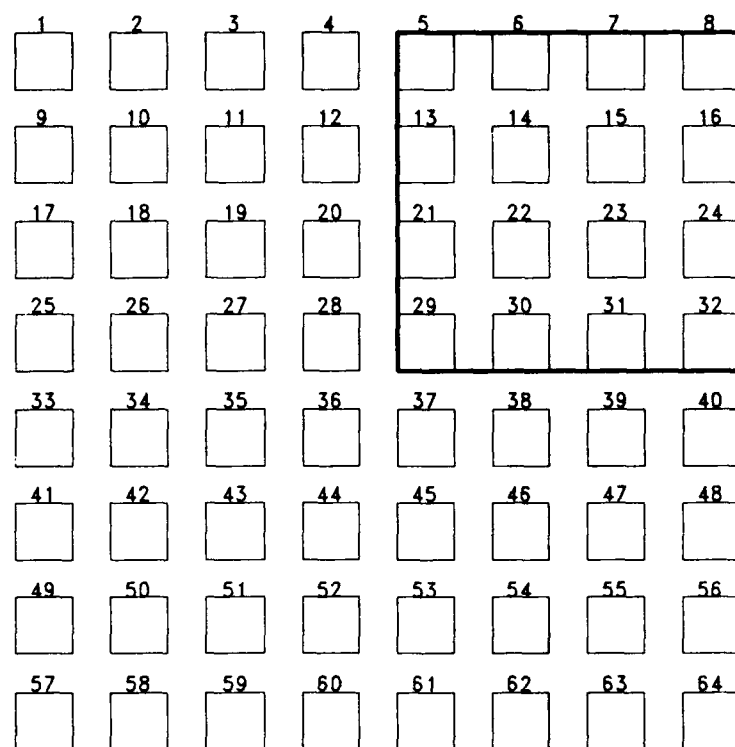
Figure 6.54.   Two-dimensional representation depicting the actual
taxel coverage of the square load as applied to the
sensor's surface.
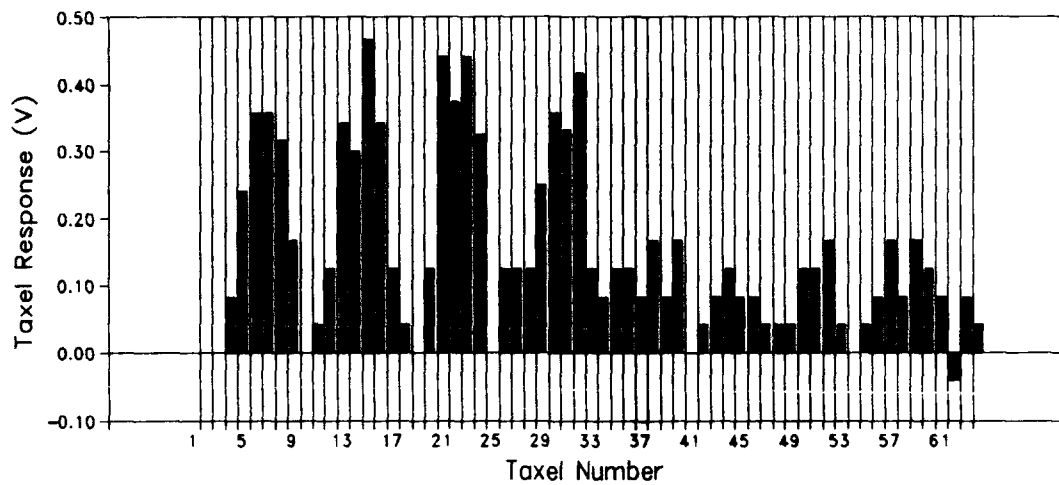
Figure 6.55.   Taxel response of the sensor to a 2.5 mm x 2.5 mm square load applied to the upper right corner with 50 gmf.
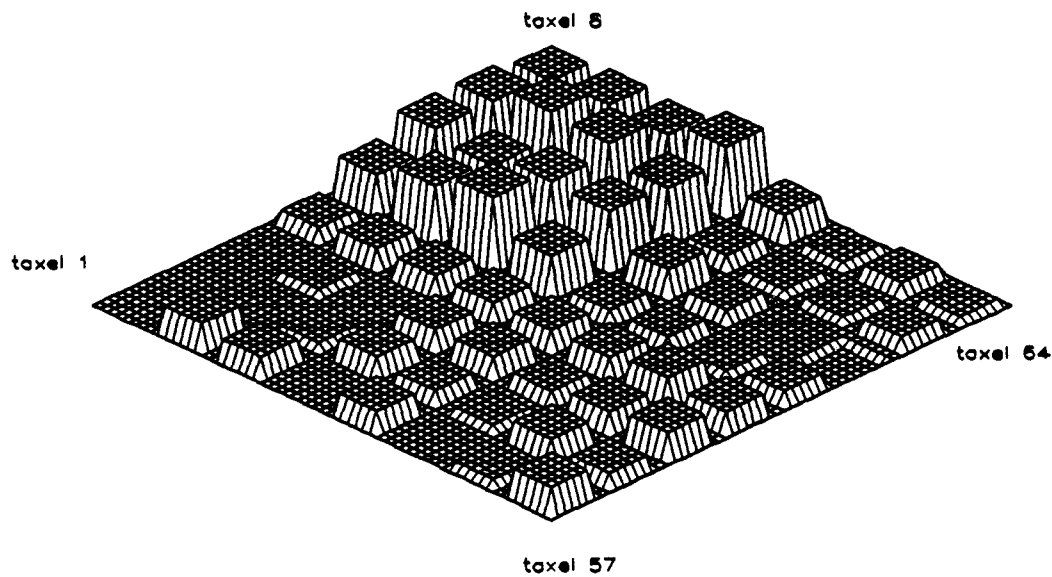
Figure 6.56.   Three-dimensional depiction of the response of the sensor to a 2.5 mm x 2.5 mm load applied to the upper right corner with 50 gmf.
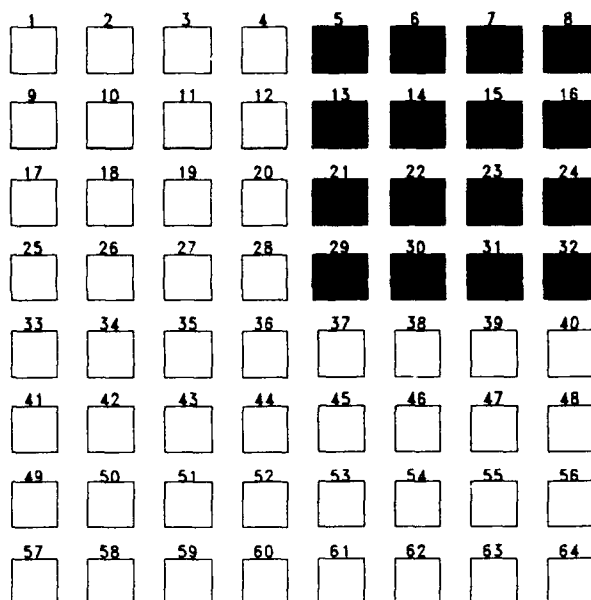
Figure 6.57. Two-dimensional representation of the sensor response showing which taxels are above the 0.2 volt threshold for the 2.5 mm x 2.5 mm load applied to the upper right corner with 50 gmf.
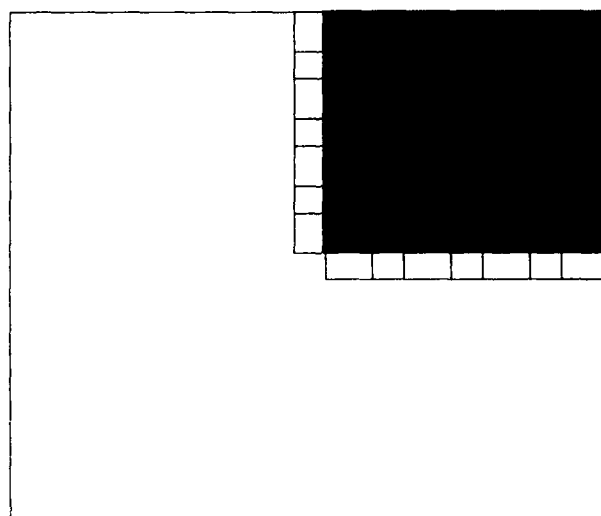
Figure 6.58. Depiction of the sensor response using a first order shape fitting algorithm to the 2.5 mm x 2.5 mm load applied to the upper right corner with 50 gmf.
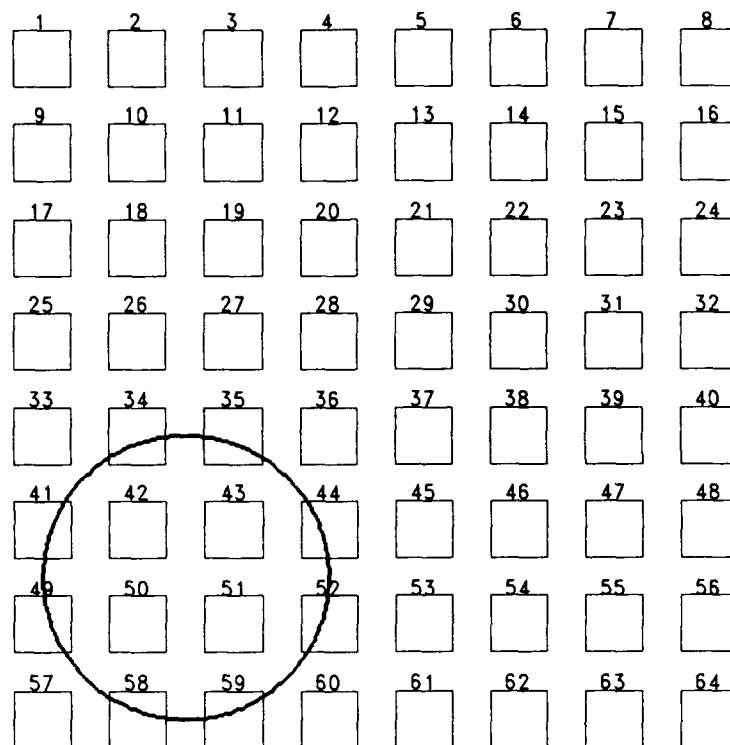
Figure 6.59.   Two-dimensional representation depicting the actual taxel coverage of the circular load as applied to the sensor's surface.
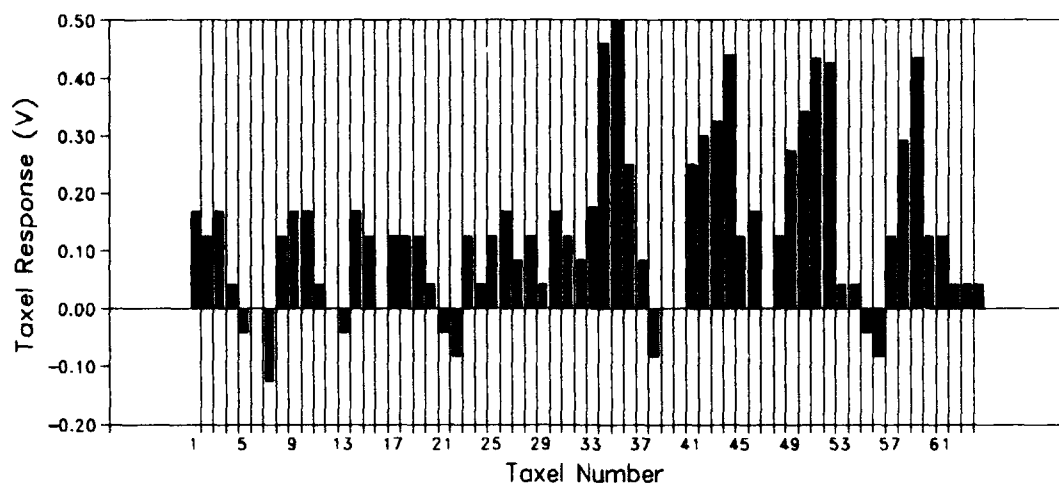
Figure 6.60.   Taxel response of the sensor to a 2 mm diameter round load applied to the lower left corner with 50 gmf.
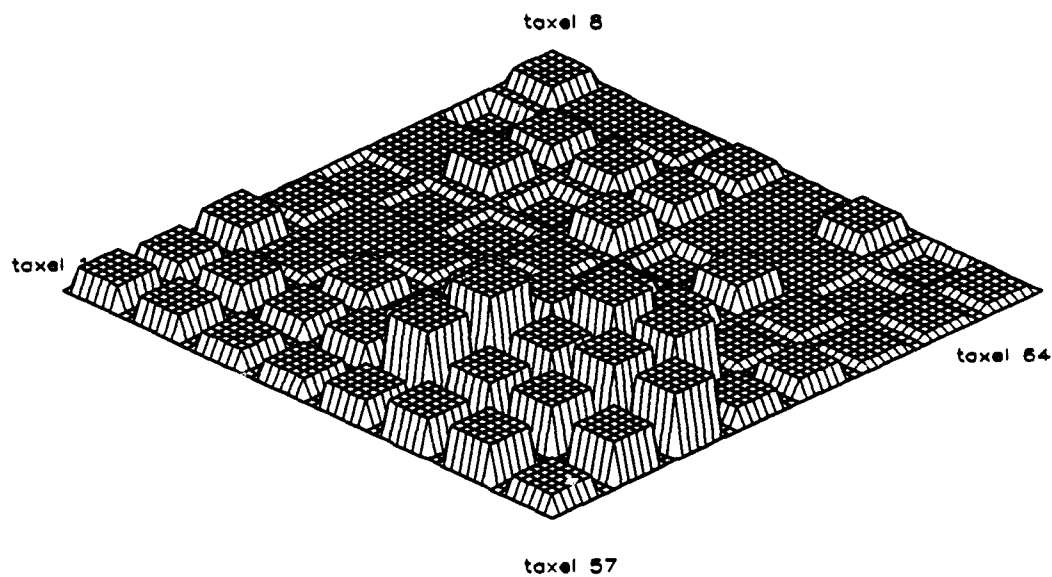
Figure 6.61.   Three-dimensional depiction of the response of the sensor to a 2 mm diameter round load applied to the lower left corner with 50 gmf.
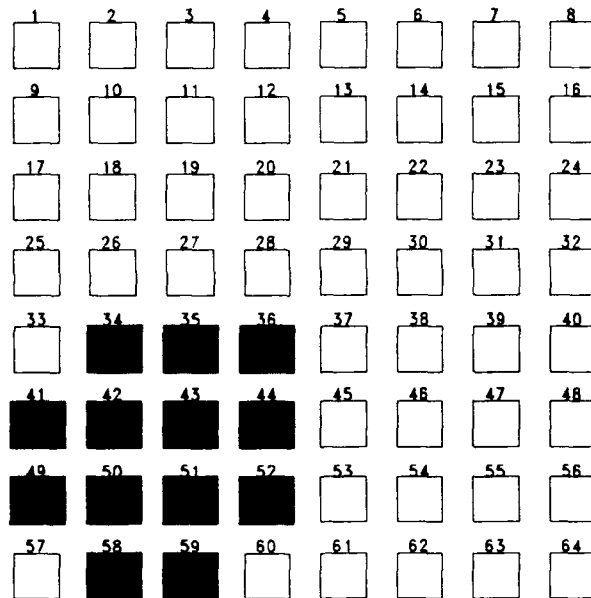
Figure 6.62.   Two-dimensional representation of the sensor
response showing which taxels are above the 0.2 volt
threshold for the 2 mm diameter round load applied
to the lower left corner with 50 gmf.
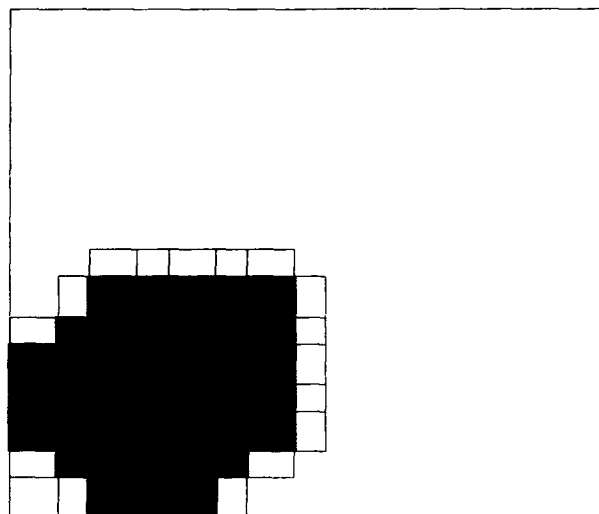
Figure 6.63.   Depiction of the sensor response using a first order
shape fitting algorithm to the 2 mm diameter round
load applied to the lower left corner with 50 gmf.

(defined in Chapter 5). Using Figure 6.45 to determine the predicted

surface area of the load, it was calculated to be 2.95 mm^2 while the

actual load is 4.2 mm^2. This situation implies a percent difference of

42%. In Figure 6.44, only taxels 15, 22, 29, 36, 43, and 50 should be

"ON". However, s'nce the width of the load is 0.7 mm, it actually

overlaps taxels 7, 14, 21, 28, 35, 42, and 49. This fact explains why

taxels 49 and 35 are also "ON."

Figure 6.46 through Figure 6.49 depict the sensor's response to a

rectangular shaped load (0.7 mm x 6 mm) applied diagonally with 75 gmf

to taxels 15, 22, 29, 36, 43, and 50 as shown in Figure 6.41.

Figure 6.46 shows the taxel response of each taxel to the load.

Figure 6.47 shows the normalized response of each sensor taxel in a

3-dimensional format. In Figure 6.48, the taxels whose voltage exceeds

the 0.2 V threshold are depicted by solid squares, and the taxels with

voltage levels below the 0.2 V threshold level are depicted as empty

squares. Figure 6.49 shows the response of the sensor using the

algorithm defined in Chapter 5 defined for area comparison. Using

Figure 6.49 to calculate the area of the load, it was calculated to be

5.14 mm^2, while the actual load is 4.2 mm^2. This gives a percent

difference of 22%. In Figure 6.48, only taxels 15, 22, 29, 36, 43, and

50 should be "ON"; however, since the width of the load is 0.7 mm, it

actually overlaps taxels 7, 14, 21, 28, 35, 42, and 49, and this is why

taxels 28, 35, 42, and 49 are also "ON." Since the load was applied so

that it did not overlap taxel 37, it is assumed that taxel 37 is "ON"

due to mechanical cros talk. This is supported by the fact that the

input and output lines of taxel 37 are separated by the input and output

lines of 4 other taxels relative to the closest stimulated taxel.

Figure 6.50 through Figure 6.53 depict the sensor's response to a rectangular shaped load (0.7 mm x 6 mm) applied diagonally with 100 gmf to taxels 15, 22, 29, 36, 43, and 50, as shown in Figure 6.41. Figure 6.50 shows the taxel response of each taxel to the load. Figure 6.51 shows the normalized response of each taxel in a 3-dimensional format. In Figure 6.52, the taxels with a voltage greater than the 0.2 V threshold are depicted by solid squares and the taxels with voltage levels below the 0.2 V threshold level are depicted as empty squares. Figure 6.53 shows the response of the sensor using the algorithm used to determine the load's area as defined in Chapter 5. Using Figure 6.53 to determine the area of the load, it was calculated to be 8.4 mm^2 while the actual load is 4.2 mm^2. This gives a percent difference of 100%. In Figure 6.52 only taxels 15, 22, 29, 36, 43, and 50 should be "ON"; however, since the width of the load is 0.7 mm, it actually overlaps taxels 7, 14, 21, 28, 35, 42, and 49, and this is why taxels 14, 21, 28, 35, 42, and 49 are also "ON." Since the load was applied so that it did not overlap taxels 8, 23, 30, 37, and 51, it is assumed that they are "ON" due to mechanical and electrical crosstalk. The input and output lines for taxel number 23 and 30 are directly adjacent to the lines for taxel 22 and 29, respectively.

Figure 6.54 shows the square shaped load (2.5 mm x 2.5 mm) applied to taxels 5, 6, 7, 8, 13, 14, 15, 16, 21, 22, 23, 24, 29, 30, 31, and 32. Figure 6.55 through Figure 6.58 depicts the sensor's response to a square shaped load applied with 50 gmf. Figure 6.55 shows the taxel response of each taxel to the load. Figure 6.56 shows the normalized response of each sensor taxel in a 3-dimensional format. In Figure 6.57, the taxels with a voltage response above the 0.2 V

threshold are depicted by solid squares, and the taxels with voltage levels below the 0.2 V threshold level are depicted as empty squares. Figure 6.58 shows the response of the sensor to the algorithm used to determine the load's area (defined in Chapter 5). Using Figure 6.58 to determine the area of the load, it was calculated to be 7.03 mm^2, while the actual load is 6.25 mm^2. This gives a percent difference of 12.5%. In Figure 6.57, all of the correct taxels are "ON."

Figure 6.59 shows the circular shaped load (2 mm diameter) applied to taxels 34, 35, 41, 42, 43, 44, 49, 50, 51, 52, 58, and 59. Figure 6.60 through Figure 6.63 depict the sensor's response to a circular shaped load applied with 50 gmf. Figure 6.60 shows the taxel response of each taxel to the load. Figure 6.61 shows the normalized response of each taxel in a 3-dimensional format. In Figure 6.62, the taxels with a voltage response greater than the 0.2 V threshold are depicted by solid squares, and the taxels with voltage levels below the 0.2 V threshold level are depicted as empty squares. Figure 6.63 shows the response of the sensor using the algorithm that determines the load's area (defined in Chapter 5). Using Figure 6.63 to determine the area of the load, it was calculated to be 5.95 mm^2, while the actual load is 3.14 mm^2. This gives a percent difference of 89%. In Figure 6.62, taxel 36 is the only taxel that is incorrectly "ON." Since the load was applied so that it did not overlap taxel 36, it is assumed that taxel 36 is "ON" due to electrical crosstalk. This is supported by the fact that the input and output lines of taxel 36 are directly adjacent to the lines of taxel 35.

6.4.5. Summary and Conclusion. The data in this section demonstrated the ability of the tactile sensor to recognize simple shapes. It was found that a 0.2 V threshold was adequate as a baseline for determining whether a taxel was "ON" or "OFF." Additionally, an area comparison algorithm was presented, and it was shown that the algorithm was not very accurate. For the worst case, the algorithm provided results that were off by a factor of two. It was also shown that electrical and mechanical crosstalk affected the sensor output.

6.5. Investigation of the Tactile Sensor's Pyroelectric Effects

This section presents the sensor's pyroelectric characterization results and analysis. The section begins with a discussion of the polarity verification experiments. Next, the sensor's pyroelectric bandwidth and sensitivity are presented. Finally, the sensor's pyroelectric accuracy and predictability are investigated.

6.5.1. Temperature Polarity Test. The pyroelectric modeling equations presented in Chapter 3 predict that a voltage decrease for each taxel will be observed when the sensor is uniformly heated. This voltage drop establishes the pyroelectric polarity of the tactile sensor. On at least 30 separate occasions, heat was applied to the tactile sensing surface of the sensor. As a result, the voltage response of the sensor's amplifiers decreased in magnitude. Similarly, when the sensor was allowed to cool, the output voltage of the sensor's amplifiers increased. Therefore, the piezoelectric tactile sensor displayed the correct pyroelectric polarity relative to the discussion in Appendix B.

6.5.2. Temperature Response Bandwidth. This section determined the pyroelectric bandwidth of the piezoelectric tactile sensor. Figure 6.64 shows the measured thermal excitation response of the piezoelectric tactile sensor. Using the time it takes the voltage to reach 63% of its steady state value, the measured thermal excitation time constant (t_r) is on the order of 12 seconds. The bandwidth can be found by inverting t_r; therefore, BW_T is 0.083 Hz.
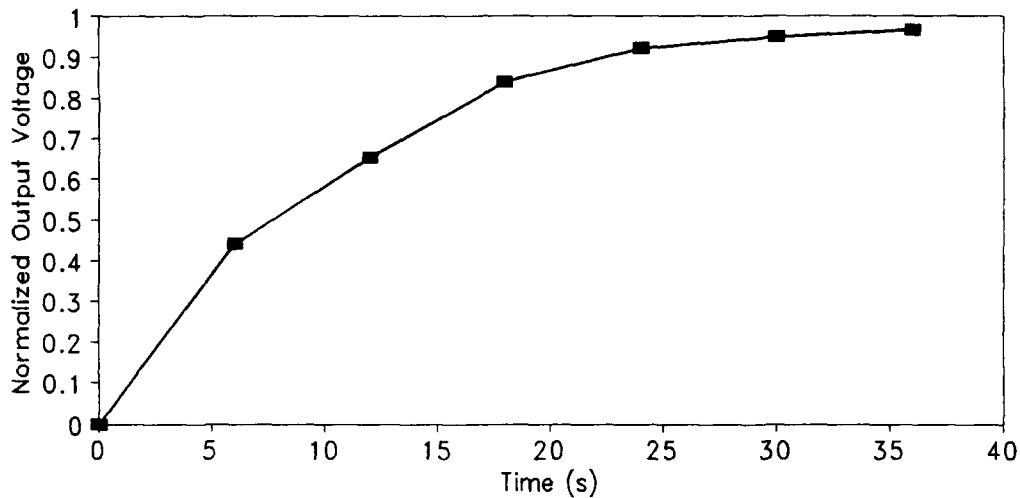
Figure 6.64.   Time response data used to determine the
                    pyroelectric excitation time constant of the sensor.

6.5.3. Sensor Temperature Sensitivity. The sensor's temperature sensitivity was found by implementing the procedure discussed in Chapter 5. The calibration curve for the temperature response of the sensor is plotted in Figure 6.65. From Figure 6.65, the data can be used to determine the following empirical equation for the temperature at the surface of the sensor as a function of the change in output voltage of the sensor when no piezoelectric effects are present:

$$\Delta T = -7.072 \cdot \Delta V - 2.633 \qquad\qquad (6.3)$$

where ΔT is the change in temperature (°C), and ΔV is the average change in voltage at the output of the sensor's amplifiers (V). By multiplying the value found previously for the minimum input voltage differential detectable at the output of the sensor's amplifiers (0.05 V) with the absolute value of slope of the calibration curve (7.702 °C/volt), the temperature sensitivity is determined to be 0.39 °C.
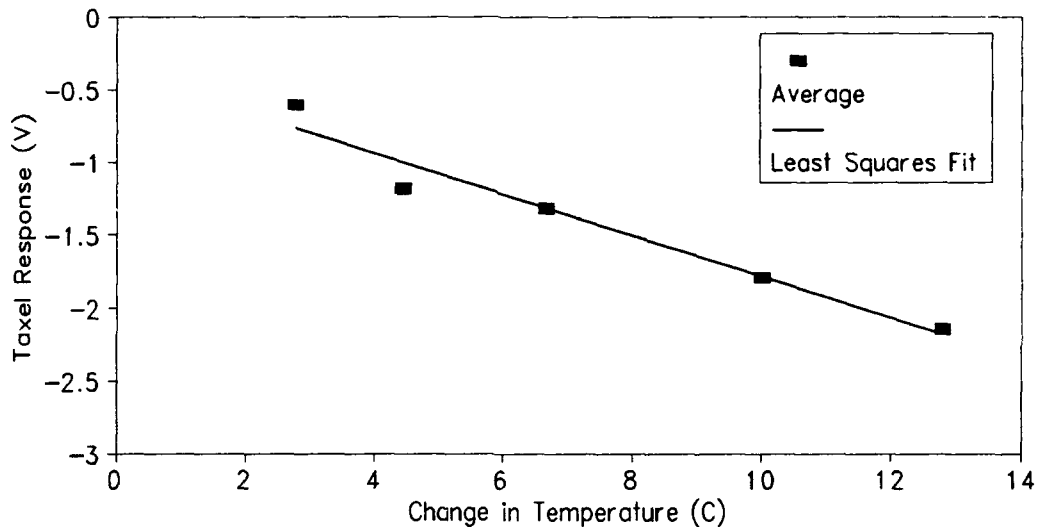
Figure 6.65.   Sensor data used to calibrate the sensor's
                      pyroelectric response.

6.5.4. Sensor Temperature Accuracy. Several voltage readings were taken to compare the actual temperature to the temperature predicted with the empirical equation. Figure 6.66 shows the percent difference between the average readings by the sensor compared to the actual temperature. The worst case percent difference was 40%, and the percent difference improved as larger temperature differences were used.
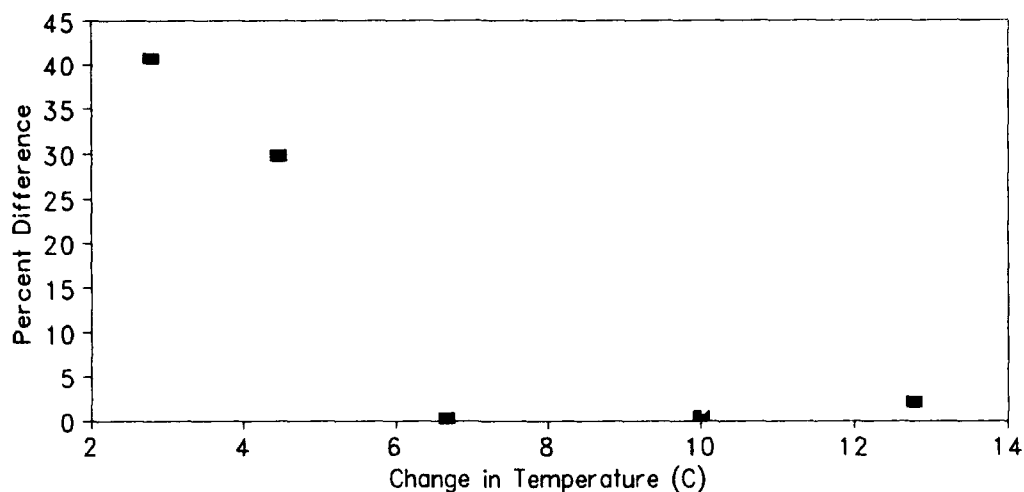
Figure 6.66.   Data depicting the worst case percent difference
                between the temperature change measured by the
                sensor and the actual temperature change.

6.5.5. Sensor Temperature Predictability. The output predicted
using Equation (5.10) was not very close to the actual response of the
sensor. For the best case, the difference between the taxel response
was off by a factor of 50 from that actually measured with the sensor.
The difference could be associated with the inaccuracy of the modeling
equations. Also, even though an attempt was made to provide the
sensor's surface with a uniform heat, it was difficult to provide
perfectly uniform heating. In addition, a significant component of the
heat meant for the active surface was absorbed by the sensor packaging.
This situation existed because the heater was permitted to directly
contact the sensor's package to avoid piezoelectric effects when taking
pyroelectric readings.

6.5.6. *Summary and Conclusion.* It was determined that the sensor temperature polarity was consistent with the equations presented in Chapter 3 and Appendix B. The temperature bandwidth of the sensor was determined to be 0.083 Hz. The temperature sensitivity was approximately 0.39 °C. The temperature accuracy was, on the average, within a 10% difference of the empirical value, and the temperature predictability was off by a factor of at least 50.

7. Conclusions and Recommendations

7.1. Introduction

In this chapter, the characteristics of the piezoelectric tactile sensor are summarized. Then, the performance figures of merit for the piezoelectric tactile sensor are compared to those of competing technologies presented in Chapter 2. This chapter concludes by presenting conclusions along with recommendations for further study of the piezoelectric tactile sensor.

7.2. Piezoelectric Tactile Sensor Characteristics

In this section, the performance characteristics of the piezoelectric tactile sensor are presented. Using the center-to-center taxel spacing as the criteria for theoretical microscopic spatial resolution, the spatial resolution of the sensor is 0.7 mm. The corresponding macroscopic array resolution of the sensor is 8 x 8. The lower detectable limit of the sensor was determined to be 1 g while the corresponding upper force sensitivity limit (limited by the amplifiers) was found to be 130 g. Therefore, the dynamic force sensitivity range of the sensor is 130:1. The maximum piezoelectric response bandwidth of the sensor was determined by Capt Dyson to be 25 Hz [8], and the force sensitivity was determined to be 7.35 grams. The pyroelectric response bandwidth of the sensor is 0.083 Hz, and the temperature sensitivity is 0.39 °C (relative to a temperature range of 2 °C to 13 °C).

7.3. Comparison of Performance Figures of Merit

In this section, the performance figures of merit for the piezoelectric tactile sensor fabricated in this thesis effort are compared to those of the competing technologies presented in Chapter 2. The spatial resolution of the sensor in this effort is higher than Harmon's ideal minimum criteria as presented in Chapter 2; however, the piezoelectric tactile sensor developed by Omata has a better spatial resolution (0.001 mm) [36]. The theoretical macroscopic array resolution of this sensor design significantly exceeds Harmon's ideal minimum resolution of 4 x 4. By comparison, sensor's fabricated with other technologies possess higher array resolutions; however, by adding internal multiplexers to this integrated circuit design, the number of allowable taxels could be increased, and therefore, the array resolution could be increased significantly. The dynamic force sensitivity range of this sensor design falls below Harmon's ideal minimum criteria of 1000:1; however, it has been shown in this thesis effort that the linear range of the taxel amplifiers can be enhanced. By enhancing the linear range of the amplifiers, the force sensitivity dynamic range of the sensor was correspondingly enhanced. The frequency response of the sensor was only 25% [8] of the minimum value that was specified by Harmon [3]. The force threshold sensitivity was only 10% of Harmon's minimum criteria; however, the force threshold sensitivity could be further reduced by lowering the baseline noise level of the sensor. Since a probable cause of the sensor's noise is the pyroelectric effect, the noise floor can be reduced when a pyroelectric compensation technique is incorporated into the sensor's circuitry. The upper force sensitivity limit of the sensor is lower than the minimum criteria

presented by Harmon [3]. Nevertheless, this limit can be overcome by incorporating an amplifier with an extended linear range (similar to the one added to the sensor's circuit design). The tactile sensor investigated in this thesis effort exceeds some of Harmon's minimum ideal criteria (spatial resolution, array resolution). Additionally, the characteristics of the sensor presented exceed those of most competing technologies (see Table 2.1). As in most research efforts, this research effort has addressed many issues concerning the piezoelectric tactile sensor; however, it has also exposed several beneficial techniques that improve the performance of the present sensor characteristics and warrant further research.

7.4. Conclusions

The objectives of this research effort were to: design and evaluate an amplifier with and extended linear range of 1 to 20 V, to design and fabricate an integrated circuit capable of being tested for electrical crosstalk, to characterize the piezoelectric response of the tactile sensor, and to characterize the pyroelectric response of the piezoelectric tactile sensor. A new amplifier was designed and added to the CIF file of the piezoelectric tactile sensor circuit. The revised amplifier design is a differential amplifier with a supply voltage of 12 V and a linear range from 1 to 17 V. The goal of a 20 V range was not satisfied. A piezoelectric tactile sensor was fabricated and tested for electrical crosstalk. However, It was found that there was a problem with the method of taking electrical crosstalk readings; therefore, the electrical crosstalk was not successfully characterized.

The tactile sensor was successfully characterized for piezoelectric and pyroelectric responses.

7.5. Recommendations

Even though the sensor in this research effort is functional, there are still many aspects of the sensor that require investigation.

7.5.1. A method of compensating for the pyroelectric effects inherent in the PVDF film needs to be developed.

7.5.2. The packaging of the sensor should be updated to allow attachment of the piezoelectric sensor to the MIT/Utah robotic hand. An ergonomic package needs to be developed that will provide the shape and size necessary to attach the piezoelectric sensor to a finger on the MIT/ Utah robotic hand.

7.5.3. In order to decrease the pin count of the sensor and simplify the external circuitry, *in situ* output multiplexers need to be added to the sensor's integrated circuit. The incorporation of *in situ* multiplexers would also simplify the wiring required to attach the sensor to the MIT/Utah robotic hand, and allow a higher array resolution by permitting an increased number of taxels.

7.5.4. Possibilities for decreasing the error in the predictability of the sensor's force sensitivity response should be investigated. A means of capturing the transients found during the acquisition of sensor data should be found, and additionally, a means of compensating for the effects of the dielectric adhesive used to bond the film to the integrated circuit should also be determined.

Appendix A. *Materials and Equipment*

Table A.1. Materials and Equipment.

Solef Polyvinylidene Fluoride Film – 40 μm thick The Solvay America Corporation 609 5th Ave. New York, NY 10017
Metal–Oxide–Semiconductor Implementation System (MOSIS) Se..ice University of Southern California Information Sciences Institute 4676 Admiralty Way Marina Del Rey, CA 90292
Urethane (MS–470/22) Miller–Stephenson Chemical Company George Washington Highway Danbury, CT 06810
MAX327 Ultra–Low Leakage, CMOS Analog Switches Maxim Integrated Products 120 San Gabriel Dr. Sunnyvale, CA 94086
MAX328 Ultra–Low Leakage, Monolithic CMOS Analog Multiplexer Chips Maxim Integrated Products 120 San Gabriel Dr. Sunnyvale, CA 94086
Keithley Electrometer, model 617 Keithley Instruments, Inc. 28775 Aurora Rd. Cleveland, OH 44139
HP Digital Storage Oscilloscope, Model 54100A Hewlett–Packard Co. 3155 Porter Dr. Palo Alto, CA 94304
Fluke Multimeter, Model 77/AN John Fluke Manufacturing Co. Everett, WA 99100
Zenith Z–248 Personal Computei (with IEEE–488 Interface) Zenith Data Systems Hilltop Rd. St Joseph, MI 49085
IEEE–488 Busses

Power Supplies, Models HP6205B, HP6624A, and HP6632A
  Hewlett–Packard Co.
  3155 Porter Dr.
  Palo Alto, CA 94304

Heaters
Thermocouples
Test Probe Fixture and Weights
Sensor Protoboard

Function Generator, Model HP3314
  Hewlett–Packard Co.
  3155 Porter Dr.
  Palo Alto, CA 94304

Elite–1 Circuit Design System
  E & L Instruments, Inc.
  70 Fulton Terrace
  New Haven, CT 06512

SPI Sputter Coater
  SPI Supplies
  P. O. Box 342
  West Chester, PA 19380

SPI Plasma Prep II
  SPI Supplies
  P. O. Box 342
  West Chester, PA 19380

VLSI Computer Aided Design (CAD) Tools
  Magic Integrated Circuit Layout Editor
  Simulation Programs Integrated Circuit
  Emphasis (HSPICE)

De–ionized Water
Glass Microscope Slides
Isopropyl Alcohol
Concentrated (37%) HCl
Ferric Chloride
Acetone
Silver Conductive Paint
Silver Conductive Epoxy
Scalpel
Syringe (3 cc)
Aluminum

Gold
Conductive Copper Tape
1-mil Diameter Wire
Heater
Thermocouple/Temperature Probe
Nitrogen Gas
Pulse Generator, Model 148 Wavetek, Inc. San Diego, CA 92123
Aluminum Wedge Bonder, Model TV909 MECH-EL Industries, Inc. Woburn, MA 01801
Electron Beam Vacuum Deposition System, Model DV602 Denton Hill, NJ 08003
Solderless Breadboard Sockets E & L Instruments, Inc. 70 Fulton Terrace New Haven, CT 06512
Digital Precision Balance, Model 500L Setra, Inc. Acton, MA 01720

Appendix B. *PVDF* *m Characterization Procedure*

Methodology for characterizing the piezoelectric film has undergone many iterations. The general procedure for characterizing the film started with Pirolo's research and was refined by Reston, Ford, Fitch, Dyson, and Yauilla [4-9].

B.1. Film polarization determination: The piezoelectric PVDF film supplied by the manufacturer is polarized, and both surfaces are metallized [63]. The surface of the PVDF film which exhibits a positive potential while being compressed will be attached to the integrated circuit electrode array. The surface of the film that is bonded to the electrode array must first have its metallization removed. Capt Ford initially developed a process to determine the polarization of the film [6]:

B.1.1. Cover two-thirds of a glass microscope slide with an aluminum thin film conductor using an electron beam vacuum deposition system as shown in Figure B.1. Apply a strip of copper tape to the surface of the slide that is coated with the aluminum thin film conductor. Apply another strip of copper tape to the uncoated surface of the slide.

B.1.2. Using a permanent laundry marker, place a small mark on one side of the piezoelectric PVDF film sheet. On the same side of the film, place a similar mark in the corner. Then, cut a small section of the film (6 mm x 6 mm) from the marked corner.

B.1.3. Attach the 6 mm x 6 mm sample (marked side up) to the central portion of the microscope slide with urethane adhesive.
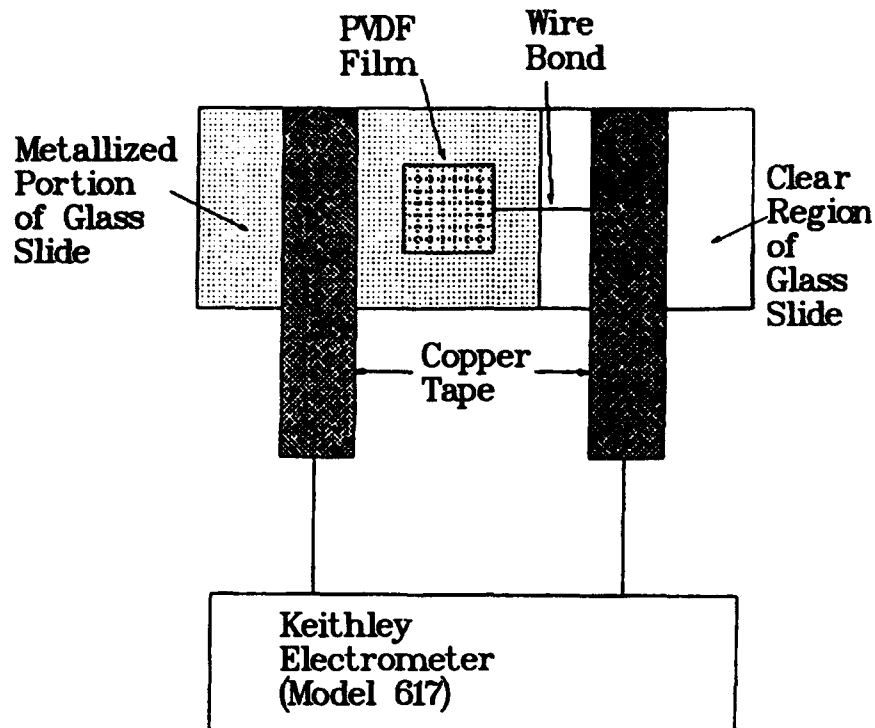
Figure B.1. Configuration for determining the piezoelectric PVDF
film's polarization [8].

Attach one end of a 1 mil diameter bond wire to the marked side of the

6 mm x 6 mm PVDF film with conductive silver paint. Attach the other

end of the 1 mil diameter wire to the copper tape that is on the

unmetallized surface of the slide.

B.1.4. Connect the voltage source (V_{source}) probe of the

electrometer to the metallized portion of the glass slide with copper

tape. Connect the voltage input (V_{in}) probe of the electrometer to the

copper tape that is attached to the unmetallized side of the glass

slide. Apply a positive 2-volt bias to the film. (Note: be sure to

attach the ground leads from the bias voltage and the input leads

together.)

B.1.5. Compress the film with a load. A positive response

implies that the V_{in} probe of the electrometer is connected to the

positive polarization (under compression) side of the film. A negative measurement implies that the V_{source} probe is connected to the positive polarization side of the film. Mark the side of the large film that corresponds to positive polarization under compression with a plus (+) sign. Mark the negative side with a minus (-) sign.

B.1.6. To verify proper markings, bring an electric heater close to the surface of the film. Verify the same polarization effect is observed. (If a compressive force causes a positive voltage response, then an increase in temperature should also cause a positive voltage response.)

B.1.7. Mark a 4" x 4" section in the corner of the 8.5" x 11" sheet of PVDF film. Mark the 4" x 4" section appropriately to indicate positive polarization. Cut out this section for subsequent processing.

B.2. Film characterization: This section outlines the procedure for recording the films piezoelectric and pyroelectric response.

B.2.1. Using the sample piece of film attached to the glass slide, apply loads ranging from 0 to 100 grams. Record the response on the computer.

B.2.2. Using an electric heating source, heat the sample piece of film attached to the glass slide and record the response on the computer.

```
*************************************************************
*        Author:   1Lt John M. Emmert
*
* This is the HSPICE deck for simulating the enhanced
*          amplifier design Vin versus Vout.
* Date: 20 May 93
* Filename: bigamp.sp
* Corrsponding VHDL File:  na
* Technology: scmos
* Description:  This HSPICE file is designed to simulate
*                the extended channel length amplifier
*************************************************************
.protect
*_____
* Power supply voltages
Vdd Vdd 0 dc 20v
*_____
* Input signals
Vin Vin 0 dc
*_____
R1 Vdd 1 7k
R2 Vdd Vout 5k
* Change the following line to reflect the desired
* channel and gate length
M1 1 Vin GND GND n L=82.0U W=205.0U
M2 Vout 1 GND GND n L=82.0U W=123.0U
*_____
* Options
.option brief post dcon= 1
*_____
* Analysis
.dc Vin 0 20 .2
*_____
* Print/plot commands
.print dc v(Vout)
*_____
* Model cards
.INCLUDE '/usr2/cad/chiplib/spicemodels/vti_hspice.lvl13'
.END
```

```
***********************************************************
*        Author:    1Lt John M. Emmert
*
* This is the HSPICE deck for simulating the response of the
* extended channel length amplifiers to changing Vdd over
* an extended length of time.
* Date: 23 Mar 93
* Filename: bigampt.sp
* Corrsponding VHDL File:  na
* Technology: scmos
* Description:  This HSPICE file is designed to simulate
*               the extended channel length amplifier
***********************************************************
.protect
*
*----------------------------------------------------------
* Input supply voltage
EVin Vin 0 Vdd 0 0.3076923
*
*----------------------------------------------------------
* Vdd signals
Vdd Vdd 0 dc
*
*----------------------------------------------------------
* Amplifier resistors
R_1_7k Vdd m1 7k
R_1_5k Vdd Vout1 5k
R_2_7k Vdd m2 7k
R_2_5k Vdd Vout2 5k
R_3_7k Vdd m3 7k
R_3_5k Vdd Vout3 5k
R_4_7k Vdd m4 7k
R_4_5k Vdd Vout4 5k
R_5_7k Vdd m5 7k
R_5_5k Vdd Vout5 5k
R_6_7k Vdd m6 7k
R_6_5k Vdd Vout6 5k
R_7_7k Vdd m7 7k
R_7_5k Vdd Vout7 5k
R_8_7k Vdd m8 7k
R_8_5k Vdd Vout8 5k
*
*----------------------------------------------------------
* Circuit extracted from the Magic file
M4 m1 Vin 0 0 n L=2.0U W=5.0U
M5 Vout1 m1 0 0 n L=2.0U W=3.0U
M1 m2 Vin 0 0 n L=18.0U W=45.0U
M0 Vout2 m2 0 0 n L=18.0U W=27.0U
M13 m3 Vin 0 0 n L=34.0U W=85.0U
M12 Vout3 m3 0 0 n L=34.0U W=51.0U
M11 m4 Vin 0 0 n L=50.0U W=125.0U
M10 Vout4 m4 0 0 n L=50.0U W=75.0U
M15 m5 Vin 0 0 n L=66.0U W=165.0U
```

```
M14 Vout5 m5 0 0 n L=66.0U W=99.0U
M9 m6 Vin 0 0 n L=82.0U W=205.0U
M8 Vout6 m6 0 0 n L=82.0U W=123.0U
M3 m7 Vin 0 0 n L=98.0U W=245.0U
M2 Vout7 m7 0 0 n L=98.0U W=147.0U
M7 m8 Vin 0 0 n L=114.0U W=285.0U
M6 Vout8 m8 0 0 n L=114.0U W=171.0U
*
*_____
* Options
.option brief post
*
*_____
* Analysis
.dc Vdd 0 50 0.25
*_____
* Print/plot commands
.print dc v(Vout8)
*_____
* Model cards
.INCLUDE '/usr2/cad/chiplib/spicemodels/vti_hspice.lvl13'
.END
```

```
****************************************************************
*          Author:    1Lt John M. Emmert
*
* This is the HSPICE deck for simulating the differential
*          amplifier design Vin versus Vout.
* Date: 20 May 93
* Filename: diffamp.sp
* Corrsponding VHDL File:   na
* Technology: scmos
* Description:   This HSPICE file is designed to simulate
*                the differential amplifier
****************************************************************
.protect
*
*──────────────────────────────────────────────────────
* Power supply voltages
Vdd Vdd 0 dc 12v
*──────────────────────────────────────────────────────
* Input signals
Vin Vin 0 dc
*──────────────────────────────────────────────────────
* Amplifier extracted from MAGIC file
M0 Vdd 6 6 Vdd p L=4.0U W=4.0U
M1 Vdd 1 1 Vdd p L=3.0U W=3.0U
M2 Vdd 1 2 Vdd p L=3.0U W=3.0U
M3 6 7 7 Vdd p L=4.0U W=4.0U
M4 1 Vin_minus 3 GND n L=2.0U W=9.0U
M5 2 7 3 GND n L=2.0U W=9.0U
M6 7 7 4 GND n L=4.0U W=4.0U
M7 5 vin GND GND n L=2.0U W=5.0U
M8 3 4 GND GND n L=2.0U W=8.0U
M9 4 4 GND GND n L=4.0U W=8.0U
M10 vout 2 Vdd Vdd p L=2.0U W=60.0U
M11 GND 4 vout GND n L=2.0U W=120.0U
* Capacitors
C0 vout GND 350F
C1 vin GND 11F
C2 5 GND 22F
C3 3 GND 62F
C4 Vin_minus GND 15F
C5 7 GND 40F
C6 1 GND 39F
C7 2 GND 45F
C8 6 GND 16F
C9 Vdd GND 257F
C10 4 GND 48F
* Resistors
R1 Vout Vin_minus 4k
R2 Vin_minus 5 1k
R3 Vdd 5 7k
*──────────────────────────────────────────────────────
```

```
* Options
.option brief post dcon= 1
*——————————————————————————————————
* Analysis
.dc Vin 0 20 .5
*——————————————————————————————————
* Print/plot commands
.print dc v(Vout)
*——————————————————————————————————
* Model cards
.INCLUDE '/usr2/cad/chiplib/spicemodels/vti_hspice.lvl13'
.END
```

```
' ************************************************************
' Data acquisition program to find the Vdd limit on the extended
' channel length amplifiers.
' filename       S_A_BD.BAS
' Language: QuickBASIC
' Instrument: Electrometer Model 617
'             HP programmable power supply model HP6624A
' Purpose:  Find single amplifier breakdown time (Long term test)
' Instructions:
'              1. Connect common ground
'                   - green wire on electrometer
'                   - ground on ps
'              2. Wire Vdd to channel 3 on PS
'              3. Wire Vin to channel 4 on PS
'              4. Red wire of electrometer to outputof amp
'************************************************************
'
'Set up the HPIB IEEE-488 interface card
REM $INCLUDE: 'QBSETUP'
CLS
PRINT "The amplifier breakdown test program is running."
ISC& = 7                              'interface select code
EM& = ISC& * 100 + 27                 'address of electrometer
PS& = ISC& * 100 + 5                  'address of pwr sup
INPUT "Enter the filename for data storage: ", DFILES$
OPEN DFILES$ FOR OUTPUT AS #3
CALL IORESET(ISC&)
IF PCIB.ERR <> NOERR THEN ERROR PCIB.BASERR   'check for errors
'Setup a timeout of 5 seconds
time! = 5
CALL IOTIMEOUT(ISC&, time!)
IF PCIB.ERR <> NOERR THEN ERROR PCIB.BASERR
CALL IOREMOTE(PS&)
       CALL IOCLEAR(PS&)
       IF PCIB.ERR <> NOERR THEN ERROR PCIB.BASERR
       CMD$ = "CLR;ISET3,.8"
       LENGTH% = LEN(CMD$)
       CALL IOOUTPUTS(PS&, CMD$, LENGTH%)
       CMD$ = "VSET3,0"
       LENGTH% = LEN(CMD$)
       CALL IOOUTPUTS(PS&, CMD$, LENGTH%)
       CMD$ = "CLR;ISET4,.8"
       LENGTH% = LEN(CMD$)
       CALL IOOUTPUTS(PS&, CMD$, LENGTH%)
       CMD$ = "VSET4,0"
       LENGTH% = LEN(CMD$)
       CALL IOOUTPUTS(PS&, CMD$, LENGTH%)
CALL IOREMOTE(EM&)
       CALL IOCLEAR(EM&)
```

```
        IF PCIB.ERR <> NOERR THEN ERROR PCIB.BASERR
        CMD$ = "C1XZ1XC0XZ0X"
        LENGTH% = LEN(CMD$)
        CALL IOOUTPUTS(EM&, CMD$, LENGTH%)
        CMD$ = "D0X"
        LENGTH% = LEN(CMD$)
        CALL IOOUTPUTS(EM&, CMD$, LENGTH%)
        CMD$ = "F0X"
        LENGTH% = LEN(CMD$)
        CALL IOOUTPUTS(EM&, CMD$, LENGTH%)
        CMD$ = "R0X"
        LENGTH% = LEN(CMD$)
        CALL IOOUTPUTS(EM&, CMD$, LENGTH%)
        CMD$ = "Q7X"
        LENGTH% = LEN(CMD$)
        CALL IOOUTPUTS(EM&, CMD$, LENGTH%)
        CMD$ = "G1X"
        LENGTH% = LEN(CMD$)
        CALL IOOUTPUTS(EM&, CMD$, LENGTH%)
INPUT "To start the test, hit <CR>.", null$
CLS
LOCATE 5, 1
PRINT "Please do not disturb!"
PRINT "Thanks,"
PRINT "Marty"
VRD$ = SPACE$(12)
VOLTS$ = SPACE$(6)
MAX% = 150: ACTUAL% = 0
' Initializations
vddvolts = 10
vinvolts = vddvolts / 3.25
N = 1800
        VOLTS$ = STR$(vddvolts)
        CMD$ = "VSET3," + VOLTS$
        LENGTH% = LEN(CMD$)
        CALL IOOUTPUTS(PS&, CMD$, LENGTH%)
        VOLTS$ = STR$(vinvolts)
        CMD$ = "VSET4," + VOLTS$
        LENGTH% = LEN(CMD$)
        CALL IOOUTPUTS(PS&, CMD$, LENGTH%)
time = 15        'delay for taking reading 15 s
t = time
t1 = TIMER
401 t2 = TIMER - t1
402 IF TIMER > 86399 GOTO 403
IF t2 < t GOTO 401
GOTO 404
403 t = time - t2
t1 = 0
GOTO 402
'Take measurements
404     CMD$ = "B0X"
        LENGTH% = LEN(CMD$)
```

```
        CALL IOOUTPUTS(EM&, CMD$, LENGTH%)
        CALL IOENTERS(EM&, VRD$, MAX%, ACTUAL%)
        IF PCIB.ERR <> NOERR THEN ERROR PCIB.BASERR
        VRD - VAL(VRD$)
        LOCATE 3, 1
        PRINT "TIME            Vdd            Vin            Vout"
        PRINT "                                "
        LOCATE 4, 1
        PRINT TIMER, vddvolts, vinvolts, VRD
        PRINT #3, TIMER, vddvolts, vinvolts, VRD
'wait 24 hours - 86400 s and meausre again
time - 86400        'set the timer in seconds
t - time
t1 - TIMER
101 t2 - TIMER - t1
102 IF TIMER > 86399 GOTO 103
IF t2 < t GOTO 101
GOTO 104
103 t - time - t2
t1 - 0
GOTO 102
104     CMD$ = "BOX"
        LENGTH% = LEN(CMD$)
        CALL IOOUTPUTS(EM&, CMD$, LENGTH%)
        CALL IOENTERS(EM&, VRD$, MAX%, ACTUAL%)
        IF PCIB.ERR <> NOERR THEN ERROR PCIB.BASERR
        VRD - VAL(VRD$)
        LOCATE 3, 1
        PRINT "TIME            Vdd            Vin            Vout"
        PRINT "                                "
        LOCATE 4, 1
        PRINT TIMER, vddvolts, vinvolts, VRD
        PRINT #3, TIMER, vddvolts, vinvolts, VRD
'increment vdd and vin
vddvolts - vddvolts + .5
vinvolts - vinvolts + .5 / 3.25
        VOLTS$ = STR$(vddvolts)
        CMD$ - "VSET3," + VOLTS$
        LENGTH% = LEN(CMD$)
        CALL IOOUTPUTS(PS&, CMD$, LENGTH%)
        VOLTS$ = STR$(vinvolts)
        CMD$ - "VSET4," + VOLTS$
        LENGTH% = LEN(CMD$)
        CALL IOOUTPUTS(PS&, CMD$, LENGTH%)
time = 15        'delay for taking reading 15 s
t - time
t1 - TIMER
301 t2 = TIMER - t1
302 IF TIMER > 86399 GOTO 303
IF t2 < t GOTO 301
GOTO 304
303 t - time - t2
t1 = 0
```

```
        GOTO 302
        304      CMD$ - "BOX"
              LENGTH% - LEN(CMD$)
              CALL IOOUTPUTS(EM&, CMD$, LENGTH%)
              CALL IOENTERS(EM&, VRD$, MAX%, ACTUAL%)
              IF PCIB.ERR <> NOERR THEN ERROR PCIB.BASERR
              VRD - VAL(VRD$)
              LOCATE 3, 1
              PRINT "TIME              Vdd          Vin            Vout"
              PRINT "                                        "
              LOCATE 4, 1
              PRINT TIMER, vddvolts, vinvolts, VRD
              PRINT #3, TIMER, vddvolts, vinvolts, VRD
IF vddvolts > 50 GOTO 1000
time - 900        'set the timer for 15 min - 900 s
t - time
t1 - TIMER
201 t2 - TIMER - t1
202 IF TIMER > 86397 GOTO 203
IF t2 < t GOTO 201
GOTO 104
203 t - time - t2
t1 - 0
GOTO 202
1000 vddvolts - 0
        vinvolts - 0
        VOLTS$ - STR$(vddvolts)
        CMD$ - "VSET3," + VOLTS$   'command for setting voltage
        LENGTH% - LEN(CMD$)
        CALL IOOUTPUTS(PS&, CMD$, LENGTH%)
        VOLTS$ - STR$(vinvolts)
        CMD$ - "VSET4," + VOLTS$   'command for setting voltage
        LENGTH% = LEN(CMD$)
        CALL IOOUTPUTS(PS&, CMD$, LENGTH%)
CALL IOLOCAL(EM&)
CALL IOLOCAL(PS&)
CLOSE
END
```

```
'****************************************************************
' Data acquisition program to find the Vin versus Vout for
' the differential or extended channel length amplifier.
' filename       AMP_CHAR.BAS
' Language: QuickBASIC
' Instrument: Electrometer Model 617
'            Power Supply: HP 6624A
' Purpose:  Find amplifier electrical characteristics
' Instructions:
'               1. Connect common ground
'                   - green wire on electrometer
'                   - ground on ps
'               2. Wire Vdd to channel 3 on PS
'               3. Wire Vin to channel 4 on PS
'               4. Red wire of electrometer to output of amp
'****************************************************************
'
'Set up the HPIB IEEE-488 interface card
REM $INCLUDE: 'QBSETUP'
CLS
ISC& = 7
EM& = ISC& * 100 + 27
PS& = ISC& * 100 + 5
INPUT "Enter the filename for data storage: ", DFILES$
OPEN DFILES$ FOR OUTPUT AS #3
CALL IORESET(ISC&)
IF PCIB.ERR <> NOERR THEN ERROR PCIB.BASERR
'Setup a timeout of 5 seconds
time! = 5
CALL IOTIMEOUT(ISC&, time!)
IF PCIB.ERR <> NOERR THEN ERROR PCIB.BASERR
CALL IOREMOTE(PS&)
        CALL IOCLEAR(PS&)
        IF PCIB.ERR <> NOERR THEN ERROR PCIB.BASERR
        CMD$ = "CLR;ISET3,.8"
        LENGTH% = LEN(CMD$)
        CALL IOOUTPUTS(PS&, CMD$, LENGTH%)
        CMD$ = "VSET3,0"
        LENGTH% = LEN(CMD$)
        CALL IOOUTPUTS(PS&, CMD$, LENGTH%)
        CMD$ = "CLR;ISET4,.8"
        LENGTH% = LEN(CMD$)
        CALL IOOUTPUTS(PS&, CMD$, LENGTH%)
        CMD$ = "VSET4,0"
        LENGTH% = LEN(CMD$)
        CALL IOOUTPUTS(PS&, CMD$, LENGTH%)
CALL IOREMOTE(EM&)
        CALL IOCLEAR(EM&)
        IF PCIB.ERR <> NOERR THEN ERROR PCIB.BASERR
        CMD$ = "C1XZ1XC0XZ0X"
        LENGTH% = LEN(CMD$)
        CALL IOOUTPUTS(EM&, CMD$, LENGTH%)
        CMD$ = "D0X"
```

```
            LENGTH% - LEN(CMD$)
            CALL IOOUTPUTS(EM&, CMD$, LENGTH%)
            CMD$ - "FOX"
            LENGTH% - LEN(CMD$)
            CALL IOOUTPUTS(EM&, CMD$, LENGTH%)
            CMD$ - "ROX"
            LENGTH% - LEN(CMD$)
            CALL IOOUTPUTS(EM&, CMD$, LENGTH%)
            CMD$ - "Q7X"
            LENGTH% - LEN(CMD$)
            CALL IOOUTPUTS(EM&, CMD$, LENGTH%)
            CMD$ - "G1X"
            LENGTH% - LEN(CMD$)
            CALL IOOUTPUTS(EM&, CMD$, LENGTH%)
INPUT "To start the test, hit <CR>.", null$
CLS
LOCATE 5, 1
VRD$ - SPACE$(12)
VOLTS$ - SPACE$(6)
MAX% - 150: ACTUAL% - 0
' Initializations
vddvolts - 12
vinvolts - 0
            VOLTS$ - STR$(vddvolts)
            CMD$ - "VSET3," + VOLTS$
            LENGTH% - LEN(CMD$)
            CALL IOOUTPUTS(PS&, CMD$, LENGTH%)
900    VOLTS$ - STR$(vinvolts)
            CMD$ - "VSET4," + VOLTS$
            LENGTH% - LEN(CMD$)
            CALL IOOUTPUTS(PS&, CMD$, LENGTH%)
time - 15          'delay for taking reading 15 s
t = time
t1 - TIMER
401 t2 - TIMER - t1
402 IF TIMER > 86399 GOTO 403
IF t2 < t GOTO 401
GOTO 404
403 t = time - t2
t1 = 0
GOTO 402
'Take measurements
404      CMD$ = "BOX"
            LENGTH% - LEN(CMD$)
            CALL IOOUTPUTS(EM&, CMD$, LENGTH%)
            CALL IOENTERS(EM&, VRD$, MAX%, ACTUAL%)
            IF PCIB.ERR <> NOERR THEN ERROR PCIB.BASERR
            VRD - VAL(VRD$)
            PRINT "TIME           Vdd          Vin              Vout"
            PRINT "                                                 "
            PRINT #3, TIMER, vddvolts, vinvolts, VRD
IF vinvolts > 12 GOTO 1000
vinvolts - vinvolts + .25
```

```
GOTO 900
1000 vddvolts - 0
     vinvolts - 0
      VOLTS$ - STR$(vddvolts)
      CMD$ - "VSET3," + VOLTS$
      LENGTH% - LEN(CMD$)
      CALL IOOUTPUTS(PS&, CMD$, LENGTH%)
      VOLTS$ - STR$(vinvolts)
      CMD$ - "VSET4," + VOLTS$
      LENGTH% - LEN(CMD$)
      CALL IOOUTPUTS(PS&, CMD$, LENGTH%)
CALL IOLOCAL(EM&)
CALL IOLOCAL(PS&)
CLOSE
END
```

```
'*******************************************************************
' Data acquisition program used to find the electrical crosstalk
' for the integrated circuit used for the base of the sensor.
' filename        TALK.BAS
' Language. QuickBASIC
' Instruments: HP 54100A DSO and HP 6624A DC pwr supply
'                HP 8082A Pulse Generator
' Purpose:  Find the electrical crosstalk
' Instructions:
'                1. Attach ps chan 1 V+ to the switch pin
'                                    V- to GND
'                2. Attach ps chan 2 V+ to the to input taxel
'                3. Pull the regular input taxel wire out of its socket
'                                    V- to GND
'                4. Attach ps chan 3 V+ to sensor V+ pin
'                                    V- to GND
'                5. Attach ps chan 4 V- to sensor V- pin
'                                    V+ to GND
'                6. Attach 2nd ps to Vcc output chips
'                                    (set to 5 V)
'                7. Attach DSO chan 1 to Vout
'                8. Attach Pulse Gen to clk set for 1.28 kHz
'                9. Attach Resistor to chan 2 DSO for triggering
'                10. Connect all grounds together
'                11. Make sure the clk is set so all 64 taxel outputs
'                    are visible on the screen (check the multiplexer
'                    counter LSB input)
'*******************************************************************
'
'Set up the HPIB IEEE-488 interface card
REM $INCLUDE: 'QBSETUP'
CLS
' change the following line to "new" for the new circuit
'       or "old" for the old integrated circuit.
chip$ = "new"
INPUT "Enter the probed taxel # (eg. 27) <CR>: ", day$
ISC& = 7
DSO& = ISC& * 100 + 7
PS& = ISC& * 100 + 5
CALL IORESET(ISC&)
IF PCIB.ERR <> NOERR THEN ERROR PCIB.BASERR  'check for errors
'Setup a timeout of 5 seconds
time! = 5
CALL IOTIMEOUT(ISC&, time!)
IF PCIB.ERR <> NOERR THEN ERROR PCIB.BASERR
        CALL IOREMOTE(PS&)
        CALL IOCLEAR(PS&)
        IF PCIB.ERR <> NOERR THEN ERROR PCIB.BASERR
        CMD$ = "CLR;ISET1,1"
        LENGTH% = LEN(CMD$)
        CALL IOOUTPUTS(PS&, CMD$, LENGTH%)
        CMD$ = "VSET1,0"
        LENGTH% = LEN(CMD$)
```

```
CALL IOOUTPUTS(PS&, CMD$, LENGTH%)
CMD$ - "CLR;ISET2,1"
LENGTH% - LEN(CMD$)
CALL IOOUTPUTS(PS&, CMD$, LENGTH%)
CMD$ - "VSET2,0"
LENGTH% - LEN(CMD$)
CALL IOOUTPUTS(PS&, CMD$, LENGTH%)
CMD$ - "CLR;ISET3,.8"
LENGTH% - LEN(CMD$)
CALL IOOUTPUTS(PS&, CMD$, LENGTH%)
CMD$ - "VSET3,0"
LENGTH% - LEN(CMD$)
CALL IOOUTPUTS(PS&, CMD$, LENGTH%)
CMD$ - "CLR;ISET4,.8"
LENGTH% - LEN(CMD$)
CALL IOOUTPUTS(PS&, CMD$, LENGTH%)
CMD$ - "VSET4,0"
LENGTH% - LEN(CMD$)
CALL IOOUTPUTS(PS&, CMD$, LENGTH%)
CALL IOREMOTE(DSO&)
CALL IOCLEAR(DSO&)
IF PCIB.ERR <> NOERR THEN ERROR PCIB.BASERR
CMD$ - "STOP"
LENGTH% - LEN(CMD$)
CALL IOOUTPUTS(DSO&, CMD$, LENGTH%)
CMD$ - "RUN"
LENGTH% - LEN(CMD$)
CALL IOOUTPUTS(DSO&, CMD$, LENGTH%)
CMD$ - "DISPLAY BRIGHTNESS HIGH"
LENGTH% - LEN(CMD$)
CALL IOOUTPUTS(DSO&, CMD$, LENGTH%)
CMD$ - "DISPLAY GRAT GRID"
LENGTH% - LEN(CMD$)
CALL IOOUTPUTS(DSO&, CMD$, LENGTH%)
CMD$ - "CHANNEL 2 SENS .5"
LENGTH% - LEN(CMD$)
CALL IOOUTPUTS(DSO&, CMD$, LENGTH%)
CMD$ - "CHANNEL 1"
LENGTH% - LEN(CMD$)
CALL IOOUTPUTS(DSO&, CMD$, LENGTH%)
CMD$ - "CHANNEL 1 PROBE 10"
LENGTH% - LEN(CMD$)
CALL IOOUTPUTS(DSO&, CMD$, LENGTH%)
CMD$ - "CHANNEL 1 SENS 2"
LENGTH% - LEN(CMD$)
CALL IOOUTPUTS(DSO&, CMD$, LENGTH%)
CMD$ - "CHANNEL 1 OFFS 7.48"
LENGTH% - LEN(CMD$)
CALL IOOUTPUTS(DSO&, CMD$, LENGTH%)
CMD$ - "TIMEBASE MODE TRIGGERED"
LENGTH% - LEN(CMD$)
CALL IOOUTPUTS(DSO&, CMD$, LENGTH%)
CMD$ - "TIMEBASE SENSITIVITY 5e-3"
```

```
      LENGTH% = LEN(CMD$)
      CALL IOOUTPUTS(DSO&, CMD$, LENGTH%)
      CMD$ = "TIMEBASE DELAY 0"
      LENGTH% = LEN(CMD$)
      CALL IOOUTPUTS(DSO&, CMD$, LENGTH%)
      CMD$ = "TRIGGER MODE EDGE"
      LENGTH% = LEN(CMD$)
      CALL IOOUTPUTS(DSO&, CMD$, LENGTH%)
      CMD$ = "TRIGGER SOURCE CHANNEL 2"
      LENGTH% = LEN(CMD$)
      CALL IOOUTPUTS(DSO&, CMD$, LENGTH%)
      CMD$ = "TRIGGER LEVEL 0.6"
      LENGTH% = LEN(CMD$)
      CALL IOOUTPUTS(DSO&, CMD$, LENGTH%)
      CMD$ = "TRIGGER SLOPE NEGATIVE"
      LENGTH% = LEN(CMD$)
      CALL IOOUTPUTS(DSO&, CMD$, LENGTH%)
CLS
'bias circuit
      CMD$ = "ISET2,1"
      LENGTH% = LEN(CMD$)
      CALL IOOUTPUTS(PS&, CMD$, LENGTH%)
      CMD$ = "ISET2,5"
      LENGTH% = LEN(CMD$)
      CALL IOOUTPUTS(PS&, CMD$, LENGTH%)
      CMD$ = "VSET2,0"
      LENGTH% = LEN(CMD$)
      CALL IOOUTPUTS(PS&, CMD$, LENGTH%)
      CMD$ = "VSET4,12"
      LENGTH% = LEN(CMD$)
      CALL IOOUTPUTS(PS&, CMD$, LENGTH%)
      CMD$ = "ISET3,0.8"
      LENGTH% = LEN(CMD$)
      CALL IOOUTPUTS(PS&, CMD$, LENGTH%)
      CMD$ = "VSET3,12"
      LENGTH% = LEN(CMD$)
      CALL IOOUTPUTS(PS&, CMD$, LENGTH%)
DIM time(1000), preload(1000), load(1000), postload(1000)
2000    CMD$ = "VSET1,5"
      LENGTH% = LEN(CMD$)
      CALL IOOUTPUTS(PS&, CMD$, LENGTH%)
      t3 = TIMER
2001 t4 = TIMER - t3
      IF t4 < 1 THEN GOTO 2001
      CMD$ = "STORE CHANNEL 1, MEMORY 3"
      LENGTH% = LEN(CMD$)
      CALL IOOUTPUTS(DSO&, CMD$, LENGTH%)
      timeconst = 1
      CMD$ = "VSET1,0"
      LENGTH% = LEN(CMD$)
      CALL IOOUTPUTS(PS&, CMD$, LENGTH%)
      t3 = TIMER
5200 t4 = TIMER - t3
```

```
        IF t4 < timeconst THEN GOTO 5200
        CMD$ = "STORE CHANNEL 1, MEMORY 4"
        LENGTH% = LEN(CMD$)
        CALL IOOUTPUTS(DSO&, CMD$, LENGTH%)
'Retreive preload data from scope
        CMD$ = "WAVEFORM SOURCE MEMORY 3 FORMAT ASCII"
        LENGTH% = LEN(CMD$)
        CALL IOOUTPUTS(DSO&, CMD$, LENGTH%)
        CMD$ = "POINTS?"
        LENGTH% = LEN(CMD$)
        CALL IOOUTPUTS(DSO&, CMD$, LENGTH%)
        R$ = SPACE$(15)
        MAX% = 150: ACTUAL% = 0
        CALL IOENTERS(DSO&, R$, MAX%, ACTUAL%)
        POINTS = VAL(R$)
        CMD$ = "YREF?"
        LENGTH% = LEN(CMD$)
        CALL IOOUTPUTS(DSO&, CMD$, LENGTH%)
        R$ = SPACE$(15)
        MAX% = 150: ACTUAL% = 0
        CALL IOENTERS(DSO&, R$, MAX%, ACTUAL%)
        YREF = VAL(R$)
        CMD$ = "YINC?"
        LENGTH% = LEN(CMD$)
        CALL IOOUTPUTS(DSO&, CMD$, LENGTH%)
        R$ = SPACE$(15)
        MAX% = 150: ACTUAL% = 0
        CALL IOENTERS(DSO&, R$, MAX%, ACTUAL%)
        YINC = VAL(R$)
        CMD$ = "YOR?"
        LENGTH% = LEN(CMD$)
        CALL IOOUTPUTS(DSO&, CMD$, LENGTH%)
        R$ = SPACE$(15)
        MAX% = 150: ACTUAL% = 0
        CALL IOENTERS(DSO&, R$, MAX%, ACTUAL%)
        YORG = VAL(R$)
        CMD$ = "XINC?"
        LENGTH% = LEN(CMD$)
        CALL IOOUTPUTS(DSO&, CMD$, LENGTH%)
        R$ = SPACE$(15)
        MAX% = 150: ACTUAL% = 0
        CALL IOENTERS(DSO&, R$, MAX%, ACTUAL%)
        XINC = VAL(R$)
        CMD$ = "XOR?"
        LENGTH% = LEN(CMD$)
        CALL IOOUTPUTS(DSO&, CMD$, LENGTH%)
        R$ = SPACE$(15)
        MAX% = 150: ACTUAL% = 0
        CALL IOENTERS(DSO&, R$, MAX%, ACTUAL%)
        XORG = VAL(R$)
        CMD$ = "XREF?"
        LENGTH% = LEN(CMD$)
        CALL IOOUTPUTS(DSO&, CMD$, LENGTH%)
```

```
              R$ - SPACE$(15)
              MAX% - 150: ACTUAL% - 0
              CALL IOENTERS(DSO&, R$, MAX%, ACTUAL%)
              XREF - VAL(R$)
CLS
X$ - SPACE$(15)
Y$ - SPACE$(15)
CMD$ - "DATA?"
LENGTH% - LEN(CMD$)
CALL IOOUTPUTS(DSO&, CMD$, LENGTH%)
FOR i - 1 TO POINTS
              CALL IOENTERS(DSO&, Y$, MAX%, ACTUAL%)
              X - (i * XINC) + XORG
              Y - ((VAL(Y$) - YREF) * YINC) + YORG
              time(i) - 0
              time(i) - X
              preload(i) - 0
              preload(i) - Y
NEXT i
'Retreive post bias data from scope
              CMD$ - "WAVEFORM SOURCE MEMORY 4 FORMAT ASCII"
              LENGTH% - LEN(CMD$)
              CALL IOOUTPUTS(DSO&, CMD$, LENGTH%)
              CMD$ - "POINTS?"
              LENGTH% - LEN(CMD$)
              CALL IOOUTPUTS(DSO&, CMD$, LENGTH%)
              R$ - SPACE$(15)
              MAX% - 150: ACTUAL% - 0
              CALL IOENTERS(DSO&, R$, MAX%, ACTUAL%)
              POINTS - VAL(R$)
              CMD$ - "YREF?"
              LENGTH% - LEN(CMD$)
              CALL IOOUTPUTS(DSO&, CMD$, LENGTH%)
              R$ - SPACE$(15)
              MAX% - 150: ACTUAL% - 0
              CALL IOENTERS(DSO&, R$, MAX%, ACTUAL%)
              YREF - VAL(R$)
              CMD$ - "YINC?"
              LENGTH% - LEN(CMD$)
              CALL IOOUTPUTS(DSO&, CMD$, LENGTH%)
              R$ - SPACE$(15)
              MAX% - 150: ACTUAL% - 0
              CALL IOENTERS(DSO&, R$, MAX%, ACTUAL%)
              YINC - VAL(R$)
              CMD$ - "YOR?"
              LENGTH% - LEN(CMD$)
              CALL IOOUTPUTS(DSO&, CMD$, LENGTH%)
              R$ - SPACE$(15)
              MAX% - 150: ACTUAL% - 0
              CALL IOENTERS(DSO&, R$, MAX%, ACTUAL%)
              YORG - VAL(R$)
              CMD$ - "XINC?"
              LENGTH% - LEN(CMD$)
```

```
                CALL IOOUTPUTS(DSO&, CMD$, LENGTH%)
                R$ - SPACE$(15)
                MAX% - 150: ACTUAL% - 0
                CALL IOENTERS(DSO&, R$, MAX%, ACTUAL%)
                XINC - VAL(R$)
                CMD$ - "XOR?"
                LENGTH% - LEN(CMD$)
                CALL IOOUTPUTS(DSO&, CMD$, LENGTH%)
                R$ - SPACE$(15)
                MAX% - 150: ACTUAL% - 0
                CALL IOENTERS(DSO&, R$, MAX%, ACTUAL%)
                XORG - VAL(R$)
                CMD$ - "XREF?"
                LENGTH% - LEN(CMD$)
                CALL IOOUTPUTS(DSO&, CMD$, LENGTH%)
                R$ - SPACE$(15)
                MAX% - 150: ACTUAL% - 0
                CALL IOENTERS(DSO&, R$, MAX%, ACTUAL%)
                XREF - VAL(R$)
CLS
X$ - SPACE$(15)
Y$ - SPACE$(15)
CMD$ - "DATA?"
LENGTH% - LEN(CMD$)
CALL IOOUTPUTS(DSO&, CMD$, LENGTH%)
FOR i - 1 TO POINTS
                CALL IOENTERS(DSO&, Y$, MAX%, ACTUAL%)
                X - (i * XINC) + XORG
                Y - ((VAL(Y$) - YREF) * YINC) + YORG
                load(i) - 0
                load(i) - Y
NEXT i
'develop weighting data
DIM taxelpre(64), taxellod(64), pre(64), lod(64), weight(64)
diff - POINTS / 64
ref - diff / 2
sumpre - 0
sumload - 0
FOR i - 1 TO 64
j - INT(diff * i - ref)
IF ABS(preload(j - 1) - preload(j)) <- .4 THEN GOTO 610
IF ABS(preload(j) - preload(j + 1)) <- .4 THEN GOTO 630
CLS
INPUT "Check clock synchronization and push <CR> to restart ", null$
GOTO 2000
630 pre(i) - (preload(j) + preload(j + 1)) / 2
GOTO 640
610 IF ABS(preload(j) - preload(j + 1)) <- .4 THEN GOTO 620
pre(i) - (preload(j - 1) + preload(j)) / 2
GOTO 640
620 pre(i) - (preload(j - 1) + preload(j) + preload(j + 1)) / 3
640 IF ABS(load(j - 1) - load(j)) <- .4 THEN GOTO 660
IF ABS(load(j) - load(j + 1)) <- .4 THEN GOTO 680
```

```
CLS
INPUT "Check clock synchronization and push <CR> to restart ", null$
GOTO 2000
680 lod(i) - (load(j) + load(j + 1)) / 2
GOTO 690
660 IF ABS(load(j) - load(j + 1)) <- .4 THEN GOTO 670
lod(i) - (load(j - 1) + load(j)) / 2
GOTO 690
670 lod(i) - (load(j - 1) + load(j) + load(j + 1)) / 3
690 weight(i) - lod(i) - pre(i)
NEXT i
1000    CMD$ - "VSET1,5"
        LENGTH% - LEN(CMD$)
        CALL IOOUTPUTS(PS&, CMD$, LENGTH%)
INPUT "Enter the test number for data storage (ie 01 for test #1): ",
TEST$
DFILES$ - "B:" + chip$ + day$ + TEST$ + ".txt"
OPEN DFILES$ FOR OUTPUT AS #3
CLS
        CMD$ - "VSET1,0"
        LENGTH% - LEN(CMD$)
        CALL IOOUTPUTS(PS&, CMD$, LENGTH%)
CMD$ - "VSET2,6.21"
LENGTH% - LEN(CMD$)
CALL IOOUTPUTS(PS&, CMD$, LENGTH%)
t3 - TIMER
5250 t4 - TIMER - t3
IF t4 < timeconst THEN GOTO 5250
CMD$ - "STORE CHANNEL 1, MEMORY 4"
LENGTH% - LEN(CMD$)
CALL IOOUTPUTS(DSO&, CMD$, LENGTH%)
t3 - TIMER
5260 t4 - TIMER - t3
IF t4 < timeconst THEN GOTO 5260
CMD$ - "VSET2,0"
LENGTH% - LEN(CMD$)
CALL IOOUTPUTS(PS&, CMD$, LENGTH%)
'Retreive loaded info from scope
        CMD$ - "WAVEFORM SOURCE MEMORY 4 FORMAT ASCII"
        LENGTH% = LEN(CMD$)
        CALL IOOUTPUTS(DSO&, CMD$, LENGTH%)
        CMD$ - "POINTS?"
        LENGTH% - LEN(CMD$)
        CALL IOOUTPUTS(DSO&, CMD$, LENGTH%)
        R$ - SPACE$(15)
        MAX% - 150: ACTUAL% - 0
        CALL IOENTERS(DSO&, R$, MAX%, ACTUAL%)
        POINTS - VAL(R$)
        CMD$ - "YREF?"
        LENGTH% - LEN(CMD$)
        CALL IOOUTPUTS(DSO&, CMD$, LENGTH%)
        R$ - SPACE$(15)
        MAX% - 150: ACTUAL% = 0
```

```
        CALL IOENTERS(DSO&, R$, MAX%, ACTUAL%)
        YREF = VAL(R$)
        CMD$ = "YINC?"
        LENGTH% = LEN(CMD$)
        CALL IOOUTPUTS(DSO&, CMD$, LENGTH%)
        R$ = SPACE$(15)
        MAX% = 150: ACTUAL% = 0
        CALL IOENTERS(DSO&, R$, MAX%, ACTUAL%)
        YINC = VAL(R$)
        CMD$ = "YOR?"
        LENGTH% = LEN(CMD$)
        CALL IOOUTPUTS(DSO&, CMD$, LENGTH%)
        R$ = SPACE$(15)
        MAX% = 150: ACTUAL% = 0
        CALL IOENTERS(DSO&, R$, MAX%, ACTUAL%)
        YORG = VAL(R$)
        CMD$ = "XINC?"
        LENGTH% = LEN(CMD$)
        CALL IOOUTPUTS(DSO&, CMD$, LENGTH%)
        R$ = SPACE$(15)
        MAX% = 150: ACTUAL% = 0
        CALL IOENTERS(DSO&, R$, MAX%, ACTUAL%)
        XINC = VAL(R$)
        CMD$ = "XOR?"
        LENGTH% = LEN(CMD$)
        CALL IOOUTPUTS(DSO&, CMD$, LENGTH%)
        R$ = SPACE$(15)
        MAX% = 150: ACTUAL% = 0
        CALL IOENTERS(DSO&, R$, MAX%, ACTUAL%)
        XORG = VAL(R$)
        CMD$ = "XREF?"
        LENGTH% = LEN(CMD$)
        CALL IOOUTPUTS(DSO&, CMD$, LENGTH%)
        R$ = SPACE$(15)
        MAX% = 150: ACTUAL% = 0
        CALL IOENTERS(DSO&, R$, MAX%, ACTUAL%)
        XREF = VAL(R$)
CLS
X$ = SPACE$(15)
Y$ = SPACE$(15)
CMD$ = "DATA?"
LENGTH% = LEN(CMD$)
CALL IOOUTPUTS(DSO&, CMD$, LENGTH%)
FOR i = 1 TO POINTS
        CALL IOENTERS(DSO&, Y$, MAX%, ACTUAL%)
        X = (i * XINC) + XORG
        Y = ((VAL(Y$) - YREF) * YINC) + YORG
        load(i) = 0
        load(i) = Y
NEXT i
diff = POINTS / 64
ref = diff / 2
sumpre = 0
```

```
sumload = 0
FOR i = 1 TO 64
j = INT(diff * i - ref)
IF ABS(preload(j - 1) - preload(j)) <= .4 THEN GOTO 510
IF ABS(preload(j) - preload(j + 1)) <= .4 THEN GOTO 530
CLS
INPUT "Check clock synchronization and push <CR> to restart ", null$
CLOSE #3
GOTO 1000
530 pre(i) = (preload(j) + preload(j + 1)) / 2
GOTO 540
510 IF ABS(preload(j) - preload(j + 1)) <= .4 THEN GOTO 520
pre(i) = (preload(j - 1) + preload(j)) / 2
GOTO 540
520 pre(i) = (preload(j - 1) + preload(j) + preload(j + 1)) / 3
540 IF ABS(load(j - 1) - load(j)) <= .4 THEN GOTO 560
IF ABS(load(j) - load(j + 1)) <= .4 THEN GOTO 580
CLS
INPUT "Check clock synchronization and push <CR> to restart ", null$
CLOSE #3
GOTO 1000
580 lod(i) = (load(j) + load(j + 1)) / 2
GOTO 590
560 IF ABS(load(j) - load(j + 1)) <= .4 THEN GOTO 570
lod(i) = (load(j - 1) + load(j)) / 2
GOTO 590
570 lod(i) = (load(j - 1) + load(j) + load(j + 1)) / 3
590 lod(i) = (lod(i) - pre(i)) - weight(i)
sumpre = pre(i) + sumpre
sumload = lod(i) + sumload
NEXT i
taxelpre(63) = pre(1)
taxelpre(55) = pre(2)
taxelpre(37) = pre(3)
taxelpre(61) = pre(4)
taxelpre(4) = pre(5)
taxelpre(28) = pre(6)
taxelpre(10) = pre(7)
taxelpre(2) = pre(8)
taxelpre(53) = pre(9)
taxelpre(45) = pre(10)
taxelpre(59) = pre(11)
taxelpre(51) = pre(12)
taxelpre(18) = pre(13)
taxelpre(27) = pre(14)
taxelpre(25) = pre(15)
taxelpre(35) = pre(16)
taxelpre(58) = pre(17)
taxelpre(44) = pre(18)
taxelpre(52) = pre(19)
taxelpre(60) = pre(20)
taxelpre(34) = pre(21)
taxelpre(36) = pre(22)
```

```
taxelpre(26) = pre(23)
taxelpre(17) = pre(24)
taxelpre(46) = pre(25)
taxelpre(54) = pre(26)
taxelpre(62) = pre(27)
taxelpre(64) = pre(28)
taxelpre(9) = pre(29)
taxelpre(1) = pre(30)
taxelpre(3) = pre(31)
taxelpre(11) = pre(32)
taxelpre(33) = pre(33)
taxelpre(42) = pre(34)
taxelpre(50) = pre(35)
taxelpre(57) = pre(36)
taxelpre(22) = pre(37)
taxelpre(24) = pre(38)
taxelpre(16) = pre(39)
taxelpre(32) = pre(40)
taxelpre(43) = pre(41)
taxelpre(41) = pre(42)
taxelpre(49) = pre(43)
taxelpre(56) = pre(44)
taxelpre(23) = pre(45)
taxelpre(15) = pre(46)
taxelpre(8) = pre(47)
taxelpre(19) = pre(48)
taxelpre(48) = pre(49)
taxelpre(39) = pre(50)
taxelpre(29) = pre(51)
taxelpre(31) = pre(52)
taxelpre(5) = pre(53)
taxelpre(13) = pre(54)
taxelpre(21) = pre(55)
taxelpre(7) = pre(56)
taxelpre(30) = pre(57)
taxelpre(40) = pre(58)
taxelpre(38) = pre(59)
taxelpre(47) = pre(60)
taxelpre(14) = pre(61)
taxelpre(6) = pre(62)
taxelpre(20) = pre(63)
taxelpre(12) = pre(64)
taxellod(63) = lod(1)
taxellod(55) = lod(2)
taxellod(37) = lod(3)
taxellod(61) = lod(4)
taxellod(4) = lod(5)
taxellod(28) = lod(6)
taxellod(10) = lod(7)
taxellod(2) = lod(8)
taxellod(53) = lod(9)
taxellod(45) = lod(10)
taxellod(59) = lod(11)
```

```
taxellod(51) = lod(12)
taxellod(18) = lod(13)
taxellod(27) = lod(14)
taxellod(25) = lod(15)
taxellod(35) = lod(16)
taxellod(58) = lod(17)
taxellod(44) = lod(18)
taxellod(52) = lod(19)
taxellod(60) = lod(20)
taxellod(34) = lod(21)
taxellod(36) = lod(22)
taxellod(26) = lod(23)
taxellod(17) = lod(24)
taxellod(46) = lod(25)
taxellod(54) = lod(26)
taxellod(62) = lod(27)
taxellod(64) = lod(28)
taxellod(9) = lod(29)
taxellod(1) = lod(30)
taxellod(3) = lod(31)
taxellod(11) = lod(32)
taxellod(33) = lod(33)
taxellod(42) = lod(34)
taxellod(50) = lod(35)
taxellod(57) = lod(36)
taxellod(22) = lod(37)
taxellod(24) = lod(38)
taxellod(16) = lod(39)
taxellod(32) = lod(40)
taxellod(43) = lod(41)
taxellod(41) = lod(42)
taxellod(49) = lod(43)
taxellod(56) = lod(44)
taxellod(23) = lod(45)
taxellod(15) = lod(46)
taxellod(8) = lod(47)
taxellod(19) = lod(48)
taxellod(48) = lod(49)
taxellod(39) = lod(50)
taxellod(29) = lod(51)
taxellod(31) = lod(52)
taxellod(5) = lod(53)
taxellod(13) = lod(54)
taxellod(21) = lod(55)
taxellod(7) = lod(56)
taxellod(30) = lod(57)
taxellod(40) = lod(58)
taxellod(38) = lod(59)
taxellod(47) = lod(60)
taxellod(14) = lod(61)
taxellod(6) = lod(62)
taxellod(20) = lod(63)
taxellod(12) = lod(64)
```

```
'substitute the following lines for the previous lines and
'remove the "'" when determining the crosstalk on the old sensor
'taxelpre(64) = pre(1)
'taxelpre(55) = pre(2)
'taxelpre(54) = pre(3)
'taxelpre(61) = pre(4)
'taxelpre(4) = pre(5)
'taxelpre(11) = pre(6)
'taxelpre(10) = pre(7)
'taxelpre(1) = pre(8)
'taxelpre(45) = pre(9)
'taxelpre(60) = pre(10)
'taxelpre(44) = pre(11)
'taxelpre(51) = pre(12)
'taxelpre(18) = pre(13)
'taxelpre(27) = pre(14)
'taxelpre(25) = pre(15)
'taxelpre(35) = pre(16)
'taxelpre(58) = pre(17)
'taxelpre(59) = pre(18)
'taxelpre(52) = pre(19)
'taxelpre(37) = pre(20)
'taxelpre(34) = pre(21)
'taxelpre(36) = pre(22)
'taxelpre(26) = pre(23)
'taxelpre(17) = pre(24)
'taxelpre(53) = pre(25)
'taxelpre(46) = pre(26)
'taxelpre(62) = pre(27)
'taxelpre(63) = pre(28)
'taxelpre(9) = pre(29)
'taxelpre(2) = pre(30)
'taxelpre(3) = pre(31)
'taxelpre(19) = pre(32)
'taxelpre(33) = pre(33)
'taxelpre(42) = pre(34)
'taxelpre(50) = pre(35)
'taxelpre(57) = pre(36)
'taxelpre(22) = pre(37)
'taxelpre(24) = pre(38)
'taxelpre(16) = pre(39)
'taxelpre(32) = pre(40)
'taxelpre(43) = pre(41)
'taxelpre(41) = pre(42)
'taxelpre(49) = pre(43)
'taxelpre(56) = pre(44)
'taxelpre(23) = pre(45)
'taxelpre(15) = pre(46)
'taxelpre(8) = pre(47)
'taxelpre(12) = pre(48)
'taxelpre(48) = pre(49)
'taxelpre(39) = pre(50)
'taxelpre(29) = pre(51)
```

```
'taxelpre(31) - pre(52)
'taxelpre(28) - pre(53)
'taxelpre(13) - pre(54)
'taxelpre(6) - pre(55)
'taxelpre(7) - pre(56)
'taxelpre(30) - pre(57)
'taxelpre(40) - pre(58)
'taxelpre(38) - pre(59)
'taxelpre(47) - pre(60)
'taxelpre(14) - pre(61)
'taxelpre(21) - pre(62)
'taxelpre(5) - pre(63)
'taxelpre(20) - pre(64)
'taxellod(64) - lod(1)
'taxellod(55) - lod(2)
'taxellod(54) - lod(3)
'taxellod(61) - lod(4)
'taxellod(4) - lod(5)
'taxellod(11) - lod(6)
'taxellod(10) - lod(7)
'taxellod(1) - lod(8)
'taxellod(45) - lod(9)
'taxellod(60) - lod(10)
'taxellod(44) - lod(11)
'taxellod(51) - lod(12)
'taxellod(18) - lod(13)
'taxellod(27) - lod(14)
'taxellod(25) - lod(15)
'taxellod(35) - lod(16)
'taxellod(58) - lod(17)
'taxellod(59) - lod(18)
'taxellod(52) - lod(19)
'taxellod(37) - lod(20)
'taxellod(34) - lod(21)
'taxellod(36) - lod(22)
'taxellod(26) - lod(23)
'taxellod(17) - lod(24)
'taxellod(53) - lod(25)
'taxellod(46) - lod(26)
'taxellod(62) - lod(27)
'taxellod(63) - lod(28)
'taxellod(9) = lod(29)
'taxellod(2) - lod(30)
'taxellod(3) - lod(31)
'taxellod(19) - lod(32)
'taxellod(33) - lod(33)
'taxellod(42) - lod(34)
'taxellod(50) - lod(35)
'taxellod(57) - lod(36)
'taxellod(22) - lod(37)
'taxellod(24) - lod(38)
'taxellod(16) - lod(39)
'taxellod(32) - lod(40)
```

```
'taxellod(43) - lod(41)
'taxellod(41) - lod(42)
'taxellod(49) - lod(43)
'taxellod(56) - lod(44)
'taxellod(23) - lod(45)
'taxellod(15) - lod(46)
'taxellod(8) - lod(47)
'taxellod(12) - lod(48)
'taxellod(48) - lod(49)
'taxellod(39) - lod(50)
'taxellod(29) - lod(51)
'taxellod(31) - lod(52)
'taxellod(28) - lod(53)
'taxellod(13) - lod(54)
'taxellod(6) - lod(55)
'taxellod(7) - lod(56)
'taxellod(30) - lod(57)
'taxellod(40) - lod(58)
'taxellod(38) - lod(59)
'taxellod(47) - lod(60)
'taxellod(14) - lod(61)
'taxellod(21) - lod(62)
'taxellod(5) - lod(63)
'taxellod(20) - lod(64)
PRINT #3, DFILES$
FOR i - 1 TO 64
        PRINT #3, i, taxelpre(i), taxellod(i)
NEXT i
CLOSE #3
INPUT "Do you want another test? (y or n):", TEST$
CLS
IF TEST$ <> "n" GOTO 1000
        CMD$ - "LOCAL"
        LENGTH% - LEN(CMD$)
        CALL IOOUTPUTS(DSO&, CMD$, LENGTH%)
        CMD$ - "VSET1,0"
        LENGTH% - LEN(CMD$)
        CALL IOOUTPUTS(PS&, CMD$, LENGTH%)
        CMD$ - "VSET2,0"
        LENGTH% - LEN(CMD$)
        CALL IOOUTPUTS(PS&, CMD$, LENGTH%)
        CMD$ - "VSET3,0"
        LENGTH% - LEN(CMD$)
        CALL IOOUTPUTS(PS&, CMD$, LENGTH%)
        CMD$ - "VSET4,0"
        LENGTH% - LEN(CMD$)
        CALL IOOUTPUTS(PS&, CMD$, LENGTH%)
CALL IOLOCAL(DSO&)
CALL IOLOCAL(PS&)
CLOSE
END
```

```
'****************************************************************
' Data aquisition program for finding the sensor or shape data for the
' piezoelectric tactile sensor.
' filename        SHAPE.BAS
' Language: QuickBASIC
' Instruments: HP 54100A DSO and HP 6624A DC pwr supply
'              HP 8082A Pulse Generator
' Purpose:  Take sensor readings
' Instructions:
'                 1. Attach ps chan 1 V+ to the switch pin
'                                     V- to GND
'                 2. Attach ps chan 2 V+ to the input bias pin
'                                     V- to GND
'                 3. Attach ps chan 3 V+ to sensor V+ pin
'                                     V- to GND
'                 4. Attach ps chan 4 V- to sensor V- pin
'                                     V+ to GND
'                 5. Attach 2nd ps to Vcc output chips
'                                     (set to 5 V)
'                 6. Attach DSO chan 1 to Vout
'                 7. Attach Pulse Gen to clk set for 1.28 kHz
'                 8. Attach Resistor to chan 2 DSO for triggering
'                 9. Connect all grounds together
'                 10. Make sure the clk is set so all 64 taxel outputs
'                     are visible on the screen (check the multiplexer
'                     counter LSB input)
'****************************************************************
'
'Set up the HPIB IEEE-488 interface card
REM $INCLUDE: 'QBSETUP'
CLS
INPUT "Enter the chip # being tested and hit <CR>: ", chip$
INPUT "Enter the date (ie 0307 for 3 July) and hit <CR>: ", day$
ISC& = 7
DSO& = ISC& * 100 + 7
PS& = ISC& * 100 + 5
CALL IORESET(ISC&)
IF PCIB.ERR <> NOERR THEN ERROR PCIB.BASERR
'Setup a timeout of 5 seconds
time! = 5
CALL IOTIMEOUT(ISC&, time!)
IF PCIB.ERR <> NOERR THEN ERROR PCIB.BASERR
CALL IOREMOTE(PS&)
      CALL IOCLEAR(PS&)
      IF PCIB.EPR <> NOERR THEN ERROR PCIB.BASERR
      CMD$ = "CLR;ISET1,1"
      LENGTH% = LEN(CMD$)
      CALL IOOUTPUTS(PS&, CMD$, LENGTH%)
      CMD$ = "VSET1,0"
      LENGTH% = LEN(CMD$)
      CALL IOOUTPUTS(PS&, CMD$, LENGTH%)
      CMD$ = "CLR;ISET2,1"
      LENGTH% = LEN(CMD$)
```

```
        CALL IOOUTPUTS(PS&, CMD$, LENGTH%)
        CMD$ - "VSET2,0"
        LENGTH% - LEN(CMD$)
        CALL IOOUTPUTS(PS&, CMD$, LENGTH%)
        CMD$ - "CLR;ISET3,.8"
        LENGTH% - LEN(CMD$)
        CALL IOOUTPUTS(PS&, CMD$, LENGTH%)
        CMD$ - "VSET3,0"
        LENGTH% - LEN(CMD$)
        CALL IOOUTPUTS(PS&, CMD$, LENGTH%)
        CMD$ - "CLR;ISET4,.8"
        LENGTH% - LEN(CMD$)
        CALL IOOUTPUTS(PS&, CMD$, LENGTH%)
        CMD$ - "VSET4,0"
        LENGTH% - LEN(CMD$)
        CALL IOOUTPUTS(PS&, CMD$, LENGTH%)
CALL IOREMOTE(DSO&)
        CALL IOCLEAR(DSO&)
        IF PCIB.ERR <> NOERR THEN ERROR PCIB.BASERR
        CMD$ - "STOP"
        LENGTH% - LEN(CMD$)
        CALL IOOUTPUTS(DSO&, CMD$, LENGTH%)
        CMD$ - "RUN"
        LENGTH% - LEN(CMD$)
        CALL IOOUTPUTS(DSO&, CMD$, LENGTH%)
        CMD$ - "DISPLAY BRIGHTNESS HIGH"
        LENGTH% - LEN(CMD$)
        CALL IOOUTPUTS(DSO&, CMD$, LENGTH%)
        CMD$ - "DISPLAY GRAT GRID"
        LENGTH% - LEN(CMD$)
        CALL IOOUTPUTS(DSO&, CMD$, LENGTH%)
        CMD$ - "CHANNEL 2 SENS .5"
        LENGTH% - LEN(CMD$)
        CALL IOOUTPUTS(DSO&, CMD$, LENGTH%)
        CMD$ - "CHANNEL 1"
        LENGTH% - LEN(CMD$)
        CALL IOOUTPUTS(DSO&, CMD$, LENGTH%)
        CMD$ - "CHANNEL 1 PROBE 10"
        LENGTH% - LEN(CMD$)
        CALL IOOUTPUTS(DSO&, CMD$, LENGTH%)
        CMD$ - "CHANNEL 1 SENS 2"
        LENGTH% - LEN(CMD$)
        CALL IOOUTPUTS(DSO&, CMD$, LENGTH%)
        CMD$ - "CHANNEL 1 OFFS 7.48"
        LENGTH% - LEN(CMD$)
        CALL IOOUTPUTS(DSO&, CMD$, LENGTH%)
        CMD$ - "TIMEBASE MODE TRIGGERED"
        LENGTH% - LEN(CMD$)
        CALL IOOUTPUTS(DSO&, CMD$, LENGTH%)
        CMD$ - "TIMEBASE SENSITIVITY 5e-3"
        LENGTH% - LEN(CMD$)
        CALL IOOUTPUTS(DSO&, CMD$, LENGTH%)
        CMD$ - "TIMEBASE DELAY 0"
```

```
      LENGTH% - LEN(CMD$)
      CALL IOOUTPUTS(DSO&, CMD$, LENGTH%)
      CMD$ - "TRIGGER MODE EDGE"
      LENGTH% - LEN(CMD$)
      CALL IOOUTPUTS(DSO&, CMD$, LENGTH%)
      CMD$ - "TRIGGER SOURCE CHANNEL 2"
      LENGTH% - LEN(CMD$)
      CALL IOOUTPUTS(DSO&, CMD$, LENGTH%)
      CMD$ - "TRIGGER LEVEL 0.6"
      LENGTH% - LEN(CMD$)
      CALL IOOUTPUTS(DSO&, CMD$, LENGTH%)
      CMD$ - "TRIGGER SLOPE NEGATIVE"
      LENGTH% - LEN(CMD$)
      CALL IOOUTPUTS(DSO&, CMD$, LENGTH%)
' bias circuit
      CMD$ - "ISET2,5"
      LENGTH% - LEN(CMD$)
      CALL IOOUTPUTS(PS&, CMD$, LENGTH%)
      CMD$ - "VSET2,4.5"
      LENGTH% - LEN(CMD$)
      CALL IOOUTPUTS(PS&, CMD$, LENGTH%)
      CMD$ - "ISET4,2"
      LENGTH% - LEN(CMD$)
      CALL IOOUTPUTS(PS&, CMD$, LENGTH%)
      CMD$ - "VSET4,12"
      LENGTH% - LEN(CMD$)
      CALL IOOUTPUTS(PS&, CMD$, LENGTH%)
      CMD$ - "ISET3,2"
      LENGTH% - LEN(CMD$)
      CALL IOOUTPUTS(PS&, CMD$, LENGTH%)
      CMD$ - "VSET3,12"
      LENGTH% - LEN(CMD$)
      CALL IOOUTPUTS(PS&, CMD$, LENGTH%)
DIM time(1000), preload(1000), load(1000), postload(1000)
CLS
PRINT "Enter the delay for taking loaded readings after the "
INPUT "bias has been removed (eg. 1 for 1 second) ", timeconst
      CMD$ - "ISET1,2"
      LENGTH% - LEN(CMD$)
      CALL IOOUTPUTS(PS&, CMD$, LENGTH%)
2000    CMD$ - "VSET1,5"
      LENGTH% - LEN(CMD$)
      CALL IOOUTPUTS(PS&, CMD$, LENGTH%)
'Now to find delay values for a particular bias value and chip #
CLS
INPUT "To find weighting values, hit <CR> ", null$
'take bias data
      CMD$ - "STORE CHANNEL 1, MEMORY 3"
      LENGTH% - LEN(CMD$)
      CALL IOOUTPUTS(DSO&, CMD$, LENGTH%)
      CMD$ - "VSET1,0"
      LENGTH% - LEN(CMD$)
      CALL IOOUTPUTS(PS&, CMD$, LENGTH%)
```

```
t1 - TIMER
9000 t2 - TIMER - t1
IF t2 < timeconst THEN GOTO 9000
'Take post bias data
        CMD$ - "STORE CHANNEL 1, MEMORY 4"
        LENGTH% - LEN(CMD$)
        CALL IOOUTPUTS(DSO&, CMD$, LENGTH%)
        CMD$ - "WAVEFORM SOURCE MEMORY 3 FORMAT ASCII"
        LENGTH% - LEN(CMD$)
        CALL IOOUTPUTS(DSO&, CMD$, LENGTH%)
        CMD$ - "POINTS?"
        LENGTH% - LEN(CMD$)
        CALL IOOUTPUTS(DSO&, CMD$, LENGTH%)
        R$ - SPACE$(15)
        MAX% - 150: ACTUAL% - 0
        CALL IOENTERS(DSO&, R$, MAX%, ACTUAL%)
        POINTS - VAL(R$)
        CMD$ - "YREF?"
        LENGTH% - LEN(CMD$)
        CALL IOOUTPUTS(DSO&, CMD$, LENGTH%)
        R$ - SPACE$(15)
        MAX% - 150: ACTUAL% - 0
        CALL IOENTERS(DSO&, R$, MAX%, ACTUAL%)
        YREF - VAL(R$)
        CMD$ - "YINC?"
        LENGTH% - LEN(CMD$)
        CALL IOOUTPUTS(DSO&, CMD$, LENGTH%)
        R$ - SPACE$(15)
        MAX% - 150: ACTUAL% - 0
        CALL IOENTERS(DSO&, R$, MAX%, ACTUAL%)
        YINC - VAL(R$)
        CMD$ - "YOR?"
        LENGTH% - LEN(CMD$)
        CALL IOOUTPUTS(DSO&, CMD$, LENGTH%)
        R$ - SPACE$(15)
        MAX% - 150: ACTUAL% - 0
        CALL IOENTERS(DSO&, R$, MAX%, ACTUAL%)
        YORG - VAL(R$)
        CMD$ - "XINC?"
        LENGTH% - LEN(CMD$)
        CALL IOOUTPUTS(DSO&, CMD$, LENGTH%)
        R$ - SPACE$(15)
        MAX% - 150: ACTUAL% - 0
        CALL IOENTERS(DSO&, R$, MAX%, ACTUAL%)
        XINC - VAL(R$)
        CMD$ - "XOR?"
        LENGTH% - LEN(CMD$)
        CALL IOOUTPUTS(DSO&, CMD$, LENGTH%)
        R$ - SPACE$(15)
        MAX% - 150: ACTUAL% - 0
        CALL IOENTERS(DSO&, R$, MAX%, ACTUAL%)
        XORG - VAL(R$)
        CMD$ - "XREF?"
```

```
                LENGTH% = LEN(CMD$)
                CALL IOOUTPUTS(DSO&, CMD$, LENGTH%)
                R$ = SPACE$(15)
                MAX% = 150: ACTUAL% = 0
                CALL IOENTERS(DSO&, R$, MAX%, ACTUAL%)
                XREF = VAL(R$)
        CLS
        X$ = SPACE$(15)
        Y$ = SPACE$(15)
        CMD$ = "DATA?"
        LENGTH% = LEN(CMD$)
        CALL IOOUTPUTS(DSO&, CMD$, LENGTH%)
        FOR i = 1 TO POINTS
                CALL IOENTERS(DSO&, Y$, MAX%, ACTUAL%)
                X = (i * XINC) + XORG
                Y = ((VAL(Y$) - YREF) * YINC) + YORG
                time(i) = 0
                time(i) = X
                preload(i) = 0
                preload(i) = Y
        NEXT i
        'Retreive post bias data from scope
                CMD$ = "WAVEFORM SOURCE MEMORY 4 FORMAT ASCII"
                LENGTH% = LEN(CMD$)
                CALL IOOUTPUTS(DSO&, CMD$, LENGTH%)
                CMD$ = "POINTS?"
                LENGTH% = LEN(CMD$)
                CALL IOOUTPUTS(DSO&, CMD$, LENGTH%)
                R$ = SPACE$(15)
                MAX% = 150: ACTUAL% = 0
                CALL IOENTERS(DSO&, R$, MAX%, ACTUAL%)
                POINTS = VAL(R$)
                CMD$ = "YREF?"
                LENGTH% = LEN(CMD$)
                CALL IOOUTPUTS(DSO&, CMD$, LENGTH%)
                R$ = SPACE$(15)
                MAX% = 150: ACTUAL% = 0
                CALL IOENTERS(DSO&, R$, MAX%, ACTUAL%)
                YREF = VAL(R$)
                CMD$ = "YINC?"
                LENGTH% = LEN(CMD$)
                CALL IOOUTPUTS(DSO&, CMD$, LENGTH%)
                R$ = SPACE$(15)
                MAX% = 150: ACTUAL% = 0
                CALL IOENTERS(DSO&, R$, MAX%, ACTUAL%)
                YINC = VAL(R$)
                CMD$ = "YOR?"
                LENGTH% = LEN(CMD$)
                CALL IOOUTPUTS(DSO&, CMD$, LENGTH%)
                R$ = SPACE$(15)
                MAX% = 150: ACTUAL% = 0
                CALL IOENTERS(DSO&, R$, MAX%, ACTUAL%)
                YORG = VAL(R$)
```

```
                CMD$ - "XINC?"
                LENGTH% - LEN(CMD$)
                CALL IOOUTPUTS(DSO&, CMD$, LENGTH%)
                R$ - SPACE$(15)
                MAX% - 150: ACTUAL% - 0
                CALL IOENTERS(DSO&, R$, MAX%, ACTUAL%)
                XINC - VAL(R$)
                CMD$ - "XOR?"
                LENGTH% - LEN(CMD$)
                CALL IOOUTPUTS(DSO&, CMD$, LENGTH%)
                R$ - SPACE$(15)
                MAX% - 150: ACTUAL% - 0
                CALL IOENTERS(DSO&, R$, MAX%, ACTUAL%)
                XORG - VAL(R$)
                CMD$ - "XREF?"
                LENGTH% - LEN(CMD$)
                CALL IOOUTPUTS(DSO&, CMD$, LENGTH%)
                R$ - SPACE$(15)
                MAX% - 150: ACTUAL% - 0
                CALL IOENTERS(DSO&, R$, MAX%, ACTUAL%)
                XREF - VAL(R$)
CLS
X$ - SPACE$(15)
Y$ - SPACE$(15)
CMD$ - "DATA?"
LENGTH% - LEN(CMD$)
CALL IOOUTPUTS(DSO&, CMD$, LENGTH%)
FOR i - 1 TO POINTS
        CALL IOENTERS(DSO&, Y$, MAX%, ACTUAL%)
        X - (i * XINC) + XORG
        Y - ((VAL(Y$) - YREF) * YINC) + YORG
        load(i) - 0
        load(i) - Y
NEXT i
'develop weighting data
DIM taxelpre(64), taxellod(64), pre(64), lod(64), weight(64)
diff - POINTS / 64
ref - diff / 2
sumpre - 0
sumload - 0
sumpost - 0
FOR i - 1 TO 64
j - INT(diff * i - ref)
IF ABS(preload(j - 1) - preload(j)) <- .4 THEN GOTO 610
IF ABS(preload(j) - preload(j + 1)) <- .4 THEN GOTO 630
CLS
INPUT "Check clock synchronization and push <CR> to restart ", null$
GOTO 2000
630 pre(i) - (preload(j) + preload(j + 1)) / 2
GOTO 640
610 IF ABS(preload(j) - preload(j + 1)) <- .4 THEN GOTO 620
pre(i) - (preload(j - 1) + preload(j)) / 2
GOTO 640
```

```
620 pre(i) = (preload(j - 1) + preload(j) + preload(j + 1)) / 3
640 IF ABS(load(j - 1) - load(j)) <= .4 THEN GOTO 660
IF ABS(load(j) - load(j + 1)) <= .4 THEN GOTO 680
CLS
INPUT "Check clock synchronization and push <CR> to restart ", null$
GOTO 2000
680 lod(i) = (load(j) + load(j + 1)) / 2
GOTO 690
660 IF ABS(load(j) - load(j + 1)) <= .4 THEN GOTO 670
lod(i) = (load(j - 1) + load(j)) / 2
GOTO 690
670 lod(i) = (load(j - 1) + load(j) + load(j + 1)) / 3
690 weight(i) = lod(i) - pre(i)
NEXT i
1000     CMD$ = "VSET1,5"
        LENGTH% = LEN(CMD$)
        CALL IOOUTPUTS(PS&, CMD$, LENGTH%)
CLS
INPUT "Enter the test number for data storage (ie 01 for test #1): ",
TEST$
DFILES$ = "B:" + chip$ + day$ + TEST$ + ".txt"
OPEN DFILES$ FOR OUTPUT AS #3
DFILESPIC$ = "B:sq" + day$ + TEST$ + ".txt"
OPEN DFILESPIC$ FOR OUTPUT AS #4
DFILESMAT$ = "B:sq" + day$ + TEST$ + ".mat"
OPEN DFILESMAT$ FOR OUTPUT AS #5
CLS
PRINT "Prepare to apply the load!  You have ", timeconst
INPUT "seconds to apply the load after you hit <CR> ", null$
        CMD$ = "VSET1,0"
        LENGTH% = LEN(CMD$)
        CALL IOOUTPUTS(PS&, CMD$, LENGTH%)
t1 = TIMER
9500 t2 = TIMER - t1
IF t2 < timeconst THEN GOTO 9500
'Take loaded measurement
        CMD$ = "STORE CHANNEL 1, MEMORY 4"
        LENGTH% = LEN(CMD$)
        CALL IOOUTPUTS(DSO&, CMD$, LENGTH%)
'Take postload measurement
CLS
INPUT "Quickly, remove load and hit <CR> to take postload measurement",
null$
        CMD$ = "STORE CHANNEL 1, MEMORY 2"
        LENGTH% = LEN(CMD$)
        CALL IOOUTPUTS(DSO&, CMD$, LENGTH%)
'Retreive loaded info from scope
        CMD$ = "WAVEFORM SOURCE MEMORY 4 FORMAT ASCII"
        LENGTH% = LEN(CMD$)
        CALL IOOUTPUTS(DSO&, CMD$, LENGTH%)
        CMD$ = "POINTS?"
        LENGTH% = LEN(CMD$)
        CALL IOOUTPUTS(DSO&, CMD$, LENGTH%)
```

```
        R$ - SPACE$(15)
        MAX% - 150: ACTUAL% - 0
        CALL IOENTERS(DSO&, R$, MAX%, ACTUAL%)
        POINTS - VAL(R$)
        CMD$ - "YREF?"
        LENGTH% - LEN(CMD$)
        CALL IOOUTPUTS(DSO&, CMD$, LENGTH%)
        R$ - SPACE$(15)
        MAX% - 150: ACTUAL% - 0
        CALL IOENTERS(DSO&, R$, MAX%, ACTUAL%)
        YREF - VAL(R$)
        CMD$ - "YINC?"
        LENGTH% - LEN(CMD$)
        CALL IOOUTPUTS(DSO&, CMD$, LENGTH%)
        R$ - SPACE$(15)
        MAX% - 150: ACTUAL% - 0
        CALL IOENTERS(DSO&, R$, MAX%, ACTUAL%)
        YINC - VAL(R$)
        CMD$ - "YOR?"
        LENGTH% - LEN(CMD$)
        CALL IOOUTPUTS(DSO&, CMD$, LENGTH%)
        R$ - SPACE$(15)
        MAX% - 150: ACTUAL% - 0
        CALL IOENTERS(DSO&, R$, MAX%, ACTUAL%)
        YORG - VAL(R$)
        CMD$ - "XINC?"
        LENGTH% - LEN(CMD$)
        CALL IOOUTPUTS(DSO&, CMD$, LENGTH%)
        R$ - SPACE$(15)
        MAX% - 150: ACTUAL% - 0
        CALL IOENTERS(DSO&, R$, MAX%, ACTUAL%)
        XINC - VAL(R$)
        CMD$ - "XOR?"
        LENGTH% - LEN(CMD$)
        CALL IOOUTPUTS(DSO&, CMD$, LENGTH%)
        R$ - SPACE$(15)
        MAX% - 150: ACTUAL% = 0
        CALL IOENTERS(DSO&, R$, MAX%, ACTUAL%)
        XORG - VAL(R$)
        CMD$ - "XREF?"
        LENGTH% - LEN(CMD$)
        CALL IOOUTPUTS(DSO&, CMD$, LENGTH%)
        R$ - SPACE$(15)
        MAX% - 150: ACTUAL% = 0
        CALL IOENTERS(DSO&, R$, MAX%, ACTUAL%)
        XREF - VAL(R$)
X$ - SPACE$(15)
Y$ - SPACE$(15)
CMD$ - "DATA?"
LENGTH% - LEN(CMD$)
CALL IOOUTPUTS(DSO&, CMD$, LENGTH%)
FOR i - 1 TO POINTS
        CALL IOENTERS(DSO&, Y$, MAX%, ACTUAL%)
```

```
            X - (i * XINC) + XORG
            Y - ((VAL(Y$) - YREF) * YINC) + YORG
            load(i) - 0
            load(i) - Y
    NEXT i
    'Retreive postload info from scope
            CMD$ - "WAVEFORM SOURCE MEMORY 2 FORMAT ASCII"
            LENGTH% - LEN(CMD$)
            CALL IOOUTPUTS(DSO&, CMD$, LENGTH%)
            CMD$ - "POINTS?"
            LENGTH% - LEN(CMD$)
            CALL IOOUTPUTS(DSO&, CMD$, LENGTH%)
            R$ - SPACE$(15)
            MAX% - 150: ACTUAL% - 0
            CALL IOENTERS(DSO&, R$, MAX%, ACTUAL%)
            POINTS - VAL(R$)
            CMD$ - "YREF?"
            LENGTH% - LEN(CMD$)
            CALL IOOUTPUTS(DSO&, CMD$, LENGTH%)
            R$ - SPACE$(15)
            MAX% - 150: ACTUAL% - 0
            CALL IOENTERS(DSO&, R$, MAX%, ACTUAL%)
            YREF - VAL(R$)
            CMD$ - "YINC?"
            LENGTH% - LEN(CMD$)
            CALL IOOUTPUTS(DSO&, CMD$, LENGTH%)
            R$ - SPACE$(15)
            MAX% - 150: ACTUAL% - 0
            CALL IOENTERS(DSO&, R$, MAX%, ACTUAL%)
            YINC - VAL(R$)
            CMD$ - "YOR?"
            LENGTH% - LEN(CMD$)
            CALL IOOUTPUTS(DSO&, CMD$, LENGTH%)
            R$ - SPACE$(15)
            MAX% - 150: ACTUAL% - 0
            CALL IOENTERS(DSO&, R$, MAX%, ACTUAL%)
            YORG - VAL(R$)
            CMD$ - "XINC?"
            LENGTH% - LEN(CMD$)
            CALL IOOUTPUTS(DSO&, CMD$, LENGTH%)
            R$ - SPACE$(15)
            MAX% - 150: ACTUAL% = 0
            CALL IOENTERS(DSO&, R$, MAX%, ACTUAL%)
            XINC - VAL(R$)
            CMD$ - "XOR?"
            LENGTH% - LEN(CMD$)
            CALL IOOUTPUTS(DSO&, CMD$, LENGTH%)
            R$ - SPACE$(15)
            MAX% - 150: ACTUAL% - 0
            CALL IOENTERS(DSO&, R$, MAX%, ACTUAL%)
            XORG - VAL(R$)
            CMD$ - "XREF?"
            LENGTH% - LEN(CMD$)
```

```
        CALL IOOUTPUTS(DSO&, CMD$, LENGTH%)
        R$ - SPACE$(15)
        MAX% - 150: ACTUAL% - 0
        CALL IOENTERS(DSO&, R$, MAX%, ACTUAL%)
        XREF - VAL(R$)
X$ - SPACE$(15)
Y$ - SPACE$(15)
CMD$ - "DATA?"
LENGTH% - LEN(CMD$)
CALL IOOUTPUTS(DSO&, CMD$, LENGTH%)
sumpre - 0
sumload - 0
FOR i - 1 TO POINTS
        CALL IOENTERS(DSO&, Y$, MAX%, ACTUAL%)
        X - (i * XINC) + XORG
        Y - ((VAL(Y$) - YREF) * YINC) + YORG
        postload(i) - Y
NEXT i
'Print taxel pattern to screen
DIM taxelpst(64), pst(64)
diff - POINTS / 64
ref - diff / 2
sumpre - 0
sumload - 0
sumpost - 0
FOR i - 1 TO 64
j - INT(diff * i - ref)
IF ABS(preload(j - 1) - preload(j)) <= .4 THEN GOTO 510
IF ABS(preload(j) - preload(j + 1)) <= .4 THEN GOTO 530
CLS
INPUT "Check clock synchronization and push <CR> to restart ", null$
CLOSE #3
CLOSE #4
CLOSE #5
GOTO 1000
530 pre(i) - (preload(j) + preload(j + 1)) / 2
GOTO 540
510 IF ABS(preload(j) - preload(j + 1)) <= .4 THEN GOTO 520
pre(i) - (preload(j - 1) + preload(j)) / 2
GOTO 540
520 pre(i) - (preload(j - 1) + preload(j) + preload(j + 1)) / 3
540 IF ABS(load(j - 1) - load(j)) <= .4 THEN GOTO 560
IF ABS(load(j) - load(j + 1)) <= .4 THEN GOTO 580
CLS
INPUT "Check clock synchronization and push <CR> to restart ", null$
CLOSE #3
CLOSE #4
CLOSE #5
GOTO 1000
580 lod(i) - (load(j) + load(j + 1)) / 2
GOTO 590
560 IF ABS(load(j) - load(j + 1)) <= .4 THEN GOTO 570
lod(i) - (load(j - 1) + load(j)) / 2
```

```
GOTO 590
570 lod(i) = (load(j - 1) + load(j) + load(j + 1)) / 3
590 pst(i) = (postload(j - 1) + postload(j) + postload(j + 1)) / 3
lod(i) = (lod(i) - pre(i)) - weight(i)
sumload = lod(i) + sumload
NEXT i
'assign taxel number
taxellod(63) = lod(1)
taxellod(55) = lod(2)
taxellod(37) = lod(3)
taxellod(61) = lod(4)
taxellod(4) = lod(5)
taxellod(28) = lod(6)
taxellod(10) = lod(7)
taxellod(2) = lod(8)
taxellod(53) = lod(9)
taxellod(45) = lod(10)
taxellod(59) = lod(11)
taxellod(51) = lod(12)
taxellod(18) = lod(13)
taxellod(27) = lod(14)
taxellod(25) = lod(15)
taxellod(35) = lod(16)
taxellod(58) = lod(17)
taxellod(44) = lod(18)
taxellod(52) = lod(19)
taxellod(60) = lod(20)
taxellod(34) = lod(21)
taxellod(36) = lod(22)
taxellod(26) = lod(23)
taxellod(17) = lod(24)
taxellod(46) = lod(25)
taxellod(54) = lod(26)
taxellod(62) = lod(27)
taxellod(64) = lod(28)
taxellod(9) = lod(29)
taxellod(1) = lod(30)
taxellod(3) = lod(31)
taxellod(11) = lod(32)
taxellod(33) = lod(33)
taxellod(42) = lod(34)
taxellod(50) = lod(35)
taxellod(57) = lod(36)
taxellod(22) = lod(37)
taxellod(24) = lod(38)
taxellod(16) = lod(39)
taxellod(32) = lod(40)
taxellod(43) = lod(41)
taxellod(41) = lod(42)
taxellod(49) = lod(43)
taxellod(56) = lod(44)
taxellod(23) = lod(45)
taxellod(15) = lod(46)
```

```
taxellod(8) = lod(47)
taxellod(19) = lod(48)
taxellod(48) = lod(49)
taxellod(39) = lod(50)
taxellod(29) = lod(51)
taxellod(31) = lod(52)
taxellod(5) = lod(53)
taxellod(13) = lod(54)
taxellod(21) = lod(55)
taxellod(7) = lod(56)
taxellod(30) = lod(57)
taxellod(40) = lod(58)
taxellod(38) = lod(59)
taxellod(47) = lod(60)
taxellod(14) = lod(61)
taxellod(6) = lod(62)
taxellod(20) = lod(63)
taxellod(12) = lod(64)
PRINT #3, DFILES$
FOR i = 1 TO 64
      PRINT #3, i, taxellod(i)
NEXT i
CLOSE #3
'find which taxels are ON, partially ON, and OFF
aveload = sumload / 64
negdelta = 0
posdelta = 0
FOR i = 1 TO 64
IF taxellod(i) >= negdelta THEN GOTO 600
negdelta = taxellod(i)
600 IF taxellod(i) < posdelta THEN GOTO 700
posdelta = taxellod(i)
700 NEXT i
delta = .5 * posdelta
DIM ONoff(64), tax(8, 8), pic(17, 17)
500 CLS
FOR i = 1 TO 64
      IF taxellod(i) > delta THEN ONoff(i) = 1
      IF taxellod(i) <= delta THEN ONoff(i) = 0
NEXT i
SCREEN 2, 1
Y1 = 41
FOR ICOL = 1 TO 8
X1 = 101
FOR IROW = 1 TO 8
i = (ICOL - 1) * 8 + IROW
X2 = X1 + 24
Y2 = Y1 + 10
' Solid => taxel is completely ON
' Empty square => taxel is completely OFF
IF ONoff(i) = 1 THEN LINE (X1, Y1)-(X2, Y2), 1, BF
IF ONoff(i) = 1 THEN tax(IROW, ICOL) = 1
IF ONoff(i) = 0 THEN LINE (X1, Y1)-(X2, Y2), 7, B
```

```
IF ONoff(i) - 0 THEN tax(IROW, ICOL) - 0
X1 - X1 + 48
NEXT IROW
Y1 - Y1 + 20
NEXT ICOL
PRINT "The maximum pos-delta and neg-delta are", posdelta, negdelta
PRINT "The current delta is", delta
INPUT "Do you want to try another weighting factor, (y or n):", TEST$
IF TEST$ - "n" GOTO 1500
INPUT "Pick the new delta for the picture, and hit <CR>", delta
GOTO 500
1500 CLS
pic(1, 1) - 2 * tax(1, 1)
pic(1, 17) - 2 * tax(1, 8)
pic(17, 1) - 2 * tax(8, 1)
pic(17, 17) - 2 * tax(8, 8)
FOR i - 2 TO 16 STEP 2
k - INT(i / 2)
pic(1, i) - 2 * tax(1, k)
pic(i, 1) - 2 * tax(k, 1)
pic(17, i) - 2 * tax(8, k)
pic(i, 17) - 2 * tax(k, 8)
NEXT i
FOR i - 3 TO 15 STEP 2
k1 - INT(i / 2 - 1 / 2)
k2 - INT(i / 2 + 1 / 2)
pic(1, i) - tax(1, k1) + tax(1, k2)
pic(i, 1) - tax(k1, 1) + tax(k2, 1)
pic(17, i) - tax(8, k1) + tax(8, k2)
pic(i, 17) - tax(k1, 8) + tax(k2, 8)
NEXT i
FOR i - 2 TO 16 STEP 2
FOR j - 2 TO 16 STEP 2
k1 - INT(i / 2)
k2 - INT(j / 2)
pic(i, j) - 2 * tax(k1, k2)
NEXT j
NEXT i
FOR i - 2 TO 16 STEP 2
FOR j - 3 TO 15 STEP 2
i1 - INT(i / 2)
j1 - INT(j / 2 - 1 / 2)
j2 - INT(j / 2 + 1 / 2)
pic(i, j) = tax(i1, j1) + tax(i1, j2)
NEXT j
NEXT i
FOR i - 3 TO 15 STEP 2
FOR j - 2 TO 16 STEP 2
j1 - INT(j / 2)
i1 - INT(i / 2 - 1 / 2)
i2 - INT(i / 2 + 1 / 2)
pic(i, j) - tax(i1, j1) + tax(i2, j1)
NEXT j
```

```
NEXT i
FOR i = 3 TO 15 STEP 2
FOR j = 3 TO 15 STEP 2
i1 = INT(i / 2 - 1 / 2)
i2 = INT(i / 2 + 1 / 2)
j1 = INT(j / 2 - 1 / 2)
j2 = INT(j / 2 + 1 / 2)
pic(i, j) = .5 * (tax(i1, j1) + tax(i1, j2) + tax(i2, j1) + tax(i2, j2))
NEXT j
NEXT i
CLS
SCREEN 2, 1
LINE (100, 24)-(509, 195), 7, B
Y1 = 25
FOR ICOL = 1 TO 17
X1 = 10'
FOR IRC  = 1 TO 17
X2 = X1 + 22
Y2 = Y1 + 9
' Solid => taxel is completely ON
' Blank => taxel is completely OFF
' Empty square => taxel is partially ON
IF pic(IROW, ICOL) >= 1.5 THEN LINE (X1, Y1)-(X2, Y2), 1, BF
IF pic(IROW, ICOL) >= 1.5 THEN GOTO 1400
IF pic(IROW, ICOL) >= 1 THEN LINE (X1, Y1)-(X2, Y2), 7, B
IF pic(IROW, ICOL) >= 1 THEN GOTO 1400
IF pic(IROW, ICOL) >= 0 THEN LINE (X1, Y1)-(X2, Y2), 0, BF
1400 X1 = X1 + 24
NEXT IROW
Y1 = Y1 + 10
NEXT ICOL
INPUT "Do you want to try another weighting factor, (y or n):", TEST$
IF TEST$ <> "y" GOTO 1600
INPUT "Pick the new delta for the picture, and hit <CR>", delta
CLS
GOTO 500
1600 CLS
PRINT #4, DFILESPIC$
FOR i = 1 TO 64
PRINT #4, ONoff(i)
NEXT i
CLOSE #4
FOR i = 1 TO 64
temp = taxellod(i)
PRINT #5, temp
NEXT i
CLOSE #5
INPUT "Do you want another test? (y or n):", TEST$
CLS
IF TEST$ <> "n" GOTO 1000
        CMD$ = "LOCAL"
        LENGTH% = LEN(CMD$)
        CALL IOOUTPUTS(DSO&, CMD$, LENGTH%)
```

```
        CMD$ - "VSET1,0"
        LENGTH% - LEN(CMD$)
        CALL IOOUTPUTS(PS&, CMD$, LENGTH%)
        CMD$ - "VSET2,0"
        LENGTH% - LEN(CMD$)
        CALL IOOUTPUTS(PS&, CMD$, LENGTH%)
        CMD$ - "VSET3,0"
        LENGTH% - LEN(CMD$)
        CALL IOOUTPUTS(PS&, CMD$, LENGTH%)
        CMD$ - "VSET4,0"
        LENGTH% - LEN(CMD$)
        CALL IOOUTPUTS(PS&, CMD$, LENGTH%)
CALL IOLOCAL(DSO&)
CALL IOLOCAL(PS&)
CLOSE
END
```

```
'*****************************************************************
' Data aquisition program for finding the sensor or pyroelectric
' response of the piezoelectric tactile sensor.
' filename        PYRO.BAS
' Language: QuickBASIC
' Instruments: HP 54100A DSO and HP 6624A DC pwr supply
'               HP 8082A Pulse Generator
'               Thermocouple
'               Heater
' Purpose:  Take pyroelectric readings
' Instructions:
'                1. Attach ps chan 1 V+ to the switch pin
'                              V- to GND
'                2. Attach ps chan 2 V+ to the input bias pin
'                              V- to GND
'                3. Attach ps chan 3 V+ to sensor V+ pin
'                              V- to GND
'                4. Attach ps chan 4 V- to sensor V- pin
'                              V+ to GND
'                5. Attach 2nd ps to Vcc output chips
'                              (set to 5 V)
'                6. Attach DSO chan 1 to Vout
'                7. Attach Pulse Gen to clk set for 1.28 kHz
'                8. Attach Resistor to chan 2 DSO for triggering
'                9. Connect all grounds together
'                10. Make sure the clk is set so all 64 taxel outputs
'                    are visible on the screen (check the multiplexer
'                    counter LSB input)
'*****************************************************************
'
'Set up the HPIB IEEE-488 interface card
REM $INCLUDE: 'QBSETUP'
CLS
INPUT "Enter the test number for data storage (ie 01 for test#1): ",
TEST$
chip$ = "T"
ISC& = 7
DSO& = ISC& * 100 + 7
PS& = ISC& * 100 + 5
CALL IORESET(ISC&)
IF PCIB.ERR <> NOERR THEN ERROR PCIB.BASERR
'Setup a timeout of 5 seconds
time! = 5
CALL IOTIMEOUT(ISC&, time!)
IF PCIB.ERR <> NOERR THEN ERROR PCIB.BASERR
CALL IOREMOTE(PS&)
     CALL IOCLEAR(PS&)
     IF PCIB.ERR <> NOERR THEN ERROR PCIB.BASERR
     CMD$ = "CLR;ISET1,1"
     LENGTH% = LEN(CMD$)
     CALL IOOUTPUTS(PS&, CMD$, LENGTH%)
     CMD$ = "VSET1,0"
     LENGTH% = LEN(CMD$)
```

```
            CALL IOOUTPUTS(PS&, CMD$, LENGTH%)
            CMD$ = "CLR;ISET2,1"
            LENGTH% = LEN(CMD$)
            CALL IOOUTPUTS(PS&, CMD$, LENGTH%)
            CMD$ = "VSET2,0"
            LENGTH% = LEN(CMD$)
            CALL IOOUTPUTS(PS&, CMD$, LENGTH%)
            CMD$ = "CLR;ISET3,.8"
            LENGTH% = LEN(CMD$)
            CALL IOOUTPUTS(PS&, CMD$, LENGTH%)
            CMD$ = "VSET3,0"
            LENGTH% = LEN(CMD$)
            CALL IOOUTPUTS(PS&, CMD$, LENGTH%)
            CMD$ = "CLR;ISET4,.8"
            LENGTH% = LEN(CMD$)
            CALL IOOUTPUTS(PS&, CMD$, LENGTH%)
            CMD$ = "VSET4,0"
            LENGTH% = LEN(CMD$)
            CALL IOOUTPUTS(PS&, CMD$, LENGTH%)
      CALL IOREMOTE(DSO&)
            CALL IOCLEAR(DSO&)
            IF PCIB.ERR <> NOERR THEN ERROR PCIB.BASERR
            CMD$ = "STOP"
            LENGTH% = LEN(CMD$)
            CALL IOOUTPUTS(DSO&, CMD$, LENGTH%)
            CMD$ = "RUN"
            LENGTH% = LEN(CMD$)
            CALL IOOUTPUTS(DSO&, CMD$, LENGTH%)
            CMD$ = "DISPLAY BRIGHTNESS HIGH"
            LENGTH% = LEN(CMD$)
            CALL IOOUTPUTS(DSO&, CMD$, LENGTH%)
            CMD$ = "DISPLAY GRAT GRID"
            LENGTH% = LEN(CMD$)
            CALL IOOUTPUTS(DSO&, CMD$, LENGTH%)
            CMD$ = "CHANNEL 2 SENS .5"
            LENGTH% = LEN(CMD$)
            CALL IOOUTPUTS(DSO&, CMD$, LENGTH%)
            CMD$ = "CHANNEL 1"
            LENGTH% = LEN(CMD$)
            CALL IOOUTPUTS(DSO&, CMD$, LENGTH%)
            CMD$ = "CHANNEL 1 PROBE 10"
            LENGTH% = LEN(CMD$)
            CALL IOOUTPUTS(DSO&, CMD$, LENGTH%)
            CMD$ = "CHANNEL 1 SENS 2"
            LENGTH% = LEN(CMD$)
            CALL IOOUTPUTS(DSO&, CMD$, LENGTH%)
            CMD$ = "CHANNEL 1 OFFS 7.48"
            LENGTH% = LEN(CMD$)
            CALL IOOUTPUTS(DSO&, CMD$, LENGTH%)
            CMD$ = "TIMEBASE MODE TRIGGERED"
            LENGTH% = LEN(CMD$)
            CALL IOOUTPUTS(DSO&, CMD$, LENGTH%)
            CMD$ = "TIMEBASE SENSITIVITY 5e-3"
```

```
        LENGTH% = LEN(CMD$)
        CALL IOOUTPUTS(DSO&, CMD$, LENGTH%)
        CMD$ = "TIMEBASE DELAY 0"
        LENGTH% = LEN(CMD$)
        CALL IOOUTPUTS(DSO&, CMD$, LENGTH%)
        CMD$ = "TRIGGER MODE EDGE"
        LENGTH% = LEN(CMD$)
        CALL IOOUTPUTS(DSO&, CMD$, LENGTH%)
        CMD$ = "TRIGGER SOURCE CHANNEL 2"
        LENGTH% = LEN(CMD$)
        CALL IOOUTPUTS(DSO&, CMD$, LENGTH%)
        CMD$ = "TRIGGER LEVEL 0.6"
        LENGTH% = LEN(CMD$)
        CALL IOOUTPUTS(DSO&, CMD$, LENGTH%)
        CMD$ = "TRIGGER SLOPE NEGATIVE"
        LENGTH% = LEN(CMD$)
        CALL IOOUTPUTS(DSO&, CMD$, LENGTH%)
' bias circuit
        CMD$ = "ISET2,5"
        LENGTH% = LEN(CMD$)
        CALL IOOUTPUTS(PS&, CMD$, LENGTH%)
        CMD$ = "VSET2,4.5"
        LENGTH% = LEN(CMD$)
        CALL IOOUTPUTS(PS&, CMD$, LENGTH%)
        CMD$ = "ISET4,2"
        LENGTH% = LEN(CMD$)
        CALL IOOUTPUTS(PS&, CMD$, LENGTH%)
        CMD$ = "VSET4,12"
        LENGTH% = LEN(CMD$)
        CALL IOOUTPUTS(PS&, CMD$, LENGTH%)
        CMD$ = "ISET3,2"
        LENGTH% = LEN(CMD$)
        CALL IOOUTPUTS(PS&, CMD$, LENGTH%)
        CMD$ = "VSET3,12"
        LENGTH% = LEN(CMD$)
        CALL IOOUTPUTS(PS&, CMD$, LENGTH%)
DIM time(1000), preload(1000), load(1000)
CLS
PRINT "Enter the delay for taking loaded readings after the "
INPUT "bias has been removed (eg. 10 for 10 seconds) ", timeconst
        CMD$ = "ISET1,2"
        LENGTH% = LEN(CMD$)
        CALL IOOUTPUTS(PS&, CMD$, LENGTH%)
2000    CMD$ = "VSET1,5"
        LENGTH% = LEN(CMD$)
        CALL IOOUTPUTS(PS&, CMD$, LENGTH%)
'Now to find delay values for a particular bias value and chip #
CLS
INPUT "To find weighting values, hit <CR> ", null$
'take bias data
        CMD$ = "STORE CHANNEL 1, MEMORY 3"
        LENGTH% = LEN(CMD$)
        CALL IOOUTPUTS(DSO&, CMD$, LENGTH%)
```

```
        CMD$ - "VSET1,0"
        LENGTH% - LEN(CMD$)
        CALL IOOUTPUTS(PS&, CMD$, LENGTH%)
t1 - TIMER
9000 t2 - TIMER - t1
IF t2 < timeconst THEN GOTO 9000
'Take post bias data
        CMD$ - "STORE CHANNEL 1, MEMORY 4"
        LENGTH% - LEN(CMD$)
        CALL IOOUTPUTS(DSO&, CMD$, LENGTH%)
        CMD$ - "WAVEFORM SOURCE MEMORY 3 FORMAT ASCII"
        LENGTH% - LEN(CMD$)
        CALL IOOUTPUTS(DSO&, CMD$, LENGTH%)
        CMD$ - "POINTS?"
        LENGTH% - LEN(CMD$)
        CALL IOOUTPUTS(DSO&, CMD$, LENGTH%)
        R$ - SPACE$(15)
        MAX% - 150: ACTUAL% - 0
        CALL IOENTERS(DSO&, R$, MAX%, ACTUAL%)
        POINTS - VAL(R$)
        CMD$ - "YREF?"
        LENGTH% - LEN(CMD$)
        CALL IOOUTPUTS(DSO&, CMD$, LENGTH%)
        R$ - SPACE$(15)
        MAX% - 150: ACTUAL% - 0
        CALL IOENTERS(DSO&, R$, MAX%, ACTUAL%)
        YREF - VAL(R$)
        CMD$ - "YINC?"
        LENGTH% - LEN(CMD$)
        CALL IOOUTPUTS(DSO&, CMD$, LENGTH%)
        R$ - SPACE$(15)
        MAX% - 150: ACTUAL% - 0
        CALL IOENTERS(DSO&, R$, MAX%, ACTUAL%)
        YINC - VAL(R$)
        CMD$ = "YOR?"
        LENGTH% - LEN(CMD$)
        CALL IOOUTPUTS(DSO&, CMD$, LENGTH%)
        R$ - SPACE$(15)
        MAX% - 150: ACTUAL% - 0
        CALL IOENTERS(DSO&, R$, MAX%, ACTUAL%)
        YORG - VAL(R$)
        CMD$ - "XINC?"
        LENGTH% - LEN(CMD$)
        CALL IOOUTPUTS(DSO&, CMD$, LENGTH%)
        R$ - SPACE$(15)
        MAX% - 150: ACTUAL% - 0
        CALL IOENTERS(DSO&, R$, MAX%, ACTUAL%)
        XINC - VAL(R$)
        CMD$ - "XOR?"
        LENGTH% - LEN(CMD$)
        CALL IOOUTPUTS(DSO&, CMD$, LENGTH%)
        R$ - SPACE$(15)
        MAX% - 150: ACTUAL% - 0
```

```
            CALL IOENTERS(DSO&, R$, MAX%, ACTUAL%)
            XORG = VAL(R$)
            CMD$ = "XREF?"
            LENGTH% = LEN(CMD$)
            CALL IOOUTPUTS(DSO&, CMD$, LENGTH%)
            R$ = SPACE$(15)
            MAX% = 150: ACTUAL% = 0
            CALL IOENTERS(DSO&, R$, MAX%, ACTUAL%)
            XREF = VAL(R$)
CLS
X$ = SPACE$(15)
Y$ = SPACE$(15)
CMD$ = "DATA?"
LENGTH% = LEN(CMD$)
CALL IOOUTPUTS(DSO&, CMD$, LENGTH%)
FOR i = 1 TO POINTS
            CALL IOENTERS(DSO&, Y$, MAX%, ACTUAL%)
            X = (i * XINC) + XORG
            Y = ((VAL(Y$) - YREF) * YINC) + YORG
            time(i) = 0
            time(i) = X
            preload(i) = 0
            preload(i) = Y
NEXT i
'Retreive post bias data from scope
            CMD$ = "WAVEFORM SOURCE MEMORY 4 FORMAT ASCII"
            LENGTH% = LEN(CMD$)
            CALL IOOUTPUTS(DSO&, CMD$, LENGTH%)
            CMD$ = "POINTS?"
            LENGTH% = LEN(CMD$)
            CALL IOOUTPUTS(DSO&, CMD$, LENGTH%)
            R$ = SPACE$(15)
            MAX% = 150: ACTUAL% = 0
            CALL IOENTERS(DSO&, R$, MAX%, ACTUAL%)
            POINTS = VAL(R$)
            CMD$ = "YREF?"
            LENGTH% = LEN(CMD$)
            CALL IOOUTPUTS(DSO&, CMD$, LENGTH%)
            R$ = SPACE$(15)
            MAX% = 150: ACTUAL% = 0
            CALL IOENTERS(DSO&, R$, MAX%, ACTUAL%)
            YREF = VAL(R$)
            CMD$ = "YINC?"
            LENGTH% = LEN(CMD$)
            CALL IOOUTPUTS(DSO&, CMD$, LENGTH%)
            R$ = SPACE$(15)
            MAX% = 150: ACTUAL% = 0
            CALL IOENTERS(DSO&, R$, MAX%, ACTUAL%)
            YINC = VAL(R$)
            CMD$ = "YOR?"
            LENGTH% = LEN(CMD$)
            CALL IOOUTPUTS(DSO&, CMD$, LENGTH%)
            R$ = SPACE$(15)
```

```
            MAX% - 150: ACTUAL% - 0
            CALL IOENTERS(DSO&, R$, MAX%, ACTUAL%)
            YORG - VAL(R$)
            CMD$ - "XINC?"
            LENGTH% - LEN(CMD$)
            CALL IOOUTPUTS(DSO&, CMD$, LENGTH%)
            R$ - SPACE$(15)
            MAX% - 150: ACTUAL% - 0
            CALL IOENTERS(DSO&, R$, MAX%, ACTUAL%)
            XINC - VAL(R$)
            CMD$ - "XOR?"
            LENGTH% - LEN(CMD$)
            CALL IOOUTPUTS(DSO&, CMD$, LENGTH%)
            R$ - SPACE$(15)
            MAX% - 150: ACTUAL% - 0
            CALL IOENTERS(DSO&, R$, MAX%, ACTUAL%)
            XORG - VAL(R$)
            CMD$ - "XREF?"
            LENGTH% - LEN(CMD$)
            CALL IOOUTPUTS(DSO&, CMD$, LENGTH%)
            R$ - SPACE$(15)
            MAX% - 150: ACTUAL% - 0
            CALL IOENTERS(DSO&, R$, MAX%, ACTUAL%)
            XREF - VAL(R$)
CLS
X$ - SPACE$(15)
Y$ - SPACE$(15)
CMD$ - "DATA?"
LENGTH% - LEN(CMD$)
CALL IOOUTPUTS(DSO&, CMD$, LENGTH%)
FOR i - 1 TO POINTS
        CALL IOENTERS(DSO&, Y$, MAX%, ACTUAL%)
        X - (i * XINC) + XORG
        Y - ((VAL(Y$) - YREF) * YINC) + YORG
        load(i) - 0
        load(i) - Y
NEXT i
'develop temperature data
DIM taxelpre(64), taxellod(64), pre(64), lod(64), weight(64)
diff - POINTS / 64
ref - diff / 2
sumpre - 0
sumload - 0
sumpost - 0
FOR i - 1 TO 64
j - INT(diff * i - ref)
IF ABS(preload(j - 1) - preload(j)) <= 4 THEN GOTO 610
IF ABS(preload(j) - preload(j + 1)) <= 4 THEN GOTO 630
CLS
INPUT "Check clock synchronization and push <CR> to restart ", null$
GOTO 2000
630 pre(i) - (preload(j) + preload(j + 1)) / 2
GOTO 640
```

```
610 IF ABS(preload(j) - preload(j + 1)) <= 4 THEN GOTO 620
pre(i) = (preload(j - 1) + preload(j)) / 2
GOTO 640
620 pre(i) = (preload(j - 1) + preload(j) + preload(j + 1)) / 3
640 IF ABS(load(j - 1) - load(j)) <= 4 THEN GOTO 660
IF ABS(load(j) - load(j + 1)) <= 4 THEN GOTO 680
CLS
INPUT "Check clock synchronization and push <CR> to restart ", null$
GOTO 2000
680 lod(i) = (load(j) + load(j + 1)) / 2
GOTO 690
660 IF ABS(load(j) - load(j + 1)) <= 4 THEN GOTO 670
lod(i) = (load(j - 1) + load(j)) / 2
GOTO 690
670 lod(i) = (load(j - 1) + load(j) + load(j + 1)) / 3
690 weight(i) = lod(i) - pre(i)
NEXT i
1000    CMD$ = "VSET1,5"
    LENGTH% = LEN(CMD$)
    CALL IOOUTPUTS(PS&, CMD$, LENGTH%)
CLS
DFILES$ = "B:" + chip$ + TEST$ + ".txt"
OPEN DFILES$ FOR OUTPUT AS #3
CLS
PRINT "Prepare to apply the heat!  You have ", timeconst
PRINT "seconds to apply the load after you hit <CR> "
INPUT "Apply heat when you hear beep", null$
    CMD$ = "VSET1,0"
    LENGTH% = LEN(CMD$)
    CALL IOOUTPUTS(PS&, CMD$, LENGTH%)
t1 = TIMER
9500 t2 = TIMER - t1
IF t2 < timeconst THEN GOTO 9500
BEEP
'Take heated measurement
CLS
time2 = 0
t5 = TIMER
500 t6 = TIMER
CLS
PRINT time2
    CMD$ = "STORE CHANNEL 1, MEMORY 4"
    LENGTH% = LEN(CMD$)
    CALL IOOUTPUTS(DSO&, CMD$, LENGTH%)
```

```
' time for measurements
IF (t6 - t5) > 45 GOTO 1600
CMD$ = "STORE CHANNEL 1, MEMORY 2"
     LENGTH% = LEN(CMD$)
     CALL IOOUTPUTS(DSO&, CMD$, LENGTH%)
'Retreive heated info from scope
     CMD$ = "WAVEFORM SOURCE MEMORY 4 FORMAT ASCII"
     LENGTH% = LEN(CMD$)
     CALL IOOUTPUTS(DSO&, CMD$, LENGTH%)
     CMD$ = "POINTS?"
     LENGTH% = LEN(CMD$)
     CALL IOOUTPUTS(DSO&, CMD$, LENGTH%)
     R$ = SPACE$(15)
     MAX% = 150: ACTUAL% = 0
     CALL IOENTERS(DSO&, R$, MAX%, ACTUAL%)
     POINTS = VAL(R$)
     CMD$ = "YREF?"
     LENGTH% = LEN(CMD$)
     CALL IOOUTPUTS(DSO&, CMD$, LENGTH%)
     R$ = SPACE$(15)
     MAX% = 150: ACTUAL% = 0
     CALL IOENTERS(DSO&, R$, MAX%, ACTUAL%)
     YREF = VAL(R$)
     CMD$ = "YINC?"
     LENGTH% = LEN(CMD$)
     CALL IOOUTPUTS(DSO&, CMD$, LENGTH%)
     R$ = SPACE$(15)
     MAX% = 150: ACTUAL% = 0
     CALL IOENTERS(DSO&, R$, MAX%, ACTUAL%)
     YINC = VAL(R$)
     CMD$ = "YOR?"
     LENGTH% = LEN(CMD$)
     CALL IOOUTPUTS(DSO&, CMD$, LENGTH%)
     R$ = SPACE$(15)
     MAX% = 150: ACTUAL% = 0
     CALL IOENTERS(DSO&, R$, MAX%, ACTUAL%)
     YORG = VAL(R$)
     CMD$ = "XINC?"
     LENGTH% = LEN(CMD$)
     CALL IOOUTPUTS(DSO&, CMD$, LENGTH%)
     R$ = SPACE$(15)
     MAX% = 150: ACTUAL% = 0
     CALL IOENTERS(DSO&, R$, MAX%, ACTUAL%)
     XINC = VAL(R$)
     CMD$ = "XOR?"
     LENGTH% = LEN(CMD$)
     CALL IOOUTPUTS(DSO&, CMD$, LENGTH%)
     R$ = SPACE$(15)
     MAX% = 150: ACTUAL% = 0
     CALL IOENTERS(DSO&, R$, MAX%, ACTUAL%)
     XORG = VAL(R$)
     CMD$ = "XREF?"
     LENGTH% = LEN(CMD$)
```

```
      CALL IOOUTPUTS(DSO&, CMD$, LENGTH%)
      R$ - SPACE$(15)
      MAX% - 150: ACTUAL% - 0
      CALL IOENTERS(DSO&, R$, MAX%, ACTUAL%)
      XREF - VAL(R$)
X$ - SPACE$(15)
Y$ - SPACE$(15)
CMD$ - "DATA?"
LENGTH% - LEN(CMD$)
CALL IOOUTPUTS(DSO&, CMD$, LENGTH%)
FOR i - 1 TO POINTS
      CALL IOENTERS(DSO&, Y$, MAX%, ACTUAL%)
      X - (i * XINC) + XORG
      Y - ((VAL(Y$) - YREF) * YINC) + YORG
      load(i) - 0
      load(i) - Y
NEXT i




'Store taxel heat information
diff - POINTS / 64
ref - diff / 2
sumpre = 0
sumload = 0
sumpost = 0
FOR i = 1 TO 64
j - INT(diff * i - ref)
IF ABS(preload(j - 1) - preload(j)) <= 4 THEN GOTO 510
IF ABS(preload(j) - preload(j + 1)) <= 4 THEN GOTO 530
CLS
INPUT "Check clock synchronization and push <CR> to restart ", null$
CLOSE #3
GOTO 1000
530 pre(i) - (preload(j) + preload(j + 1)) / 2
GOTO 540
510 IF ABS(preload(j) - preload(j + 1)) <= 4 THEN GOTO 520
pre(i) - (preload(j - 1) + preload(j)) / 2
```

```
GOTO 540
520 pre(i) = (preload(j - 1) + preload(j) + preload(j + 1)) / 3
540 IF ABS(load(j - 1) - load(j)) <= 4 THEN GOTO 560
IF ABS(load(j) - load(j + 1)) <= 4 THEN GOTO 580
CLS
INPUT "Check clock synchronization and push <CR> to restart ", null$
CLOSE #3
GOTO 1000
580 lod(i) = (load(j) + load(j + 1)) / 2
GOTO 590
560 IF ABS(load(j) - load(j + 1)) <= 4 THEN GOTO 570
lod(i) = (load(j - 1) + load(j)) / 2
GOTO 590
570 lod(i) = (load(j - 1) + load(j) + load(j + 1)) / 3
590 lod(i) = (lod(i) - pre(i)) - weight(i)
sumload = lod(i) + sumload
NEXT i
'assign taxel number
taxellod(63) = lod(1)
taxellod(55) = lod(2)
taxellod(37) = lod(3)
taxellod(61) = lod(4)
taxellod(4) = lod(5)
taxellod(28) = lod(6)
taxellod(10) = lod(7)
taxellod(2) = lod(8)
taxellod(53) = lod(9)
taxellod(45) = lod(10)
taxellod(59) = lod(11)
taxellod(51) = lod(12)
taxellod(18) = lod(13)
taxellod(27) = lod(14)
taxellod(25) = lod(15)
taxellod(35) = lod(16)
taxellod(58) = lod(17)
taxellod(44) = lod(18)
taxellod(52) = lod(19)
taxellod(60) = lod(20)
taxellod(34) = lod(21)
taxellod(36) = lod(22)
taxellod(26) = lod(23)
taxellod(17) = lod(24)
taxellod(46) = lod(25)
taxellod(54) = lod(26)
taxellod(62) = lod(27)
taxellod(64) = lod(28)
taxellod(9) = lod(29)
taxellod(1) = lod(30)
taxellod(3) = lod(31)
taxellod(11) = lod(32)
taxellod(33) = lod(33)
taxellod(42) = lod(34)
taxellod(50) = lod(35)
```

```
taxellod(57) = lod(36)
taxellod(22) = lod(37)
taxellod(24) = lod(38)
taxellod(16) = lod(39)
taxellod(32) = lod(40)
taxellod(43) = lod(41)
taxellod(41) = lod(42)
taxellod(49) = lod(43)
taxellod(56) = lod(44)
taxellod(23) = lod(45)
taxellod(15) = lod(46)
taxellod(8) = lod(47)
taxellod(19) = lod(48)
taxellod(48) = lod(49)
taxellod(39) = lod(50)
taxellod(29) = lod(51)
taxellod(31) = lod(52)
taxellod(5) = lod(53)
taxellod(13) = lod(54)
taxellod(21) = lod(55)
taxellod(7) = lod(56)
taxellod(30) = lod(57)
taxellod(40) = lod(58)
taxellod(38) = lod(59)
taxellod(47) = lod(60)
taxellod(14) = lod(61)
taxellod(6) = lod(62)
taxellod(20) = lod(63)
taxellod(12) = lod(64)
PRINT #3, DFILES$
time2 = t6 - t5
PRINT #3, time2
FOR i = 1 TO 64
     PRINT #3, i, taxellod(i)
NEXT i

GOTO 500




1600 CLS
     CLOSE #3
     CMD$ = "LOCAL"
     LENGTH% = LEN(CMD$)
     CALL IOOUTPUTS(DSO&, CMD$, LENGTH%)
     CMD$ = "VSET1,0"
     LENGTH% = LEN(CMD$)
     CALL IOOUTPUTS(PS&, CMD$, LENGTH%)
     CMD$ = "VSET2,0"
     LENGTH% = LEN(CMD$)
     CALL IOOUTPUTS(PS&, CMD$, LENGTH%)
```

```
        CMD$ = "VSET3,0"
        LENGTH% = LEN(CMD$)
        CALL IOOUTPUTS(PS&, CMD$, LENGTH%)
        CMD$ = "VSET4,0"
        LENGTH% = LEN(CMD$)
        CALL IOOUTPUTS(PS&, CMD$, LENGTH%)
CALL IOLOCAL(DSO&)
CALL IOLOCAL(PS&)
CLOSE
END
```

Appendix E. *Three-Dimensional Shape Processing Program*

```
% Matlab file for 3-D sensor plots
% make sure the data to plot has been copied to the file "d.mat"
load d
for i=1:8,
      for j=1:8,
            A(i,j)=d(8*(i-1)+j);
      end
end
% zero out P
for i=1:64,
      for j=1:64,
            P(i,j)=0;
      end
end
% put A matrix values in P
for i=1:8,
      for j=1:8,
            for k=2:7,
                  for l=2:7,
                        P(8*(i-1)+k,8*(j-1)+l)=A(i,j);
                  end
            end
      end
end
% set azimuth angle
az = -45
% set the elevation angle
el = 75
M = [az el]
% plot the data
mesh(P,M)
text(.05,.55,'taxel 1','sc')
text(.5,1,'taxel 8','sc')
text(.88,.4,'taxel 64','sc')
text(.5,.05,'taxel 57','sc')
% clear old graph file
!del c:\matlab\bin\test.met
% save the plot to a file named test.met
meta c:\matlab\bin\test
% convert the file to HPGL format
!gpp c:\matlab\bin\test /dhpgl
% print the file to the Epson DOT Matric printer
%     use dlqf for final quality
%     use dlqd for draft quality
%!gpp c:\thesis\wpg\test.met /dlqd/fprn
% print the file to the HP laser printer
%!gpp c:\thesis\wpg\test.met /djet/fprn
```

Bibliography

[1]   B. E. Robertson, *Robot Sensors, Tactile and Non-Vision* (vol. 2). New
      York: Springer–Verlag, 1986.

[2]   R. A. Russell, *Robotic Tactile Sensing*. Englewood Cliffs, NJ:
      Prentice Hall, 1990.

[3]   L. D. Harmon. "Automated Tactile Sensing," *International Journal of
      Robotics Research*, vol. 1, pp. 3–32, 1982.

[4]   D. G. Pirolo, "Piezoelectric Polymer Tactile Sensor Arrays for
      Robotics," M.S. thesis, Air Force Institute of Technology, 1987.

[5]   R. R. Reston, "Robotic Tactile Sensor Fabricated from Piezoelectric
      Polyvinylidene Fluoride Films," M.S. thesis, Air Force Institute of
      Technology, 1988.

[6]   D. G. Ford, "Multiplexed Robotic Tactile Sensor Fabricated from
      Polyvinylidene Fluoride Films," M.S. thesis, Air Force Institute of
      Technology, 1989.

[7]   R. C. Fitch, "A Robotic Tactile Sensor Incorporating Silicon Planar
      Technology, a Piezoelectric Polyvinylidene Fluoride Film, and On–Chip
      Signal Processing," M.S. thesis, Air Force Institute of Technology,
      1990.

[8]   C. S. Dyson, "Robotic Tactile Sensor Fabricated from a Monolithic
      Silicon Integrated Circuit and a Piezoelectric Polyvinylidene Fluoride
      Thin Film," M.S. thesis, Air Force Institute of Technology, 1991.

[9]   N. C. Yauilla, "Characterization of an Integrated Circuit Tactile
      Sensor Fabricated from a Piezoelectric Polyvinylidene Fluoride (PVDF)
      Polymer Film," Report for EENG 799 Special Study, School of
      Engineering, Air Force Institute of Technology (AU), Wright Patterson
      AFB, OH, June 19. .

[10] E. S. Kolesar, R. R. Reston, D. G. Ford, and R. C. Fitch, "Multiplexed
      Piezoelectric Polymer Tactile Sensor," *Journal of Robotic Systems*,
      vol. 9, pp. 37–63, 1992.

[11] KYNAR Piezo Film Department. *Kynar Piezo Film Technical Manual*.
      Manual 10–M–11–83–M. King of Prussia, PA: Pennwalt Corporation, 1983.

[12] W. G. Cady, *Piezoelectricity. An Introduction to the Theory and
      Application of Electromechanical Phenomena in Crystals* (revised
      edition, vol. 1 and 2). New York: Dover Publications, 1964.

[13] J. G. Webster (ed.), "Piezoelectric Sensors," *Tactile Sensors for
      Robotics and Medicine*. New York: John Wiley and Sons, 1988.

[14]   L. D. Harmon, "Robotic Taction for Industrial Assembly," *International Journal of Robotics Research*, vol. 3, pp. 72–76, 1983.

[15]   M. R. Wolffenbuttel, R. F. Wolffenbuttel, and P. P. L. Regtien, "An Integrated Charge Amplifier for a Smart Tactile Sensor," *Sensors and Actuators*, vol. A 31, pp. 101–109, 1991.

[16]   M. R. Wolffenbuttel and P. P. L. Regtien, "Polysilicon Bridges for the Realization of Tactile Sensors," *Sensors and Actuators*, vol. A 25, pp. 257–264, 1991.

[17]   K. Suzuki, K. Najafi, and K. D. Wise, "A 1024–Element High–Performance Silicon Tactile Imager," in *IEEE Electron Devices Meeting*. San Francisco, CA: IEEE Electron Device Society Press, 1988, pp. 674–677.

[18]   H. Crazzolara, W. Munch, and M. Nagele, "Silicon Pressure Sensor with Integrated Bias Stabilization and Temperature Compensation," *Sensors and Actuators*, vol. A 30, pp. 241–247, 1992.

[19]   L. Liu, X. Zheng, and Z. Li, "An Array Tactile Sensor with Piezoresistive Single–Crystal Silicon Diaphragm," *Sensors and Actuators*, vol. A 32, pp. 193–196, 1993.

[20]   T. H. Speeter, "A Tactile Sensing System for Robotic Manipulation," *The International Journal of Robotics Research*, vol. 9, pp. 25–36, 1990.

[21]   R. C. Luo, F. Wang, and Y. Liu, "An Imaging Tactile Sensor with Magnetostrictive Transduction," *Robot Sensors (Tactile and Non-Vision*, vol. 2) (A. Pugh, ed.). Kempston, Bedford, UK: IFS Publications, 1986.

[22]   P. Adl, Z. A. Memon, D. J. Mapps, and R. T. Rakowski, "Serpentine Magnetoresistive Elements for Tactile Sensor Applications," *IEEE Transactions on Magnetics*, vol. 26, pp. 2047–2049, 1990.

[23]   J. J. Clark, "A Magnetic Field Based Compliance Matching Sensor for High Resolution, High Compliance Tactile Sensing," *Proceedings of the IEEE International Conference on Robotics and Automation*, vol. 2, pp. 772–777, 1988.

[24]   W. D. Drotning and P. Garcia, "A VMEbus Ultrasonic Sensor for Robotic System Control," *Sensors*, pp. 22–31, May 1993.

[25]   J. Borenstein and Y. Koren, "Obstacle Avoidance with Ultrasonic Sensors," *IEEE Journal of Robotics and Automation*, vol. 4, pp. 213–218, 1988.

[26]   H. Ermert, J. Schmolke, and G. Weth, "An Adaptive Ultrasonic Sensor for Object Identification," *Proceedings of the IEEE Ultrasonics Symposium*. Williamsburg, VA, 1986, pp. 555–558.

[27]   A. R. Grahn and L. Astle, "Robotic Ultrasonic Force Sensor Arrays,"
        Conference Proceedings of Robotics Society of Manufacturing Engineers,
        vol. 8, Dearborn, MI, 1984, pp. 21.1-21.17.

[28]   J. Rebman and K. A. Morris, "A Tactile Sensor with Electrooptical
        Transduction," in *Robot Sensors (Tactile and Non-Vision*, vol. 2)
        (A. Pugh, ed.,). Kempston, Bedford, UK: IFS Publications, 1986.

[29]   J. C. Walker, R. Holmes, and G. R. Jones, "Nine Element Optical Sensor
        Matrix Network Using a Spatial Light Modulator," *Electronic Letters*,
        vol. 30, pp. 1627-1628, 1992.

[30]   S. R. Emge and C. Chen, "Two-Dimensional Contour Imaging with a Fiber
        Optic Microbend Tactile Sensor Array," *Sensors and Actuators*, vol. B
        3, pp. 31-42, 1991.

[31]   M. Mehdian and H. Rahnejat, "A Sensory Gripper Using Tactile Sensors
        for Object Recognition, Orientation Control, and Stable Manipulation,"
        IEEE Transactions on Systems, Man, and Cybernetics, vol. 19, pp. 1250-
        1261, 1989.

[32]   S. Begej, "Planar and Finger-Shaped Optical Tactile Sensors for
        Robotic Applications," *IEEE Journal of Robotics and Automation*, vol.
        4, pp. 472-484, 1988.

[33]   R. S. Muller and J. Conragan, "Piezoelectric-Semiconductor,
        Electromechanical Transducer," U.S. Patent No. 3,351,786, Nov. 7,
        1967.

[34]   H. S. Tzou and S. Pandita, "A Multi-Purpose Dynamic and Tactile Sensor
        for Robot Manipulators," *Journal of Robotics Systems*, vol. 4, pp. 719-
        741, 1987.

[35]   K. Park, R. D. Klafter, and P. E. Bloomfield, "A PVDF Tactile Sensor
        for Industrial Robots," *Conference of Robots*. vol. 10, Dearborn, MI:
        Society of Manufacturing Engineers, 1986, pp. 4/47-4/72.

[36]   S. Omata and T. Yoshikazu, "New Tactile Sensor Like the Human Hand and
        Its Applications," *Sensors and Actuators*, vol. 35, pp. 9-15, 1992.

[37]   C. Domenici and D. D. Rossi, "A Stress-Component-Selective Tactile
        Sensor Array," *Sensors and Actuators*, vol. 13, pp. 97-100, 1992.

[38]   J. Curie and P. Curie, "Development by Pressure of Polar Electricity
        in Hemihedral Crystals with Inclined Faces," *Bulletin de Soci 'et 'e
        min 'eralogique de France*, vol. 3, pp. 90-93, 1880.

[39]   A. H. Soukhanov (ed.), *Webster's II New Riverside University
        Dictionary*. Boston, MA: Houghton Mifflin Company, 1984.

[40]   C. Z. Rosen, B. V. Hiremath, and R. Newnham (ed.), "IEEE Standard on Piezoelectricity (ANSI/IEEE Standard 176-1987, 1988)," *Key Papers in Physics*. New York: The American Institute of Physics, 1992.

[41]   J. D. Kraus, *Electromagnetics*. New York: McGraw-Hill, 1984.

[42]   C. R. Paul and S. A. Nasar, *Introduction To Electromagnetic Fields*. New York: McGraw-Hill, 1982.

[43]   G. S. Kino, *Acoustic Waves*. New Jersey: Prentice-Hall, 1987.

[44]   R. G. Kepler and R. A. Anderson, "Ferroelectric Polymers," *Advances in Physics*, vol. 41, pp. 1-57, 1992.

[45]   R. K. Wangsness, *Electromagnetic Fields*. New York: John Wiley and Sons, 1979.

[46]   M. A. Marcus, "Orientation Effects on Dielectric and Piezoelectric Properties of Polyvinylidene Fluoride Films," *Proceedings of the 5th International Symposium on Electrets*. Heidelberg: 1985, pp. 894-899.

[47]   R. W. Whatmore, "Pyroelectric Devices and Materials," *Reports on Progress in Physics*, vol. 49, pp. 1335-1386, 1986.

[48]   M. A. Marcus, "Applications of Polyvinylidene Fluoride Films," *Proceedings of the 5th International Symposium on Electrets*, Heidelberg: 1985, pp. 724-731.

[49]   D. K. Das-Gupta, "On the Nature of Pyroelectricity in Polyvinylidene Fluoride," *Ferroelectrics*, vol. 33, pp. 75-89, 1981.

[50]   M. A. Bachmann and J. B. Lando, "A Reexamination of the Crystal Structure of Phase II of Poly(Vinylidene Fluoride)," *Macromolecules*, vol. 14, pp. 40-46, 1981.

[51]   S. B. Lang, A. S. Dereggi, M. G. Broadhurst, and G. T. Davis, "Effects of Poling Field and Time on Pyroelectric Coefficient and Polarization Uniformity in Polyvinyl Fluoride," *Ferroelectrics*, vol. 33, pp. 119-125, 1981.

[52]   J. E. McKinney, G. T. Davis, and M. G. Broadhurst, *Plasma Poling of Poly(Vinylidene Fluoride): Piezo- and Pyroelectric Response* (Contract N00014-74-C) (AD-A070750). Washington DC: National Bureau of Standards, Polymer Science and Standards Division, June 1979.

[53]   A. H. Franzan, N. F. Leite, and L. C. M. Miranda, "Investigation of Poling Field Effects on PVDF Pyroelectric Detectors: Photoacoustic Thermal Diffusivity Measurements," *Applied Physics*, vol. A 50, pp. 431-438, 1990.

[54]   G. M. Sessler, "Piezoelectricity in Polyvinylidene Fluoride," *Journal of Acoustical Society of America*, vol. 70, pp. 1586-1608, 1981.

[55] H. Kawai, "The Piezoelectricity of Poly (vinylidene Fluoride),"
Japanese Journal of Applied Physics, vol. 8, pp. 975-976, 1969.

[56] R. Al-Jishi and P. L. Taylor, "Equilibrium Polarization and
Piezoelectric and Pyroelectric Coefficients in Poly(vinylidene
Fluoride)," *Journal of Applied Physics*, vol. 57, pp. 902-905, 1985.

[57] R. Al-Jishi and P. L. Taylor, "Field Sums for Extended Dipoles in
Ferroelectric Polymers," *Journal of Applied Physics*, vol. 57, pp. 897-
901, 1985.

[58] R. G. Kepler and R. A. Anderson, "On the Origin of Pyroelectricity in
Polyvinylidene Fluoride," *Journal of Applied Physics*, vol. 49, pp.
4918-4921, 1978.

[59] R. G. Kepler and R. A. Anderson, "Piezoelectricity and Pyroelectricity
in Polyvinylidene Fluoride," *Journal of Applied Physics*, vol. 49, pp.
4490-4494, 1978.

[60] R. G. Kepler, R. A. Anderson, and R. R. Lagasse, "Pyroelectricity and
the Electric Field Dependence of Crystallinity in Polyvinylidene
Fluoride," *Ferroelectrics*, vol. 57, pp. 151-158, 1984.

[61] C. K. Purvis and P. L. Taylor, "Piezoelectric and Pyroelectric
Coefficients for Ferroelectric Crystals with Polarized Molecules,"
Physical Review, vol. 26, pp. 4564-4570, 1982.

[62] C. K. Purvis and P. L. Taylor, "Piezoelectricity and Pyroelectricity
in Polyvinylidene Fluoride: Influence of the Lattice Structure,"
Journal of Applied Physics, vol. 54, pp. 1021-1028, 1983.

[63] Solef Piezo Film. *Technical Data Sheet*. S. A. Brussels, Belgium:
Solvay & Cie.

[64] M. A. Marcus, "Ferroelectric Polymers and Their Appliciations,"
Ferroelectrics, vol 40, pp. 29-41, 1982.

[65] P. Dario, D. D. Rossi, C. Domenici, and R. Francesconi.
"Ferroelectric Polymer Tactile Sensors with Anthropomorphic Features,"
Proceedings of the IEEE Conference on Robotics. New York: IEEE Press,
1984, pp. 332-340.

[66] T. Y. Chan, P. K. Ko, and C. Hu, "Dependence of Channel Electric Field
on Device Scaling," *IEEE Electron Device Letters*, vol. EDL-6, pp. 551-
553, Oct. 1985.

[67] M. Kakumu, M. Kinugawa, and K. Hashimoto, "Choice of Power-Supply
Voltage for Half-Micrometer and Lower Submicrometer CMOS Devices,"
IEEE Transactions on Electron Devices, vol. 37, pp. 1334-1342, 1990.

[68] C. M. Leonard, *Fundamentals of Thermodynamics*. Englewood Cliffs, NJ:
Prentice-Hall, 1958.

[69]   C. L. Nachtigal, *Instrumentation and Control. Fundamentals and Applications*. New York: John Wiley and Sons, 1990.

Vita

Capt John M. Emmert was born 4 May 1964 in Lexington, Kentucky. He graduated from Lafayette High School in Lexington, Kentucky in 1982, and entered the University of Kentucky in September of that year. In 1987 he graduated from the University of Kentucky with a Bachelor of Science in Electrical Engineering. Following completion of Officer Training School he was assigned to the 6545th Test Group at Hill AFB in Utah. From 1989 to 1992 he served as a flight test engineer. In May 1992, he entered the School of Engineering, Air Force Institute of Technology.

Permanent Address: 500 Andrea Dr.
                     Lexington KY 40503

REPORT DOCUMENTATION PAGE

1. AGENCY USE ONLY (Leave blank)	2. REPORT DATE	3. REPORT TYPE AND DATES COVERED
	December 1993	Master's Thesis

4. TITLE AND SUBTITLE

Obejct Imaging Accomplished with an Integrated Circuit Robotic Tactile Sensor Incorporating a Piezoelectric Polyvinylidene Fluoride Thin Film

5. FUNDING NUMBERS

6. AUTHOR(S)

John M. Emmert

7. PERFORMING ORGANIZATION NAME(S) AND ADDRESS(ES)

Air Force Institute of Technology, WPAFB OH 45433-7765

8. PERFORMING ORGANIZATION REPORT NUMBER

AFIT/GE/ENG/93D-06

9. SPONSORING/MONITORING AGENCY NAME(S) AND ADDRESS(ES)

Capt Paul Whalen
Armstrong Laboratory (AL/CFBA)
Wright-Patterson AFB, OH 45433

10. SPONSORING/MONITORING AGENCY REPORT NUMBER

11. SUPPLEMENTARY NOTES

13. ABSTRACT (Maximum 200 words)

The purpose of this research effort was to investigate the performance of a piezoelectric tactile sensor design and appropriately refine it. The sensor was fabricated from an 8 x 8 electrode array MOS integrated circuit. Each taxel in the array was 400 microns x 400 microns. A 6 mm x 6 mm piece of piezoelectric polyvinylidene fluoride was adhered to the electrode array using a urethane dielectric adhesive to form the active sensing area of the sensor.

An amplifier was investigated to enhance the range of the tactile sensor's output signal. The amplifier is a high input impedance differential amplifier with a linear range from 1 to 17 V. The unique feature of the differential amplifier was that it used a power supply of only 12 V.

The spatial resolution of the sensor is 0.7 mm. The lower force limit of the sensor is 1 g while the upper limit, limited by a previous amplifier design with a range from 2.5 to 7 V, is 130 g. The dynamic range of the sensor is 130:1. The sensor's force sensitivity is 7.35 g. The pyroelectric bandwidth of the sensor is 0.083 Hz, and the temperature sensitivity of the sensor is 0.39 degrees Celsius.

14. SUBJECT TERMS

Tactile Sensor, Sensors, Piezoelectric, Pyroelectric, PVDF, Thin Film

15. NUMBER OF PAGES

259

16. PRICE CODE

17. SECURITY CLASSIFICATION OF REPORT	18. SECURITY CLASSIFICATION OF THIS PAGE	19. SECURITY CLASSIFICATION OF ABSTRACT	20. LIMITATION OF ABSTRACT
UNCLASSIFIED	UNCLASSIFIED	UNCLASSIFIED	UL